

**Development of New *N*-Cyclopropyl Based Electron Transfer Probes for
Cytochrome P-450 and Monoamine Oxidase Catalyzed Reactions**

Michelle L. Grimm

Dissertation submitted to the faculty of the Virginia Polytechnic Institute and State University in
partial fulfillment of the requirements for the degree of

Doctor of Philosophy

In

Chemistry

James M. Tanko, Committee Chair

J. Paige Buchanan

Neal Castagnoli Jr.

James Mahaney

May 4, 2011
Blacksburg, Virginia

Keywords: Single electron transfer, Hydrogen atom transfer, Cyclopropyl amines, Radical
cation, Cyclopropane ring opening

Copyright 2011, M. L. Grimm

Development of New *N*-Cyclopropyl Based Electron Transfer Probes for Cytochrome P-450 and Monoamine Oxidase Catalyzed Reactions

Michelle L. Grimm

ABSTRACT

The recent upsurge of degenerative diseases believed to be the result of oxidative stress has sparked an increased interest in utilizing the fundamental principles of physical organic chemistry to understand biological problems. Enzyme pathways can pose several experimental complications due to their complexity, therefore the small molecule probe approach can be utilized in an attempt understand the more complex enzyme mechanisms. The work described in this dissertation focuses on the use of *N*-cyclopropyl amines that have been used as probes to study the mechanism of monoamine oxidase (MAO) and cytochrome P-450 (cP-450).

A photochemical model study of benzophenone triplet (³BP) with the MAO-B substrate 1-methyl-4-phenyl-1,2,3,6-tetrahydropyridine (MPTP) and two of its derivatives, 1-cyclopropyl-4-phenyl-1,2,3,6-tetrahydropyridine and (+/-)-[*trans*-2-phenylcyclopropyl-4-phenyl-1,2,3,6-tetrahydropyridine is presented in Chapter 2. The barrier for ring opening of aminyl radical cations derived from *N*-cyclopropyl derivatives of tertiary amines (such as MPTP) is expected to be low. Reactions of ³BP with all three compounds are very similar. The results suggest that the reaction between benzophenone triplet and tertiary aliphatic amines proceed via a simple hydrogen atom transfer reaction. Additionally these model examinations provide evidence that oxidations of *N*-cyclopropyl derivatives of MPTP catalyzed by MAO-B may not be consistent with a pure SET pathway.

The chemistry of *N*-cyclopropyl amines has been used to study the mechanism of amine oxidations by cP-450. Until recently, the rate constant for these ring opening reactions has not been reported. Direct electrochemical examinations of *N*-cyclopropyl-*N*-methylaniline showed that the radical cation undergoes a unimolecular rearrangement consistent with a cyclopropyl ring opening reaction. Examination of both the direct and indirect electrochemical data showed that the oxidation potential *N*-cyclopropyl-*N*-methylaniline to be +0.528 V (0.1 M Ag⁺/Ag), and rate constant for ring opening of $4.1 \times 10^4 \text{ s}^{-1}$. These results are best explained by two phenomena: (i) a resonance effect in which the spin and charge of the radical cation in the ring closed form is delocalized into the benzene ring hindering the overall rate of the ring opening reaction, and/or (ii) the lowest energy conformation of the molecule does not meet the stereoelectronic requirements for a ring opening pathway. Therefore a new series of spiro cyclopropanes were designed to lock the cyclopropyl group into the appropriate bisected conformation. The electrochemical results reported herein show that the rate constant for ring opening of 1'-methyl-3',4'-dihydro-1'*H*-spiro[cyclopropane-1,2'-quinoline] and 6'-chloro-1'-methyl-3',4'-dihydro-1'*H*-spiro[cyclopropane-1,2'-quinoline] are $3.5 \times 10^2 \text{ s}^{-1}$ and $4.1 \times 10^2 \text{ s}^{-1}$ with redox potentials of 0.3 and 0.366 respectively. In order to examine a potential resonance effect a derivative of *N*-methyl-*N*-cyclopropylaniline was synthesized to provide a driving force for the ring opening reaction thereby accelerating the overall rate of the ring opening pathway. The electrochemical results show that the rate constant for ring opening of 4-chloro-*N*-methyl-*N*-(2-phenylcyclopropyl)aniline to be $1.7 \times 10^8 \text{ s}^{-1}$. The formal oxidation potential (E°_{ox}) of this substrate was determined to be 0.53 V.

The lowered redox potentials of 1'-methyl-3',4'-dihydro-1'*H*-spiro[cyclopropane-1,2'-quinoline] and 6'-chloro-1'-methyl-3',4'-dihydro-1'*H*-spiro[cyclopropane-1,2'-quinoline] can be directly

attributed to the electron donating character of the ortho alkyl group of the quinoline base structure of these spiro derivatives, and therefore the relative energy of the ring closed radical cations directly affects the rate of ring opening reactions. The relief of ring strain coupled with the formation of the highly resonance stabilized benzylic radical explains the rate increase for the ring opening reaction of 4-chloro-*N*-methyl-*N*-(2-phenylcyclopropyl)aniline.

Acknowledgments

I will always have some very fond memories of my graduate career. If nothing else this experience has taught me that nothing of real value comes without sweat, tenacity and dedication. I have thoroughly enjoyed my time in graduate school, however difficult it may have seemed at the time.

First and foremost I would like to thank my research director, Dr. James Tanko, for all of the support and guidance (coupled with a few dumb looks along the way) that he has given me through the years. I am truly indebted to him for aiding me through this process, without him I would have never obtained my PhD. Lastly, I want to thank him for his friendship and caring advice he has provided me with during my time in Blacksburg.

Additionally I want to thank members of my PhD committee for mentoring me through my education: Dr. Neal Castagnoli deserves special thank you for asking the difficult question that I may or may not have thought about. In addition to providing me with experimental advice and helpful discussion along the way, he has been an invaluable resource throughout my studies. Dr. Paige Buchanan has served as a mentor to me both as a previous supervisor and as a friend throughout my career as a scientist. Dr. James Mahaney for serving on my committee and providing positive feedback on my PhD project. Lastly I would like to thank Dr. Tim Long for serving on my committee despite his hectic schedule. Additionally, I feel I should give thanks to Dr. Paul Deck for his patience with all of my arduous questions about bureaucratic paperwork - he is a very patient man.

I would also like to thank the members of the Tanko group that I have gotten to know very well through the years: Dr. Xiangzong Li, Dr. Hayati Celik, Dr. Susan Mitroka, Jared Spencer, Amber Hancock, Akiko Nakamura, Shraddha Patil-Patwardhan, and Liang Chen, I enjoyed working

with all of you. I would like to give a special thank you to Jared Spencer for several fond memories through the years. If I ever feel the need to drive around the McDonalds parking lot at 3 in the morning I'll know whom to call. In all seriousness thank your for all your help with electrochemistry throughout my graduate studies. Secondly, I would like to thank Amber Hancock for being such a loyal and caring friend during my time at Virginia Tech. I know we will friends for a lifetime, and you can't get rid of me.

I would also like to thank the close circle of friends that have been my support group during my time in Blacksburg. Thanks to all my 'stragglers': Jason Baldwin, Dawn Stoneking, Jeff Bunting, Brandie Lemon, Amy Splitt, Pris Sears, Knic Umstead, Sarah Brunner, Mary Baker, Farrell Kelleher, and Chuck Ronco (Sorry if I forgot anyone). I love all of you guys.

A special expression of gratitude goes out to my brother in law Darren Snelgrove who offered words of wisdom along with some humorous stories in an attempt to keep me motivated throughout my education. I also would like to thank two of my closest friends Terri Denslow and Andrea Thornberry for the late night phone conversations and supportive words even though they are both three thousand miles away.

I want to thank my parents for their support throughout my education. Thanks again for doing everything in your power to ensure I would be successful from the time I went off to kindergarten to this point in my career, culminating in the terminal degree in my field. Thank you for the love and support all these years.

Lastly, thank you to my husband Bruce Snelgrove who has been with me through all the great times and supported me in the truly difficult times of this journey. I love you with all my heart.

This manuscript is dedicated to Bruce P. Snelgrove

Table of Contents

Title Page.....	i
Abstract.....	ii
Acknowledgments.....	v
List of Equations.....	iv
List of Figures.....	viii
List of Schemes.....	xiii
List of Tables.....	xvi
List of Abbreviations.....	xvii
Chapter 1 Reactive Intermediates: Photochemical and Electrochemical Methods.....	1
1.1 Introduction	1
1.2 Organic Photochemistry	1
1.2.1 Theoretical Concepts Relating to Organic Photochemistry	3
1.2.2 Rehm-Weller Equation.....	12
1.3 Electrochemical methods	16
1.3.1 Reversible Cyclic Voltammetry.....	18
1.3.2 Quasireversible Cyclic Voltammetry	18
1.3.3 Irreversible Cyclic Voltammetry	19
1.3.4 Mixed Kinetic Control.....	22
1.3.5 Indirect Electrochemistry.....	22
1.4 Dissertation Description	26
Chapter 2 Reaction of Benzophenone Triplet with Aliphatic Amines. What a Potent Neurotoxin Can Tell Us About the Reaction Mechanism.....	31
2.1 Introduction	33
2.2 Results and Discussion	40
2.2.1 Calculations.....	40
2.2.2 Laser Flash Photolysis (LFP).	45
2.3 Conclusions	48
2.4 Experimental Section	49
2.4.1 Materials.	49
2.4.2 Apparatus.....	50

2.4.3	Laser Flash Photolysis (LFP).	50
2.4.4	Calculations.	50
2.4.5	Calculations. (Experimental).	50
Chapter 3 Development of New N-Cyclopropyl Based Electron Transfer Probes for Enzyme Catalyzed Reactions: Stereoelectronic Effects55		
3.1	Introduction	58
3.1.1	Cyclopropane Chemistry	58
3.1.2	Cytochrome P-450	59
3.1.3	SET Pathway	60
3.1.4	HAT Pathway	61
3.1.5	Mechanistic Debate	63
3.2	Results and Discussion	65
3.2.1	<i>N</i> -Cyclopropyl- <i>N</i> -Methylaniline	65
3.2.2	1'-methyl-3',4'-dihydro-1' <i>H</i> -spiro[cyclopropane-1,2'-quinoline] (25)	68
3.2.3	6'-chloro-1'-methyl-3',4'-dihydro-1' <i>H</i> -spiro[cyclopropane-1,2'-quinoline] (41)	85
3.2.4	Preparative Scale Electrolysis (Bulk Electrolysis)	90
3.2.5	Electrochemical Electrospray Mass Spectroscopy (EC-ESI/MS)	94
3.3	Conclusions	100
3.4	Experimental Section	100
3.4.1	Materials and Purification	100
3.4.2	Instrumentation	100
3.4.3	Synthesis	101
3.4.4	Photochemical Apparatus.	104
3.4.5	Laser Flash Photolysis (LFP).	105
3.4.6	Direct and Indirect Electrochemistry	105
3.4.7	Preparative Scale Electrolysis	106
3.4.8	Digital Simulations	106
Chapter 4 Development of New <i>N</i>-Cyclopropyl Based Electron Transfer Probes for Cytochrome P-450 Oxidations: Resonance Effects112		
4.1	Introduction	114
4.1.1	Cyclopropyl Carbinyl Neutral Radical	114
4.1.2	Aromatic Amines	115
4.2	Results and Discussion	117
4.2.1	Substrate Synthesis	117
4.2.2	(4-chloro- <i>N</i> -methyl- <i>N</i> -(2-phenylcyclopropyl)aniline) (7)	117
4.2.3	Direct Electrochemistry	118
4.2.4	Indirect Electrochemistry	126
4.2.5	Preparative Scale Electrolysis (Bulk Electrolysis)	131
4.3	Conclusions	133
4.4	Experimental Section	133
4.4.1	Materials and Purification	133

4.4.2	Instrumentation	133
4.4.3	Synthesis.....	134
4.4.4	Direct and Indirect Electrochemistry	135
4.4.5	Preparative Scale Electrolysis	136
4.4.6	Digital Simulations.....	137
Chapter 5 Rational for Experimental Findings and Concluding Remarks		140
5.1	Introduction	141
5.2	Summary of Results Presented in Chapters 4 and 5.....	142
5.3	Substituent Effects Correlated to Redox Potentials.....	143
5.4	Linear Free Energy Relationships.....	146
5.5	Activation Barriers and Trends in Redox Potentials.....	149
5.6	Spin Density Analysis of Compound $5^{\bullet+}$	151
5.7	Comparison of 5 to 7 and 8.....	153
5.8	Spin Density Analysis of Substrate $6^{\bullet+}$	155
5.9	Comparison of Experimental Data with Computational Results.....	156
5.10	Final Thoughts and Conclusions	161
Appendix A: Supplementary Information for Chapter 2.....		163
Appendix B: Supplementary Information for Chapter 4.....		170
Appendix C: Supplementary Information for Chapter 5.....		173

List of Equations

Equation 1-1 Leffler relationship	5
Equation 1-2 Hammett equation.....	6
Equation 1-3 Marcus equation	6
Equation 1-4 Marcus equation without the electrostatic term.....	7
Equation 1-5 Marcus treatment of the Eyring equation.....	9
Equation 1-6 Steady state treatment of the Eyring equation.....	9
Equation 1-7 Weller equation.....	13
Equation 1-8 Free energy change with respect to redox potentials.....	15
Equation 1-9 Nernst equation.....	18
Equation 1-10 Boundary conditions for the heterogeneous electron transfer rate constant used for LSV analysis.....	19
Equation 1-11 Boundary conditions for the rate constant of the chemical step used for LSV analysis	19
Equation 1-12 Change in peak potential with respect to the scan rate for an electron transfer rate limiting pathway.....	20
Equation 1-13 Predicted peak widths for an electron transfer rate limiting pathway	20
Equation 1-14 Relationship between the heterogenous electron transfer rate constant and the peak potential for an electron transfer process.....	20
Equation 1-15 Definition of the transfer coefficient	20
Equation 1-16 Change in peak potential with respect to the scan rate for a chemical step rate limiting pathway	21
Equation 1-17 Predicted peak widths for a chemical step rate limiting pathway	21
Equation 1-18 Predicted change in the peak potential with respect to the substrate concentration for a first order chemical step rate limiting process.....	21
Equation 1-19 Relationship between the rate constant for the chemical step and the peak potential for a chemical step rate limiting pathway	21

Equation 1-20 Change in peak potential with respect to the scan rate for a dimerization pathway..	21
Equation 1-21 Predicted change in the peak potential with respect to the substrate concentration for a dimerization process.....	21
Equation 1-22 Predicted peak widths for a dimerization pathway	21
Equation 1-23 Relationship between the rate constant for dimerization and the peak potential for a second order process.....	21
Equation 1-24 Boundary conditions for mixed kinetic control used for LSV analysis.....	22
Equation 1-25 Boundary conditions for mixed kinetic control used for LSV analysis.....	22
Equation 1-26 Boundary conditions used in redox catalysis for an electron transfer rate limiting pathway.....	24
Equation 1-27 Mediator to substrate ratio.....	24
Equation 1-28 Boundary conditions used in redox catalysis for a chemical step rate limiting pathway.....	25
Equation 1-29 Boundary conditions used in redox catalysis for a chemical step rate limiting pathway.....	25
Equation 1-30 Relationship between the redox potential of the substrate to the rate constant of the chemical step for a chemical step rate limiting pathway	26
Equation 2-1 Equation to obtain the pseudo first order rate constants for the reaction of benzophenone triplet (³ BP) with MPTP	164
Equation 3-1 Dimensionless parameter λ	78
Equation 3-2 Dimensionless parameter λ_1	78
Equation 3-3 Dimensionless parameter λ_{-1}	78
Equation 3-4 Mediator to substrate ratio	79
Equation 3-5 Expression for the composite rate constant k_{obs}	83
Equation 3-6 Relationship between the rate constant for the chemical step and the peak potential for a chemical step rate limiting pathway	83

Equation 3-7 Relationship between the redox potential of the substrate to the rate constant of the chemical step for a chemical step rate limiting pathway.....	83
Equation 4-1 Boundary conditions for the heterogeneous electron transfer rate constant used for LSV analysis.....	119
Equation 4-2 Boundary conditions for the rate constant of the chemical step used for LSV analysis.....	119
Equation 4-3 Change in peak potential with respect to the scan rate for an electron transfer rate limiting pathway.....	120
Equation 4-4 Predicted peak widths for an electron transfer rate limiting pathway.....	120
Equation 4-5 Relationship between the heterogenous electron transfer rate constant and the peak potential for an electron transfer process.....	120
Equation 4-6 Change in peak potential with respect to the scan rate for a chemical step rate limiting pathway.....	120
Equation 4-7 Predicted peak widths for a chemical step rate limiting pathway.....	120
Equation 4-8 Predicted change in the peak potential with respect to the substrate concentration for a first order chemical step rate limiting process.....	120
Equation 4-9 Relationship between the rate constant for the chemical step and the peak potential for a chemical step rate limiting pathway.....	120
Equation 4-10 Boundary conditions for mixed kinetic control used for LSV analysis.....	121
Equation 4-11 Boundary conditions for mixed kinetic control used for LSV analysis.....	121
Equation 4-12 Solved solution for extraction of the C_1 term.....	124
Equation 4-13 Solved solution for extraction of the C_2 term.....	124
Equation 4-14 Relationship between the rate constant for the chemical step and the peak potential for a mixed kinetic control pathway.....	125
Equation 4-15 Boundary conditions used in redox catalysis for an electron transfer rate limiting pathway.....	127
Equation 4-16 Mediator to substrate ratio.....	127
Equation 4-17 Gibbs free energy change of reaction.....	129

Equation 4-18 Relationship between the homogenous electron transfer rate constant and the redox potential of the substrate	129
Equation 5-1 Hammett Equation	147
Equation 5-2 Equation for adjusted σ^+ values accounting for the effect of an ortho alkyl group...	148
Equation 5-3 Predicted peak widths for a concerted dissociative electron transfer process.....	158
Equation 5-4 Equation for adjusted σ^+ values accounting for a resonance effect.....	159

List of Figures

Figure 1-1 Schematic representation of reaction progress for the reaction $A \rightarrow B$. ΔG^\ddagger represents the activation barrier for the reaction, and ΔG° represents the relative energy of the reactants and products.....	3
Figure 1-2 Schematic representation of the relative position of the T.S. of a reaction according to the Hammond postulate.....	4
Figure 1-3 Reaction of Fe^{2+} and Fe^{3+} depicting the changes in internal reorganization energy for a favorable electron transfer pathway	8
Figure 1-4 Graphical representation of $\log k$ vs. ΔG°	10
Figure 1-5 Reaction coordinate diagrams depicting (i) thermoneutral reaction progress, (ii) extremely exothermic progress, and (iii) Marcus ‘inverted’ region	11
Figure 1-6 Orbital Diagrams depicting (i) reduction of a desired substrate by an organic sensitizer and (ii) oxidation of a desired substrate by an organic sensitizer.....	14
Figure 1-7 Representative voltammogram	17
Figure 1-8 Representation of a mediated redox catalysis experiment	24
Figure 1-9 Representation of the procedure to extract k_1 and $E^\circ_{(A/A\cdot)}$ from experimental data.....	25
Figure 2-1 Reaction coordinate diagram for the ring opening of 14^{*+} calculated at the UHF/6-31G* level of theory.....	41
Figure 2-2 Reaction coordinate diagram for the ring opening of 15^{*+} calculated at the UHF/6-31G* level of theory.....	42
Figure 2-3 Reaction coordinate diagram for the ring opening of 16^{*+} calculated at the UHF/6-31G* level of theory.....	43
Figure 2-4 Depiction of how variation on C-C bond length of 14^{*+} is accompanied by simultaneous rotation of the <i>N</i> -methyl group.....	43
Figure 2-5 Reaction coordinate diagram for the ring opening of 17^{*+} calculated at the UHF/6-31G* level of theory.....	44
Figure 2-6 Transient absorption spectra of (i) MPTP (1) in CH_3CN and, (ii) <i>N</i> -cyclopropylphenyl MPTP (10) in CH_3CN	47
Figure 2-7 Transient absorption spectra of MPTP (1) in benzene.....	165

Figure 2-8 Transient absorption spectra of MPTP (1) in CH ₃ CN in the presence of LiOCl ₄	165
Figure 2-9 Transient absorption spectra of <i>N</i> -cyclopropylphenyl MPTP (10) in benzene.....	166
Figure 2-10 Transient absorption spectra of <i>N</i> -cyclopropylphenyl MPTP (10) in CH ₃ CN in the presence of LiOCl ₄	166
Figure 2-11 Concentration profile for the reaction of benzophenone triplet (³ BP) with MPTP (1) in acetonitrile.....	167
Figure 2-12 Concentration profile for the reaction of benzophenone triplet (³ BP) with MPTP (1) in acetonitrile in the presence of 0.5M LiOCl ₄	167
Figure 2-13 Concentration profile for the reaction of benzophenone triplet (³ BP) with <i>N</i> -cyclopropyl-MPTP (9) in benzene.....	168
Figure 2-14 Concentration profile for the reaction of benzophenone triplet (³ BP) with <i>N</i> -cyclopropyl MPTP (9) in acetonitrile.....	168
Figure 2-15 Concentration profile for the reaction of benzophenone triplet (³ BP) with <i>N</i> -cyclopropyl MPTP (9) in acetonitrile in the presence of 0.5M LiOCl ₄	169
Figure 3-1 Depiction of the orbital interaction of the cyclopropyl group and a π system: (i) interaction depicted in the bisected conformation, and (ii) interaction shown in the perpendicular conformation.....	59
Figure 3-2 Compounds used to examine the <i>N</i> -dealkylation reaction of <i>N</i> -alkyl- <i>N</i> -cyclopropyl- <i>p</i> -chloroaniline probes by cP-450	62
Figure 3-3 Direct photoionization of anilines at 266 nm	67
Figure 3-4 New series of compounds for study.....	68
Figure 3-5 Cyclic voltammogram of 27 (0.1 M LiOCl ₄ , 0.5 M CH ₃ OH/CH ₃ CN, $\nu = 100$ mV/sec, 4.65 mM substrate).....	72
Figure 3-6 LSV analysis of 27 , $\partial E_p/\partial \log \nu$ at 2.6 mM concentration. (0.1 M LiClO ₄ , 0.5 M CH ₃ OH/CH ₃ CN, $\nu = 100$ -1000 mV/sec)	72
Figure 3-7 LSV analysis of 27 , $\partial E_p/\partial \log \nu$ at 4.6 mM concentration. (0.1 M LiClO ₄ , 0.5 M CH ₃ OH/CH ₃ CN, $\nu = 100$ -1000 mV/sec)	73
Figure 3-8 LSV analysis of 27 , $\partial E_p/\partial \log \nu$ at 8.7 mM concentration. (0.1 M LiClO ₄ , 0.5 M CH ₃ OH/CH ₃ CN, $\nu = 100$ -1000 mV/sec)	73

Figure 3-9 LSV analysis of 27 , $\partial E_p/\partial \log C_A$ at multiple concentrations. (0.1 M LiClO ₄ , 0.5 M CH ₃ OH/CH ₃ CN, $\nu = 100$ mV/sec)	74
Figure 3-10 [i_p/i_{pd} vs. $\log(1/\nu)$] – Mediated redox catalysis of 27 by 4-cyanophenylferrocene (36f), (0.1 M LiClO ₄ , 0.5 M CH ₃ OH/CH ₃ CN, $\gamma = 1$, $\nu = 100$ -8000 mV/sec)	79
Figure 3-11 [i_p/i_{pd} vs. $\log C_M^0/\nu$] – Mediated redox catalysis of 27 by 4-cyanophenylferrocene (36f), (0.1 M LiClO ₄ , 0.5 M CH ₃ OH/CH ₃ CN, $\gamma = 1$, $\nu = 100$ -8000 mV/sec)	80
Figure 3-12 Mediated redox catalysis of 25 by 4-cyanophenylferrocene (36f), (0.1 M LiClO ₄ , 0.5 M CH ₃ OH/CH ₃ CN, $\gamma = 1$, (i) $\nu = 100$ mV, (ii) $\nu = 400$ mV, (iii) $\nu = 600$ mV, (iv) $\nu = 1000$ mV ..	81
Figure 3-13 Mediated redox catalysis of 27 with 4-cyanophenylferrocene (36f), (CH ₃ CN, 0.5M CH ₃ OH, 0.5M nBu ₄ N ⁺ •BF ₄ ⁻ , $\nu = 25$ mV, $\gamma = 1, 2.24, 3.48, 4.73, 5.97$)	82
Figure 3-14 Fitting results of the results for mediated catalysis of 27 with 4-cyanophenylferrocene (36f) with digitally simulated working curves ($k_0 = 1.1 \times 10^5$).	83
Figure 3-15 Redox Catalysis of 27 with 2-nitrophenylferrocene (36g) (CH ₃ CN, 0.5M CH ₃ OH, 0.5M nBu ₄ N ⁺ •BF ₄ ⁻ , $\nu = 25$ mV, $\gamma = 1, 2.1, 3.2, 4.3, 5.4$)	84
Figure 3-16 Fitting results of the results for mediated catalysis of 27 with 2-nitrophenylferrocene (36g) with digitally simulated working curves ($k_0 = 9.7 \times 10^4$)	85
Figure 3-17 Cyclic voltammogram of 41 (0.1 M LiClO ₄ , 0.5 M CH ₃ OH/CH ₃ CN, $\nu = 100$ mV/sec, 4.65 mM substrate)	87
Figure 3-18 LSV analysis of 41 , $\partial E_p/\partial \log \nu$ at 2.2 mM concentration. (0.1 M LiClO ₄ , 0.5 M CH ₃ OH/CH ₃ CN, $\nu = 100$ -1000 mV/sec)	87
Figure 3-19 LSV analysis of 41 , $\partial E_p/\partial \log \nu$ at 5.3 mM concentration. (0.1 M LiClO ₄ , 0.5 M CH ₃ OH/CH ₃ CN, $\nu = 100$ -1000 mV/sec)	88
Figure 3-20 Redox Catalysis of 41 with 2,4-dinitrophenylferrocene (36h) (CH ₃ CN, 0.5M CH ₃ OH, 0.5M nBu ₄ N ⁺ •BF ₄ ⁻ , $\nu = 25$ mV/sec, $\gamma = 1, 2.1, 3.3, 4.4, 5.6$)	89
Figure 3-21 Fitting results of the results for mediated catalysis of 41 with 2,4-dinitrophenylferrocene (36h) with digitally simulated working curves.	89
Figure 3-22 Mass voltammograms of 41 and its oxidation product ($m/z = 240$)	94
Figure 3-23 Mass Spectra of 41 post ESI oxidation.	95
Figure 3-24 ESI MS results for experiments conducted in H ₂ ¹⁸ O water.	98
Figure 3-25 ESI MS results for experiments conducted in oxygen ¹⁸ O.	99

Figure 4-1 Cyclic voltammogram of 6 (0.1 M NBu ₄ ⁺ •BF ₄ ⁻ , 0.5 M CH ₃ OH/CH ₃ CN, ν = 100 mV/sec, 2.3 mM substrate).....	122
Figure 4-2 LSV analysis of 6 , $\partial E_p/\partial \log \nu$ at 1.5 mM concentration. (0.1 M NBu ₄ ⁺ •BF ₄ ⁻ , 0.5 M CH ₃ OH/CH ₃ CN, ν = 100-4000 mV/sec).....	123
Figure 4-3 LSV analysis of 6 , $\partial E_p/\partial \log \nu$ at 2.3 mM concentration. (0.1 M NBu ₄ ⁺ •BF ₄ ⁻ , 0.5 M CH ₃ OH/CH ₃ CN, ν = 100-1000 mV/sec).....	123
Figure 4-4 LSV analysis of 6 , $\partial E_p/\partial \log \nu$ at 2.5 mM concentration. (0.1 M NBu ₄ ⁺ •BF ₄ ⁻ , 0.5 M CH ₃ OH/CH ₃ CN, ν = 100-1000 mV/sec).....	124
Figure 4-5 Working curve for the change in peak width ($E_p - E_{p/2}$) with respect to the log of the scan rate (ν) to extract a value for C ₁	125
Figure 4-6 Working curve for the change in peak potential (E_p) with respect to the log of the scan rate (ν) to extract a value for C ₂	126
Figure 4-7 Representation of the procedure to extract k_1 and $E^\circ_{(A/A^{\bullet+})}$ from experimental data	127
Figure 4-8 [ip/ipd vs. log (1/ ν)] – Mediated redox catalysis of 6 by ferrocene carboxylic acid, (0.1M LiOCl ₄ , 0.5M CH ₃ OH/CH ₃ CN, γ = 1, ν = 100 – 8000 mV/sec).....	128
Figure 4-9 [ip/ipd vs. log (C ^o _M / ν)] – Mediated redox catalysis of 6 by ferrocene carboxylic acid, (0.1M LiOCl ₄ , 0.5M CH ₃ OH/CH ₃ CN, γ = 1, ν = 100 – 8000 mV/sec)	129
Figure 4-10 [ip/ipd vs. log (1/ ν)] – Mediated redox catalysis of 6 by 4-cyanophenyl ferrocene, (0.1M LiOCl ₄ , 0.5M CH ₃ OH/CH ₃ CN, γ = 1, ν = 100 – 8000 mV/sec).....	130
Figure 4-11 [ip/ipd vs. log (C ^o _M / ν)] – Mediated redox catalysis of 6 by 4-cyanophenyl ferrocene, (0.1M LiOCl ₄ , 0.5M CH ₃ OH/CH ₃ CN, γ = 1, ν = 100 – 8000 mV/sec)	130
Figure 5-1 Correlation of calculated ionization potentials to experimentally determined redox potentials of compounds 1-8	146
Figure 5-2 Hammett plot correlating the redox potential of 1-8 to σ^+	148
Figure 5-3 Hammett plot correlating the redox potential of 1-8 to adjusted σ^+ constants accounting for the added electron donating character of compounds 7 and 8	149
Figure 5-4 Reaction coordinate diagram depicting the relative energies of compounds 5^{•+} , 9^{•+} , and 10^{•+}	151

Figure 5-5 Depiction of the spin and charge delocalization of (i) the ring closed radical cation, (ii) the transition state, and (iii) the product arising from the ring opening of 5^{•+}	153
Figure 5-6 Depiction of the spin and charge delocalization of (i) the ring closed radical cation, (ii) the transition state, and (iii) the product arising from the ring opening of 7^{•+}	154
Figure 5-7 Depiction of the spin and charge delocalization of (i) the ring closed form, (ii) the transition state, and (iii) the product arising from the ring opening of 6^{•+}	156
Figure 5-8 Reaction coordinate diagram for compounds 5-8	156
Figure 5-9 Hammett plot correlating the redox potential of 1-8 to modified σ^+ constants accounting for the added resonance effect for 8	160
Figure 5-10 Depiction of the spin and charge delocalization of (i) the ring closed radical cation, (ii) the transition state, and (iii) the product arising from the ring opening of 8^{•+}	174
Figure 5-11 Transition state structure for compound 5^{•+}	174
Figure 5-12 Transition state structure for compound 9^{•+}	175
Figure 5-13 Transition state structure for compound 10^{•+}	175
Figure 5-14 Transition state structure for compound 13^{•+}	176

List of Schemes

Scheme 1-1	Reactive intermediate generation.....	2
Scheme 1-2	Representation of an electron transfer process resulting in oxidation of the substrate ...	3
Scheme 1-3	Electron transfer reaction used for the steady state approximation	9
Scheme 1-4	Representation of the Rehm-Weller experiment.....	12
Scheme 1-5	Parameters for calculating a thermodynamic cycle for ET	15
Scheme 1-6	Representation of the EC mechanism.....	16
Scheme 1-7	Representation of the mechanism for mediated redox catalysis.....	23
Scheme 2-1	Proposed Pathways for MAO oxidations	34
Scheme 2-2	Degradation of MPPP to MPTP.....	34
Scheme 2-3	The MAO-B catalyzed bioactivation of MPTP (2) to MPDP ⁺ (4 ⁺) and MPP ⁺ (5 ⁺).	35
Scheme 2-4	Reaction of benzophenone triplet (³ BP) with aromatic amines	36
Scheme 2-5	Ring opening of the cyclopropylcarbinyl neutral radical	38
Scheme 2-6	Ring opening of <i>N</i> -(2-phenylcyclopropyl) aminyl radical cations	39
Scheme 2-7	Resonance stabilization of the distonic radical cation derived from 10 ⁺ and 16 ⁺	45
Scheme 2-8	Reaction pathways for ³ BP with MPTP 1) SET, and 2) HAT.....	46
Scheme 3-1	Stoichiometry of the cP-450 catalyzed oxidation.	60
Scheme 3-2	Pathways for the oxidation of P-450: (A) SET mechanism, and (B) HAT mechanism.	60
Scheme 3-3	Ring opening of <i>N</i> -benzyl- <i>N</i> -cyclopropylamine following an SET pathway.....	61
Scheme 3-4	Oxidation of <i>N</i> -methyl- <i>N</i> -cyclopropyl amine by HRP and cP-450.....	64
Scheme 3-5	Products stemming from the oxidation of ¹³ C labeled oxidation of 1-cyclopropyl-4-phenyl-1,2,3,6-tetrahydropyridine.	64
Scheme 3-6	Reaction of 4-phenyl-1-(<i>trans</i> -2-phenyl)cyclopropyl amine with cP-450.....	65

Scheme 3-7 Depiction of (i) resonance delocalization of the radical cation, and (ii) stereoelectronic requirements for ring opening.....	67
Scheme 3-8 Attempted synthesis of 1'-methylspiro[cyclopropane-1,2'-indoline]: (i) NaH, dimethylsulfate, xylene, reflux 2hr.; (ii) Ti(O ⁱ Pr) ₄ , CH ₃ CH ₂ MgBr, -78°C to RT, 17 hrs.....	68
Scheme 3-9 Proposed cyclopropane ring opening reaction in the presence of mild acid.	69
Scheme 3-10 Attempted synthesis of 1',3',3'-trimethylspiro[cyclopropane-1,2'-indoline]: (i) NaH, dimethylsulfate, xylene, reflux 2hr.; (ii) LDA, 2x CH ₃ I -78°C; (iii) Ti(O ⁱ Pr) ₄ , CH ₃ CH ₂ MgBr, -78°C to RT, 17 hrs.....	69
Scheme 3-11 Synthesis of 1'-methyl-3',4'-dihydro-1' <i>H</i> -spiro[cyclopropane-1,2'-quinoline]: (i) ClC(O)CH ₂ CH ₂ Cl, acetone, reflux 2.5 hrs.; (ii) AlCl ₃ , 17 hrs.; (iii) Ti(O ⁱ Pr) ₄ , CH ₃ CH ₂ MgBr, -78°C to RT, 15 hrs.....	70
Scheme 3-12 Representation of the EC mechanism.....	71
Scheme 3-13 Synthesis of modified ferrocenes for reductive catalysis experiments: (i) NaNO ₂ , 20% H ₂ SO ₄ , 0° C; (ii) ferrocene, 0° C to RT, 48hrs.....	78
Scheme 3-14 Mechanism used to model the chemical step rate limiting pathway for compound 27.	83
Scheme 3-15 Synthesis of 6'-chloro-1'-methyl-3',4'-dihydro-1' <i>H</i> -spiro[cyclopropane-1,2'-quinoline]: (i) ClC(O)CH ₂ CH ₂ Cl, acetone, reflux 2.5 hr.; (ii) AlCl ₃ , 17 hr.; (iii) NaH, dimethylsulfate, xylene, reflux 2 hr. (iv) Ti(O ⁱ Pr) ₄ ,CH ₃ CH ₂ MgBr, -78 C to RT.....	86
Scheme 3-16 Bulk electrolysis with a sodium borohydride workup.....	90
Scheme 3-17 Sample electrolysis of 41. Solutions were subjected to a reductive work up and analyzed by GC-MS.....	91
Scheme 3-18 Sample electrolysis of 41. Solutions were exposed to an H-donor, subjected to a reductive work up, and analyzed by GC-MS.....	92
Scheme 3-19 Proposed mechanism for the oxidation of 42 leading to the products 41 and 43a.....	93
Scheme 3-20 Proposed mechanism for 42 abstract a hydrogen from the <i>N</i> -methyl group.	93
Scheme 3-21 Proposed mechanism accounting for the reaction of 41 with water post ESI-MS.....	96
Scheme 3-22 Proposed mechanism for the reaction of 41 with molecular oxygen post ESI.....	97
Scheme 3-23 Predicted products from reaction of 41 with H ₂ ¹⁸ O water.....	98

Scheme 3-24 Predicted products from reaction of 41 with ^{18}O molecular oxygen.....	99
Scheme 4-1 Ring opening of <i>N</i> -benzyl- <i>N</i> -cyclopropyl amine following an SET pathway.....	114
Scheme 4-2 Ring opening of the cyclopropyl carbinyl neutral radical.....	115
Scheme 4-3 Ring opening of <i>N</i> -methyl- <i>N</i> -cyclopropylaniline radical cation.....	116
Scheme 4-4 Depiction of (i) resonance delocalization of the radical cation, and (ii) stereo-electronic requirements for ring opening.....	116
Scheme 4-5 Ring opening reaction of 4-chloro- <i>N</i> -methyl- <i>N</i> -(2-phenylcyclopropyl)aniline	117
Scheme 4-6 Attempted synthesis of 4-chloro- <i>N</i> -methyl- <i>N</i> -(2-phenylcyclopropyl)aniline (6).....	118
Scheme 4-7 Synthesis of 4-chloro- <i>N</i> -methyl- <i>N</i> -(2-phenylcyclopropyl)aniline (6)	118
Scheme 4-8 Representation of the EC mechanism.....	119
Scheme 4-9 Proposed mechanism for the reaction of 6 following bulk electrolysis.	132
Scheme 4-10 Mechanism used to generate the theoretical working curves.....	171
Scheme 5-1 Ring opening of <i>N</i> -methyl- <i>N</i> -cyclopropylaniline radical cation (5^{•+}).....	141
Scheme 5-2 Depiction of (i) resonance delocalization of the radical cation, and (ii) stereo-electronic requirements for ring opening.....	142
Scheme 5-3 Solvolysis reaction of cumyl chloride that defines the σ^+ substituent constant.	147
Scheme 5-4 Ring opening reaction of 5^{•+}	152

List of Tables

Table 1-1 Photophysical Data for several known organic sensitizers.....	16
Table 2-1 Rate constants for the reaction of ³ BP with 2 and 9	48
Table 3-1 Rate constants for the decay of radical cations used in the Maslak study.....	66
Table 3-2 Summary of direct electrochemical results.....	75
Table 3-3 Listing of mediators used in our laboratory. Compounds in black denote commercially available compounds. Compounds in blue were synthesized in our laboratory.....	77
Table 3-4 Sample electrolysis of 41 . Solutions were subjected to a reductive work up (NaBH ₄) and analyzed by GC-MS.....	91
Table 3-5 Sample electrolysis of 41 . Solutions were subjected to a reductive work up (NaBH ₄ or NaBD ₄) and analyzed by GC-MS.....	91
Table 3-6 Sample electrolysis of 41 . Solutions were subjected to a reductive work up (NaBH ₄ or NaBD ₄) and analyzed by GC-MS.....	92
Table 5-1 Redox Potentials for the anilines examined and rate constants for the ring opening of the corresponding radical cations.....	145
Table 5-2 Calculated activation barriers for compounds 5^{•+} , 9^{•+} , and 10^{•+} at the B3YLP/6-311+G(d,p) level of theory.....	150
Table 5-3 Comparison of experimentally derived rate constants and computational results at the B3YLP/6-311+G(d,p) level of theory.....	158

List of Abbreviations

A	Reactant
BDE	Bond Dissociation Energy
BP	Benzophenone
C	Celsius
cP-450	Cytochrome P-450
CV	Cyclic Voltammetry
D	Donor Substrate
D	Diffusion Coefficient
DET	Dissociative Electron Transfer
DTBPO	Di- <i>t</i> -butyl peroxide
E°	Redox Potential
E_p	Peak Potential
$E_{p/2}$	Half Wave Potential
EC	Electron Transfer followed by a Chemical Step
ET	Electron Transfer
F	Faraday's Constant
ΔG°	Free Energy change for a Reaction
ΔG^\ddagger	Free Energy of Activation
ΔG_{ET}	Free Energy of Electron Transfer
HAT	Hydrogen Atom Transfer
HOMO	Highest Occupied Molecular Orbital
HRP	Horse Radish Peroxidase
i_p	Peak Current
k	Rate Constant
k_0	Rate Constant for the Chemical Step
K_{eq}	Equilibrium Constant
k_G	Heterogeneous Rate Constant
K_H	Ionization Constant of Benzoic Acid
k_{obs}	Observed Rate Constant
K_X	Ionization Constant of substituted benzoic acid
KIEs	Kinetic Isotope Effects
LC-MS	Liquid Chromatography Mass Spectrometry
LFP	Laser Flash Photolysis
LSV	Linear Sweep Voltammetry
LUMO	Lowest Unoccupied Molecular Orbital
M	Mediator
MAO	Monoamine Oxidase
MPDP	1-methyl-4-phenyl-2,3-dihydropyridinium
MPP ⁺	1-methyl-4-phenylpyridinium

MPPP	1-methyl-4-phenyl-4-propionoxypiperidine
MPTP	1-methyl-4-phenyl-1,2,3,6-tetrahydropyridine
mM	Millimolar
mol	Mole
mV	Millivolts
n	Number of Moles
nm	Nanometers
NHE	Normal Hydrogen Electrode
P	Products
R	Ideal Gas Constant
S	Sensitizer
SET	Single Electron Transfer
SSIP	Solvent Separated Ion Pair
T	Temperature
ν	Scan Rate
V	Volts
UV/vis	Ultraviolet/visible
ρ	Hammett Reaction Constant
σ	Hammett Substituent Parameters
λ	Reorganization Energy

Chapter 1 Reactive Intermediates: Photochemical and Electrochemical Methods

1.1 Introduction

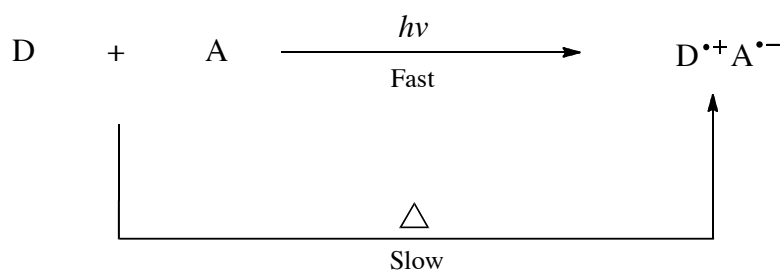
The increasing occurrence of neurodegenerative conditions such as Parkinson's and Alzheimer's disease, as well as various cancers that are believed to be the result of oxidative stress, has renewed interest in utilizing the principles of mechanistic organic chemistry to study fundamental biological problems at the molecular level. Due to the complexity of enzyme pathways, many biological problems are approached through the use of small molecule probes to gain insight into the mechanism of a specific pathway. This is done through the use of a model system that emulates an enzyme but is much less complex. By gaining an understanding of the simpler processes, one can extrapolate and make a hypothesis for the behavior of the more complex systems. For the scope of this review, only mechanisms of oxidation of amines catalyzed by monoamine oxidase (MAO) and cytochrome P-450 are discussed. These enzymes are believed to catalyze oxidations via mechanisms involving reactive intermediates (e.g. free radicals and radical ions). Photochemical and electrochemical methods provide a means of generating radical ions, and therefore this review begins with an overview of organic photochemistry and culminates in a review in organic electrochemistry.

1.2 Organic Photochemistry

Organic photochemistry is a field that employs the disciplines of organic, physical and mechanistic chemistry. The field has been more generally accepted since the advent of the Woodward-Hoffman rules, which defined a set of basic principles based on molecular orbital theory. These rules dictate whether a chemical transformation will occur thermally or photochemically, and also have the ability to accurately predict the stereochemistry of the

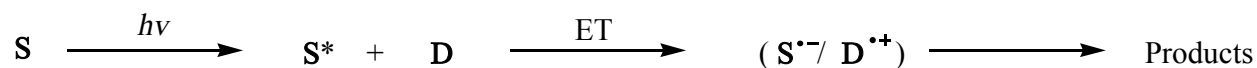
reaction products.¹ These ideas have been utilized extensively by synthetic chemists in pericyclic and Diels-Alder reactions² and by physical organic chemists to study reaction mechanisms.³

Photochemistry utilizes a photon of light to provide the energy to drive a chemical transformation. Photochemistry provides a means to generate reactive species that are not easily studied by traditional thermal reactions due to the fact that the chemistry involving radicals and radical ions occurs on a time regime that is much faster than thermal reactions (**Scheme 1-1**).



Scheme 1-1 Reactive intermediate generation

This review focuses on the mechanistic aspects of electron transfer reactions (**Scheme 1-2**), where an organic sensitizer (**S**) is elevated to its singlet or triplet excited state (**S*** based on the spin multiplicity of the excited state). In the example provided, **S*** serves as an electron acceptor, oxidizing the donor substrate (**D**). First **S*** and **D** must diffuse together to form a contact ion pair. Electron transfer leads to the radical ion pair (**D^{•+}/S^{•-}**), which may undergo subsequent chemical reactions leading to stable products. **S*** can act as an oxidant or a reductant depending on the redox properties of the sensitizer and the donor. Experimental techniques, advances in photochemistry, and a discussion of physical properties with respect to experimental methodology (e.g. oxidation potentials), are addressed in greater detail later in this review.



Scheme 1-2 Representation of an electron transfer process resulting in oxidation of the donor (**D**) by a photochemical sensitizer molecule (**S**).

1.2.1 Theoretical Concepts Relating to Organic Photochemistry

Organic chemists have developed theories both qualitative and quantitative to describe reaction phenomena (e.g., stereochemistry, reaction rates, and structure activity relationships). It is well established that a reactant must overcome an energy barrier to lead to a product (**Figure 1-1**). This barrier is denoted as the free energy of activation (ΔG^\ddagger), and represents a kinetic barrier that must be overcome in order for the reaction to progress. The relative position of the reactants and products on the energy coordinate diagram dictate whether or not a reaction is spontaneous. These parameters are dictated by the Gibbs free energy relationship and are thermodynamic properties.

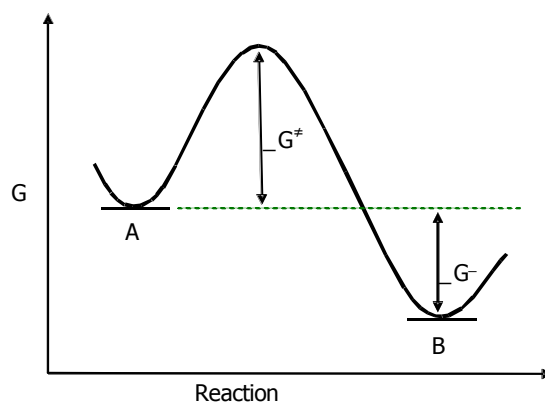


Figure 1-1 Schematic representation of reaction progress for the reaction $A \rightarrow B$. ΔG^\ddagger represents the activation barrier for the reaction, and ΔG° represents the relative energy of the reactants and products.

The Hammond postulate predicts the approximate structure and energy of the transition state based on the endothermicity or exothermicity of the reaction assuming the change ΔS in is small.

The Hammond postulate formally states that: “If two states, as for example, a transition state and an unstable intermediate, occur consecutively during a reaction process and have nearly the same energy content, their interconversion will involve only a small reorganization of the molecular structures”.⁴ The fundamental concept that this statement eloquently describes is that the transition state more closely resembles the reactant for an exothermic process and the product for an endothermic process (**Figure 1-2**).

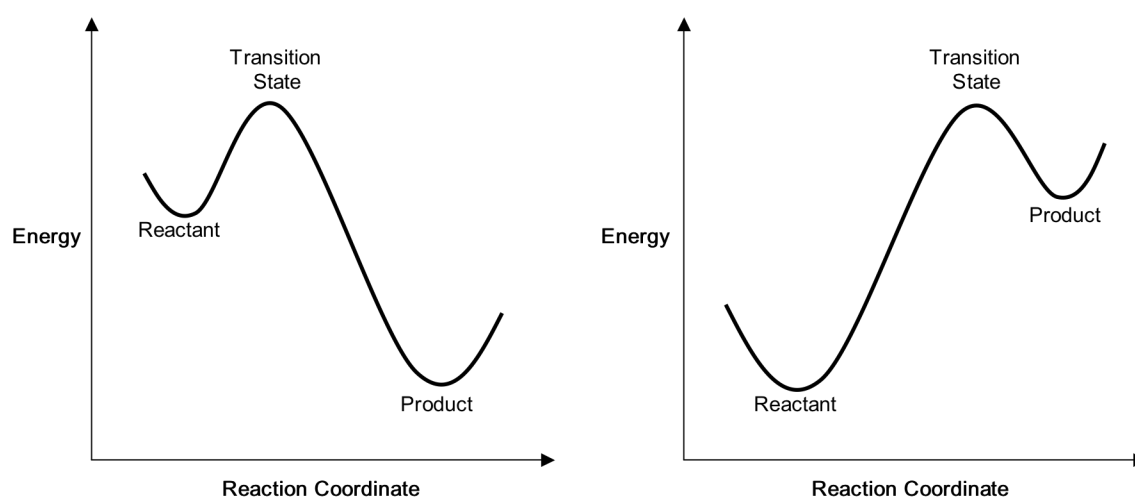


Figure 1-2 Schematic representation of the relative position of the T.S. of a reaction according to the Hammond postulate.

Although the previous example describing kinetic barriers and thermodynamic properties is more qualitative in nature, several theories were developed to explain these ideas in a quantitative fashion. Based on an idea similar to the Hammond postulate, Leffler predicted that the location of the transition state would be expressed by a parameter based on the endothermic or exothermic nature of the reaction. This parameter was based on the assumption that the structure of the transition state would be dependent on the structure and relative energies of the reactants

and product molecules. This idea led to the development of the Leffler relationship^{5,6} (**Equation 1-1**).

$$\delta G^\ddagger = \alpha \delta G_p + (1 - \alpha) \delta G_R \quad \text{Equation 1-1}$$

In **Equation 1-1**: δG^\ddagger is the change in free energy of the transition state, δG_p is the change in free energy of the products of the reaction, δG_R is the change in free energy of the reactants, and α is the measure of transition state structure. Expressed in another way, $\alpha = \delta G^\ddagger / \delta G^\circ$. The measure of transition state structure (α) is a value between 0-1 that will predict the location of the transition state on the reaction coordinate. A value of $\alpha = 0.5$ is indicative of a symmetrical transition state, $\alpha < 0.5$ indicates an early (reactant-like) transition state, and $\alpha > 0.5$ indicates a late (product-like) transition state.

The nature of the transition state can also be probed through the use of the Hammett Equation.^{7,8} Hammett derived a mathematical expression to quantitatively assess the electronic effects of a chemical transformation based on the hydrolysis of benzoic acid (**Equation 1-2**), where σ is constant based on the electronic nature of the substituent, ρ is the reaction constant (dependent upon the nature of the reaction, solvent, and temperature)⁹, and K_X and K_H are the ionization constants for a substituted benzoic acid and for benzoic acid, respectively. By correlating ionization constants against the electronic substituent constants, one can deduce a value for the reaction constant ρ . A positive ρ value is indicative of a more negative transition state structure of that of the reactant, and the reaction will be accelerated by the presence of electron withdrawing groups. Conversely a negative ρ value is indicative of a more positive transition state structure, and the reaction will be accelerated in the presence of electron donating groups. The Leffler and Hammett equations are well established examples of “linear free energy

relationships”, which predict that the free energy of activation of a chemical reaction changes in a linear fashion with the free energy of reaction.

$$\rho\sigma = \log \frac{K_X}{K_H} \quad \text{Equation 1-2}$$

In contrast to the previous examples, Marcus developed a quadratic relationship between ΔG^\ddagger and ΔG° which has become the touchstone of electron transfer theory. Marcus theory accounts for several factors that can influence the activation barrier of an electron transfer reaction:¹⁰ This theory, accounts for the internal (molecule) and external (solvent) changes that occur in the progression from reactants to transition state, and it defines the relationship between the activation barrier and driving force necessary for electron transfer chemistry to occur. This idea, although quantum mechanical in nature, is easily understood. The basic premise of the equation relates reaction rates and Gibbs free energy in a quadratic relationship as opposed to a linear relationship, as is the case of the Hammett equation and other linear free energy relationships. The important features of the Marcus equation involve two terms: the first term is an electrostatic term, and the second term is related to the reorganization energy of the system (**Equation 1-3**).

$$\Delta G^\ddagger = \frac{Z_1 Z_2 e^2 f}{D r_{12}} + \frac{\lambda}{4} \left(1 + \frac{\Delta G_{ET}}{\lambda} \right)^2 \quad \text{Equation 1-3}$$

In equation 3, ΔG^\ddagger is the activation energy for electron transfer, Z_1 and Z_2 are the charges on the reacting species, e is the electronic charge, f is a factor taking into account the ionic strength of the solution, D is a factor related to the dielectric constant of the solvent, r_{12} is a parameter that takes into account the distance that two molecules must move to be within collision distance, λ is the reorganization energy for the overall electron transfer, and ΔG_{ET} is the free energy of the reaction. The electrostatic term goes to zero if one species is neutral, and the equation simplifies to **Equation 1-4**.

$$\Delta G^{\ddagger} = \frac{\lambda}{4} \left(1 + \frac{\Delta G_{ET}}{\lambda} \right)^2 \quad \text{Equation 1-4}$$

The second form of the equation is the most relevant for the purpose of this review, due to the fact that the electron transfer reactions of interest involve an excited state sensitizer reacting with a neutral ground state donor molecule.

The innovative quality of Marcus theory is that it takes into account the reorganization energy (λ) of the system, which represents the energy needed to transform the nuclear configurations in the starting material and the solvent to those of the transition state. The reorganization energy is usually separated into two terms: (i) the molecules reacting (λ_1), and (ii) the reorganization energy of the solvent molecules during the course of the reaction (λ_2), resulting in the overall reorganization energy (λ) for the reaction where $\lambda = \lambda_1 + \lambda_2$. Initially, the two molecules that are involved must orient themselves in such a way as to facilitate a favorable geometry. The energy levels must be within +/- RT in the transition state, based on the Franck-Condon factor.¹¹ This process requires an initial increase in energy of the system in order to achieve the geometry of the transition state. This reorganization energy is dependent on a geometric distortion that must occur for both molecules to make this process favorable. Once in the transition state, the electron can be transferred, and the two molecules can then diffuse apart. This idea is depicted in **Figure 1-3**, where the redox reaction of Fe²⁺ going to Fe³⁺ is shown.

In Figure 3 the two molecules first diffuse together. The larger Fe²⁺ must then shrink in size while the Fe³⁺ grows in size, in order to achieve the appropriate nuclear conformation in the transition state. The electron can then be transferred, at which point the two molecules can achieve their final geometries and diffuse apart.¹²

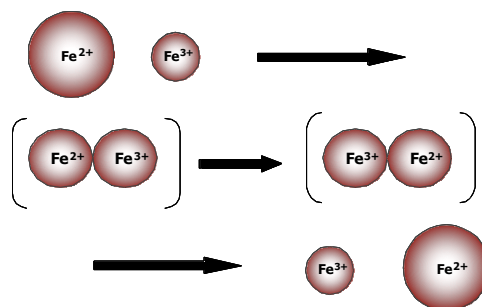


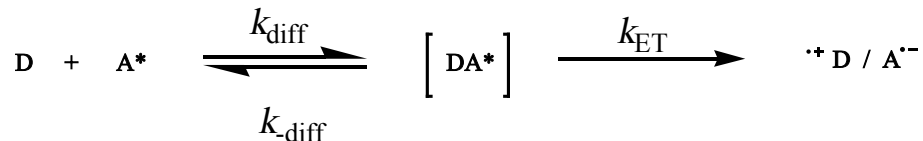
Figure 1-3 Reaction of Fe²⁺ and Fe³⁺ depicting the changes in internal reorganization energy for a favorable electron transfer pathway.

The second component to Marcus theory is the solvent reorganization energy component (λ_2). The magnitude of λ_2 is directly related to the charge on the reacting species and the dielectric constant of the solvent in which the reaction is taking place. In considering the solvent reorganization energy, it must be noted that the change in entropy of the solvent can be a major factor in achieving the desired transition state. When working in a polar medium, the solvent molecule must adopt a specific orientation in order to stabilize the transition state during the course of electron transfer. In essence, the solvent molecules must present the appropriate ends of their dipoles in order to stabilize the charge in the transition state. When conducting experiments in non-polar solvents, the magnitude of the aforementioned component is lessened due to the fact that the net stabilization of these solvents during the course of the electron transfer is generally negligible.

Marcus theory is a powerful relationship that can be used to examine the dynamics of an electron transfer reaction, but it must be manipulated mathematically to relate these values to parameters that can be measured experimentally. Through the use of the simplified Marcus equation (without the electrostatic term) and the use of the Eyring equation, a new equation can be derived (**Equation 1-5**).

$$k_{obs} = KZ \exp \left(\frac{\frac{\lambda}{4} \left(1 + \frac{\Delta G^\circ}{\lambda} \right)^2}{RT} \right) \quad \text{Equation 1-5}$$

Terms in **Equation 1-5** are defined as follows: k_{obs} is the observed rate constant, K is the transmission coefficient typically assumed to be unity, Z is a universal frequency factor, R is the ideal gas constant, T is temperature, and ΔG° and λ have the same meanings factors as they do in the Marcus equation. This expression can then be used, after steady state treatment of the reaction pathway, to derive a relationship between k_{obs} and ΔG° (**Scheme 1-3**).



Scheme 1-3 Electron transfer reaction used for the steady state approximation

The reaction pathway depicted in **Scheme 1-3** is a steady state problem: the reactants combine to form an initial complex, which can either proceed in a forward direction and undergo electron transfer, or it can dissociate back to reactants. The steady state approximation can then be applied on the complex $[DA^*]$. After the kinetic expression is solved, the k_{obs} value can then be inserted into the modified form of the Eyring equation leading to the following relationship (**Equation 1-6**).

$$k_{obs} = \frac{k_{diff}}{1 + \frac{k_{diff}}{K_{diff}Z} \exp \left\{ \frac{\left[\frac{\lambda}{4} \left(1 + \frac{\Delta G^\circ}{\lambda} \right)^2 \right]}{RT} \right\}} \quad \text{Equation 1-6}$$

This equation is used to relate the log of the observed rate constant to ΔG° . The resulting curve takes the form of an inverted parabola with three regions that are defined by the kinetic parameters described by the reaction pathway that was used to derive the steady state approximation (**Figure 1-4**). The first region (region I) is dominated by diffusion, and therefore the process will proceed at a diffusion controlled rate; the second region (region II) is a linear component of the relationship, governed by the equilibrium between back electron transfer or the forward process going to products; the third region (region III) is the area of interest in which the reorganization energy comes into effect.¹²

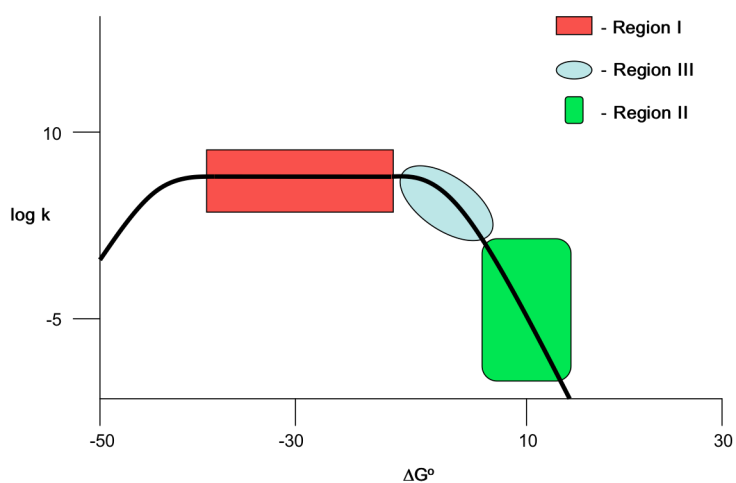


Figure 1-4 Graphical representation of log k vs. ΔG°

Generally one expects that as the reaction becomes more exothermic, the rate of reaction increases. Marcus theory predicts, however, that as the electron transfer reaction becomes increasingly exothermic (-15 kcal/mol), the reaction rate actually decreases. This phenomenon, counterintuitive to transition state theory, is defined as the Marcus 'inverted' region. In **Figure 1-5** the first reaction coordinate diagram represents a thermoneutral reaction where the rate can be measured based on the Gibbs free energy in a traditional fashion, and experimental

parameters of the reaction can be obtained through the use of the Arrhenius equation. The second diagram represents a scenario in which the reaction is exothermic and there is virtually no activation barrier, resulting in a very fast reaction. The last reaction coordinate represents a scenario in which the reaction is exceedingly exothermic, so that the reaction actually goes backwards, and as a result the rate of reaction actually begins to decrease.

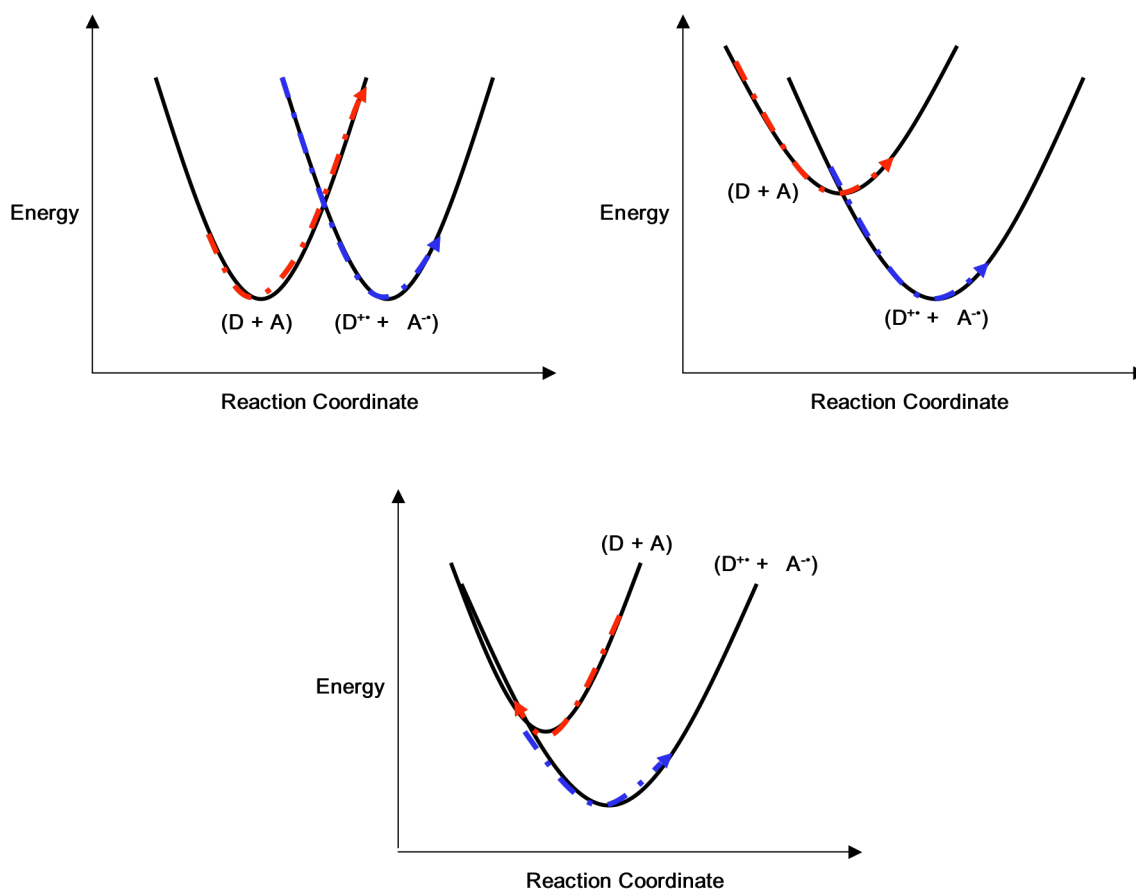


Figure 1-5 Reaction coordinate diagrams depicting (i) thermoneutral reaction progress, (ii) extremely exothermic progress, and (iii) Marcus 'inverted' region.

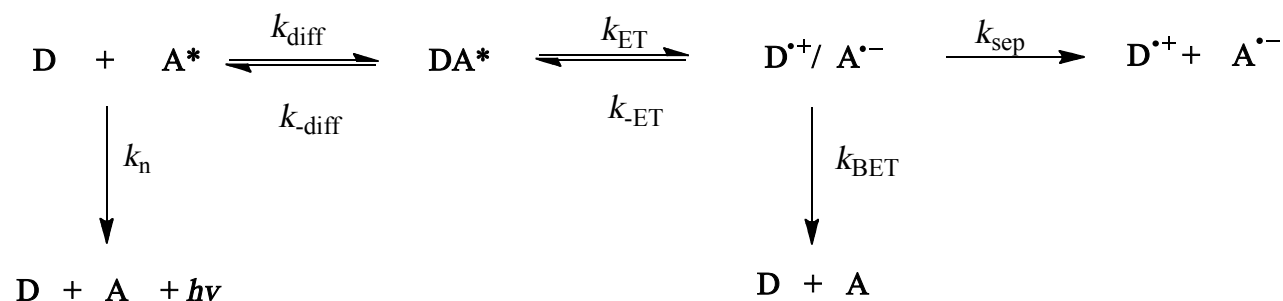
This idea has been tested and observed in a variety of fashions. In one classic experiment performed by Beitz and Miller,¹³ radiolysis was used to generate solvated electrons in the presence of an electron acceptor to generate radical anions. The novelty of the experiment is that

the electron transfer was conducted in a solid matrix. The experiment was then repeated in the presence of several electron acceptors with a range of reduction potentials. In doing so they were able to show that extremely exothermic reactions resulted in up to a 10^6 (s^{-1}) reduction in rate.

This phenomenon was further addressed in the solution phase, where donor acceptor relationships were studied through a competition experiment.¹⁴ The excited state ion separation and excited state recombination back to the ground state were compared. Several donors and acceptors of varying oxidation and reduction potentials were selected. These variables changed the driving force of the reaction. If the reaction progressed in the Marcus ‘normal’ region, then charge separation prevailed; in the ‘inverted’ region, recombination back to ground state was the dominating process.

1.2.2 Rehm-Weller Equation

After the inception of Marcus theory and the idea defining reaction energetics as a function of reactant and solvent reorganization energy, Rehm and Weller performed a series of experiments where they monitored the lifetime of the excited state molecule concentration in the presence of varying concentrations of quencher. They interpreted the results according to **Scheme 1-4**.^{10,15}



Scheme 1-4 Representation of the Rehm-Weller experiment

Based on the Marcus ‘inverted’ region one would expect the reaction rate to increase initially in the normal region and then decrease when in the ‘inverted’ region. Through the course of these experiments, even when $\Delta G_{ET} = -60$ kcal/mol, they saw no decrease in the rate of electron transfer. Experimentally obtained rate constants were on the order of diffusion controlled (10^{9-10} s⁻¹). Although the Rehm-Weller experiment did not conclusively show direct evidence of the ‘inverted’ region, it did lead to the development of the Weller equation (**Equation 1-7**), which is now used to predict the rate constants for electron transfer reactions using thermodynamic parameters that can be obtained experimentally.

$$k_{ET} = \frac{2 * 10^{10}}{1 + 0.25 \left[\exp\left(\frac{\Delta G_{ET}^*}{RT}\right)^2 + \exp\left(\frac{\Delta G_{ET}}{RT}\right) \right]} \quad \text{Equation 1-7}$$

Terms in **Equation 1-7** are defined as follows: ΔG_{ET}^* is the excitation energy of the sensitizer and ΔG_{ET} is the energy of the ion pair, and R and T have their usual designations. This equation can be interpreted by the following statement: “if the excitation energy of the sensitizer is greater than energy of the ion pair by a few kcal/mol the electron transfer is expected to proceed at a diffusion controlled rate”.¹⁶

Ideally one would like to design a system in which a sensitizer will promote oxidation or reduction of the desired substrate. Experimental or published photophysical parameters, such as reduction potentials and excitation energies, give the quantitative values of the relative energies of the Highest Occupied Molecular Orbital (HOMO) and Lowest Unoccupied Molecular Orbital (LUMO) of the sensitizer and where those values lie on an energy profile. These values are important when examining electron transfer reactions (**Scheme 1-2**), specifically where an organic sensitizer (**S**) is elevated to its excited state (**S***), followed by the formation of a contact pair (**DS***), resulting in the oxidation or reduction of the substrate of interest (**+D S***). The

oxidation or reduction of the substrate of interest is driven by the oxidation potential of the organic sensitizer selected (**Figure 1-6**). In the first diagram, the HOMO and LUMO energies of the sensitizer are higher than that of the desired substrate, leading to reduction of the desired substrate (R). Conversely, in the second diagram the HOMO and LUMO energies of the sensitizer are lower than that of the desired substrate leading to oxidation of the substrate (R).

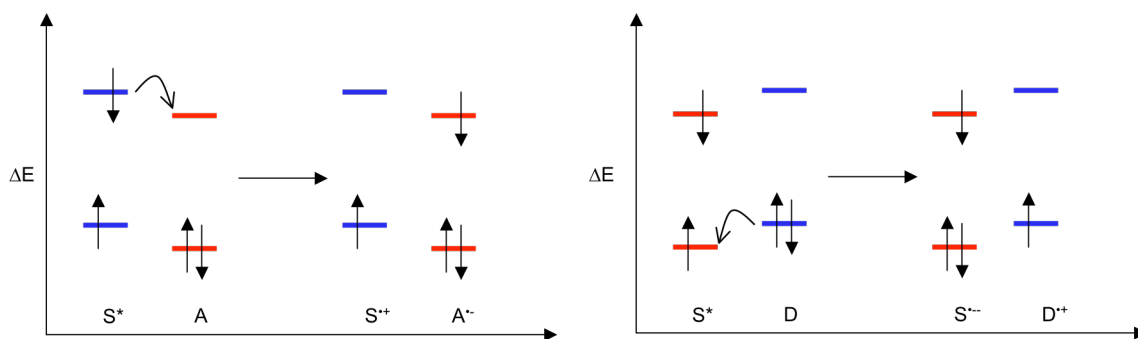


Figure 1-6 Orbital Diagrams depicting (i) reduction of a desired substrate by an organic sensitizer and (ii) oxidation of a desired substrate by an organic sensitizer

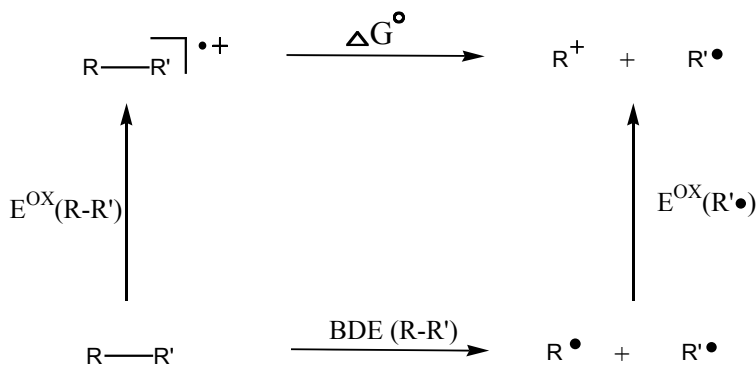
The ability of a molecule to gain electrons (reduction) or lose electrons (oxidation) is based on the redox potential of the chemical reaction. These reactions are broken down into two half reactions: an oxidation half reaction and a reduction half reaction. For the sake of simplicity, this discussion is limited to that of reduction potentials. These values are dependent on a substrate's ability to be reduced in the presence of an electron. These values are derived from the Nernst equation and have been standardized vs. the normal hydrogen electrode (NHE, $E^\circ = 0.000\text{V}$). The more positive the value for E° for a given substrate, the more favorable the reduction.¹⁷ A more extensive discussion of the Nernst equation is provided later in this review.

Through the use of the Weller equation one may design a system that promotes the oxidation or reduction of a desired substrate. The Weller equation can then be manipulated through the use of the Marcus relationship to give a simple expression that relates ΔG° to oxidation and reduction

potentials as well as taking into account the excitation energy of the sensitizer that is being utilized in the experiment (**Equation 1-8**). This information allows for the construction of a thermodynamic cycle.

$$\Delta G^\circ = [E(\text{Donor})^{\text{ox}} + E(\text{Acceptor})^{\text{red}}] - E_{\text{excitation}} \quad \text{Equation 1-8}$$

This refined version of the Weller equation can be utilized to extract information about a system in which a given experimental parameter may be extremely difficult to measure.¹⁶ Using this relationship one can create a thermodynamic cycle which utilizes a substrate's oxidation potential as well as the bond dissociation energy of the neutral molecule to predict the value of ΔG° (**Scheme 1-5**).



Scheme 1-5 Parameters for calculating a thermodynamic cycle for ET

After the construction of the thermodynamic cycle, one may obtain several of these values experimentally or by the use of calculations to solve for the last variable. The parameters for a given thermodynamic cycle can be obtained experimentally as well as augmented by the use of theoretical molecular modeling calculations. Although oxidation and reduction potentials can be difficult to obtain experimentally, several sources for these values are available in primary literature. The values for oxidation/reduction potentials can be used to evaluate ΔG° within the governing parameters of a thermodynamic cycle for the system that one intends to examine.

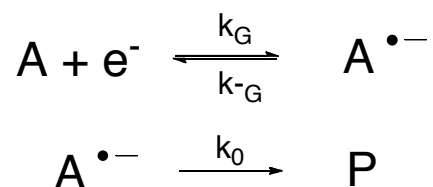
Table 1-1 shows a listing of several sensitizers that have been studied previously in the literature.

Sensitizer	E (Acceptor) ^{RED} (V)	λ_{max} (nm)	E (singlet)	E (triplet)
acetophenone	-1.86	386	3.41	3.20
4-methoxyacetophenone	-1.5	353	3.51	3.10
9,10-dicyanoanthracene	-0.89	433	2.86	NA
2,6,9,10-tetracyanoanthracene	-0.45	440	2.82	NA
p-dicyanobenzene	-1.60	290	4.27	3.06
benzophenone	-1.68	384	3.23	3.00
naphthalene	-2.29	311	3.99	2.64
1-cyanonaphthalene	-1.98	320	3.88	2.49
1,4-dicyanonaphthalene	-1.28	359	3.45	2.41
trans-stilbene	-2.26	304	3.53	2.12
phenanthrene	-2.20	345	3.59	2.69

Table 1-1 Photophysical Data for several known organic sensitizers¹⁸

1.3 Electrochemical methods

Although LFP is commonly used to examine electron transfer reactions, cyclic voltammetry is a popular method that can also be used to examine the kinetics of an electron transfer process. If a substrate can undergo a subsequent chemical transformation post electron transfer, the process is deemed to proceed via an EC mechanism (Electron transfer followed by a Chemical step) (**Scheme 1-6**).^{17, 19} During an EC process the substrate is reduced at the electrode surface to generate $A^{\bullet-}$, and $A^{\bullet-}$ can then go on to form products. For simplicity, the following discussion of electrochemical methods will be explained as a reduction reaction. These techniques are viable for oxidative pathways, but the sign convention is reversed.



Scheme 1-6 Representation of the EC mechanism

A common technique used to study electron transfer reactions is linear sweep voltammetry (LSV). This technique entails applying a potential over a fixed potential range within a given time regime, where a chemical transformation will occur to generate an i vs. E curve. The applied potential can then be switched back to the initial potential. The implementation of reverse sweep is called cyclic voltammetry (CV). From the resulting $i - E$ curve several initial observations can be made after a few initial experiments (**Figure 1-7**). Key components of the voltammogram will give kinetic data about the chemical process. Important attributes of the voltammogram include the following: (i) E_p – peak potential, (ii) i_p – peak current, (iii) $E_{p/2}$ – half wave potential, and (iv) $(E_p - E_{p/2})$ – peak width.

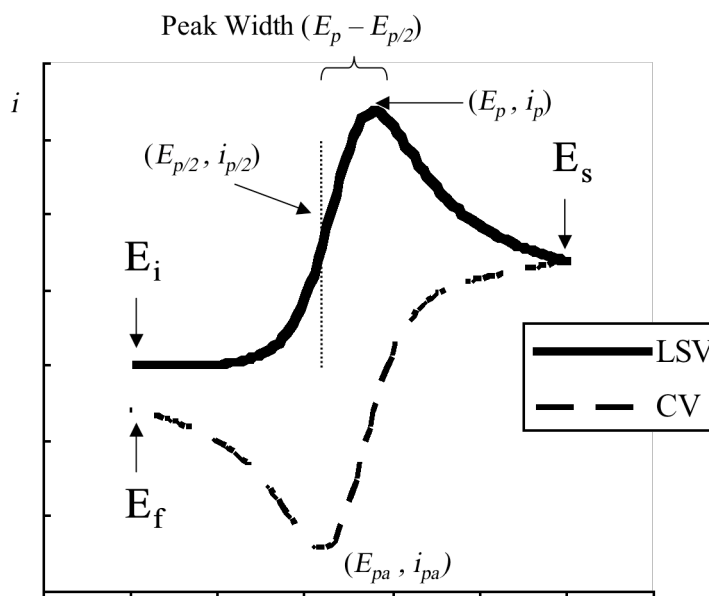


Figure 1-7 Representative voltammogram

Following the reverse sweep one of three things can happen: (i) the reverse wave will consist of a wave shaped like the forward wave plotted in the reverse direction (reversible), (ii) the reverse

wave will be present but not draw the same amount of current (quasireversible), and (iii) the reverse wave will not be present (irreversible).

1.3.1 Reversible Cyclic Voltammetry

A reversible cyclic voltammogram is characterized by a symmetrical wave on the reverse sweep. A typical experiment involves collecting voltammograms at several different scan rates (v). The chemistry at the electrode surface is governed by the Nernst equation (**Equation 1-9**), where the concentration of **A** and **A^{*}** are in equilibrium at the electrode surface. For equation **1-9**: E is the electrode potential, E^0 is the formal potential, $[A]$ is the concentration of the oxidized form, $[A^{*-}]$ is the concentration of the reduced form, and n , R , T , F all have their usual designations.

$$E = E^0 + \frac{2.3RT}{nF} \log \frac{[A]}{[A^{*-}]} \quad \text{Equation 1-9}$$

For a reversible system the subsequent chemical transformation shown in **Scheme 1-10** does not take place either because (i) there is not a follow up chemical reaction or (ii) because the resulting chemistry is slow compared to the reverse electron transfer reaction. Therefore as the scan rate is varied, there will be no change in the peak potential, and no kinetic data can be obtained. Other important features of a reversible voltammogram include that the peak current ratios i_p/i_{pa} will be equal to 1 and a peak potential difference ($E_p - E_{pa}$) of 59 mV will exist.¹⁷

1.3.2 Quasireversible Cyclic Voltammetry

A quasireversible electrochemical process is defined as a pathway where some of the reduced form of the substrate has undergone a follow up transformation prior to the reverse sweep. This results in a reverse oxidative wave that does not draw as much current as the forward sweep. Kinetic information for the chemical step can be obtained from the voltammograms by plotting the peak current ratio i_p/i_{pa} against $k[A]^z/FvRT$ (for an EC mechanism $z = 0$).²⁰ These working

curves can be generated for any given sweep rate to give the rate constant k for the chemical step.

1.3.3 Irreversible Cyclic Voltammetry

An irreversible voltammogram is characterized by the lack of a wave on the reverse sweep. When this case arises the technique is deemed linear sweep voltammetry (LSV) because no information can be obtained from the reverse wave. This phenomena can be the result of several mechanistic scenarios: (i) the electron transfer step is rate limiting, (ii) the chemical step is rate limiting, or (iii) a combination of both (mixed kinetic control). All three cases have been solved through the use of dimensionless variables (**Equations 1-10** and **1-11**) to solve the boundary value problem for each mechanistic scenario.¹⁹ Terms are defined as follows: v is the scan rate, D is the diffusion coefficient, k_G is the heterogeneous electron transfer rate constant, k_0 is the rate constant for the subsequent chemical step, n is the number of electrons in the electron transfer step, and F , R and T all have their usual designations. These solutions will give rise to important features of the voltammogram.

$$\Lambda = k_G \left(\frac{DnFv}{RT} \right)^{-\frac{1}{2}} \quad \text{Equation 1-10}$$

$$\lambda = \frac{RTk_0}{nFv} \quad \text{Equation 1-11}$$

In the case where electron transfer is rate limiting, the EC mechanism will give rise to the following set of solutions to the boundary problem (**Equations 1-12** and **1-13**).¹⁹ Characteristic voltammograms for an electron transfer rate limiting process are characterized by peak widths of 95 mV, and the change in peak potential with respect to scan rate will vary cathodically by 59 mV per tenfold change in scan rate (v). **Equation 1-14** gives the relationship between the heterogeneous rate constant (k_G) and the peak potential (E_p). If the formal reduction potential is

known for the substrate of interest, then the heterogeneous rate constant k_G for electron transfer can be found from **Equation 1-14**.

$$\frac{dE_p}{d\log v} = -\frac{29.6}{\alpha n} mV \quad \text{Equation 1-12}$$

$$E_p - E_{p/2} = \frac{1.85RT}{\alpha nF} \approx 95 mV \quad \text{Equation 1-13}$$

$$E_p = E^\circ - \frac{0.783RT}{\alpha nF} - \frac{RT}{\alpha nF} \left(\ln \frac{D_0^{1/2}}{k_G} + \ln \left(\frac{nFv\alpha}{RT} \right)^{1/2} \right) \quad \text{Equation 1-14}$$

The term α is deemed the transfer coefficient, which gives information about the symmetry of the transition state. The transfer coefficient relates the change in the free energy of activation to the change in free energy of the reaction **Equation 1-15**.^{21, 22} The term α determines the fraction of change in the electrode potential that causes a change in the activation energy. For most electron transfer processes, this value can be assumed to be 0.5. This approximation can be made if no bonds are broken concurrent with electron transfer.²³

$$\alpha = \frac{\partial G^\ddagger}{\partial G^\circ} \quad \text{Equation 1-15}$$

The circumstance where the chemical step is rate limiting will give rise to a separate set of solutions to the boundary problem (**Equations 1-16 and 1-17**).¹⁹ Important diagnostic features for voltammograms of a system undergoing a chemical step rate limiting pathway include peak widths of 48 mV, and the change in peak potential with respect to scan rate will vary by approximately 30 mV. The concentration of **A** will have no bearing on the change in peak potential (**Equation 1-18**). **Equation 1-18** will hold true if the subsequent chemical transformation is a first order process; discussions of higher order pathways will be addressed in the following section. The solution to the boundary problem relating peak potential (E_p) to the rate constant for the chemical step (k) is shown in **Equation 1-19**. If the formal reduction

potential of the compound is known, then this equation can be used to solve for the rate constant for the chemical step.

$$\frac{dE_p}{d\log v} = -\frac{29.6}{n} mV \quad \text{Equation 1-16}$$

$$E_p - E_{p/2} = 1.85 \frac{RT}{nF} \approx 48 mV \quad \text{Equation 1-17}$$

$$\frac{dE_p}{d\log[A]} = 0 \quad \text{Equation 1-18}$$

$$E_p = E^0 - \frac{0.783RT}{nF} + \frac{RT}{2nF} \ln \frac{k_0 RT}{vnF} \quad \text{Equation 1-19}$$

In the case where the subsequent chemical step is not a first order process but 2nd order as in the case with dimerization (EC_{dim} mechanism), the solutions to the boundary problem are as follows. Voltammograms will differ from the traditional first order reaction in the following ways: peak widths will be on the order of 39 mV (**Equation 1-22**), and peak potentials will vary by -20 mV per ten fold increase in scan rate (**Equation 1-20**).¹⁹ Peak potentials will also have a variance of 20 mV per tenfold increase in concentration (**Equation 1-21**). This equation can be used to distinguish between a followup dimerization process or a rearrangement pathway. The relationship between the rate constant for the chemical step (k) and the peak potential (E_p) is given in **Equation 1-23**.

$$\frac{dE_p}{d\log v} = -\frac{19.7}{n} mV \quad \text{Equation 1-20}$$

$$\frac{dE_p}{d\log[A]} = \frac{19.7}{n} mV \quad \text{Equation 1-21}$$

$$E_p - E_{p/2} = 1.512 \frac{RT}{nF} \approx 39.2 mV \quad \text{Equation 1-22}$$

$$E_p = E^0 - 0.502 \frac{RT}{nF} + \frac{RT}{3nF} \ln \frac{2k_0[A]}{3v} \frac{RT}{nF} \quad \text{Equation 1-23}$$

1.3.4 Mixed Kinetic Control

The third situation that can occur when examining the EC mechanism is the case of mixed kinetic control. This phenomenon arises when the rate constants for the electron transfer step and the chemical step are within an order of magnitude of one another. Therefore one may observe changes in the voltammograms as the scan rate is increased tenfold.¹⁹ To solve for solutions of the boundary problem, it is necessary to introduce two new variables, p and ξ . ξ is a dimensionless variable that defines the electrode potential and the heterogeneous rate constant for electron transfer **Equation 1-24**. The parameter p measures the competition kinetics of the electron transfer step and the chemical step (for an α value of 0.5) **Equation 1-25**. The k_G term dominates as the function p approaches zero, conversely as p approaches infinity kinetic control is governed by k_0 . Experimentally one can diagnose mixed kinetic control by examining voltammograms ranging from low to high scan rate. At lower scan rates electrochemical runs will have features indicative of chemical step rate limiting, while at high scan rates voltammograms will have properties that resemble electron transfer rate limiting behavior. Characteristic features of voltammograms for a system under mixed kinetic control include, peak widths between 48-95 mV, and the change in peak potential with respect to scan rate will exhibit changes between 30 and 60 mV.

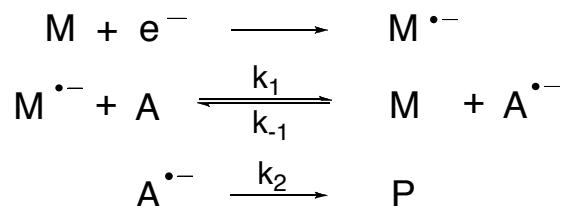
$$\xi = -\frac{\alpha F}{RT} (E - E_{A/A^{*+}}) + \ln \left(k_G \sqrt{\frac{RT}{\alpha F v D}} \right) \quad \text{Equation 1-24}$$

$$p = \frac{F v}{2RT} \frac{k_0 D^2}{k_G^4} \quad \text{Equation 1-25}$$

1.3.5 Indirect Electrochemistry

Due to the fact that several of the equations discussed in the previous section contain equations that relate the formal redox potential to the rate constant, additional experiments may be needed

to extract more information to solve for both variables. Therefore a series of indirect methods have been developed to circumvent this problem. A convenient method used for this purpose is a methodology known as homogeneous redox catalysis. **Scheme 1-7** shows a mechanistic depiction of the pathway, where mediator **M** is reduced to form **M^{•-}**, **M^{•-}** will react with **A** to give **A^{•-}**, and **A^{•-}** can then go on to form products.



Scheme 1-7 Representation of the mechanism for mediated redox catalysis

In a successful mediated redox catalysis experiment, the mediator must contain three basic properties: (i) the mediator must be reduced at a potential more positive than the substrate, (ii) the reduction of the mediator should be fast at the electrode surface, and (iii) the electrochemistry of the mediator should be reversible (Nernstian).²³ The main thermodynamic requirements for redox catalysis are that the mediator needs to be more easily reduced than the redox couple **A/A^{•-}** and the followup reaction needs to be fast and irreversible.²⁴ If these requirements are not met, there will be no driving force for the homogeneous electron transfer step, and redox catalysis will not occur.

The mediator will give rise to a reversible cyclic voltammogram, and when substrate is added the reductive wave will draw more current and lose its characteristic reversibility (**Figure 1-8**). The loss of **A^{•-}** will result in an overpotential, which is needed to drive the electron transfer reaction to attempt to maintain an equilibrium at the electrode surface as governed by the Nernst equation. A typical experiment involves comparing the peak current ratio i_p/i_{pd} at several

different scan rates; as the scan rate is increased the peak current ratio will begin to approach 1.^{23,}

^{25,26} From this data kinetic information can be obtained.

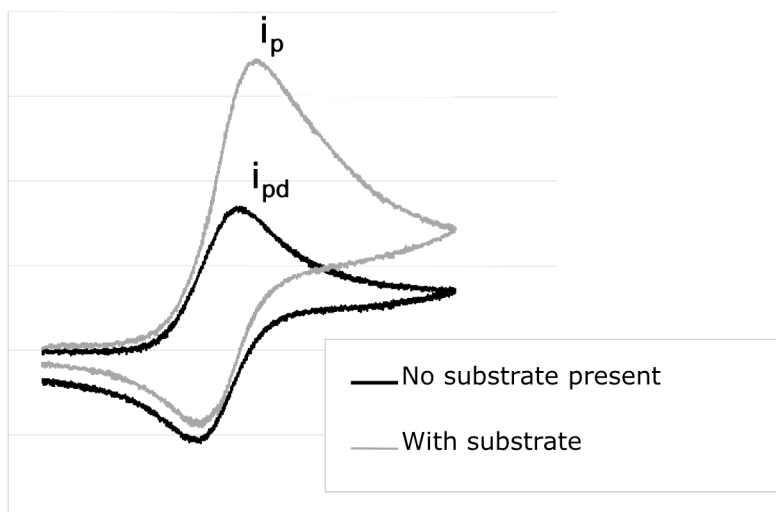


Figure 1-8 Representation of a mediated redox catalysis experiment

From **Scheme 1-7** one can envision two scenarios that may occur: (i) homogeneous electron transfer is rate limiting and (ii) the chemical step is rate determining. When electron transfer is rate limiting, the system is dependent on two dimensionless parameters, λ_1 and γ (**Equations 1-26** and **1-27**). As a result there will be a concentration dependence on the mediator at constant gamma.

$$\lambda_1 = \left(\frac{RT}{F} \right) \left(\frac{k_1[M]}{v} \right) \quad \text{Equation 1-26}$$

$$\gamma = \frac{[A]}{[M]} \quad \text{Equation 1-27}$$

Although no kinetic information about the chemical step can be obtained if the electron transfer step is rate limiting, two important values can be extracted from these experiments: (i) the

standard redox potential compound of interest ($E^{\circ}_{(A/A^{\bullet-})}$) and (ii) the rate constant for the electron transfer of the mediator and the substrate (k_1). This information can be obtained by examining a series of mediators that differ in redox potential. By plotting the rate constants of the forward electron transfer against the driving force (ie: $E^{\circ}_{(M/M^{\bullet-})} - E^{\circ}_{(A/A^{\bullet-})}$), k_1 and $E^{\circ}_{(A/A^{\bullet-})}$ can be obtained for the system if the data lies in the ‘activation’ and ‘counter diffusion’ regions (**Figure 1-9**).²³

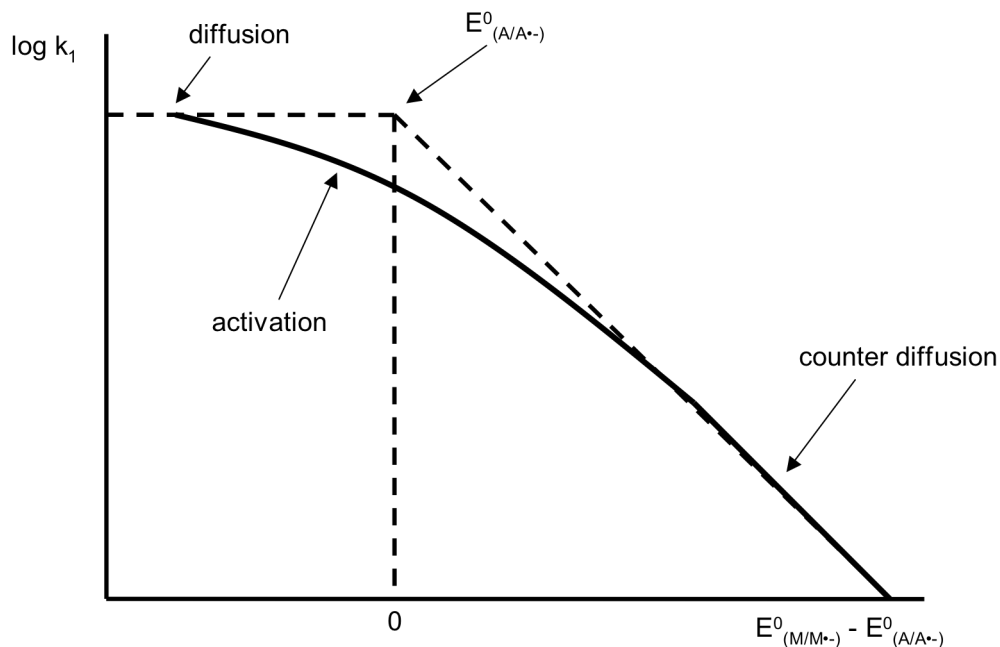


Figure 1-9 Representation of the procedure to extract k_1 and $E^{\circ}_{(A/A^{\bullet-})}$ from experimental data

When the chemical step is rate limiting, the electron transfer step between the mediator and the substrate is in a pre-equilibrium; therefore, the mediator concentration is independent of the peak current ratio. The system is governed by λ_1 and γ , as well as two new dimensionless parameters λ and λ_{-1} that are expressed in the form $\lambda\lambda_1/\lambda_{-1}$ (**Equations 1-28** and **1-29**).

$$\lambda = \left(\frac{RT}{F} \right) \left(\frac{k_2}{v} \right) \quad \text{Equation 1-28}$$

$$\lambda_{-1} = \left(\frac{RT}{F} \right) \left(\frac{k_{-1}[M]}{v} \right) \quad \text{Equation 1-29}$$

A series of theoretical working curves have been developed for this mechanistic regime that compare the peak current ratio (i_p/i_{pd}) to the dimensionless parameter $\lambda\lambda_1/\lambda_{-1}$. The difference between the experimental data and the theoretical values obtained from the working curves is directly related to the rate constant for the chemical step. **Equations 1-30** and **1-19** can then be used to solve for the rate constant of the chemical step k_2 and the formal redox potential of the substrate $E^\circ_{(A/A^{\bullet-})}$.²⁵

$$\frac{\lambda\lambda_1}{\lambda_{-1}} = \left(\frac{RT}{F}\right)\left(\frac{k_2k_1}{k_{-1}v}\right) = \left(\frac{RT}{F}\right)\left(\frac{k}{v}\right)e^{\left[\left(\frac{F}{RT}\right)\left(E^\circ_{(A/A^{\bullet-})} - E^\circ_{(M/M^{\bullet-})}\right)\right]} \quad \text{Equation 1-30}$$

1.4 Dissertation Overview

The introductory chapter of this dissertation focused on techniques that can be used to examine the chemistry of reactive intermediates. Due to the fact both, an electron transfer mechanism and a hydrogen atom transfer pathway, have been proposed for the mechanism of cP-450 and MAO oxidations, a detailed discussion of the techniques used to study radical and radical ion intermediates was presented in Chapter 1.

A photochemical model study of benzophenone triplet (^3BP) with the MAO-B substrate 1-methyl-4-phenyl-1,2,3,6-tetrahydropyridine (MPTP) and two of its derivatives, 1-cyclopropyl-4-phenyl-1,2,3,6-tetrahydropyridine and (+/-)-[*trans*-2-phenylcyclopropyl-4-phenyl-1,2,3,6-tetrahydropyridine] is presented in Chapter 2. The barrier for ring opening of aminyl radical cations derived from *N*-cyclopropyl derivatives of tertiary amines (such as MPTP) is expected to be low. Reactions of ^3BP with all three compounds are very similar. The results suggest that the reaction between benzophenone triplet and tertiary aliphatic amines proceed via a simple hydrogen atom transfer reaction. Additionally these model examinations provide evidence that oxidations of *N*-cyclopropyl derivatives of MPTP catalyzed by MAO-B may not be consistent with a pure SET pathway.

Chapter 3 examines the chemistry of *N*-cyclopropyl amines that have been used in enzymatic examinations of cP-450 to probe for an SET pathway. To date, the work done on these cyclopropanes made the assumption that the ring opening of these probes should be on the order of 10^8 s^{-1} , based on the known rate constant for the ring opening of the cyclopropyl carbinyl neutral radical. Photochemical and electrochemical examinations of *N*-methyl-*N*-cyclopropylaniline revealed that the rate constant for cyclopropyl ring opening to be $4 \times 10^4 \text{ s}^{-1}$. Molecular modeling calculations of *N*-cyclopropylaniline radical cation revealed that the perpendicular conformation was more favorable by 3.6 kcal/mol, leading to the hypothesis that the cyclopropyl group did not meet the appropriate stereoelectronic requirements for ring opening. Therefore a new series of spiro cyclopropanes were designed to lock the cyclopropyl group into the appropriate bisected conformation. The electrochemical results reported herein show that the rate constant for ring opening of 1'-methyl-3',4'-dihydro-1'*H*-spiro[cyclopropane-1,2'-quinoline] (**27**) and 6'-chloro-1'-methyl-3',4'-dihydro-1'*H*-spiro[cyclopropane-1,2'-quinoline] (**41**) are $3.5 \times 10^2 \text{ s}^{-1}$ and $4.1 \times 10^2 \text{ s}^{-1}$ respectively. Results from preparative scale electrolysis and ESI-MS are consistent with a ring opening process being operative for the chemical step.

The research presented in Chapter 4 examines the ring opening reaction of 4-chloro-*N*-methyl-*N*-(2-phenylcyclopropyl)aniline radical cation. *N*-methyl-*N*-cyclopropylaniline has been used in previous studies to probe the mechanism of amine oxidations by cP-450. Photochemical and electrochemical examinations of this substrate, revealed that the rate constant for cyclopropyl ring opening to be $4 \times 10^4 \text{ s}^{-1}$. This result can be explained by a resonance effect in which the spin and charge of the radical cation in the ring closed form is delocalized into the benzene ring hindering the overall rate of the ring opening reaction. Therefore a derivative of *N*-methyl-*N*-cyclopropylaniline was synthesized to provide a driving force for the ring opening reaction

thereby accelerating the overall rate of the ring opening pathway. The electrochemical results reported herein show that the rate constant for ring opening of 4-chloro-*N*-methyl-*N*-(2-phenylcyclopropyl)aniline to be $1.7 \times 10^8 \text{ s}^{-1}$. The formal oxidation potential (E°_{ox}) of this substrate was determined to be 0.53 V. Results from preparative scale electrolysis are consistent with a ring opening process being operative for the chemical step.

Lastly, Chapter 5 will address the factors that govern the rate of ring opening of these reactive radical cations. Computational analysis of all compounds at the B3YLP level of theory is presented for all compounds discussed in this dissertation. Rational for experimentally obtained redox potentials and ring opening rate constants will be presented in this section of the dissertation.

References

1. Woodward, R. B.; Hoffman, R., *The Conservation of Orbital Symmetry*. Academic Press: New York, 1970.
2. Nicolaou, K. C.; Snyder, S. A.; Montagnon, T.; Vassilikogiannakis, G., The Diels-Alder reaction in total synthesis. *Angewandte Chemie-International Edition* **2002**, *41* (10), 1668-1698.
3. Evans, T. R.; Wake, R. W.; Sifain, M. M., Singlet Quenching Mechanisms III (1). Sensitized Isomerization of Hexamethylbicyclo[2.2.0] Hexa-2,5-diene. A Chain Reaction. *Tetrahedron Lett* **1973**, *14*, 701-704.
4. Hammond, G. S., A Correlation of Reaction Rates. *J Am Chem Soc* **1955**, *77*, 334-338.
5. Leffler, J. E., Parameters for the Description of Transition States. *Science* **1953**, *117*, 340-341.
6. Pross, A., *Theoretical & Physical Principles of Organic Reactivity*. Wiley: New York, 1995.
7. Jaffe, H. H., A Reexamination of the Hammett Equation. *Chem Rev* **1953**, *53*, 191-261.
8. Lowry, T. H.; Richardson, K. S., *Mechanism and Theory in Organic Chemistry*. 3rd ed.; Harper Collins Publishers: New York, 1987.
9. Hammett, L. P., The Effect of Structure upon the Reactions of Organic Compounds. Benzene Derivatives. *J Am Chem Soc* **1937**, *59*, 96-103.
10. Marcus, R. A., Chemical and Electrochemical Electron Transfer Theory. *Annual Reviews of Physical Chemistry* **1964**, *15*, 155.
11. Schuster, G. B., *Advances in Electron Transfer Chemistry*. JAI Press Inc.: 1991.
12. Ebersson, L., *Electron Transfer Reactions in Organic Chemistry*. Springer-Verlag: Berlin, 1987.
13. Beitz, J. V.; Miller, J. R., Exothermic Rate Restrictions on Electron-Transfer in a Rigid Medium. *J Chem Phys* **1979**, *71* (11), 4579-4595.
14. Gould, I. R.; Moser, J. E.; Ege, D.; Moody, R.; Armitage, B.; Farid, S., Electron-Transfer within Geminate Radical Ion-Pairs. *Journal of Imaging Science* **1989**, *33* (2), 44-46.
15. Rehm, D.; Weller, A., *Ber. Bunsenges. Phys. Chem.* **1969**, *73*, 834-839.
16. Mattes, S. L.; Farid, S., *Organic Photochemistry*. Marcel Decker: New York, 1983; Vol. 6.

17. Bard, A. J.; Faulkner, L. R., *Electrochemical Methods. Fundamentals and Applications*. John Wiley & Sons, Inc.: New York, 2001.
18. Kavarnos, G. J.; Turro, N. J., Photosensitization by Reversible Electron-Transfer - Theories, Experimental-Evidence, and Examples. *Chem Rev* **1986**, *86* (2), 401-449.
19. Nadjo, L.; Saveant, J. M., Linear Sweep Voltammetry: Kinetic Control by Charge Transfer and or Secondary Chemical Reactions. *Electroanalytical Chemistry and Interfacial Electrochemistry* **1973**, *48*.
20. Parker, V. D., *Linear Sweep and Cyclic Voltammetry*. Elsevier: New York, 1986; Vol. 26.
21. Holder, G. N.; McClure, L. L.; Rarrar, D. G., Voltammetric Reductions of Ring Substituted Acetophenones. 2. A Senior Level Experiment Requiring Classification of an Electrochemical Mechanism as Stepwise or Concerted. *Chem. Educator* **2002**, *7*, 74-80.
22. Antonello, S.; Maran, F., The role and relevance of the transfer coefficient α in the study of dissociative electron transfers: Concepts and examples from the electroreduction of perbenzoates. *J Am Chem Soc* **1999**, *121* (41), 9668-9676.
23. Andrieux, C. P.; Hapiot, P.; Saveant, J. M., Fast Kinetics by Means of Direct and Indirect Electrochemical Techniques. *Chem Rev* **1990**, *90* (5), 723-738.
24. Andrieux, C. P.; Dumas-Bouchiat, J. M.; Saveant, J. M., Homogeneous Redox Catalysis of Electrochemical Reactions. *Journal of Electroanalytical Chemistry* **1978**, *87*, 39-53.
25. Andrieux, C. P.; Blocman, C.; Dumas-Bouchiat, J. M.; M'halla, F.; Saveant, J. M., Homogeneous Redox Catalysis of Electrochemical Reactions - Part V. Cyclic Voltammetry. *Journal of Electroanalytical Chemistry* **1980**, *113*, 19-40.
26. Phillips, J. P.; Gillmore, J. G.; Schwartz, P.; Brammer, L. E.; Berger, D. J.; Tanko, J. M., Radical ion probes. 8. Direct and indirect electrochemistry of 5,7-di-tert-butylspiro[2.5]octa-4,7-dien-6-one and derivatives. *J Am Chem Soc* **1998**, *120* (1), 195-202.
27. Newcomb, M.; Johnson, C. C.; Manek, M. B.; Varick, T. R., Picosecond Radical Kinetics. Ring Opening of Phenyl-Substituted Cyclopropylcarbinyl Radicals. *J. Am. Chem. Soc* **1992**, *114*, 10915-10921.

Chapter 2 Reaction of benzophenone triplet with aliphatic amines. What a potent neurotoxin can tell us about the reaction mechanism

Contributions

This chapter represents a modified version of a published article focusing on the reaction of benzophenone triplet and two of its derivatives.¹ Contributions from the authors are as follows: Michelle L. Grimm, (author of this dissertation) performed the laser flash photolysis of 1-cyclopropyl-4-phenyl-1,2,3,6-tetrahydropyridine (**9**) and (+/-)-[trans-2-phenylcyclopropyl-4-phenyl-1,2,3,6-tetrahydropyridine (**10**), and made significant contributions to the writing and editing of the manuscript. Rate constants for **2** and **9** and laser flash photolysis of 1-methyl-4-phenyl-1,2,3,6-tetrahydropyridine [MPTP (**2**)] were performed by Meghan Finn. Computational work was performed by William J. Allen. Selected calculations and manuscript preparation were performed by Dr. James M. Tanko. Lastly Dr. Neal Castagnoli (committee member) made significant contributions to the writing and editing of the manuscript as well as aided significantly in the intellectual contributions for this work.

1. Grimm, M. L.; Allen, W. J.; Finn, M.; Castagnoli, N.; Tanko, J. M. Reaction of Benzophenone Triplet with Aliphatic Amines. *Bioorg. Med. Chem.* **2011**, *19*, 1458-1463.

Abstract

A photochemical model study of benzophenone triplet (^3BP) with the MAO-B substrate 1-methyl-4-phenyl-1,2,3,6-tetrahydropyridine [MPTP (**2**)] and two of its derivatives, 1-cyclopropyl-4-phenyl-1,2,3,6-tetrahydropyridine (**9**) and (+/-)-[*trans*-2-phenylcyclopropyl-4-phenyl-1,2,3,6-tetrahydropyridine (**10**)] were performed. Literature precedent and calculations reported herein suggest that the barrier to ring opening for aminyl radical cations derived from *N*-cyclopropyl derivatives of tertiary amines (such as MPTP) will be low. The LFP results reported herein demonstrate that pathways for the reaction of ^3BP with **2**, **9**, and **10** are very similar. In each instance, disappearance of ^3BP is accompanied solely by appearance of bands corresponding to the diphenylhydroxymethyl radical and neutral radical derived from MPTP and its two derivatives **9** and **10**. These results suggest that the reaction between benzophenone triplet and tertiary aliphatic amines proceed via a simple hydrogen atom transfer reaction. Additionally these model examinations provide evidence that oxidations of *N*-cyclopropyl derivatives of MPTP catalyzed by MAO-B may not be consistent with a pure SET pathway.

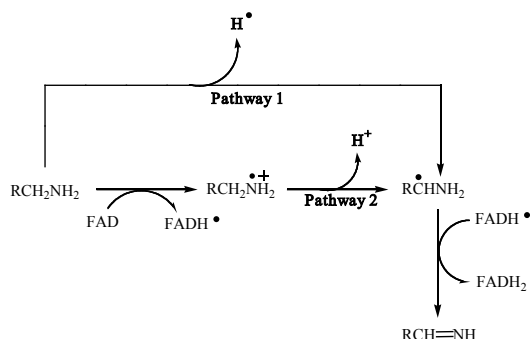
2.1 Introduction

Monoamine oxidase (MAO) A and B are flavoenzymes that catalyze the oxidation of various monoaminergic neurotransmitters, including serotonin and dopamine,¹ as well as some xenobiotics.² MAO-A selectively catalyzes the oxidation of serotonin; the B form is the principal enzyme that catalyzes the oxidation of dopamine.³ MAO-B has gained additional attention since it catalyzes the bioactivation of certain tetrahydropyridinyl derivatives to neurotoxic metabolites that mediate the degradation of dopaminergic neurons in the substantia nigra resulting in a parkinsonian syndrome closely resembling idiopathic Parkinson's disease.⁴

Model studies have led to several proposals to account for the catalytic activity of MAO-B. A polar pathway involving the addition of the aminyl substrate across the 4a-5 double bond of the covalently bound FAD co-factor followed by an intramolecular redox reaction has been proposed by Mariano^{5, 6} and, more recently, Edmondson.⁷ Two radical-based pathways also have been considered. Silverman has been a strong proponent of the single electron transfer (SET) mechanism^{1, 8} and Castagnoli has presented evidence consistent with a hydrogen atom transfer (HAT) mechanism^{2, 9} (**Scheme 2-1**).

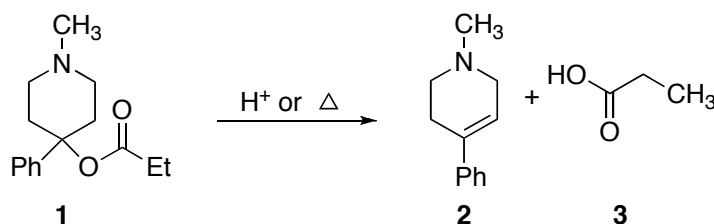
Scheme 2-1 outlines the differences between the SET and HAT proposals. Although these two pathways can account for some of the behaviour of substrates and inhibitors, it is our view that neither of these radical-based mechanisms nor the polar pathway account for all of the available experimental evidence. Since our interests are linked to the MAO-catalyzed metabolic activation of cyclic tertiary allylamines, the discussion that follows will focus on the radical pathways since nucleophilic addition of tertiary amines across the 4a-5 double bond (the polar pathway) should be sterically prohibited. The present chapter describes the results of our attempts to provide evidence to help distinguish the potential contributions of the SET and HAT mechanisms using

photochemically activated benzophenone as the electron or hydrogen atom acceptor and various tetrahydropyridinyl derivatives that are known MAO-B substrates and/or for which independent documentation of the fate of electrochemically mediated 1-electron oxidations is available.



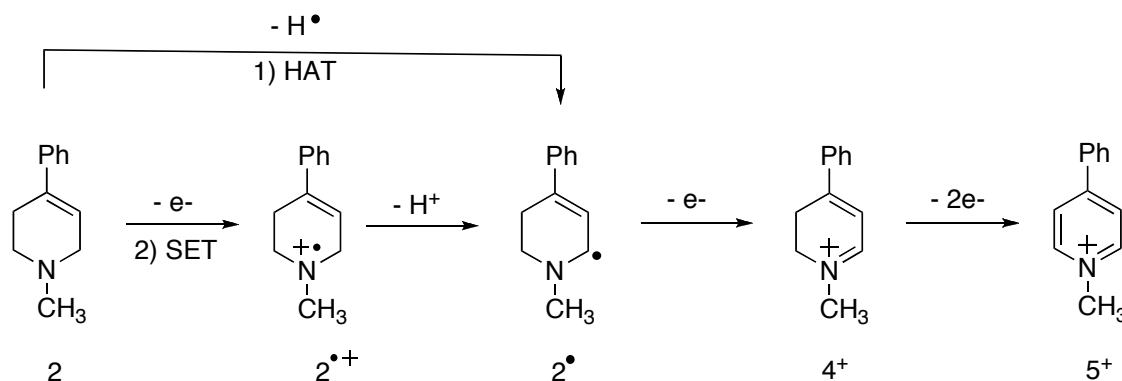
Scheme 2-1 Proposed Pathways for MAO oxidations

Over the past 30 years much focus has been given to 1-methyl-4-phenyl-1,2,3,6-tetrahydropyridine [MPTP (**2**)], a compound known to induce an irreversible parkinsonian disorder in humans and animal models.^{10, 11} This hypothesis was made after the deaths of several young patients suffering from irreversible parkinsonian symptoms. The common thread between these cases was the fact that all the patients had ingested a contaminated merperidine analogue that had been administered by self injection.¹² This analogue (MPPP) (**1**) was believed to have been contaminated through the synthetic route that led to the formation of 1-Methyl-4-phenyl-1,2,5,6-tetrahydropyridine (MPTP) (**2**) and propionic acid (**3**) as an impurity (**Scheme 2-2**).



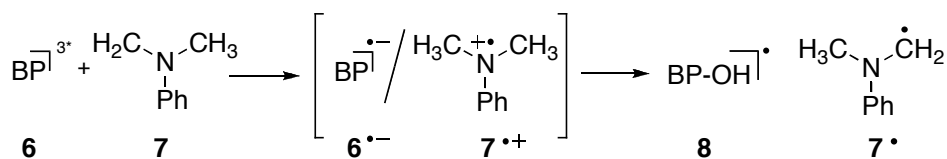
Scheme 2-2 Degradation of MPPP to MPTP

Subsequent biochemical studies led to the discovery that MPTP is oxidatively metabolized in the brain to give the dihydropyridiniumyl species MPDP⁺ (**4**) that subsequently undergoes a two electron oxidation to give the toxic pyridiniumyl product MPP⁺ (**5**) (**Scheme 2-3**).⁹ MPP⁺ is thought to mediate the degeneration of dopaminergic neurons.⁴ Mechanistic details of this important bioactivation pathway remain poorly understood. What is known is that the initial 2-electron oxidation is catalyzed efficiently by MAO-B.



Scheme 2-3 The MAO-B catalyzed bioactivation of MPTP (**2**) to MPDP⁺ (**4**⁺) and MPP⁺ (**5**⁺).

Benzophenone is a common photosensitizer; its chemistry with aromatic amines has been well characterized. Although the products of the reaction give the *appearance* of a hydrogen atom transfer process, laser flash photolysis (LFP) experiments have shown that the reaction of benzophenone triplet (**6**) with aromatic amines proceeds by a single electron transfer, generating a solvent separated ion pair (SSIP) consisting of benzophenone radical anion [(**6^{•-}**) λ_{max} = 715 nm] and an aminyl radical cation (**7^{•+}**).^{13, 14} This caged-pair subsequently reacts via proton transfer, with the aminyl radical cation acting as an acid and the benzophenone radical anion as a base, generating diphenylmethanol radical [(**8**) λ_{max} = 545 nm] and the neutral aminyl radical (**7[•]**) (**Scheme 2-4**).

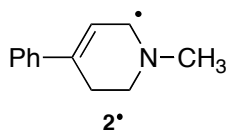


Scheme 2-4 Reaction of benzophenone triplet (^3BP) with aromatic amines

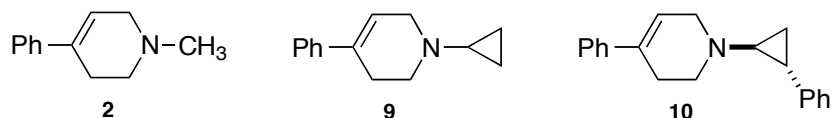
Similarly, ^3BP reacts readily with aliphatic amines with a reactivity order $3^\circ > 2^\circ > 1^\circ$.⁹ Rate constants for tertiary and secondary amines are on the order of diffusion controlled, while primary amines are on the order of $10^7 \text{ M}^{-1}\text{s}^{-1}$.¹⁵ Although the reaction is also a formal hydrogen atom transfer process, the details of the mechanism remain ambiguous. Assuming electron transfer occurs, proton transfer between the initially produced $\mathbf{6}^{\cdot-}/\mathbf{7}^{\cdot+}$ caged pair may occur too rapidly for these species to be detected. Also, unlike aromatic amines, spectroscopic characterization of the initially formed $\text{R}_3\text{N}^{\cdot+}$ is difficult because these species absorb weakly and thus are invisible by UV. Consequently, both hydrogen atom transfer and single electron transfer mechanisms have been suggested for the reactions of benzophenone triplet and aliphatic amines. Achieving an unambiguous assignment of the reaction mechanism has proven problematic.

Recently, we reported rate constants for the reaction of *t*-butoxyl radical ($^t\text{BuO}^\bullet$) with the potent neurotoxin 1-methyl-4-phenyl-1,2,3,6-tetrahydropyridine (MPTP).^{16, 17} In this study, $^t\text{BuO}^\bullet$ was generated by the photolysis of di-*t*-butyl peroxide (DTBPO). This method was employed to measure the absolute rate constants for hydrogen atom abstractions from MPTP by $^t\text{BuO}^\bullet$, generated by laser flash photolysis (LFP), in order to gain insight into the radical-based chemistry of MPTP. Unlike the radicals derived from HAT in simple aliphatic amines,^{18, 19} the MPTP derived radical ($\mathbf{2}^\bullet$) gave rise to a transient species ($\lambda_{\text{max}} = 385 \text{ nm}$) that could be easily monitored. The strongly absorbing species was assigned to the α -allylic MPTP radical based on

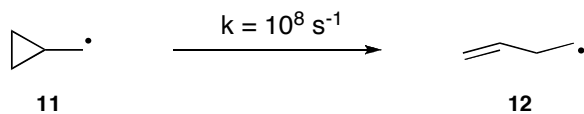
isotopic labeling studies. The observed rate constant for the formation of the MPTP derived radical was determined to be $2.27 \times 10^8 \text{ M}^{-1}\text{s}^{-1}$.^{16,17}



In principle, hydrogen atom abstraction can occur at each of the carbons alpha to the nitrogen in MPTP, as was demonstrated for hydrogen abstractions by t-butoxyl radical.¹⁵ However, only **2•** possesses a suitable chromophore that can be readily monitored at 385 nm. Accordingly, it was envisioned that this radical would provide a unique spectroscopic handle to study the mechanism of the reaction between benzophenone triplet and aliphatic amines. This manuscript describes the photochemical investigation of reaction of ³BP with 1-methyl-4-phenyl-1,2,3,6-tetrahydropyridine (MPTP) (**2**) and two of its derivatives; 1-cyclopropyl-4-phenyl-1,2,3,6-tetrahydropyridine [*N*-cyclopropyl MPTP] (**9**) and (+/-)-[*trans*-2-phenylcyclopropyl-4-phenyl-1,2,3,6-tetrahydropyridine] [*N*-cyclopropylphenyl MPTP] (**10**).



The *N*-cyclopropyl MPTP derivatives provide a unique way to probe the mechanism of these benzophenone triplet-mediated oxidations because in direct analogy to the cyclopropylcarbinyl \rightarrow homoallyl neutral radical rearrangement (**Scheme 2-5**),²⁰ the derived radical cations (if produced) are expected to undergo instantaneous ring opening. Moreover, because the barrier to this ring opening is exceedingly small (*vide infra*), this process should be competitive with deprotonation of the aminyl radical cation.



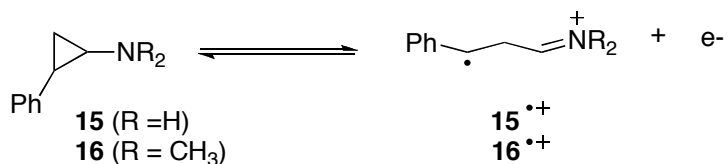
Scheme 2-5 Ring opening of the cyclopropylcarbinyl neutral radical

Literature precedent suggests that $\mathbf{9}^{*+}$ and $\mathbf{10}^{*+}$ will have little or no barrier to ring opening. Indeed, 1-electron oxidation of $\mathbf{10}$ may occur via a dissociative electron transfer (DET) reaction, wherein electron transfer and ring opening occur simultaneously.²¹ Electron paramagnetic resonance (EPR) examinations of the radical cation generated from *N*-cyclopropylamine ($\mathbf{13}$) support this statement.¹⁹ EPR experiments in a solid matrix have provided evidence for the distonic radical cation (ring opened) structure based upon hyperfine coupling constants and have shown that the aminyl radical cation ring-opens to the distonic radical cation rapidly upon electron removal.^{22, 23} Subsequent molecular orbital calculations at the MP2 and other levels of theory have suggested that the removal of an electron from *N*-cyclopropylamine occurs simultaneously with ring opening; the only stable structure is the distonic radical ion, which collapses to a more stable aminopropenyl ion.^{24, 25}

Studies on MPTP and the cyclopropyl analogs $\mathbf{9}$ and $\mathbf{10}$ by online coupling of electrochemistry and mass spectrometry (EC-ESI-MS) have been reported.²⁶ The technique involves passing a substrate solution through a porous graphite electrode and varying the potential from 0 to 1500mV. The concentrations of substrates and products resulting from 1-electron oxidation are then monitored via LC-MS. Experiments conducted with compound $\mathbf{2}$ showed evidence for electron transfer to generate the aminyl radical cation $\mathbf{2}^{*+}$ followed by subsequent deprotonation at the allylic position to yield $\mathbf{2}^{\cdot}$. On the other hand, the analogous reactions with compounds $\mathbf{9}$ and $\mathbf{10}$ were consistent with rapid ring opening of the aminyl radical cations to give

corresponding distonic radical cation. No dihydropyridinium products corresponding to electron transfer followed by allylic α -carbon deprotonation were detected. These experiments were further probed by computational analysis at the UHF level of theory. No global minima corresponding to the ring closed aminyl radical cations **10**^{•+} were ever obtained indicating that the electron transfer and ring opening proceed by a concerted process.

Dinnocenzo, *et al.*²⁷ studied the fate of a series of structurally-related *N*-(2-phenylcyclopropyl) aminyl radical cations (**15**^{•+} and **16**^{•+}) by nanosecond laser flash photolysis. Ring opening of the radical cation was estimated to be exothermic by -26 kcal/mol. It was suggested that ring opening and electron transfer were occurring in a concerted fashion and that *N*-(2-phenylcyclopropyl) aminyl radical cations have virtually no barrier for ring opening (**Scheme 2-6**).



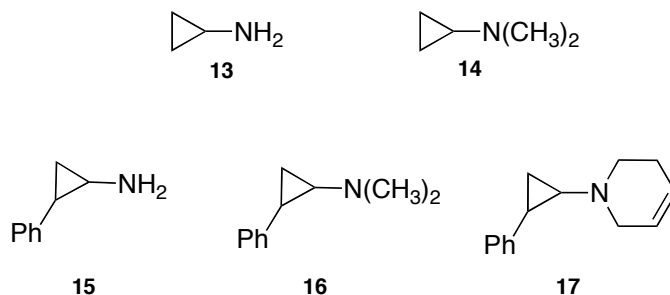
Scheme 2-6 Ring opening of *N*-(2-phenylcyclopropyl) aminyl radical cations

Literature precedent as well as higher order molecular orbital calculations suggest that the barrier for ring opening of tertiary amine radical cations such as *N*-(2-phenylcyclopropyl) derivative (**10**) to be virtually nonexistent. Due to the unique chromophore derived from **2**, laser flash photolysis can be used to spectroscopically observe a reactive intermediate that is generated from excitation, be it radical or radical ion. Herein we report: (1) computational analysis of ring opening reactions of relevant cyclopropyl amines, and (2) the results of model studies on the photochemically-mediated oxidation of MPTP and two of its derivatives that are designed to evaluate the HAT vs. the SET pathways.

2.2 Results and Discussion

2.2.1 Calculations

The ring opening of radical cations derived from: *N*-cyclopropylamine (**13**), *N,N*-dimethylaminocyclopropane (**14**), 2-phenylcyclopropylamine (**15**), *N,N*-dimethyl-*N*-(2-phenylcyclopropyl)amine and (**16**) 1-cyclopropylphenyl-1,2,3,6-tetrahydropyridine (**17**) were examined computationally. As noted, calculations pertaining to the ring opening chemistry of **13**^{•+} have been previously reported,²²⁻²⁵ thereby allowing us to validate the computational methods before examining the chemistry of compounds **13**^{•+} → **17**^{•+}. The following are the specific issues to be addressed: Will a tertiary aminyl radical cation such as **14**^{•+} be more stable than primary radical **13**^{•+} and thus have a barrier to ring opening? Will phenyl substitution on the cyclopropyl group lower or eliminate the barrier to ring opening, if indeed such a barrier exists?



2.2.1.1 *N*-cyclopropylaminyl radical cation (**13**^{•+}).

Consistent with published results,²²⁻²⁵ an energy profile (plot of energy vs. C-C bond length) of **13**^{•+} at the UHF/6-31G* level of theory suggest that the ring-closed form of **13**^{•+} does not exist at a potential energy minimum. Attempts to minimize the energy of the cyclopropyl ring-closed form of **13**^{•+} led to a minimized structure corresponding to the distonic (ring-opened) radical cation. Similar results were obtained at the UMP2/6-31G* and UMP4SDTQ/6-311G** levels of theory/basis sets. Geometry optimization led exclusively to the ring-opened form. These results confirm that there is no barrier associated with the ring-opening of **13**^{•+}. Because these results

correspond with previously published studies,²²⁻²⁵ it can be said with confidence that these computational methods can also be utilized to examine $14^{*+} \rightarrow 17^{*+}$.

2.2.1.2 *N,N*-dimethyl-*N*-cyclopropylaminyl radical cation (14^{*+}).

Energy profiles on 14^{*+} at the UHF/6-31G*, UMP2/6-31G*, and, UMP4SDTQ/6-31G** levels all reveal a) the ring-closed and ring-opened forms of 14^{*+} reside at potential energy minima (no imaginary frequencies), and b) that there is small barrier to the ring opening reaction (**Figure 2-1**). A transition state for ring opening was successfully located, characterized by one imaginary frequency corresponding to C-C bond cleavage. In the case of UHF/6-31G*, the energy of activation for the ring opening pathway was found to be 4.7 kcal/mol. Ring opening was exothermic by ca. -7.5 kcal/mol.

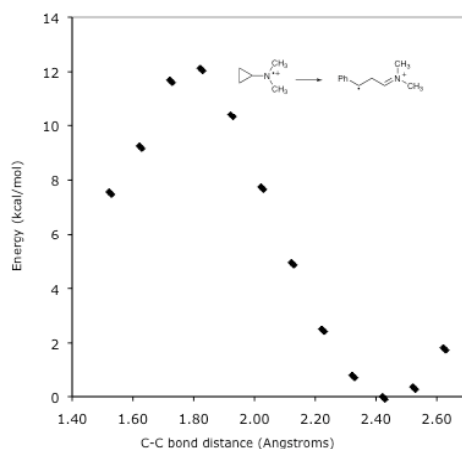


Figure 2-1 Reaction coordinate diagram for the ring opening of 14^{*+} calculated at the UHF/6-31G* level of theory.

2.2.1.3 *N*-(2-phenylcyclopropyl)aminyl radical cation (15^{*+}).

As was the case for 13^{*+} , calculations at the UHF/6-31G* level of theory revealed that ring-opening of 15^{*+} occurs with essential no barrier (**Figure 2-2**), consistent with the results of Dinnocenzo, *et al.* The interaction between C1 and C3 is purely repulsive. Similar results were obtained at UMP2/G-31G*, and UMP4STDQ/6-31G** levels of theory, further confirming that

the ring closed form of $15^{+\bullet}$ does not exist at a potential energy minimum, and that no barrier to ring opening exists.

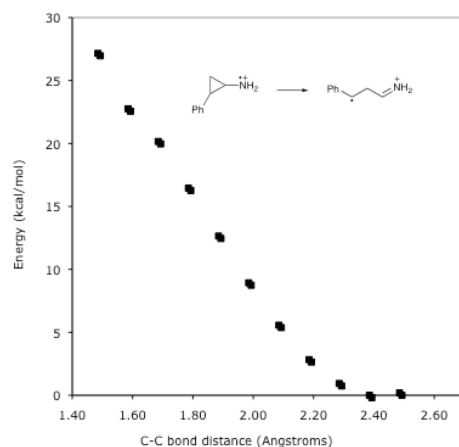


Figure 2-2 Reaction coordinate diagram for the ring opening of $15^{+\bullet}$ calculated at the UHF/6-31G* level of theory.

2.2.1.4 *N,N*-dimethyl-*N*-(2-phenylcyclopropyl)aminyl radical cation ($16^{+\bullet}$).

Geometry optimizations at UHF/6-31G* revealed a stable ring-opened form and a stable ring-closed form of the radical cation with no imaginary frequencies for either. ΔE° for ring opening was found to be -27.0 kcal/mol, consistent with the results of Dinnocenzo, *et al.*²⁷ Curiously, an energy profile of the cyclopropyl ring opening reaction (**Figure 2-3**) did not reveal either a minimum for the ring-closed form of $16^{+\bullet}$ or a transition state for ring opening. Similarly, geometry optimization calculations at the UMP2 level of theory using the 6-31G* basis set also found both the ring-opened and ring-closed form of $16^{+\bullet}$. Again, the barrier to ring opening was nonexistent. (Unfortunately, the limitations of the computational system used in this study prevented us from probing this problem further as energy profiles at UMP2/6-31G* and UMP4STDQ/6-31G** levels of theory were unsuccessful).

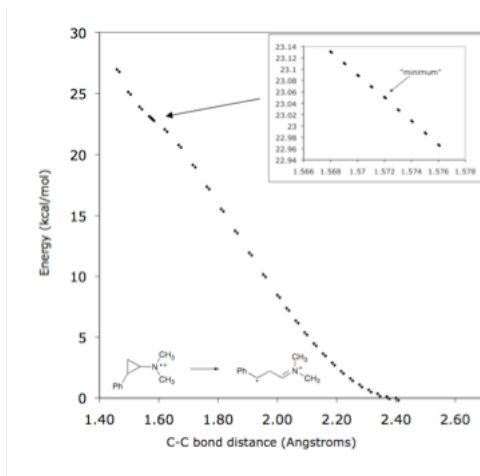


Figure 2-3 Reaction coordinate diagram for the ring opening of 16^{*+} calculated at the UHF/6-31G* level of theory.

Careful inspection of the profile for 16^{*+} , varying the C-C bond length in very small increments (0.001 Å) in the vicinity of the ring-closed minimum proved informative. Variation of the C-C bond length is accompanied by a simultaneous rotation of one of the methyl groups as depicted in **Figure 2-4**. Thus, a simple, two-dimensional reaction coordinate diagrams such as in **Figure 2-3** does not depict the full dynamics of the system, explaining why no minimum appears in this plot. All attempts to locate a transition state for ring opening failed, and as the calculations pertain to 0 K, we conclude that there is no significant barrier to ring opening of 16^{*+} at room temperature.

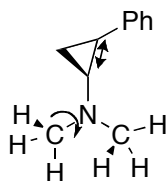


Figure 2-4 Depiction of how variation on C-C bond length of 14^{*+} is accompanied by simultaneous rotation of the *N*-methyl group.

Because of the anomaly with rotation of the methyl groups in **16⁺**, ring opening of cyclic aminyl radical cation **17⁺** was reexamined as a model for the ring opening of the radical cation generated from *trans*-2-phenylcyclopropyl-4-phenyl-1,2,3,6-tetrahydro-pyridine (**10**). No minimum corresponding to a cyclopropane ring-closed structure could be located at any level of theory. The reaction coordinate diagram (**Figure 2-5**) is unambiguous in showing that the interaction between C1 and C3 is purely repulsive, consistent with earlier observations.²¹ Accordingly, it appears quite reasonable to assume that ring-opening of **10⁺** is barrier-free.

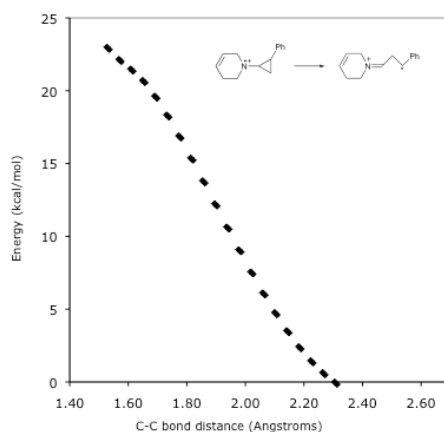


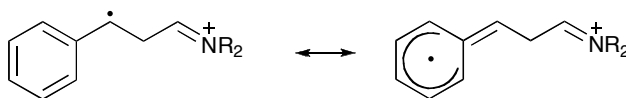
Figure 2-5 Reaction coordinate diagram for the ring opening of **17⁺** calculated at the UHF/6-31G* level of theory.

2.2.1.5 Comparison of **13⁺** and **14⁺**.

Computationally, we observed that **13⁺** exhibits no stable ring closed form and opens spontaneously with the transfer of an electron, consistent with earlier reports on this system. On the other hand, **14⁺** can lose an electron and remain a stable ring-closed radical cation. A barrier to ring-opening exists, thus a transition state exists. A chemical reason for this is that the electron donating character of the methyl groups on **14⁺** can stabilize the radical cation in the ring-closed form.

2.2.1.6 Comparison of $14^{*\bullet}$ and $16^{*\bullet}$.

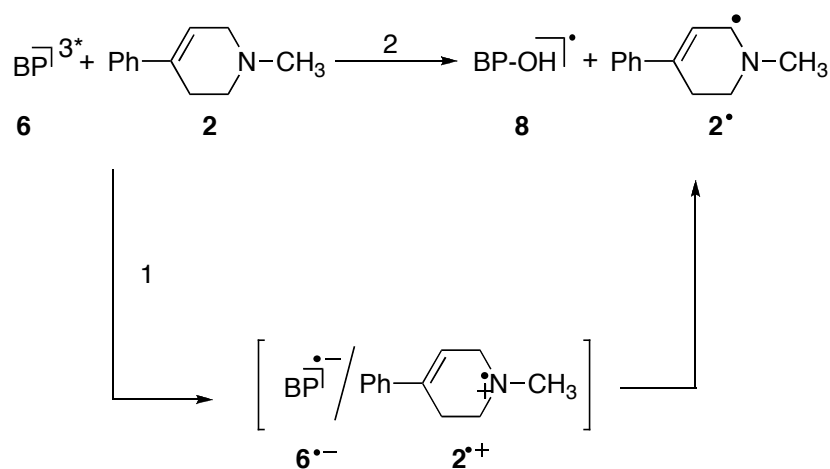
Computational analysis of $14^{*\bullet}$ clearly reveals a barrier to ring opening. Conversely, ring opening of $16^{*\bullet}$ is highly exothermic ($\Delta E^\circ = -27$ kcal/mol) with no significant barrier to ring opening, consistent with the report of Dinnocenzo and coworkers.²⁷ One electron oxidation of **10** and **16** likely occurs via a concerted dissociative electron transfer reaction. This process is driven by the fact that the ring-opened form is stabilized by the formation of a benzylic radical (Scheme 2-7). For $12^{*\bullet}$, no such stabilization exists resulting in a 4.71 kcal/mol barrier for the ring opening pathway.



Scheme 2-7 Resonance stabilization of the distonic radical cation derived from $10^{*\bullet}$ and $16^{*\bullet}$

2.2.2 Laser Flash Photolysis (LFP).

The transient absorption spectra for the reaction of ^3BP with MPTP (**2**) in benzene are presented in **Figure 2-6**; virtually identical results were obtained in acetonitrile. The key features of these spectra are that for MPTP, the data suggest that the decay of benzophenone triplet [6^{3*} ($\lambda_{max} = 520$)]¹² is accompanied by the formation of two new species at $\lambda_{max} = 545$ ¹² and 385 nm.¹⁶ These two species are the diphenylhydroxymethyl radical [**8** (545 nm)] and MPTP-H \bullet [**2 \bullet** (385 nm)], which are formed either by in-cage proton abstraction in the caged ion pair, or direct hydrogen atom abstraction (**Scheme 2-8**). The spectra showed no indication that the benzophenone radical anion [$6^{\bullet-}$ ($\lambda_{max} = 650$ nm)] was formed.



Scheme 2-8 Reaction pathways for ³BP with MPTP 1) SET, and 2) HAT

In order to probe further the mechanism of this system, and to differentiate between the direct HAT and SET pathways, an analogous LFP study was conducted on the corresponding *N*-cyclopropyl MPTP derivatives **9** and **10**. In the case of MPTP, either hydrogen atom abstraction, or SET followed by in-cage deprotonation, would result in the formation of **2[•]**. However in the case of the two cyclopropyl derivatives, if SET is occurring, cyclopropyl ring opening is expected to compete with deprotonation because there is little (in the case of **9^{•+}**) or no (in the case of **10^{•+}**) barrier to ring opening (*vide supra*). Electron transfer from **10** is likely to be concerted with ring opening. This system is an ultrasensitive probe for single electron transfer—competitive with events such as deprotonation which may be occurring within the lifetime of a caged-radical ion pair.

For each, the reaction of ³BP produced only species absorbing at 540 nm, corresponding to diphenylmethanol radical (**8**) and 380 nm corresponding to the hydrogen atom abstraction product. In examining the chemistry of these compounds, using benophenone triplet as a sensitizer it has been inferred that the “hydrogen atom abstraction” is the only observable process.

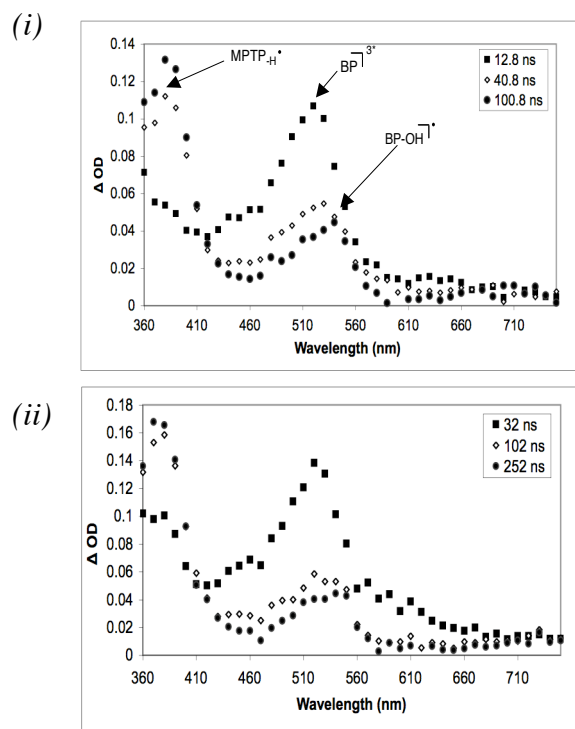


Figure 2-6 Transient absorption spectra of (i) MPTP (**2**) in CH_3CN and, (ii) *N*-cyclopropylphenyl MPTP (**10**) in CH_3CN .

These experiments were also conducted in the presence of 0.5 M lithium perchlorate, which has been shown to aid in the separation of the contact ion pair to facilitate the diffusion of the contact ion pair forming a solvent separated ion pair.²⁸ Lithium cation will complex with benzophenone radical anion, which can be monitored at $\lambda_{\text{max}} = 650$ nm on a nanosecond time regime. Examination of all three compounds showed no evidence of benzophenone radical anion in the presence of lithium perchlorate. In the case of the *N*-cyclopropyl derivatives, the MPTP derived radical absorption band (**9'**) should be diminished and the band corresponding to the benzophenone radical anion should be visible in the absorption spectra, making the reasonable assumption that ring opening is competitive with deprotonation. In the case of compound **10**, the molecule is expected to undergo a concerted dissociative electron transfer reaction, and therefore neither the band at 385 nm (corresponding to the MPTP derived radical (**10'**)) or band at 545 nm (corresponding to **8'**) are expected to be present. Because both of these bands *are* observed, it

can be surmised that an electron transfer process is not occurring in this system. These results are fully consistent with the proposal that these oxidations of MPTP and its derivatives by benzophenone occur by a HAT process.

Rate constants for the reaction of benzophenone triplet with **2** and **9** were examined by varying the concentration of MPTP derivatives and monitoring the growth of the MPTP radical species on a nanosecond time regime as described previously¹⁵. For both substrates, the rate constants were on the order of diffusion controlled and not significantly affected by added electrolyte (Table 2-1).

Substrate	Solvent	k_{obs} ($\text{M}^{-1}\text{s}^{-1}$)
2	Benzene	2.12×10^9
2	Acetonitrile	8.34×10^9
2	Acetonitrile/ LiOCl ₄	5.83×10^9
9	Benzene	2.19×10^9
9	Acetonitrile	5.47×10^9
9	Acetonitrile/LiOCl ₄	6.37×10^9

Table 2-1 Rate constants for the reaction of ³BP with **2** and **9**.

2.3 Conclusions

Literature precedent and the calculations reported herein suggest for tertiary amines (such as these MPTP derivatives) that the barrier to ring opening of the corresponding radical cations is anticipated to be low for the *N*-cyclopropyl derivative (*e.g.*, **9**⁺)²²⁻²⁵ and non-existent for the *N*-(2-phenylcyclopropyl) derivative (*e.g.*, **10**⁺).^{21, 27} These systems are thus expected to be ultrasensitive probes for single electron transfer. The LFP results reported herein demonstrate that for the reaction of ³BP with **2**, **9**, and **10**, the intermediates formed are very similar. In each instance, disappearance of ³BP is accompanied solely by appearance of bands corresponding to the diphenylhydroxymethyl radical and neutral radical derived from MPTP and its derivatives. In principle, this is consistent with either an apparent hydrogen abstraction from the MPTP derivative, or deprotonation within the radical ion pair formed by single electron transfer.

However, the results obtained for **9**, and especially for **10** do not support an electron transfer pathway. Electron transfer from **9** is expected to lead immediately to the cyclopropyl ring opened product. If this were occurring, the observations would be drastically different: a) Bands corresponding to either the diphenylhydroxymethyl radical ($\lambda_{max} = 540$ nm) or neutral radical derived from the MPTP derivative ($\lambda_{max} = 380$) would *not* be observed because the ring opening would beat out deprotonation, and b) a band corresponding to the benzophenone radical anion ($\lambda_{max} = 650$ nm) *would* be observed. Accordingly, these results suggest that the reaction between benzophenone triplet and tertiary aliphatic amines proceed via a hydrogen atom transfer reaction. Additionally these models provide evidence that oxidations of N-cyclopropyl derivatives of MPTP catalyzed by MAO-B may not proceed by a pure SET pathway.

2.4 Experimental Section

2.4.1 Materials

All solvents and fine chemicals used in this study were obtained from Aldrich and used as received unless otherwise noted. Benzophenone was recrystallized in methanol prior to use. Syntheses of MPTP and derivatives have been described previously;^{21, 29} these compounds were stored as their oxalate salts. For sample preparation, the oxalate salts were suspended in saturated potassium carbonate and extracted using ethyl acetate to render the free base prior to use. Solution concentrations were calculated using the mass of the free base. **Caution:** MPTP is a known neurotoxin and should be handled in a well-ventilated hood and proper personal protective equipment should be worn while working with this material. Procedures for the safe handling of MPTP have been documented.³⁰

2.4.2 Apparatus

Steady-state UV/Vis spectra were recorded on a Hewlett Packard diode array UV/Visible spectrophotometer (HP 8452A). Laser flash photolysis (LFP) experiments were conducted using an Applied Photophysics LKS.60 spectrometer using the third harmonic of a Continuum Surelite I-10 Nd:YAG laser (4 - 6 ns pulse, 355 nm). Absorption spectra were monitored by a Hewlett Packard Infinium digital oscilloscope and analyzed with an Applied Photophysics SpectraKinetic Workstation software package (v. 4.59). Experiments were performed with a jacketed cell holder connected to a VWR Scientific Products (PolyScience) variable temperature circulating bath (model 1150-A) thermally equilibrated to 25C.

2.4.3 Laser Flash Photolysis (LFP)

Sample solutions were prepared in benzene or acetonitrile and deoxygenated with argon prior to use. (Steady-state UV/Visible spectra were recorded to ensure that benzophenone was the only species absorbing at the excitation wavelength). In most LFP experiments, 1:1 concentrations of the MPTP derivatives and benzophenone (4.5 mM) were examined in acetonitrile with varying concentrations of lithium perchlorate.

2.4.4 Calculations

Density functional theory calculations were performed using the Titan³¹ molecular modeling software and/or Gaussian 03.³²

2.4.5 Calculations. (Experimental)

Initial calculations for all four compounds (**11-15**) included the structure of the radical cation in the ring-closed form, transition state, and ring-opened form of each of the compounds were isolated at the AM1 level of theory. Structural results were imported from the AM1 level calculations, followed by geometry optimization and frequency calculations at the UHF level of

theory with the 6-31G* basis set. The results (structural coordinates) from this calculation were taken to a higher energy level, and once again geometry optimization and frequency calculations were performed at the UMP2 level of theory with the 6-31G* basis set. Finally, the energies of the structures that were determined at UMP2 were calculated once more at the UMP4SDTQ level of theory with the 6-311G** basis set.

Acknowledgements

This work was funded by the National Science Foundation (CHE-0548129). MLG was partially supported by NSF-IGERT (DGE-0333378).

Supplementary Data

Supplementary Information is shown in Appendix A: Transient absorption spectra for and MPTP and N-cyclopropylphenyl MPTP as well as concentration profiles of MPTP and N-cyclopropyl MPTP in benzene and acetonitrile.

References

1. Silverman, R. B., Radical Ideas About Monoamine-Oxidase. *Accounts of Chemical Research* **1995**, *28* (8), 335-342.
2. Kalgutkar, A. S.; Dalvie, D. K.; Castagnoli, N.; Taylor, T. J., Interactions of nitrogen-containing xenobiotics with monoamine oxidase (MAO) isozymes A and B: SAR studies on MAO substrates and inhibitors. *Chemical Research in Toxicology* **2001**, *14* (9), 1139-1162.
3. Scrutton, N. S., Chemical aspects of amine oxidation by flavoprotein enzymes. *Natural Product Reports* **2004**, *21* (6), 722-730.
4. Singer, T. P.; Salach, J. I.; Castagnoli, N.; Trevor, A., Interactions of the Neurotoxic Amine 1-Methyl-4-Phenyl-1,2,3,6-Tetrahydropyridine with Monoamine Oxidases. *Biochemical Journal* **1986**, *235* (3), 785-789.
5. Kim, J. M.; Bogdan, M. A.; Mariano, P. S., Mechanistic Analysis of the 3-Methylflavin-Promoted Oxidative Deamination of Benzylamine - a Potential Model for Monoamine-Oxidase Catalysis. *Journal of the American Chemical Society* **1993**, *115* (23), 10591-10595.
6. Kim, J. M.; Hoegy, S. E.; Mariano, P. S., Flavin Chemical-Models for Monoamine-Oxidase Inactivation by Cyclopropylamines, Alpha-Silylamines, and Hydrazines. *Journal of the American Chemical Society* **1995**, *117* (1), 100-105.
7. Miller, J. R.; Edmondson, D. E., Structure-activity relationships in the oxidation of para-substituted benzylamine analogues by recombinant human liver monoamine oxidase A. *Biochemistry* **1999**, *38* (41), 13670-13683.
8. Silverman, R. B.; Hoffman, S. J.; Catus, W. B., A Mechanism for Mitochondrial Monoamine-Oxidase Catalyzed Amine Oxidation. *Journal of the American Chemical Society* **1980**, *102* (23), 7126-7128.
9. Franot, C.; Mabic, S.; Castagnoli, N., Chemical model studies on the monoamine oxidase-B catalyzed oxidation of 4-Substituted 1-cyclopropyl-1,2,3,6-tetrahydropyridines. *Bioorganic & Medicinal Chemistry* **1998**, *6* (3), 283-291.
10. Markey, S. P.; Johannessen, J. N.; Chiueh, C. C.; Burns, R. S.; Herkenham, M. A., Intraneuronal Generation of a Pyridinium Metabolite May Cause Drug-Induced Parkinsonism. *Nature* **1984**, *311* (5985), 464-467.
11. Markey, S. P.; Burns, R. S., Mptp Exposure Victims. *Chemical & Engineering News* **1984**, *62* (6), 2-&.
12. Langston, J. W.; Ballard, P.; Tetrud, J. W.; Irwin, I., Chronic Parkinsonism in Humans Due to a Product of Meperidine-Analog Synthesis. *Science* **1983**, *219* (4587), 979-980.

13. Simon, J. D.; Peters, K. S., Picosecond Studies of Organic Photoreactions. *Accounts of Chemical Research* **1984**, *17*, 277-283.
14. Peters, K. S., *Advances in Electron Transfer Chemistry*. JAI Press: 1994; Vol. 4.
15. Griller, D.; Howard, J. A.; Marriott, P. R.; Scaiano, J. C., *J. Am. Chem. Soc.* **1981**, *103*, 619 - 623.
16. Suleman, N. K.; Flores, J.; Tanko, J. M.; Isin, E. M.; N. Castagnoli, J., *Bioorg. Med. Chem.* **2008**, *16*, 8557 - 8562.
17. Tanko, J. M.; Friedline, R.; Suleman, N. K.; N. Castagnoli, J., *J. Am. Chem. Soc.* **2001**, *123*, 5808 - 5809.
18. Finn, M.; Friedline, R.; Suleman, N. K.; Wohl, C. J.; Tanko, J. M., *J. Am. Chem. Soc.* **2004**, *126*, 7578 - 7584.
19. Lalevée, J.; Graff, B.; Allonas, X.; Fouassier, J. P., *J. Phys. Chem. A* **2007**, *111*, 6991 - 6998.
20. Newcomb, M.; Varick, T. R.; Ha, C.; Manek, M. B.; Yue, X., *J. Am. Chem. Soc.* **192**, *114*, 8158 - 8163.
21. Jurva, U.; Bissel, P.; Isin, E. M.; Igarashi, K.; Kuttub, S.; N. Castagnoli, J., *J. Am. Chem. Soc.* **2005**, *127*, 12366 - 12377.
22. Qin, X.-Z.; Williams, F., *J. Am. Chem. Soc.* **1987**, *109*, 595 - 597.
23. Knolle, W.; Janovský, I.; Naumov, S.; Williams, F., *J. Phys. Chem. A* **2006**, *110*, 13816 - 13826.
24. Bouchoux, G.; Alcaraz, C.; Dutuit, O.; Nguyen, M. T., *J. Am. Chem. Soc.* **1998**, *120*, 152 - 160.
25. Nguyen, M. T.; Creve, S.; Ja, T.-K., *Chem. Phys. Lett.* **1998**, *293*, 90 - 96.
26. Jurva, U.; Bissel, P.; Isin, E. M.; Igarashi, K.; Kuttub, S.; Castagnoli, N., Model electrochemical-mass spectrometric studies of the cytochrome P450-catalyzed oxidations of cyclic tertiary allylamines. *Journal of the American Chemical Society* **2005**, *127* (35), 12368-12377.
27. Wang, Y.; Luttrull, D. K.; Dinnocenzo, J. P.; Goodman, J. L.; Farid, S.; Gould, I. R., *Photochem. Photobiol. Sci.* **2003**, *2*, 1169 - 1176.
28. Simon, J. D.; Peters, K. S., Na⁺ and Li⁺ Effects on the Photo-Reduction of Benzophenone - a Picosecond Absorption Study. *Journal of the American Chemical Society* **1983**, *105*, 4875-4882.

29. Nimkar, S. K.; Anderson, A. H.; Rimoldi, J. M.; Stanton, M.; Castagnoli, K. P.; Mabic, S.; Wang, Y. X.; Castagnoli, N., Synthesis and monoamine oxidase B catalyzed oxidation of C-4 heteroaromatic substituted 1,2,3,6-tetrahydropyridine derivatives. *Chemical Research in Toxicology* **1996**, *9*(6), 1013-1022.
30. Pitts, S. M.; Markey, S. P.; Murphy, D. L.; Weisz, A.; Lunn, G., Recommended Practices for the Safe Handling of MPTP In MPTP-A Nuerotoxin Producing a Parkinsonian Syndrome Academic: New York, 1986; pp 703-716.
31. Wavefunction, Inc.: Irvine, CA 92612, 1998.
32. Frisch, M. J.; Trucks, G. W.; Schlegel, H. B.; Scuseria, G. E.; Robb, M. A.; Cheeseman, J. R.; J. A. Montgomery, J.; Vreven, T.; Kudin, K. N.; Burant, J. C.; Millam, J. M.; Iyengar, S. S.; Tomasi, J.; Barone, V.; Mennucci, B.; Cossi, M.; Scalmani, G.; Rega, N.; Petersson, G. A.; Nakatsuji, H.; Hada, M.; Ehara, M.; Toyota, K.; Fukuda, R.; Hasegawa, J.; Ishida, M.; Nakajima, T.; Honda, Y.; Kitao, O.; Nakai, H.; Klene, M.; Li, X.; Knox, J. E.; Hratchian, H. P.; Cross, J. B.; Adamo, C.; Jaramillo, J.; Gomperts, R.; Stratmann, R. E.; Yazyev, O.; Austin, A. J.; Cammi, R.; Pomelli, C.; Ochterski, J. W.; Ayala, P. Y.; Morokuma, K.; Voth, G. A.; Salvador, P.; Dannenberg, J. J.; Zakrzewski, V. G.; Dapprich, S.; Daniels, A. D.; Strain, M. C.; Farkas, O.; Malick, D. K.; Rabuck, A. D.; Raghavachari, K.; Foresman, J. B.; Ortiz, J. V.; Cui, Q.; Baboul, A. G.; Clifford, S.; Cioslowski, J.; Stefanov, B. B.; Liu, G.; Liashenko, A.; Piskorz, P.; Komaromi, I.; Martin, R. L.; Fox, D. J.; Keith, T.; Al-Laham, M. A.; Peng, C. Y.; Nanayakkara, A.; Challacombe, M.; Gill, P. M. W.; Johnson, B.; Chen, W.; Wong, M. W.; Gonzalez, C.; Pople, J. A. *Gaussian 03, Revision C.02*, Gaussian, Inc.: Wallingford CT, 2004.

Chapter 3 Development of New N-Cyclopropyl Based Electron Transfer Probes for Enzyme Catalyzed Reactions: Stereoelectronic Effects

Contributions

This chapter represents contributions from two sources: (i) a summary of published work describing the rate constant for the ring opening of *N*-cyclopropyl-*N*-methylaniline (**9**),¹ and (ii) the design, synthesis, and reaction kinetics of 1'-methyl-3',4'-dihydro-1'*H*-spiro[cyclopropane-1,2'-quinoline] (**27**) and 6'-chloro-1'-methyl-3',4'-dihydro-1'*H*-spiro[cyclopropane-1,2'-quinoline] (**41**).² Contributions from the authors are as follows: Michelle L. Grimm (author of this dissertation) performed the photochemistry of all compounds.¹ Dr. Xiangzhong Li performed the electrochemistry and product studies of compounds **9** and **22**.¹ Dr. Kazuo Igarashi provided the mass-spectral data for the manuscript.¹ Dr. James M. Tanko and Dr. Neal Castagnoli contributed to the writing and editing of the manuscript, as well as aided in the intellectual contributions of the work. Dr. James M. Tanko prepared and submitted the manuscript.

For the second manuscript (now in preparation), contributions from the authors are as follows: synthesis, electrochemistry and product studies of compounds **27** and **41** were all conducted by Michelle L. Grimm.² Selected synthetic steps were repeated by Eveline Reichert and Amber N. Hancock. Dr. Medhi Ashraf and Dr. N. Kamrudin Suleman performed all ESI-MS examinations. Dr. Neal Castagnoli aided with the ESI-MS experimental work and made significant intellectual contributions to the manuscript. Branden Fanovic provided the computational data, and Dr. Travis Dudding aided significantly to the intellectual merit of the document. Dr. James M. Tanko contributed to the writing and editing of the manuscript in addition to preparing the work for publication.

1. Li, X.; Grimm, M. L.; Castagnoli, N.; Igarashi, K.; Tanko, J. M. The First Calibration of an Aminiumyl Radical Ion Clock: Why N-cyclopropylanilines May Be Poor Mechanistic Probes for Single Electron Transfer. *Chem. Commun.* **2007**, 2648-2650.
2. Grimm, M. L.; Hancock, A. N.; Reichert, E.; Fonovic, B.; Suleman, N. K.; Ashraf, M.; Dudding, T.; Castagnoli, N.; Tanko, J. M. Development of New N-cyclopropyl Based Electron Transfer Probes for Enzyme Catalyzed Reactions: Stereoelectronic Effects and Resonance Effects. (Manuscript in preparation).

Abstract

N-cyclopropyl amines have been used in enzymatic examinations of cP-450 to probe for an SET pathway. To date, the work done on these cyclopropanes made the assumption that the ring opening of these probes should be on the order of 10^8 s^{-1} , based on the known rate constant for the ring opening of the cyclopropyl carbonyl neutral radical. Photochemical and electrochemical examinations of *N*-cyclopropyl-*N*-methylaniline (**9**) revealed that the rate constant for cyclopropyl ring opening to be $4 \times 10^4 \text{ s}^{-1}$. Molecular modeling calculations of **9**^{••} revealed that the perpendicular conformation was more favorable by 3.6 kcal/mol, leading to the hypothesis that the cyclopropyl group did not meet the appropriate stereoelectronic requirements for ring opening. Therefore a new series of spiro cyclopropanes were designed to lock the cyclopropyl group into the appropriate bisected conformation. The electrochemical results reported herein show that the rate constant for ring opening of 1'-methyl-3',4'-dihydro-1'*H*-spiro[cyclopropane-1,2'-quinoline] (**27**) and 6'-chloro-1'-methyl-3',4'-dihydro-1'*H*-spiro[cyclopropane-1,2'-quinoline] (**41**) are $3.5 \times 10^2 \text{ s}^{-1}$ and $4.1 \times 10^2 \text{ s}^{-1}$ respectively. Results from preparative scale electrolysis and ESI-MS are consistent with a ring opening process being operative for the chemical step.

3.1 Introduction

This chapter of the dissertation will focus on the cyclopropane chemistry of amine radical cations that have been used as mechanistic probes for the cytochrome P-450 (cP-450) family of enzymes. Although cyclopropyl amines have been used to probe the mechanism of enzymatic pathways for several enzymes including cP-450 and monoamine oxidase (MAO); the formal rate constants for these ring opening reactions have never been reported. Several reasonable hypotheses have been proposed based on the chemistry of cyclopropyl carbinyl neutral radical, but a detailed kinetic examination of the analogous amine radical cations has yet to be reported. The background information will review the ongoing experimental discrepancies between the mechanistic proposals (e.g., single electron transfer vs. hydrogen atom transfer), and will highlight the conflicting conclusions that have arisen from the use of traditional mechanistic probes for cP-450. This chapter will encompass the design, synthesis, and electrochemistry of a new generation of substrates that were envisioned to serve as better probes for these enzymes.

3.1.1 Cyclopropane Chemistry

Cyclopropane reactivity has been examined extensively for several decades.¹ The cyclopropyl group can act as an electron donor, and therefore it will readily stabilize electron poor substituents such as radicals and carbocations when in the appropriate conformation.³ When the molecule adopts the bisected conformation, the p-orbitals of the cyclopropane are aligned with the electron deficient center. It has been proposed that the interaction between the HOMO and the LUMO are maximized in this conformation, and therefore it is capable of donating electron density (**Figure 3-1**). Conversely, when the molecule adopts a perpendicular conformation (orthogonal orbitals) the electron donating properties of the cyclopropyl group are greatly minimized.⁴ Additionally the molecule must adopt the bisected conformation for ring opening to

occur due to maximal overlap between the HOMO and the electron deficient radical/radical cation center. If this stereoelectronic requirement is not met, the overall rate of ring opening will be inhibited.⁵

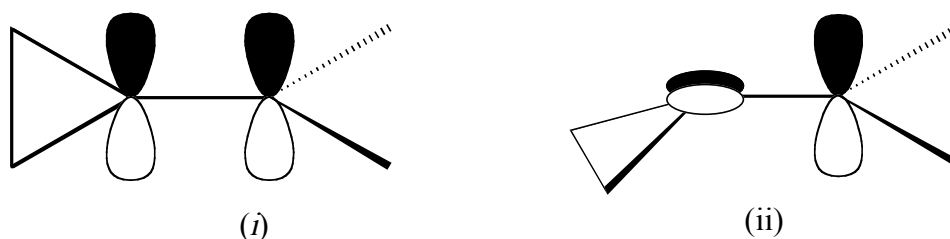
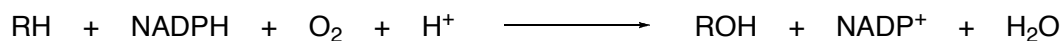
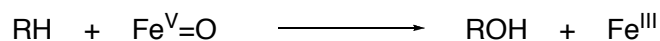
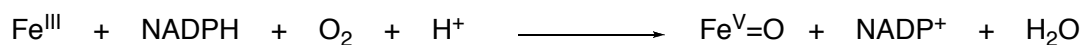


Figure 3-1 Depiction of the orbital interaction of the cyclopropyl group and a π system: (i) interaction depicted in the bisectioned conformation, and (ii) interaction shown in the perpendicular conformation.

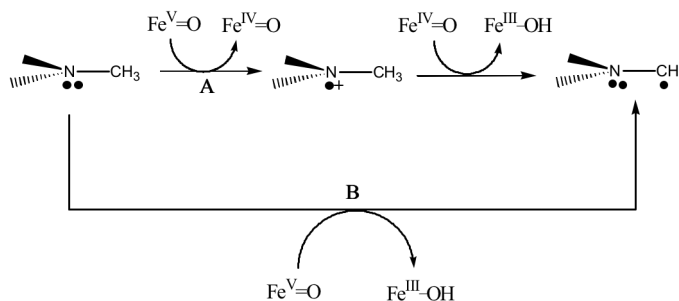
3.1.2 Cytochrome P-450

Cytochrome P-450 is a heme containing metalloenzyme involved in the oxidation of a variety of compounds ranging from xenobiotics⁶ to pharmaceutical drugs.⁷ The cP-450 enzymes belong to the oxygenase class of compounds, and to date over 2000 forms of the enzyme have been identified.⁸ Cytochrome P-450 consists of an iron porphyrin ring covalently bound to a protein via a cystine linkage.⁹ Over the past 40 years, cP-450 has gained much attention in the scientific community due to its ability to oxidize a variety of organic molecules that includes alkanes, olefins, and amines.⁸⁻¹⁰ Cytochrome P-450 oxidations are a result of a catalytic cycle involving a high valent iron-oxo ($\text{Fe}^{\text{V}}=\text{O}$) species that can be easily reduced to the corresponding iron alcohol ($\text{Fe}^{\text{III}}-\text{OH}$) **Scheme 3-1**. The high valent iron-oxo species is the key intermediate that has been implicated in the oxidation of a variety of substrates.⁸



Scheme 3-1 Stoichiometry of the cP-450 catalyzed oxidation.

The oxidation of amines by cP-450 has sparked considerable debate within the scientific community (**Scheme 3-2**). Two mechanisms have been proposed for the oxidation of amines by cP-450: (i) single electron transfer (SET),^{11, 12} and (ii) hydrogen atom transfer (HAT).¹³⁻¹⁵ The SET mechanism involves an electron transfer step that generates an amine radical cation followed by a proton transfer step to generate a neutral radical species. The HAT mechanism is a concerted hydrogen atom abstraction that results in a neutral radical.

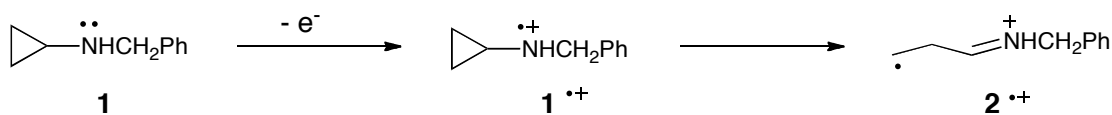


Scheme 3-2 Pathways for the oxidation of P-450: (A) SET mechanism, and (B) HAT mechanism.

3.1.3 SET Pathway

Several cyclopropylamines have been reported to undergo oxidation by cP-450. Among these substrates, *N*-benzyl-*N*-cyclopropylamine (**1**) has been commonly used to study the enzyme's mechanism; compound **1** renders the enzyme inert upon exposure.¹¹ This observation led to the hypothesis that the initial oxidation is an electron transfer step resulting in the formation of an

aminyl radical cation ($1^{+\bullet}$) which will rapidly ring open to generate the corresponding distonic radical cation **2** (**Scheme 3-3**). **2** is believed to covalently bind to the enzyme irreversibly, and render the enzyme inert. Inactivation of cP-450 by cyclopropylamines provides the best evidence for an SET pathway.^{11, 12} Secondary evidence supporting this hypothesis is based on the chemistry of horse radish peroxidase (HRP). HRP, an enzyme known to oxidize amines through an SET mechanism, has a higher reduction potential than cP-450 indicating that the initial oxidation step is more favorable for cP-450.¹⁶



Scheme 3-3 Ring opening of *N*-benzyl-*N*-cyclopropylamine following an SET pathway.

The rate constants for the ring opening of *N*-cyclopropylamines are expected to be within the same order of magnitude as the neutral cyclopropyl carbonyl free radical rearrangement.^{17, 18} Rate constants for the neutral carbon based radical are known to be on the order of 10^8 s^{-1} .¹⁹ Experimental evidence in conjunction with MO calculations imply that this assumption is valid for aliphatic amines, but the data detailing the behavior of aromatic amines remains ambiguous.^{20, 21} Due to the fact that *N*-cyclopropyl-*N*-methylaniline and several of its derivatives have been used as SET probes in cP-450 oxidations, the ring opening reaction must be competitive in relation to other competing pathways (e.g., deprotonation) for the probe to be effective.²²

3.1.4 HAT Pathway

The alternative mechanism proposed for the oxidation of cP-450 is the hydrogen atom transfer (HAT) mechanism. The HAT mechanism is a concerted hydrogen atom abstraction reaction resulting in the formation of a neutral radical. A recent examination conducted by Bhakta

provided evidence supporting the HAT mechanism.²³ This hypothesis stems from examination of the *N*-dealkylation reaction of *N*-alkyl-*N*-cyclopropyl-*p*-chloroanilines by cP-450 (**Figure 3-2**). Several key observations were drawn from this study: (i) The magnitude of isotope effects of **5** and **7** as compared to **5** and **8** were 3.2 +/- 0.1 and 3.1 +/- 0.1 respectively, indicating that the *N*-deisopropylation reaction proceeds via a mechanism similar to the *N*-decyclopropylation reaction, (ii) Reaction of **4** and **6** results only in *N*-demethylated products, only trace amounts of *N*-decyclopropylation were observed, and (iii) exposure of all six compounds to a known 1 electron oxidant $\text{Fe}^{\text{III}}(\text{phen})_3^{3+}(\text{PF}_6)_3^{3-}$ in the presence of base resulted in ring opened compounds. Products resulting from *N*-demethylation were minimal. These observations led to the idea that the *N*-decyclopropylation reaction catalyzed by cP-450 proceeds via a mechanism that leaves the cyclopropyl group unperturbed.

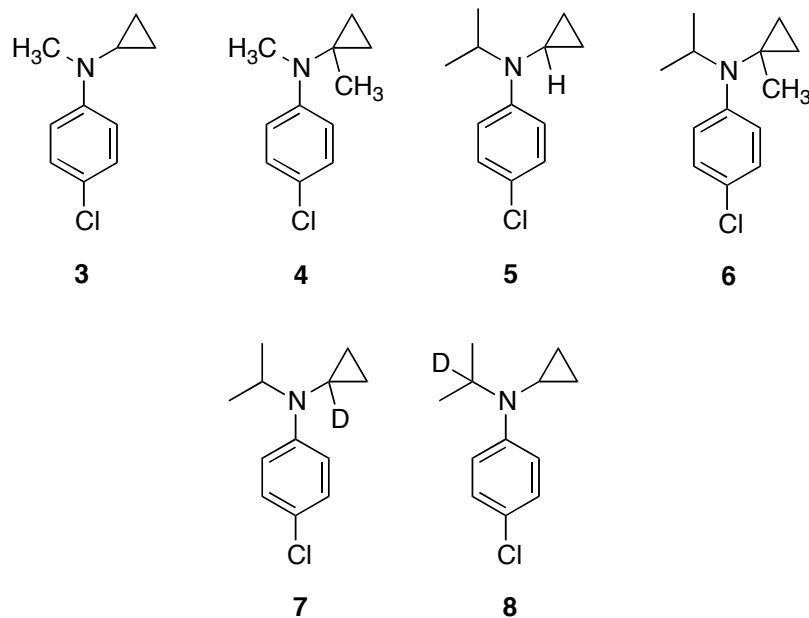
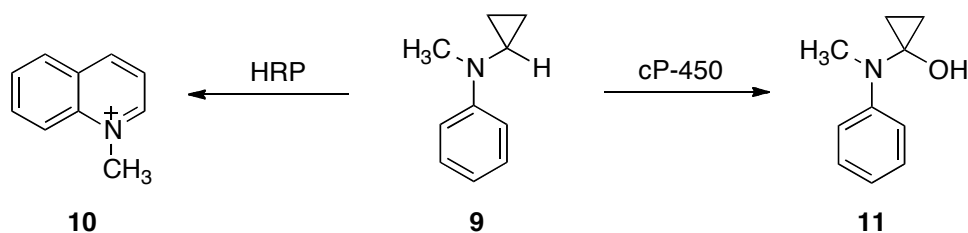


Figure 3-2 Compounds used to examine the *N*-dealkylation reaction of *N*-alkyl-*N*-cyclopropyl-*p*-chloroaniline probes by cP-450

3.1.5 Mechanistic Debate

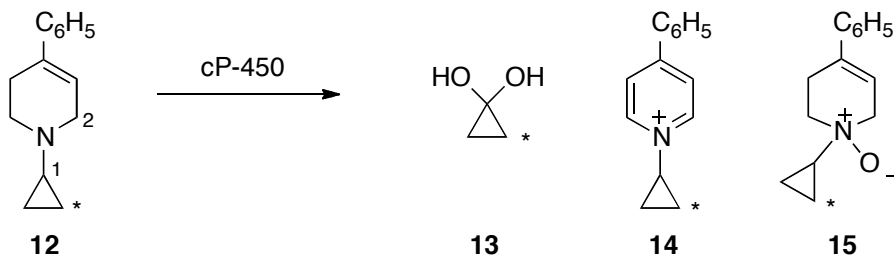
Several examinations utilizing kinetic isotope effects (KIEs) have been used to distinguish between a hydrogen atom abstraction pathway vs. an electron transfer mechanism. KIEs for a hydrogen abstraction process are estimated to be large ($k_H/k_D = 7$) conversely; KIEs for a SET process are expected to be smaller ($k_H/k_D = 1$).²⁴ Kinetic isotope effect experiments were conducted utilizing substituted *N,N*-dimethylaniline derivatives, in which one of the *N*-methyl groups showed an effect with a range of 1-2. This led to the hypothesis that the enzyme pathway was a result of a single electron transfer mechanism. To further elaborate on these examinations, several aliphatic and aromatic amines were exposed to HAT conditions utilizing *t*-butoxyl radical as the probe. KIEs on the order of 1.4 for aliphatic amines and 2-3.5 for aromatic amines were reported. These experiments concluded that electron transfer and hydrogen atom abstraction could not be distinguished by the magnitude of isotope effects alone.¹³

A set of experiments performed by Schaffer *et al.*, have yielded evidence against a SET mechanism.²⁵ Exposure of *N*-cyclopropyl-*N*-methylaniline (**9**) to HRP, an enzyme known to oxidize via an SET pathway, led exclusively to the formation of *N*-methylquinolinium (**10**). The formation of the quinolinium results from a ring opening reaction of the cyclopropyl group forming a primary carbon radical that adds to the phenyl ring. Analogous experiments utilizing cP-450 resulted in the formation of cyclopropanone hydrate (**11**), and did not show any evidence of cP-450 inactivation (**Scheme 3-4**).



Scheme 3-4 Oxidation of N-methyl-N-cyclopropyl amine by HRP and cP-450

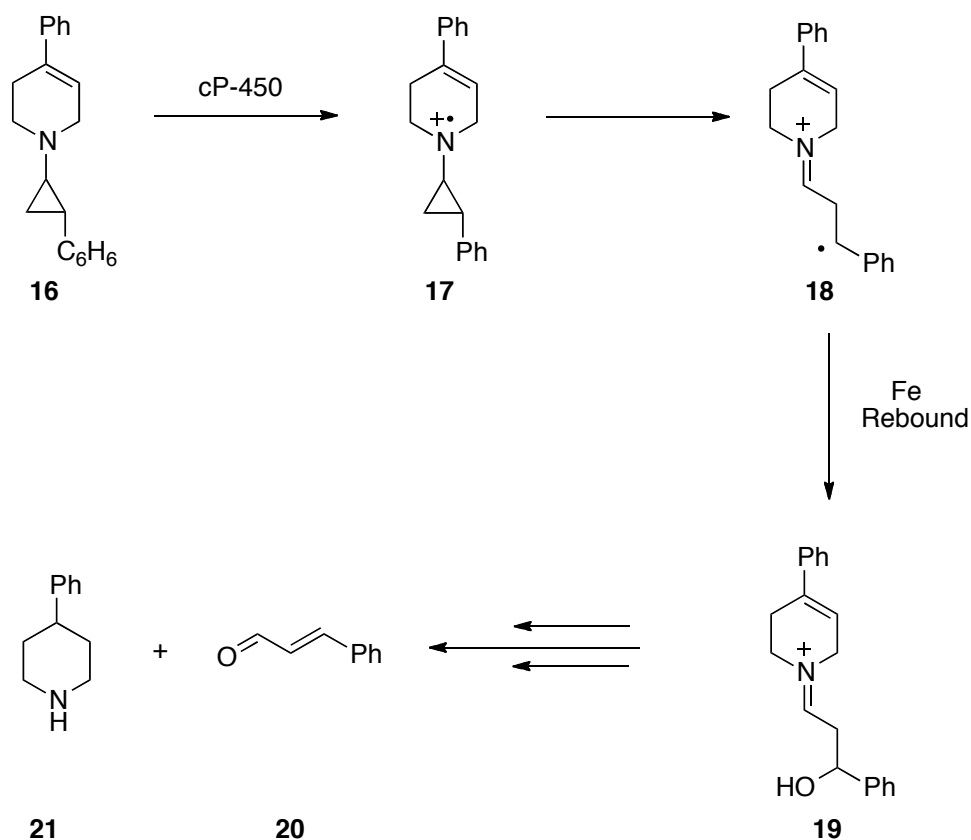
A recent enzymatic study utilizing ^{13}C labeled **12** as a substrate for cP-450 oxidation led to observation of four distinct products: (i) cyclopropanone-2-hydrate (**13**), (ii) 1-cyclopropyl-4-phenylpyridinium (**14**), and (iii) a diastereomeric mixture of 1-cyclopropyl-4-phenylpyridinium-N-oxide (**15**) (**Scheme 3-5**).²⁶ Compound **13** is presumably formed from the hydrogen atom abstraction reaction of **12** from the cyclopropyl carbon (C_1). Subsequent hydrolysis of the carbinolamine stemming from recombination of hydroxyl radical yields the corresponding cyclopropanone-2-hydrate (**13**). Compound **14** is formed by a hydrogen atom abstraction of the allylic (C_2) carbon of **12**. Four electron oxidation of the tetrahydropyridine by cP-450 results in the observed product **14**. The diastereomeric mixture **15** was formed via oxidation the amino nitrogen by the enzyme. These results provide evidence that the decyclopropylation reaction of cyclopropylamines proceeds via a HAT pathway.



Scheme 3-5 Products stemming from the oxidation of ^{13}C labeled oxidation of 1-cyclopropyl-4-phenyl-1,2,3,6-tetrahydropyridine.

Although initial examinations conducted by Bissel *et al.* provide compelling evidence for a HAT pathway, several mechanistic ambiguities have arisen based upon exposure of 4-phenyl-1-(*trans*-2-phenyl)cyclopropyl amine (**16**) to the enzyme. Analogous treatment of **16** to cP-450 resulted in products consistent with an SET pathway. The isolation of cinnamaldehyde (**20**) can best be explained via an SET process (**Scheme 3-6**). The authors conclude that the stability of the benzylic radical **18** may be the driving force for an SET pathway in this system, essentially

posing the question as to whether SET and HAT pathways are governed by a conformational effect or a resonance effect.



Scheme 3-6 Reaction of 4-phenyl-1-(*trans*-2-phenyl)cyclopropyl amine with cP-450.

3.2 Results and Discussion

3.2.1 *N*-Cyclopropyl-*N*-Methylaniline

Maslak *et al* developed a photochemical methodology to study the decay of a series of reactive radical cations.²⁷ A series of 1,2-dialkyl-1-(4'-(dimethylamino)phenyl)-2phenylethanes were selected due to their ability to fragment post excitation by the initial laser pulse (**Table 3-1**). Compounds were photolyzed directly at 266 nm utilizing nanosecond laser flash photolysis (LFP) to generate the parent radical cation. The initial laser pulse led to the formation of the reactive radical cation, which was characterized by an absorption maxima of 490 nm. Following

initial excitation a fragmentation reaction ensued due to a significant amount of strain about the C-C bond. The decay of the radical cation was accompanied by the appearance of a new band at 385 nm that was assigned to the formation of the benzyl cation. The rate of decay of all radical cations were measured to be on the order of 10^5 s^{-1} .

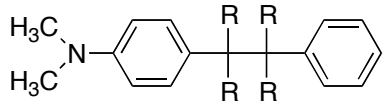
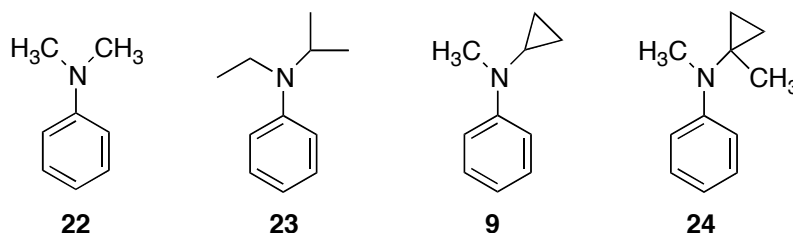
	$k \text{ (s}^{-1}\text{)}$	$\lambda_{\text{max}} \text{ (nm)}$
R = Ethyl	1.6×10^5	490
R = Propyl	4.4×10^5	490
R = Butyl	5.4×10^5	490

Table 3-1 Rate constants for the decay of radical cations used in the Maslak study.

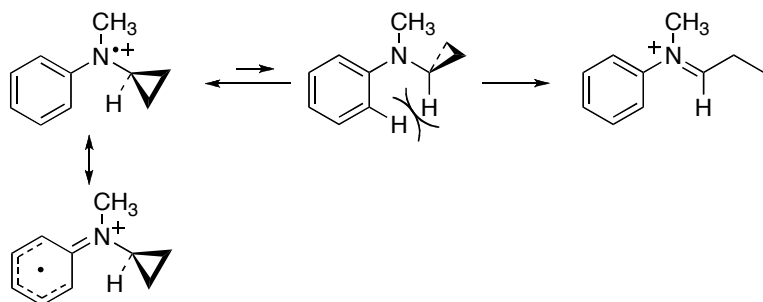
Recently in our laboratory, the kinetics of a series of aniline derivatives were examined (**Figure 3-3**).²² Direct photoionization at 266 nm (5% CH_3OH in CH_3CN) of *N,N*-dimethylaniline (**22**), *N*-ethyl-*N*-methylaniline (**23**), *N*-cyclopropyl-*N*-methylaniline (**9**), and *N*-methyl-*N*-cyclopropylaniline (**24**) utilizing LFP showed absorption maxima in the region 460-490 nm consistent with the formation of a reactive radical cation.²⁷ Although the molecules did show transient decays on the order of 10^6 s^{-1} with a λ_{max} of 460-490 nm, there was no indication that a ring opening pathway was occurring (**Figure 3-3**). This assumption is based on the fact that no rate enhancement was observed for the *N*-cyclopropyl derivatives (**9^{••}** and **24^{••}**) when compared to the parent compound *N,N*-dimethylaniline (**22^{••}**). Considering the fact that the rate constants for **22^{••}** and **23^{••}** were of the same order of magnitude as the *N*-cyclopropyl derivatives (**9^{••}** and **24^{••}**) - if ring opening is occurring, the rate constant must be less than or equal to 10^6 s^{-1} .



λ_{max} (nm)	460	470	480	490
k_{obs} (s^{-1})	3.1×10^6	1.07×10^6	2.6×10^6	6.4×10^6

Figure 3-3 Direct photoionization of anilines at 266nm

Photochemical experiments were augmented through linear sweep voltammetry and homogeneous redox catalysis examinations. Direct electrochemical examinations of $\mathbf{9}^{+\bullet}$ showed that the compound undergoes a unimolecular rearrangement consistent with a cyclopropyl ring opening reaction. Homogeneous redox catalysis experiments showed chemical step rate limiting behavior for three separate mediators. Examination of both the direct and indirect electrochemical data showed that the oxidation potential of *N,N*-dimethylaniline (+0.491 V) and *N*-methyl-*N*-cyclopropylaniline are comparable (+0.528 V vs. 0.1 M Ag+/Ag). Further examination of these results show that the rate constant for ring opening of $\mathbf{9}^{+\bullet}$ was $4.1 \times 10^4 \text{ s}^{-1}$. These results are best explained by two phenomena (**Scheme 3-7**): (i) a resonance effect in which the spin and charge of the radical cation in the ring closed form is delocalized into the benzene ring hindering the overall rate of the ring opening reaction, and/or (ii) the lowest energy conformation of the molecule does not meet the stereoelectronic requirements for a ring opening pathway. This chapter of the manuscript will address the stereoelectronic effects. A detailed discussion of resonance effects will be presented in the subsequent chapter.



Scheme 3-7 Depiction of (i) resonance delocalization of the radical cation, and (ii) stereoelectronic requirements for ring opening.

Profiles of compound **9⁺** examining rotation about the *N*-cyclopropyl bond at the B3YLP level of theory revealed a 3.6 kcal/mol difference in energy between the bisected and perpendicular conformations. In light of these results, a new generation of substrates were synthesized in order to overcome these stereoelectronic effects (**Figure 3-4**). The novel substrates were designed to effectively lock the cyclopropyl group in the bisected conformation, therefore allowing one to study the rate constant for ring opening without the added rotational barrier that exists for the *N*-cyclopropyl aniline systems.

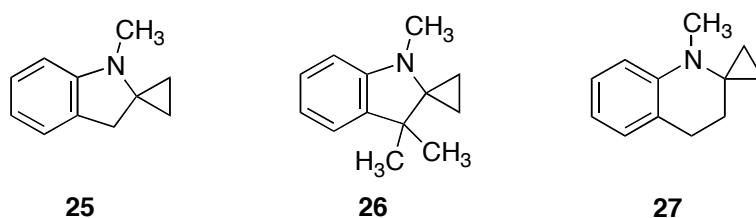
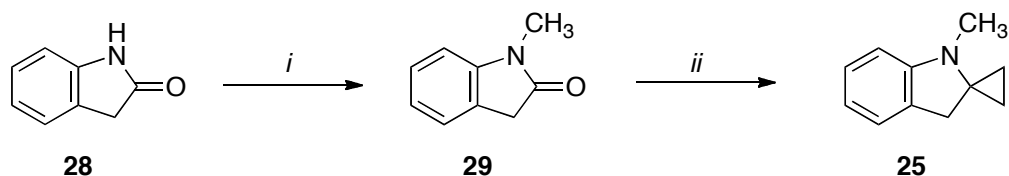


Figure 3-4 New series of compounds for study

3.2.2 1'-methyl-3',4'-dihydro-1*H*-spiro[cyclopropane-1,2'-quinoline] (**25**):

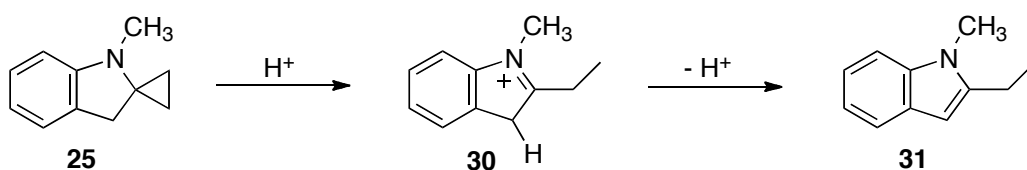
3.2.2.1 Substrate Synthesis

Compound **25** was envisioned to come from the commercially available indole **28**. Addition of a methyl group to the amide utilizing sodium hydride and dimethyl sulfate was expected to give rise to 1-methylindolin-2-one (**29**).²⁸ The desired product **25** was to be formed by a titanium mediated cyclopropanation reaction (**Scheme 3-8**).²⁹

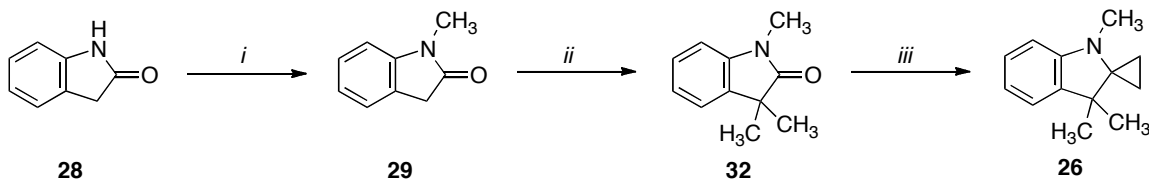


Scheme 3-8 Attempted synthesis of 1'-methylspiro[cyclopropane-1,2'-indoline]: (i) NaH, dimethylsulfate, xylene, reflux 2hr.; (ii) Ti(O^{*i*}Pr)₄, CH₃CH₂MgBr, -78°C to RT, 17 hrs.

The first step of the synthesis was successful in yielding the amide **29** in 57% yield. The subsequent cyclopropanation reaction was unsuccessful: the only material isolated was 2-ethyl-1-methyl-1*H*-indole (**31**). **25** was presumed to undergo a ring opening reaction to generate the unstable iminium ion **30**, which can then lose a proton and isomerize to give the corresponding conjugated ring system (**Scheme 3-9**). Driving force for this reaction was the formation of the aromatic indole **31**.



Scheme 3-9 Proposed cyclopropane ring opening reaction in the presence of mild acid. In order to circumvent the formation of the aromatic indole **31**, a modification to the original synthesis was proposed. Two methyl groups would be installed alpha to the amide carbonyl to prevent isomerization (**32**). The synthesis would utilize the first step of the previous sequence, but a step to install two methyl groups prior to the cyclopropanation reaction would be added to the synthetic plan (**Scheme 3-10**).

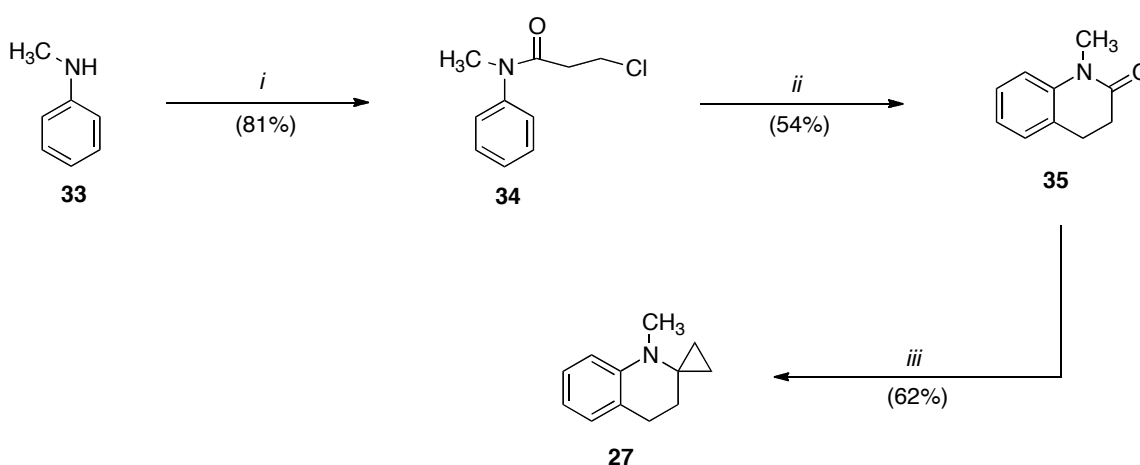


Scheme 3-10 Attempted synthesis of 1',3',3'-trimethylspiro[cyclopropane-1,2'-indoline]: (i) NaH, dimethylsulfate, xylene, reflux 2hr.; (ii) LDA, 2x CH₃I -78°C; (iii) Ti(OⁱPr)₄, CH₃CH₂MgBr, -78°C to RT, 17 hrs.

Compound **29** was treated with lithium diisopropyl amine (LDA) and an excess of methyl iodide to yield the 1,3,3-trimethylindolin-2-one (**32**) in 56% yield. The following reaction utilizing titanium isopropoxide and ethyl magnesium bromide was attempted, but only recovered starting

material **32** was ever isolated. No product was ever detected, presumably due to the steric bulk created by the additional methyl groups alpha to the reactive carbonyl.

Although neither attempt to synthesize the indole derivative resulted in the desired product, the issue was resolved by changing the base structure to a quinoline derivative. Compound **34** was synthesized by treatment of *N*-methylaniline with the 3-chloropropanoyl chloride to give the corresponding 3-chloro-*N*-methyl-*N*-phenylpropanamide (**34**) in 81% yield. **34** was subjected to a Friedel Crafts reaction to generate 1-methyl-3,4-dihydroquinolin-2(1*H*)-one (**35**) in 54% yield. The final reaction, a titanium mediated cyclopropylation reaction was successful in giving the final product, 1'-methyl-3',4'-dihydro-1'*H*-spiro[cyclopropane-1,2'-quinoline], (**27**) in 62% yield (**Scheme 3-11**).



Scheme 3-11 Synthesis of 1'-methyl-3',4'-dihydro-1'*H*-spiro[cyclopropane-1,2'-quinoline]: (i) ClC(O)CH₂CH₂Cl, acetone, reflux 2.5 hrs.; (ii) AlCl₃, 17 hrs.; (iii) Ti(O^{*i*}Pr)₄, CH₃CH₂MgBr, -78C to RT, 15 hrs.

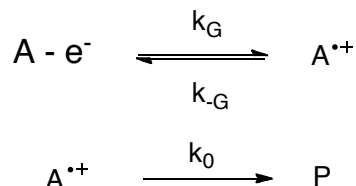
3.2.2.2 Laser Flash Photolysis

Direct photoionization of **27** at 266 nm (5% CH₃OH in CH₃CN) utilizing laser flash photolysis showed an absorption maxima of 500 nm, consistent with the formation of the reactive radical cation **27^{•+}**. Transient absorption spectra showed a rate of decay of 1.1 x 10⁶ s⁻¹ for compound

27^{•+}. Comparing the LFP results of **9** and **27** with compound **22**, it is readily apparent that no rate enhancement can be attributed to cyclopropane ring opening. Because the rate of decay of **27^{•+}** is of the same order of magnitude as **22^{•+}**, it can be surmised that if ring opening is occurring, then the rate constant must be less than or equal to 10^6 s^{-1} .

3.2.2.3 Direct Electrochemistry

Cyclic voltammetry is a method that can be used to examine the kinetics of an electron transfer process. If a substrate can undergo a subsequent chemical transformation post electron transfer, the process is deemed to proceed via an EC mechanism (Electron transfer followed by a Chemical step) (**Scheme 3-12**).^{17, 19} During an EC process the substrate is oxidized at the electrode surface to generate $A^{\bullet+}$, and $A^{\bullet+}$ can then go on to form products. Kinetic information can be gained from voltammograms once several key components have been identified. Important components of the voltammogram include: (i) E_p – peak potential, (ii) i_p – peak current, (iii) $E_{p/2}$ – half wave potential, and (iv) $(E_p - E_{p/2})$ – peak width.



Scheme 3-12 Representation of the EC mechanism.

Experimental runs of compound **27** consisted of measuring the peak potential at multiple scan rates ($\nu = 100 - 1000 \text{ mV/sec}$). Sample runs were measured at multiple concentrations. Characteristic features of the voltammograms included: (i) Peak potentials (E_p) on the order of 270 mV at 100 mV, (ii) Peak widths ($E_p - E_{p/2}$) between 50-60 mV, and (iii) a change in peak potential with respect to the scan rate ($dE_p/d\log \nu$) of 27.01 +/- 3 mV. A representative voltammogram is shown in **Figure 3-5**.

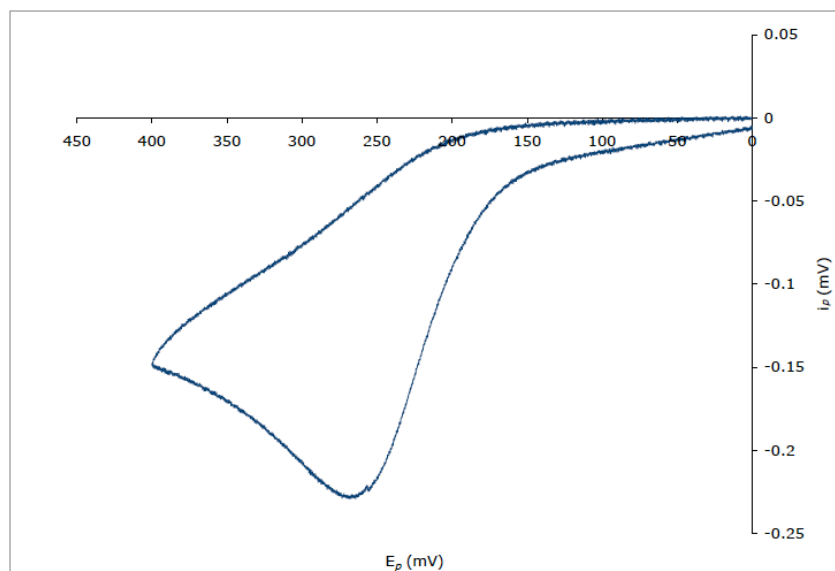


Figure 3-5 Cyclic voltammogram of **27** (0.1 M LiClO₄, 0.5 M CH₃OH/CH₃CN, $\nu = 100$ mV/sec, 4.65 mM substrate)

Theoretical parameters for chemical step rate limiting behavior predict a change in peak potential with respect to the log of the scan rate to be 30 mV/decade. Results for this system suggest a rate limiting chemical step following an EC mechanism (**Figures 3-6, 3-7, and 3-8**).

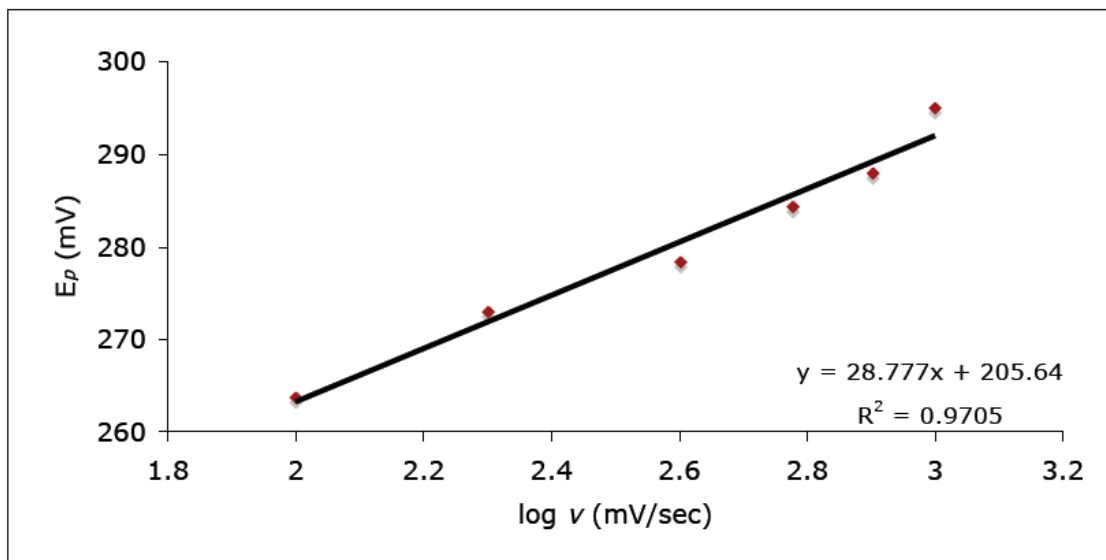


Figure 3-6 LSV analysis of **27**, $\partial E_p / \partial \log \nu$ at 2.6 mM concentration. (0.1 M LiClO₄, 0.5 M CH₃OH/CH₃CN, $\nu = 100$ -1000 mV/sec)

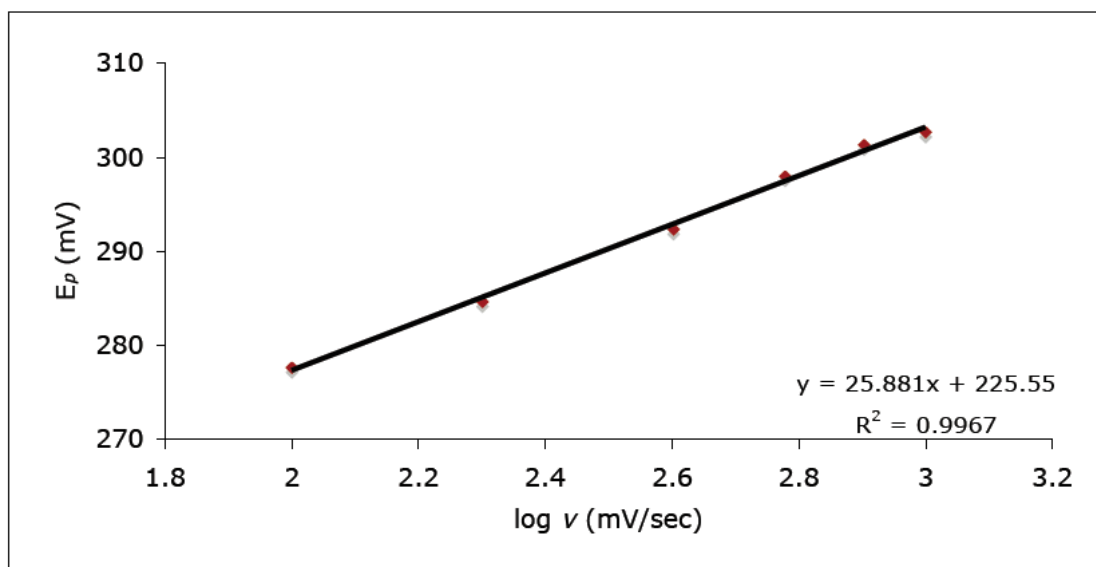


Figure 3-7 LSV analysis of **27**, $\partial E_p/\partial \log v$ at 4.6 mM concentration. (0.1 M LiClO₄, 0.5 M CH₃OH/CH₃CN, $v = 100$ -1000 mV/sec)

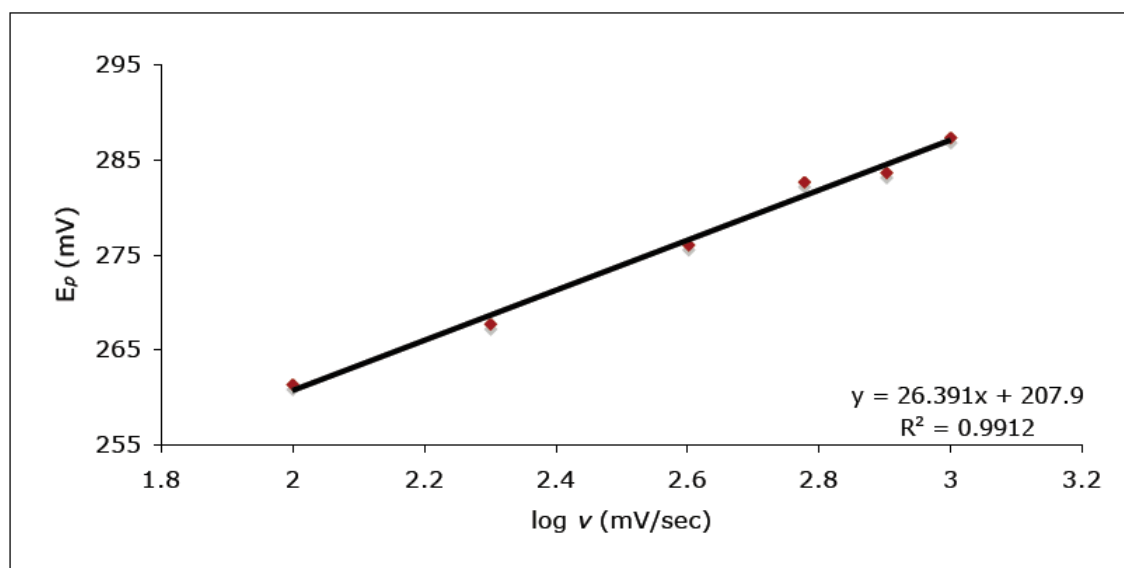


Figure 3-8 LSV analysis of **27**, $\partial E_p/\partial \log v$ at 8.7 mM concentration. (0.1 M LiClO₄, 0.5 M CH₃OH/CH₃CN, $v = 100$ -1000 mV/sec)

Secondary experiments were conducted in order to probe for a nucleophilic assisted pathway.

These studies entailed varying methanol concentration and holding the substrate concentration

constant. Theoretical parameters for a nucleophilic pathway are as follows: peak potentials will vary by 30 mV per ten fold increase in scan rate, and peak potentials will also have a variance of 30 mV per tenfold increase in concentration of nucleophile.³⁰ No correlation between peak potential and methanol concentration was ever observed, indicating the rate of decay of the radical cation is zero order in methanol. This result essentially demonstrates that a nucleophile (methanol)-assisted ring opening is not occurring.

Lastly, a dimerization mechanism was probed for this system. Experiments consisted of varying the substrate concentration and measuring peak potentials at constant scan rate. Theoretical parameters for a dimerization mechanism are as follows: peak widths on the order of 39 mV, and peak potentials will vary by 20 mV per ten fold increase in scan rate.³⁰ Peak potentials will also have a variance of 20 mV per tenfold increase in concentration. **Figure 3-9** shows no correlation between peak potential and concentration, indicating that a dimerization pathway is unlikely.

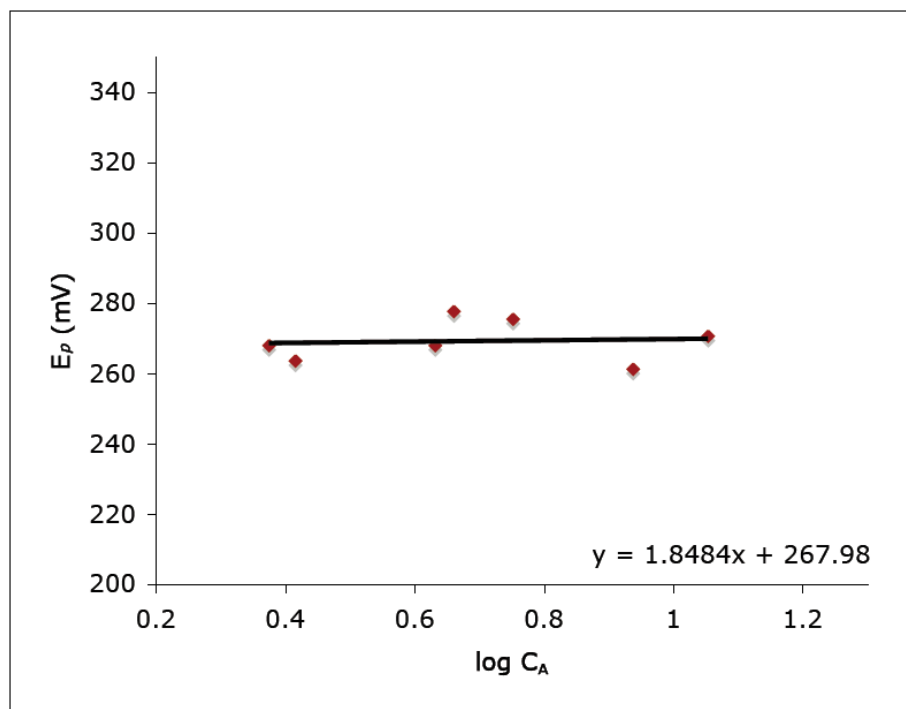


Figure 3-9 LSV analysis of **27**, $\partial E_p/\partial \log C_A$ at multiple concentrations. (0.1 M LiClO₄, 0.5 M CH₃OH/CH₃CN, $\nu = 100$ mV/sec)

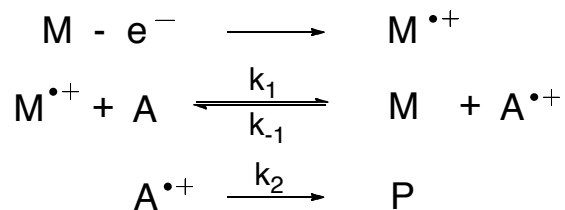
From the above analysis we can conclude that the chemistry of **27** is governed by chemical step rate limiting behavior. Subsequent analysis shows that a dimerization pathway is unlikely. A potential nucleophilic pathway was eliminated due to the fact that there was no correlation of peak potential with respect to methanol concentration. These results are summarized in **Table 3-2**.

Mechanism	$\frac{dE_p}{d \log v}$	$\frac{dE_p}{d \log C_A}$	$\frac{dE_p}{d \log C_{MeOH}}$
$k[B][X]$ $B + X \rightarrow C$	30	0	30
$k[B]^2$ $2B \rightarrow C$	19.7	19.7	0
$k[B]$ $B \rightarrow C$	30	0	0
Experimental Values	27 ± 2	1.85 ± 10.5	0 ± 1.2

Table 3-2 Summary of direct electrochemical results.

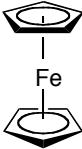
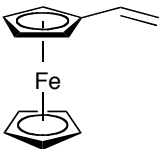
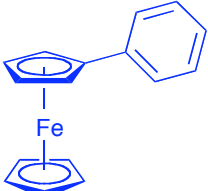
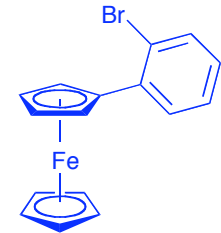
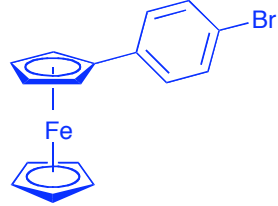
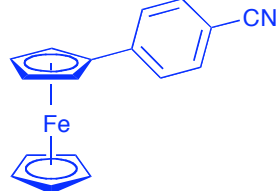
3.2.2.4 Indirect Electrochemistry

Mediated redox catalysis is a common technique used to further gain kinetic data through electrochemical methods. This methodology differs from direct electrochemical methods because an electroactive compound is used to facilitate homogeneous electron transfer. Mediator **M** is oxidized to form **M^{•+}**, **M^{•+}** will react with **A** to give **A^{•+}**, and **A^{•+}** can then go on to products.



In a successful mediated redox catalysis experiment the mediator must contain three basic properties: (i) the mediator must be easier to oxidize than the substrate, (ii) the oxidation of the

mediator should be fast at the electrode surface, and (iii) the electrochemistry of the mediator must be reversible (Nernstian). Below is a table of mediators used for our efforts.

Ferrocene	E_{ox} (0.1 M Ag+/Ag)
 36a	32 mV
 36b	55 mV
 36c	70 mV
 36d	100 mV
 36e	94 mV**
 36f	145 mV**

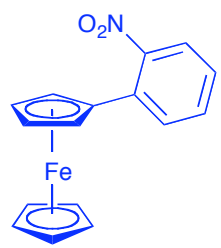
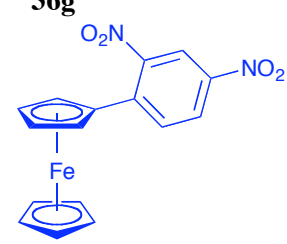
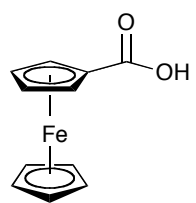
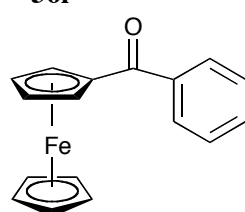
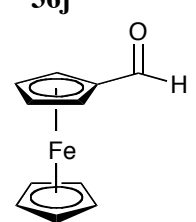
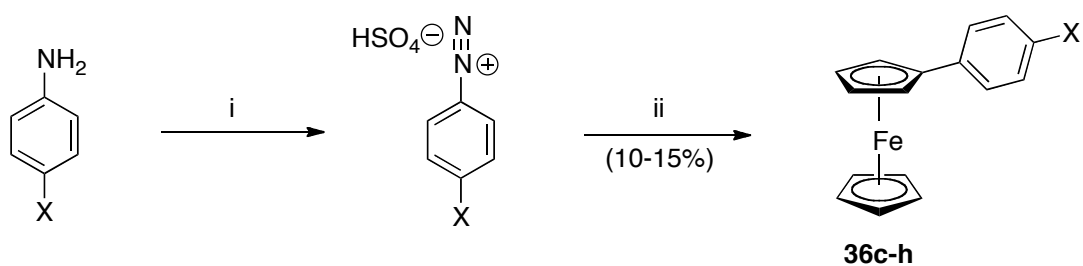
 <p>36g</p>	143 mV**
 <p>36h</p>	280 mV
 <p>36i</p>	264 mV
 <p>36j</p>	290 mV
 <p>36k</p>	310 mV

Table 3-3 Listing of mediators used in our laboratory. Compounds in black denote commercially available compounds. Compounds in blue were synthesized in our laboratory.

For our system, commercially available mediators were not in the appropriate potential range for redox catalysis. Therefore several mediators were synthesized in our laboratory. The synthesis of these mediators was achieved with the use of commercially available anilines and ferrocene. Anilines were suspended in aqueous sulfuric acid, sodium nitrite was then added to the mixture

to form a diazonium ion. Following formation of the diazonium, ferrocene was added and solutions were allowed to react for several days (**Scheme 3-13**). This methodology was employed for all non-commercially available mediators used for this study. Mediators were all successfully prepared, albeit in low yields.



Where X = H, CN, Br, NO₂

Scheme 3-13 Synthesis of modified ferrocenes for reductive catalysis experiments: (i) NaNO₂, 20% H₂SO₄, 0° C; (ii) ferrocene, 0° C to RT, 48hrs.

Traditional data analysis of redox catalysis data is processed by analyzing peak current ratios ((i) i_p – current drawn from mediator and substrate, and (ii) i_{pd} – current drawn from mediator by itself) and plotting them against mediator concentration (C_M^o) at constant γ . When the chemical step is rate limiting, the electron transfer step is a pre-equilibrium and the concentration of the mediator is independent of the peak current ratio. The system is governed by the dimensionless parameters λ , λ_1 , λ_{-1} , and γ that are expressed in the form $\lambda\lambda_1/\lambda_{-1}$ (**Equations 3-1 through 3-4**).⁵

31, 32

$$\lambda = \left(\frac{RT}{F}\right) \left(\frac{k_2}{v}\right) \quad \text{Equation 3-1}$$

$$\lambda_1 = \left(\frac{RT}{F}\right) \left(\frac{k_1[M]}{v}\right) \quad \text{Equation 3-2}$$

$$\lambda_{-1} = \left(\frac{RT}{F}\right) \left(\frac{k_{-1}[M]}{v}\right) \quad \text{Equation 3-3}$$

$$\gamma = \frac{[A]}{[M]} \quad \text{Equation 3-4}$$

A series of theoretical working curves have been developed for this mechanistic regime that compare the peak current ratio (i_p/i_{pd}) to the dimensionless parameter $\lambda\lambda_1/\lambda_{-1}$. Comparison of plots [i_p/i_{pd} vs. $\log(1/\nu)$] and [i_p/i_{pd} vs. $\log C_M^0/\nu$] will unambiguously show any mediator dependence in the system. Peak current ratio (i_p/i_{pd}) is a function of $\log(1/\nu)$ when the chemical step is rate limiting, thus plots of [i_p/i_{pd} vs. $\log(1/\nu)$] will converge to one line, while plots of [i_p/i_{pd} vs. $\log C_M^0/\nu$] will show three distinct curves. The difference between the experimental data and the theoretical values obtained from the working curves is directly related to the rate constant for the chemical step. **Figure 3-10** and **3-11** show some representative examples of the data obtained for compound **27**.

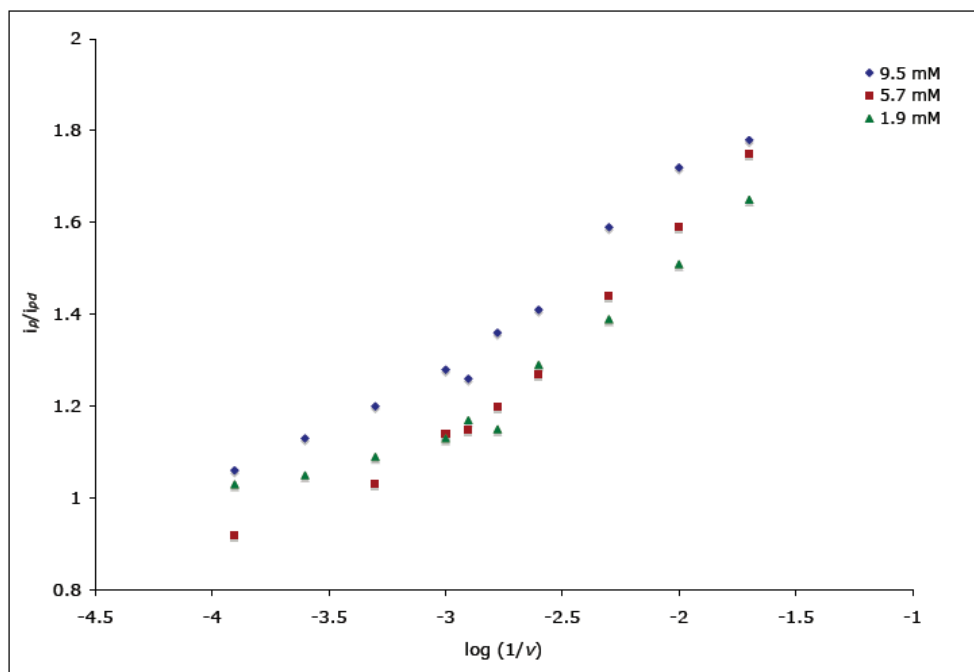


Figure 3-10 [i_p/i_{pd} vs. $\log(1/\nu)$] – Mediated redox catalysis of **27** by 4-cyanophenylferrocene (**36f**), (0.1 M LiClO₄, 0.5 M CH₃OH/CH₃CN, $\gamma = 1$, $\nu = 100$ -8000 mV/sec)

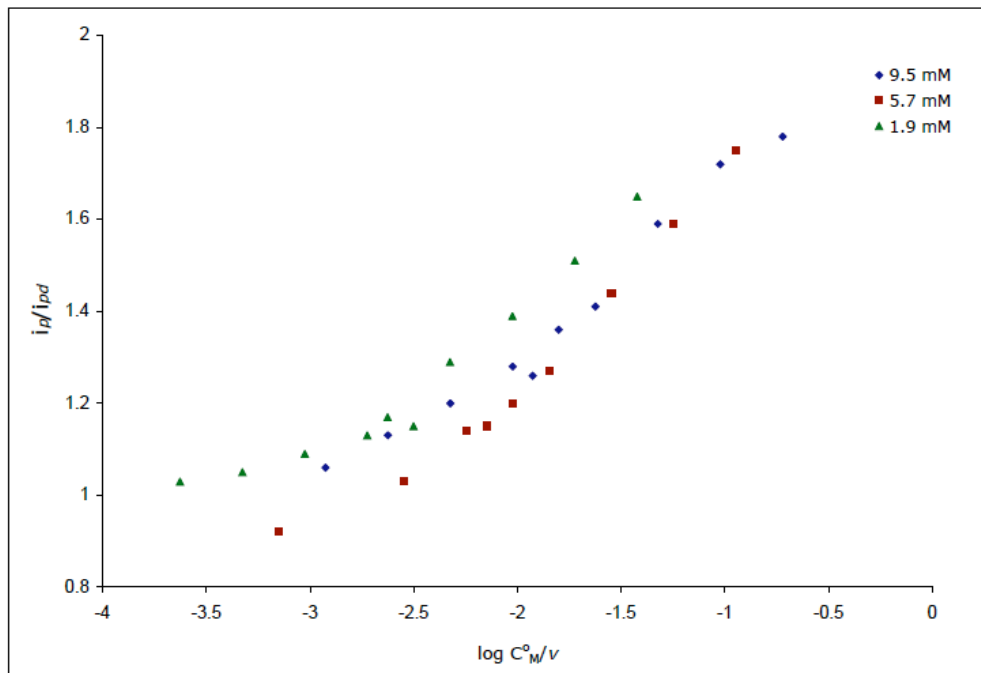


Figure 3-11 $[i_p/i_{pd}]$ vs. $\log C_M^o/v$ – Mediated redox catalysis of **27** by 4-cyanophenylferrocene (**36f**), (0.1 M LiClO₄, 0.5 M CH₃OH/CH₃CN, $\gamma = 1$, $v = 100$ -8000 mV/sec)

Electron transfer or chemical step rate limiting behavior cannot be resolved from these plots (**Figures 3-10** and **3-11**). This results from the fact that the data shows a second oxidative wave that can be seen at higher scan rates. At low scan rates typical redox catalysis behavior is observed, but as the scan rate is increased one can observe the appearance of two distinct oxidative waves: the first can be attributed to the catalytic wave, and the second wave is due to the oxidation of the substrate itself (**Figure 3-12**). The main thermodynamic requirements for redox catalysis are as follows: the mediator should be more easily oxidized than the redox couple A/A^{*+} , and the follow up reaction must be fast and irreversible.³³ Catalysis arises from the driving force of the followup chemical reaction; therefore, for a typical redox catalysis experiment, the loss of substrate will result in an overpotential that is needed to drive the electron transfer step in an attempt to maintain equilibrium as governed by the Nernst equation. If these

requirements are not met, there will be no driving force for the homogeneous electron transfer and redox catalysis will not occur. The formation of the second oxidative wave directly results from the fact that the follow up chemistry is slow, and therefore does not efficiently facilitate catalysis.

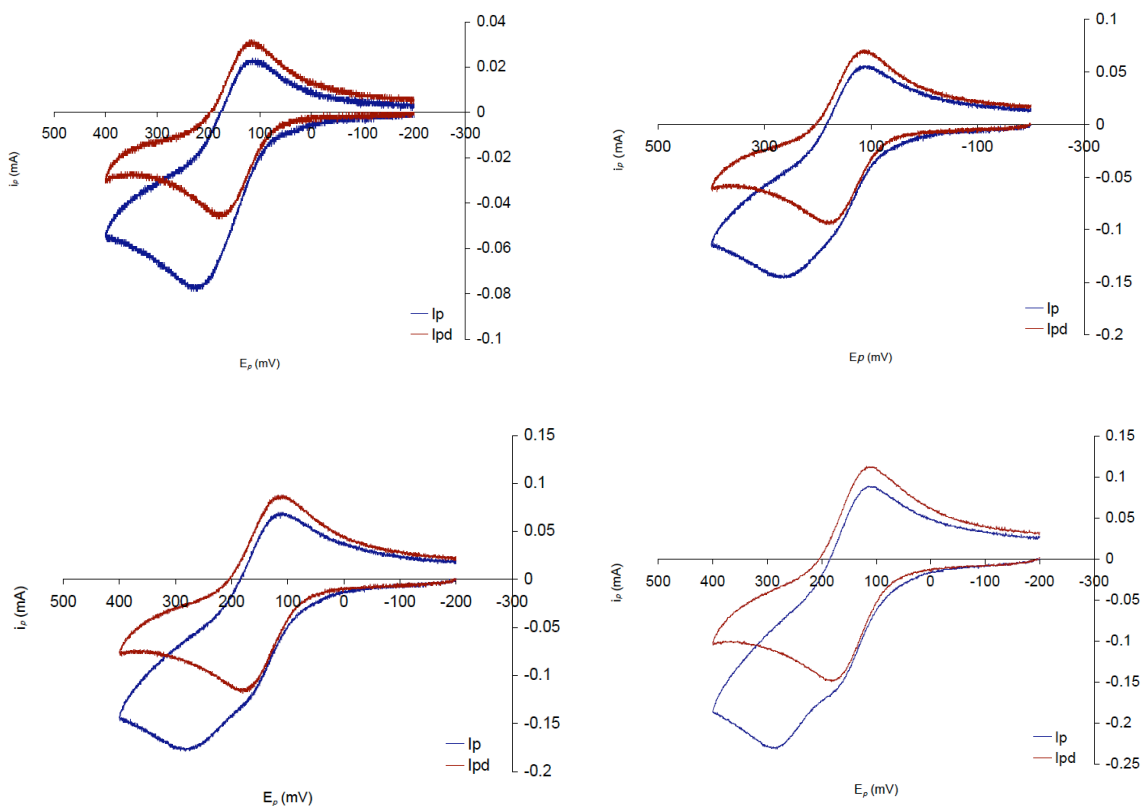


Figure 3-12 Mediated redox catalysis of **27** by 4-cyanophenylferrocene (**36f**), (0.1 M LiClO₄, 0.5 M CH₃OH/CH₃CN, $\gamma = 1$, (i) $\nu = 100$ mV, (ii) $\nu = 400$ mV, (iii) $\nu = 600$ mV, (iv) $\nu = 1000$ mV

To circumvent this problem, experiments were run in the presence of additional substrate to drive the equilibrium of the followup chemistry to the right. This was achieved by adding substrate to the mediator while keeping the scan rates low to ensure efficient catalysis (**Figure 3-13**). From **Figure 3-13** it is evident that as substrate is added, catalytic activity increases, and therefore catalysis is occurring.

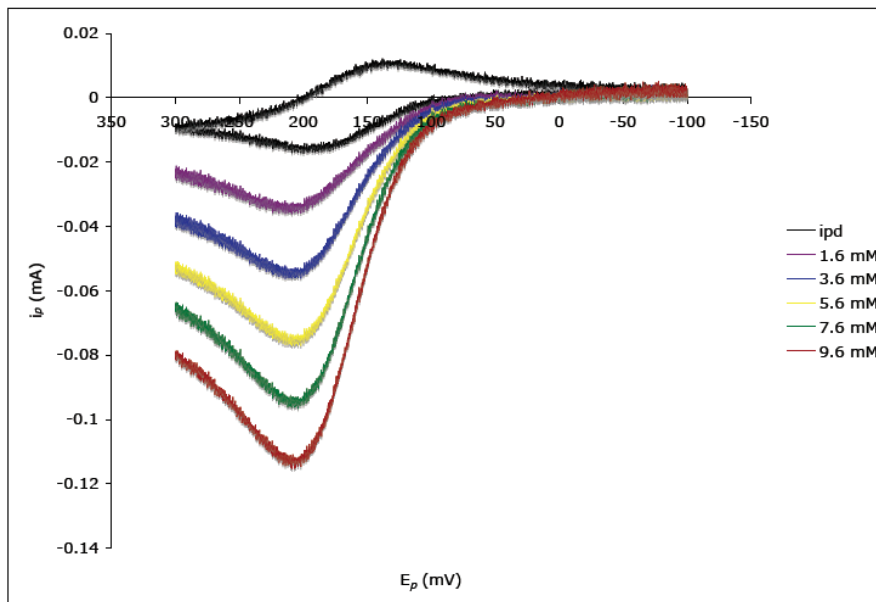
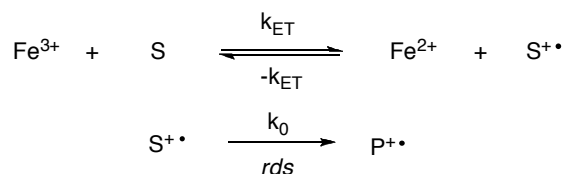


Figure 3-13 Mediated redox catalysis of **27** with 4-cyanophenylferrocene (**36f**), (CH_3CN , 0.5M CH_3OH , 0.5M $\text{nBu}_4\text{N}^+\text{BF}_4^-$, $\nu = 25$ mV, $\gamma = 1, 2.24, 3.48, 4.73, 5.97$)

Working curves have been derived previously to describe the behavior of mediator and substrate to express i_p/i_{pd} as a function of γ .³¹ The data could not be evaluated using the traditional methods that have been employed in our laboratory, therefore a series of theoretical working curves were generated by modeling the reaction mechanism using digital simulation software (**Scheme 3-14**). Experimental conditions (e.g., γ and E_{ox} of the mediator) were entered into the simulations as dictated by the experiment. Values for k_0 were methodically adjusted to obtain a curve that best fit the experimental data. The appropriate working curves were derived by plotting $1/\gamma^*(I_p/I_{pd})$ vs. γ , to obtain a value for a composite rate constant k_{obs} (**Equation 3-5**). A detailed explanation of the parameters used to generate these working curves is described in the experimental section.



Scheme 3-14 Mechanism used to model the chemical step rate limiting pathway for compound **27**.

Once a value of the composite rate constant (k_{obs}) was obtained from the theoretical working curves, equations **3-6** and **3-7** could be used to solve for the formal oxidation potential ($E^{\circ}_{substrate}$) and rate constant for ring opening (k_0) for each mediator^{31, 34}

$$k_{obs} = K_{eq}k_0 \quad \text{Equation 3-5}$$

$$E_p = E_{ox} - \left(\frac{0.78RT}{nF} \right) - \frac{RT}{2nF} \ln \left(\frac{k_0RT}{vnF} \right) \quad \text{Equation 3-6}$$

$$k_{obs} = k_0 e^{\left[\frac{F}{RT} (E^{\circ}_{substrate} - E^{\circ}_{mediator}) \right]} \quad \text{Equation 3-7}$$

Experimental data correlated to the ‘best fit’ theoretical working curve is shown in **Figure 3-14**.

After obtaining a value for k_{obs} from equation **3-5** and solving equations **3-6** and **3-7**, a value of 0.299V was obtained for $E^{\circ}_{substrate}$ and a value of $3.1 \times 10^2 \text{ s}^{-1}$ was obtained k_0 using **36f** as a mediator.

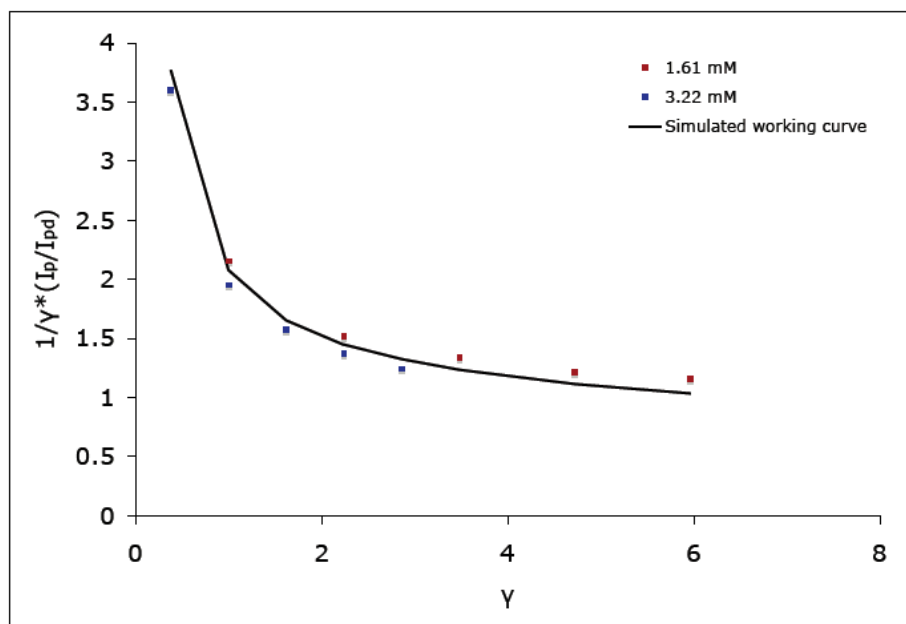


Figure 3-14 Fitting results of the results for mediated catalysis of **27** with 4-cyanophenylferrocene (**36f**) with digitally simulated working curves ($k_0 = 1.1 \times 10^5$).

To ensure validation for the values obtained with **36f**, a second series of experiments was conducted utilizing 2-nitrophenylferrocene (**36g**) as a mediator for compound **27**. **Figure 3-15** shows that redox catalysis is indeed occurring with this mediator. Analysis utilizing the same methodology resulted in a value of 0.301V for $E^{\circ}_{\text{substrate}}$ and the rate constant (k_0) was found to be $3.8 \times 10^2 \text{ s}^{-1}$.

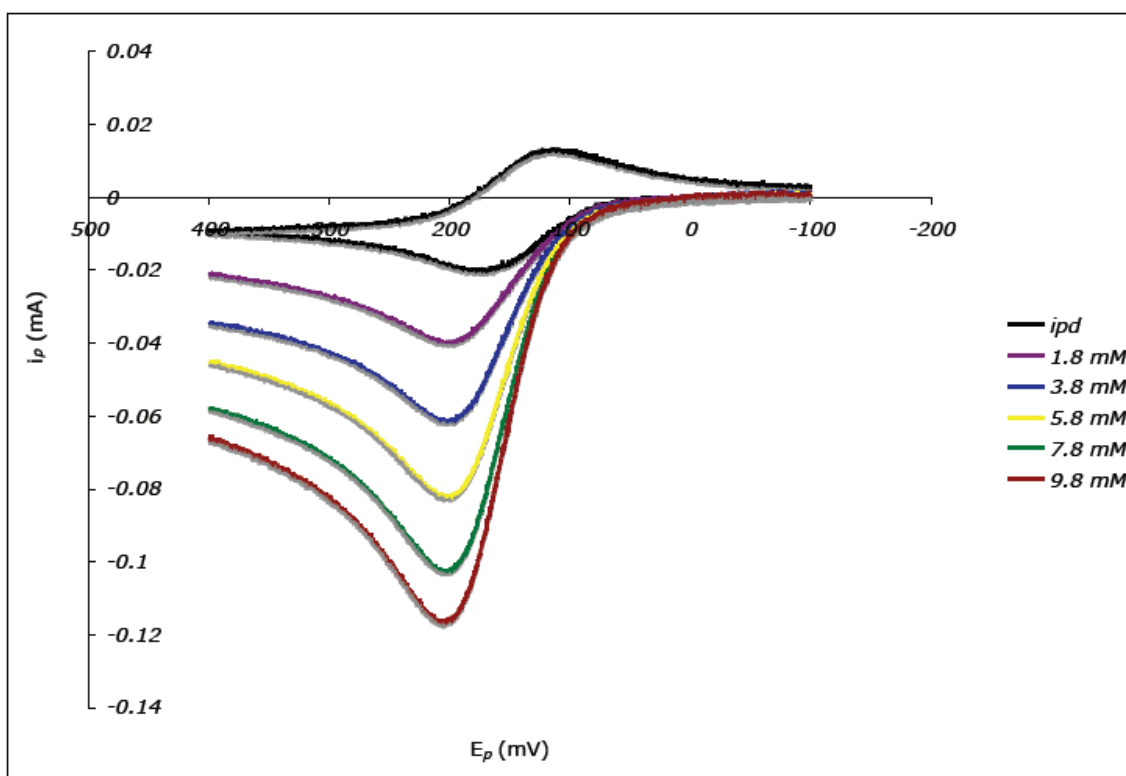


Figure 3-15 Redox Catalysis of **27** with 2-nitrophenylferrocene (**36g**) (CH_3CN , 0.5M CH_3OH , 0.5M $\text{nBu}_4\text{N}^+\text{BF}_4^-$, $\nu = 25 \text{ mV}$, $\gamma = 1, 2.1, 3.2, 4.3, 5.4$)

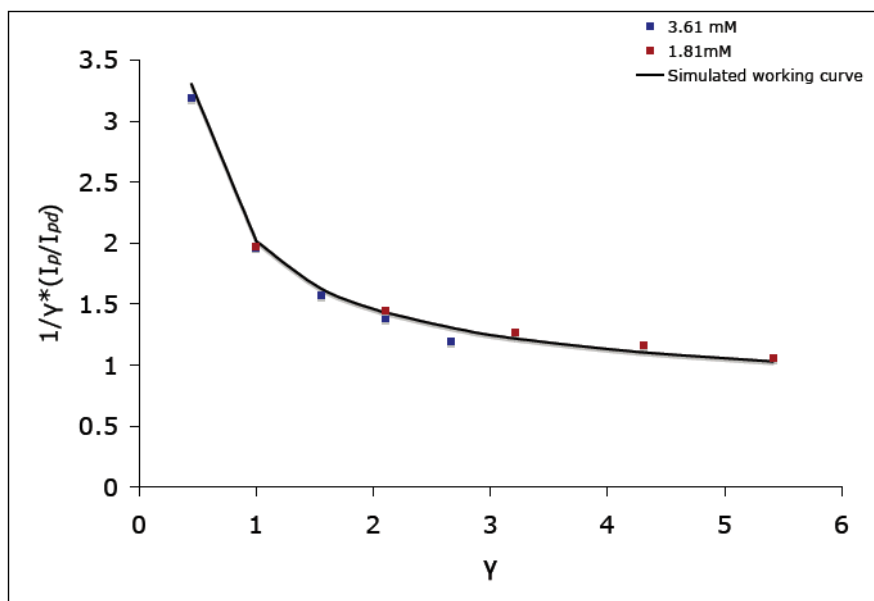


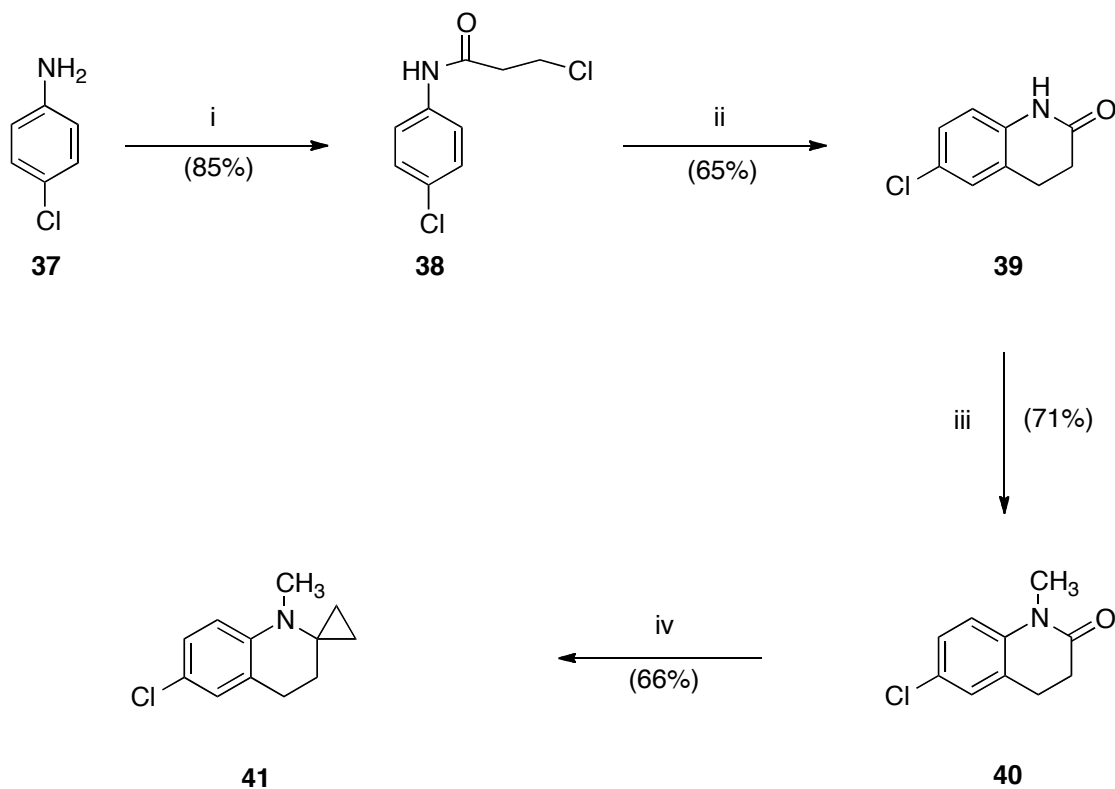
Figure 3-16 Fitting results of the results for mediated catalysis of **27** with 2-nitrophenylferrocene (**36g**) with digitally simulated working curves ($k_0 = 9.7 \times 10^4$).

3.2.3 6'-chloro-1'-methyl-3',4'-dihydro-1'H-spiro[cyclopropane-1,2'-quinoline] (**41**)

3.2.3.1 Substrate Synthesis

Due to the fact that 4-chloro- *N*-cyclopropyl-*N*-methylaniline has been used as an electron transfer probe for cP-450 oxidations the chlorinated version of compound **27** was also examined. A second desirable feature of this structure is that the potential for a dimerization pathway is eliminated due to the chlorine blocking the 4-position of the quinoline ring. The synthetic route to generate compound **41** was modified by adding a step in the sequence to install the *N*-methyl group. Attempts to use the same methodology for **41** that was used for **25** were unsuccessful. Treatment of 4-chloroaniline (**37**) with the 3-chloropropanoyl chloride gave the corresponding amide **38** in 85% yield. The amide was then subjected to a Freidel Crafts reaction to generate the quinoline **39** in 65% yield. The amide nitrogen was then alkylated utilizing sodium hydride and dimethyl sulfate yielding compound **40** in 71% yield. The final titanium mediated

cyclopropylation reaction was successful in giving the final product 6'-chloro-1'-methyl-3',4'-dihydro-1'*H*-spiro[cyclopropane-1,2'-quinoline] (**41**) in 66% yield (**Scheme 3-15**).



Scheme 3-15 Synthesis of 6'-chloro-1'-methyl-3',4'-dihydro-1'*H*-spiro[cyclopropane-1,2'-quinoline]: (i) ClC(O)CH₂CH₂Cl, acetone, reflux 2.5 hr.; (ii) AlCl₃, 17 hr.; (iii) NaH, dimethylsulfate, xylene, reflux 2 hr. (iv) Ti(O^{*i*}Pr)₄, CH₃CH₂MgBr, -78 C to RT.

3.2.3.2 Direct Electrochemistry

Experimental runs of compound **41** consisted of measuring the peak potential at multiple scan rates ($\nu = 100\text{-}1000$ mV/sec). Sample runs were measured at multiple concentrations. Characteristic features of the voltammograms included: (i) Peak potentials (E_p) on the order of 310 mV at 100 mV, (ii) Peak widths ($E_p - E_{p/2}$) between 50-60 mV, and (iii) a change in peak potential with respect to the scan rate ($dE_p/d\log \nu$) of 27.01 ± 1.3 mV. A representative voltammogram is shown in **Figure 3-17**.

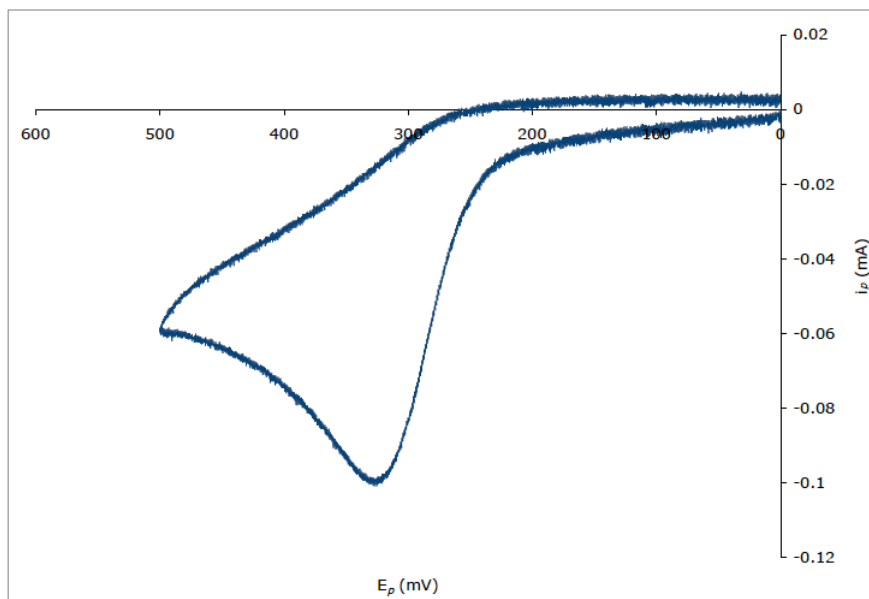


Figure 3-17 Cyclic voltammogram of **41** (0.1 M LiOCl₄, 0.5 M CH₃OH/CH₃CN, $\nu = 100$ mV/sec, 4.65 mM substrate)

Theoretical parameters for chemical step rate limiting behavior predict a change in peak potential with respect to the log of the scan rate to be 30 mV/decade. Results for this system suggest rate limiting chemical step following an EC mechanism (**Figures 3-18** and **3-19**).

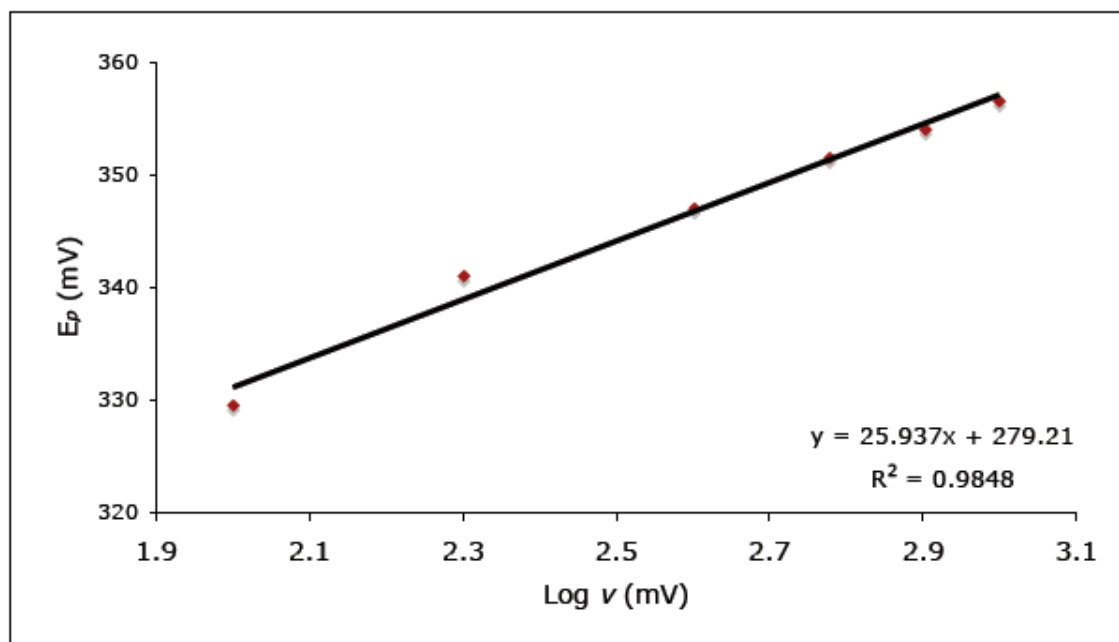


Figure 3-18 LSV analysis of **41**, $\partial E_p/\partial \log \nu$ at 2.2 mM concentration. (0.1 M LiClO₄, 0.5 M CH₃OH/CH₃CN, $\nu = 100$ -1000 mV/sec).

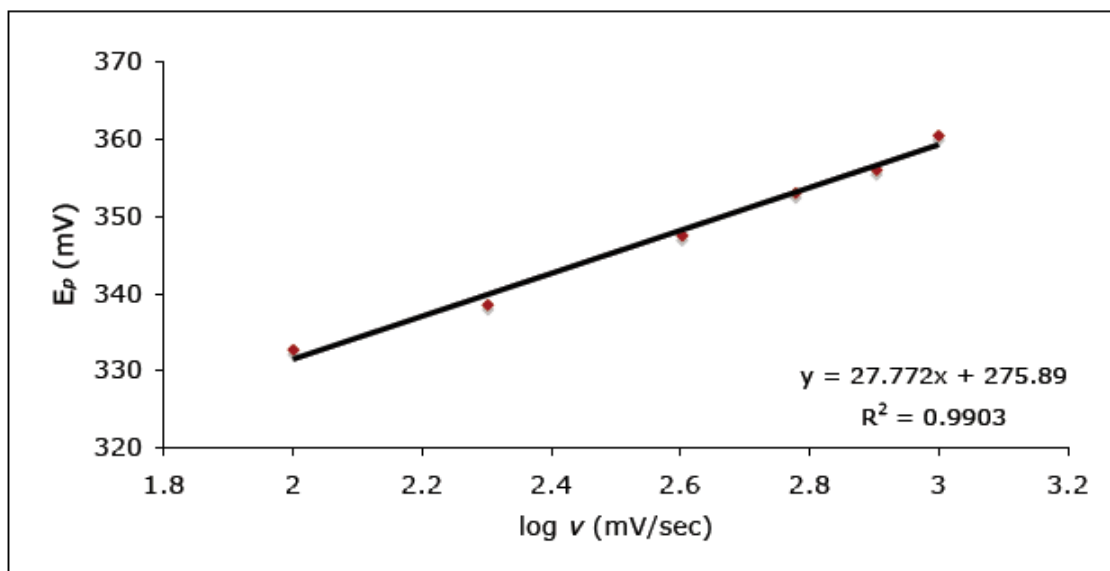


Figure 3-19 LSV analysis of **41**, $\partial E_p/\partial \log v$ at 5.3 mM concentration. (0.1 M LiClO₄, 0.5 M CH₃OH/CH₃CN, $v = 100$ -1000 mV/sec).

3.2.3.3 Indirect Electrochemistry

Based upon the behavior of compound **27**, traditional treatment of redox catalysis data (analysis of peak current ratio (i_p/i_{pd}) and plotting against mediator concentration (C_M^0) at constant γ), was not attempted on compound **41**. Sample runs were conducted by adding additional substrate to the mediator while keeping scan rates low to ensure catalysis (**Figure 3-20**). Only one mediator, 2,4-dinitrophenylferrocene (**34h**), was utilized for these experiments due to the synthetic availability of mediators available in the appropriate potential range. Analysis of the data utilizing the same methodology described previously resulted in a value of 0.366V for $E_{\text{substrate}}^0$ and the rate constant (k_0) was found to be $4.1 \times 10^2 \text{ s}^{-1}$.

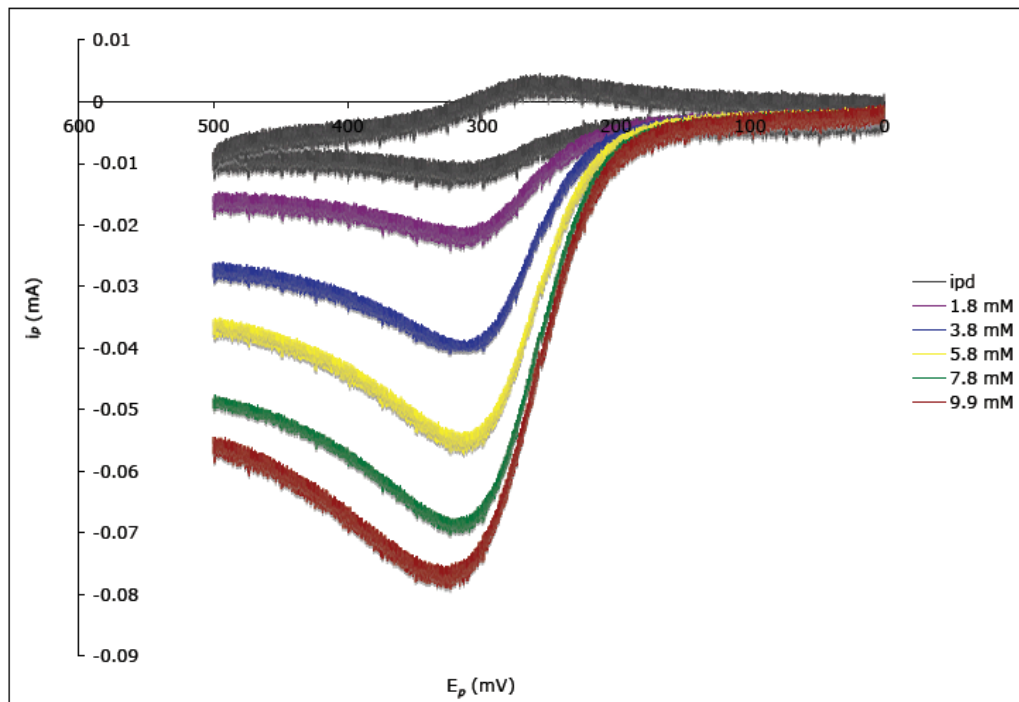


Figure 3-20 Redox Catalysis of **41** with 2,4-dinitrophenylferrocene (**36h**) (CH_3CN , 0.5M CH_3OH , 0.5M $\text{nBu}_4\text{N}^+\text{BF}_4^-$, $\nu = 25 \text{ mV/sec}$, $\gamma = 1, 2.1, 3.3, 4.4, 5.6$)

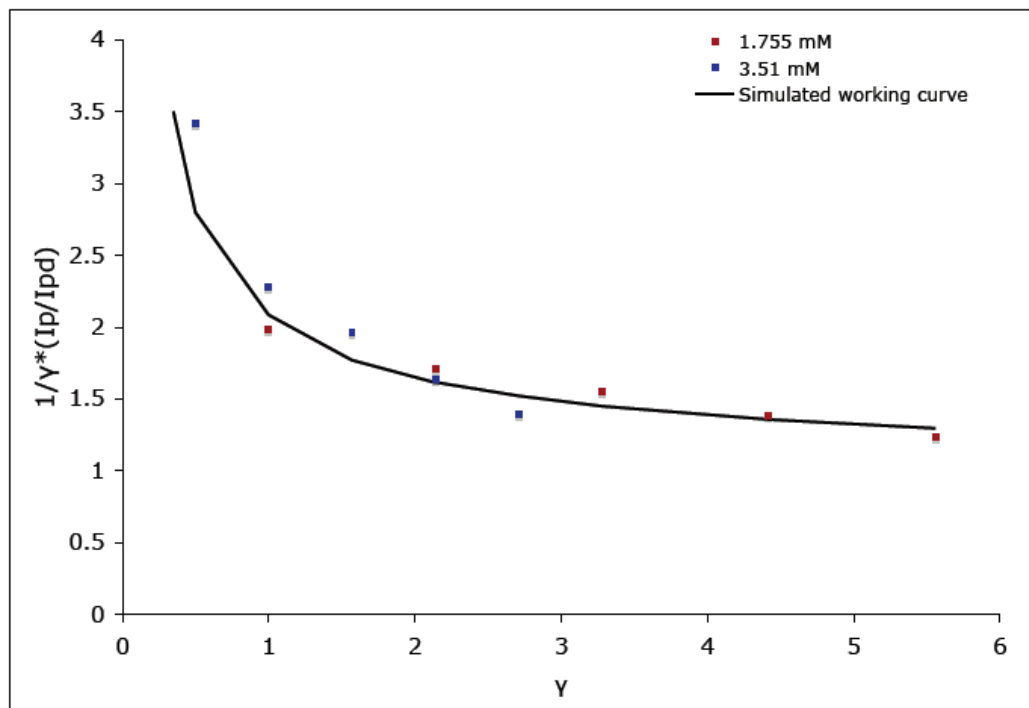
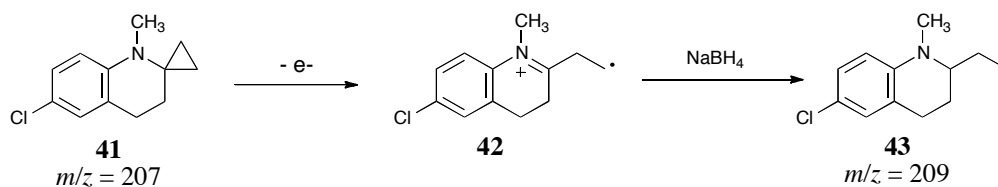


Figure 3-21 Fitting results of the results for mediated catalysis of **41** with 2,4-dinitrophenylferrocene (**36h**) with digitally simulated working curves.

3.2.4 Preparative Scale Electrolysis (Bulk Electrolysis)

To ensure that a ring opening pathway was indeed occurring following the direct and indirect electrochemistry, preparative scale electrolysis was performed on compound **41**. Preparative scale oxidations were conducted in a standard H-cell containing a glass frit serving as a salt bridge. Compounds were oxidized for a fixed amount of time, corresponding to the number of moles of electrons passed through the solution over the course of the experiment. Sample solutions were then quenched and analyzed by GC-MS. Unfortunately, large samples (e.g., gram quantities) were unable to be examined utilizing this method due to problems with electrode fouling. For this reason micro-molar solutions had to be utilized for the work described herein; attempts to isolate and characterize products via traditional analytical techniques were unsuccessful.

Initial experiments were run at a constant potential 100 mV more positive than the peak potential of the substrate. This method was abandoned fairly rapidly due to issues with electrode fouling despite working at lowered concentrations. Constant current electrolysis proved to be more effective for this examination. **Table 3-4** shows only one product corresponding to the ring opened material **43** ($m/z = 209$). Unreacted starting material ($m/z = 207$) was the only other material present in the sample solutions post electrolysis. Reproducible product yields were not obtained, presumably due to electrode fouling. Results have been summarized in **Table 3-4**.

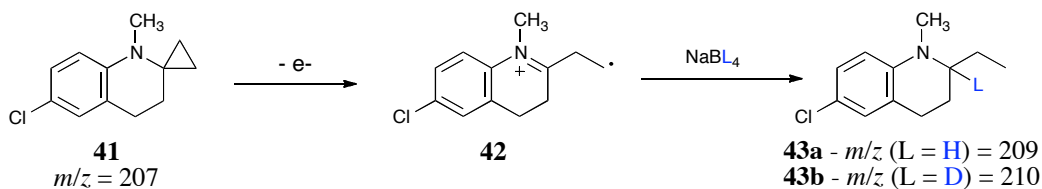


Scheme 3-16 Bulk electrolysis with a sodium borohydride workup.

Conditions	Solvent	Workup	<i>m/z</i>
500 mV, 1hr.	CH ₃ CN/CH ₃ OH	NaBH ₄	207, 209
500 mV, 1hr.	CH ₃ CN	NaBH ₄	207, 209
-3 mA, 1 hr.	CH ₃ CN/CH ₃ OH	NaBH ₄	207, 209
-3 mA, ½ hr.	CH ₃ CN/CH ₃ OH	NaBH ₄	209

Table 3-4 Sample electrolysis of **41**. Solutions were subjected to a reductive work up (NaBH₄) and analyzed by GC-MS.

Secondary experiments mirrored that of the first experiments, but the work up procedure was changed to account for mass balance post reaction. Due to the fact that sodium borohydride is known to reduce iminyl bonds, quenching with sodium borodeuteride should yield the deuterium substituted analogue of the ring opened structure (**Scheme 3-17**).³⁵ GC-MS analysis of the product solution should clearly resolve the two compounds post reaction. A summary of these results is presented in **Table 3-5**. Addition of sodium borodeuteride following the electrolysis yields a new structure **43b** (*m/z* = 210). This is consistent with the proposed mechanism shown in **Scheme 3-16**, therefore it can be inferred that the iminium **42** was formed post reaction electrolysis.

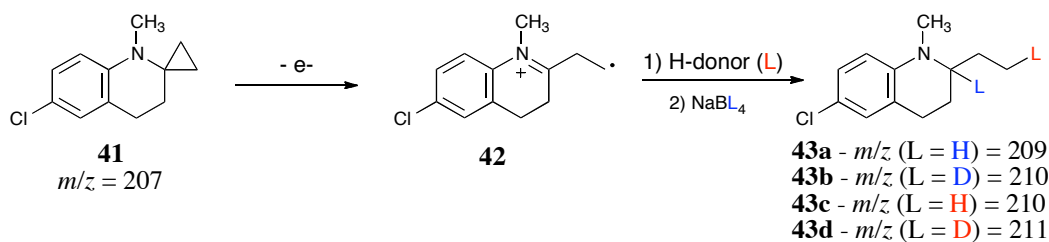


Scheme 3-17 Sample electrolysis of **41**. Solutions were subjected to a reductive work up and analyzed by GC-MS.

Conditions	Solvent	Workup	<i>m/z</i>
-3 mA, 1hr.	CH ₃ CN/CH ₃ OH	NaBH ₄	207, 209
-3 mA, 1 hr.	CH ₃ CN/CH ₃ OH	NaBD ₄	207, 210/mix
-3 mA, ¾ hr.	CH ₃ CN/CH ₃ OH	NaBH ₄	207, 209
-3 mA, ¾ hr.	CH ₃ CN/CH ₃ OH	NaBD ₄	209, 210

Table 3-5 Sample electrolysis of **41**. Solutions were subjected to a reductive work up (NaBH₄ or NaBD₄) and analyzed by GC-MS.

Lastly, experiments were conducted in the presence of hydrogen atom donors of varying bond dissociation energy. These experiments were conducted to account for quenching of the primary radical formed post formation of the distonic radical cation **42** (Scheme 3-18). Experiments could not be attempted with a more labile H-atom donor because compounds found in this range would likely interfere with the electrolysis of **41**. One electron oxidation of **41**, followed by deuterium atom abstraction of the donor should yield the deuterated substituted methyl group derived from **42**. Subsequent reduction with NaBD₄ would give **43d** (*m/z* = 211). No hydrogen atom abstraction from the donor was observed (Table 3-6).



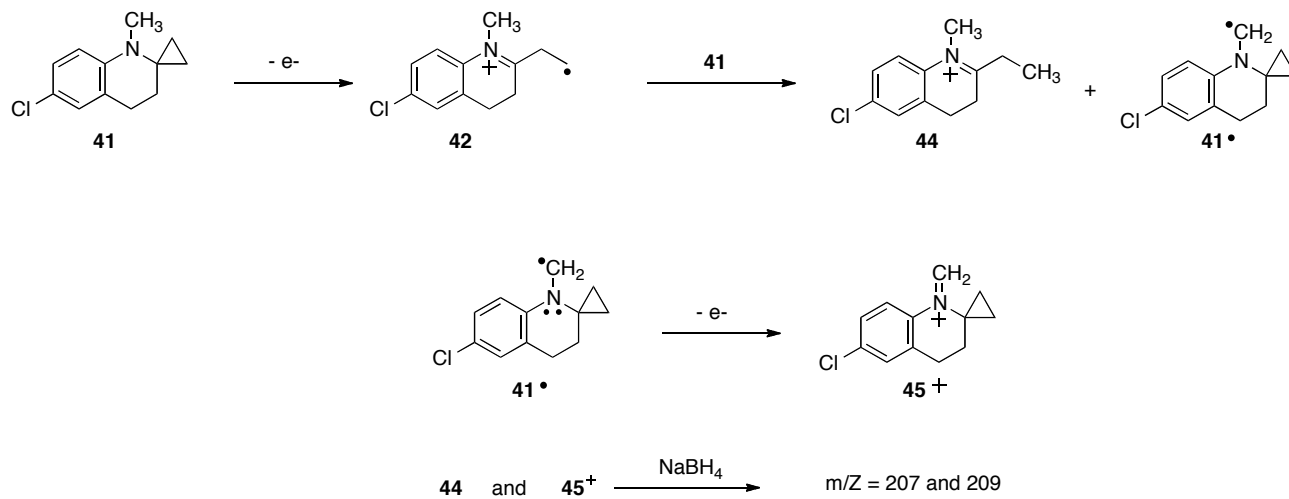
Scheme 3-18 Sample electrolysis of **41**. Solutions were exposed to an H-donor, subjected to a reductive work up, and analyzed by GC-MS.

Conditions	Solvent	Workup	H/D-Donor	<i>m/z</i>
-3 mA, ¾ hr.	CD ₃ CN	NaBH ₄	CD ₃ CN	209
-3 mA, ¾ hr.	CD ₃ CN	NaBH ₄	CD ₃ OD	209
-3 mA, 1 hr.	-----	NaBH ₄	Toluene - <i>d</i> ⁸	209
-3 mA, ½ hr.	CD ₃ CN	NaBD ₄	CD ₃ CN	210/mix
-3 mA, ¾ hr.	CD ₃ CN	NaBD ₄	CD ₃ OD	210
-3 mA, ¾ hr.	-----	NaBD ₄	Toluene - <i>d</i> ⁸	210

Table 3-6 Sample electrolysis of **41**. Solutions were subjected to a reductive work up (NaBH₄ or NaBD₄) and analyzed by GC-MS.

Two mechanisms have been proposed to account for the mass balance of the hydrogen atom abstraction step. The first potential pathway begins with oxidation of **41** at the electrode surface to generate the ring opened distonic radical cation **42**. Compound **42** then can abstract a hydrogen atom from the starting material to yield **44** and **41**[•] (Scheme 3-19). **41**[•] can undergo a

second oxidation at the electrode surface to lose a second electron yielding the imine **45⁺**. Reduction of sodium borohydride will give the results presented in **Tables 3-4** and **3-5**, but reduction of compound **45⁺** with sodium borodeuteride should give an *m/z* of 208. This mechanism does not fully account for the data presented in **Tables 3-4** and **3-5**, therefore another mechanism was considered.



Scheme 3-19 Proposed mechanism for the oxidation of **42** leading to the products **41** and **43a**.

The first step of the second proposed mechanism begins with an oxidation at the electrode surface to yield **42**. Compound **42** can abstract a hydrogen atom from its own *N*-methyl group yielding **46a** (**Scheme 3-20**), which will exist as the more stable resonance form **46b**. Compound **46b**, a tertiary radical is much more stable than compound **42** or **46a**, therefore a hydrogen atom abstraction by **46b** with the H-atom donors studied in **Table 3-5** is unlikely. This mechanistic scenario potentially accounts for the observed chemistry.



Scheme 3-20 Proposed mechanism for **42** abstract a hydrogen from the *N*-methyl group.

3.2.5 Electrochemical Electrospray Mass Spectroscopy (EC-ESI/MS)

Online coupling mass spectrometry and electrochemistry can provide important chemical information about an oxidized species post reaction. This method allows one to directly monitor the products of an electrochemical reaction as a function of electrode potential.³⁶ The technique involves passing a substrate solution through a porous carbon electrode and varying the potential. The substrate solution is then passed through a mass spectrometer, and its oxidation products (MH^+ or M^+) as generated by ESI can then be monitored online by mass spectroscopy. Mass voltammograms are obtained by plotting the ion intensities vs. potential.³⁷

A representative mass voltammogram of compound **41** is shown in **Figure 3-22**. At approximately 120 mV the intensity of the MH^+ ion of compound **41** at m/z 208 begins to decrease and is replaced with a species at m/z 240. Mass spectra corresponding to the product voltammogram ($m/z = 240$) is provided in **Figure 3-23**.

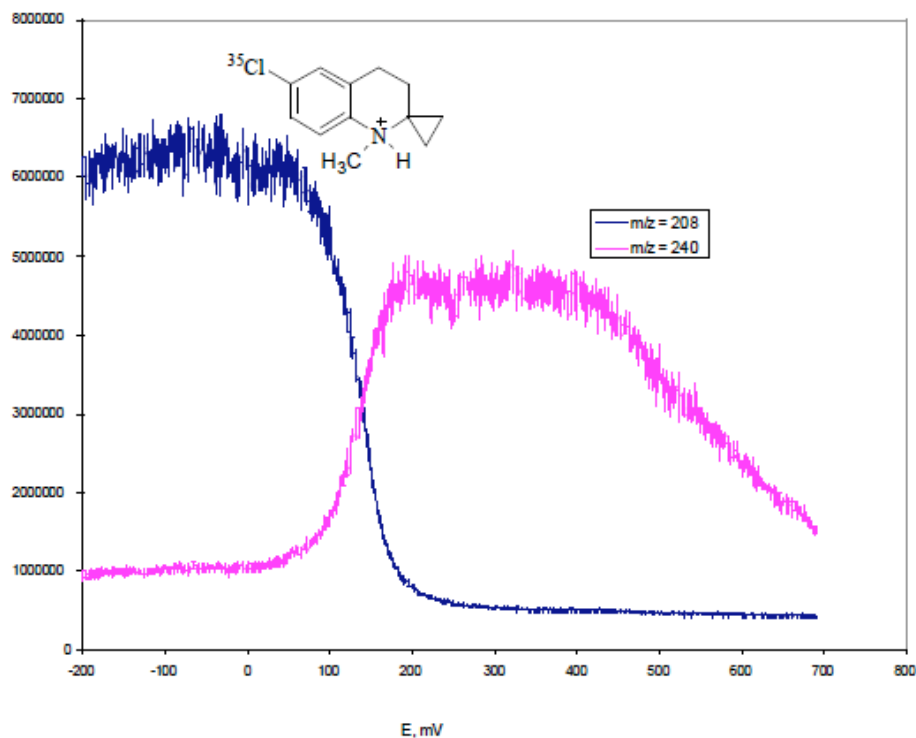


Figure 3-22 Mass voltammograms of **41** and its oxidation product ($m/z = 240$).

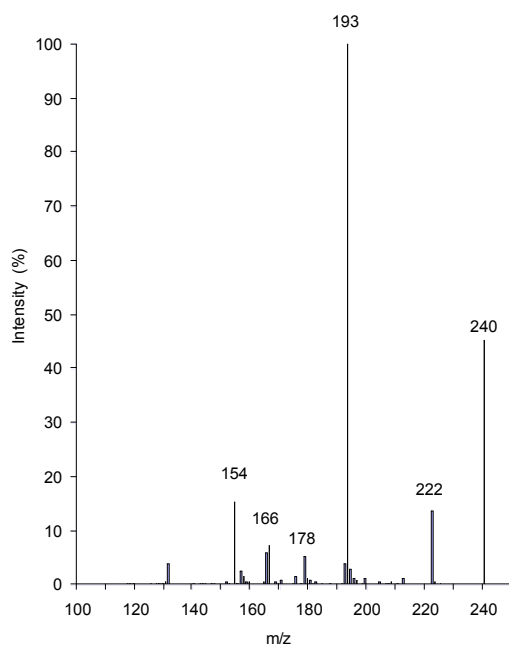
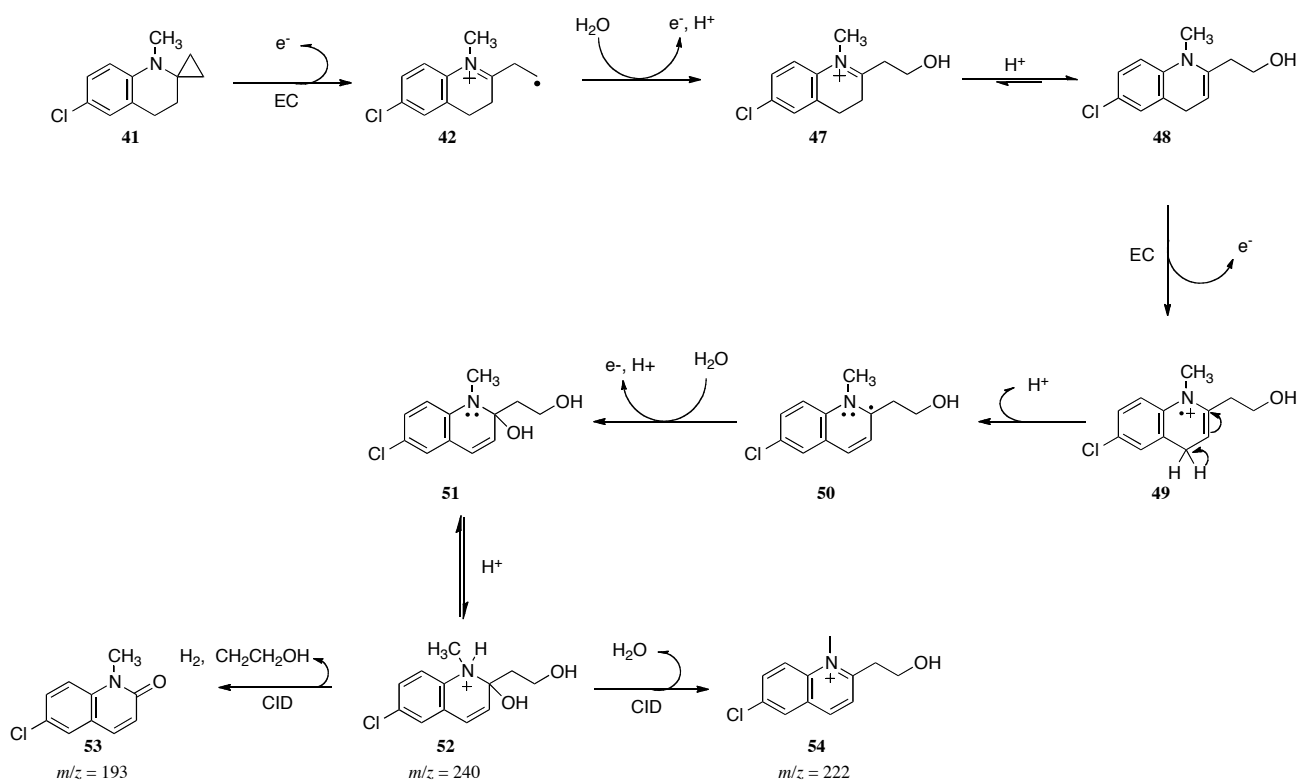


Figure 3-23 Mass Spectra of the product from **41** following ESI oxidation.

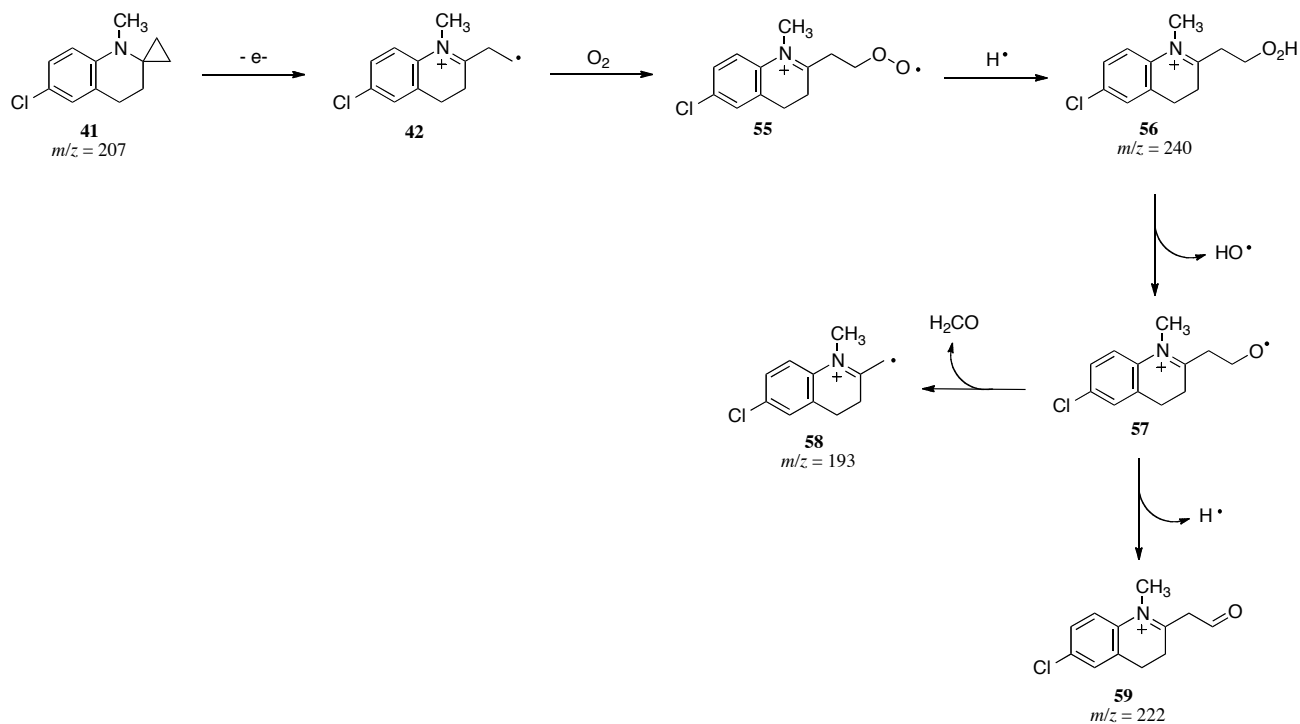
To account for the fragmentation patterns observed in the mass spectroscopy following the initial oxidation, a mechanism was proposed in which compound **41** was initially oxidized to yield the distonic radical cation **42**. This compound could then go on to react with water to yield the corresponding primary alcohol **47** ($m/z = 240$). This base structure could then undergo a second electrochemical oxidation and lose a proton to yield a tertiary radical **50**. Compound **50** could then react with water and gain a proton to yield a di-hydroxyl **52**. This compound could then either fragment to yield the amide fragment (**53**) ($m/z = 193$) or it could eliminate water to give the quinolinium species **54** ($m/z = 222$). Details of the mechanism are presented in **Scheme 3-21**.



Scheme 3-21 Proposed mechanism accounting for the reaction of **41** with water post ESI-MS.

A second potential pathway was proposed that accounts for the mass peak of 240. This mechanism differs from **Scheme 3-21** in that compound **42** reacts with molecular oxygen to ultimately lead to hydroperoxide **56**. The peroxide bond then fragments to give an oxygen centered radical **57**. The oxygen centered radical can then either lose a hydrogen atom to yield an aldehyde **59** ($m/z = 222$), or it can undergo β -cleavage to give a methyl radical **58** ($m/z = 193$).

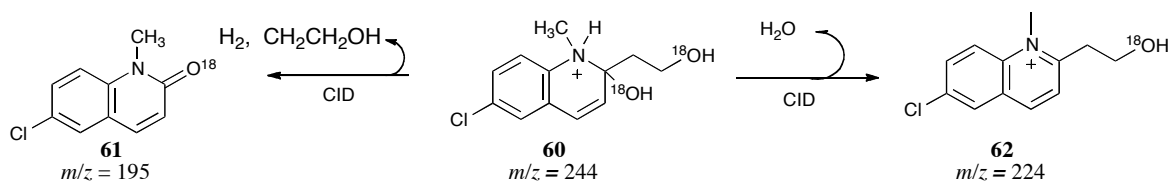
This mechanism is shown in **Scheme 3-22**.



Scheme 3-22 Proposed mechanism for the reaction of **41** with molecular oxygen post ESI.

Both of these mechanisms account for the fragmentation patterns seen from the EC/ESI-MS data. In order to differentiate between these two pathways, a second series of experiments was conducted that utilized H_2^{18}O as the solvent. If **Scheme 3-21** were the predominant mechanism leading to the formation of compounds **53** and **54**, one would expect the fragmentation peak corresponding compound **54** ($m/z = 222$) to be shifted by two molecular mass units ($m/z = 224$) to yield **62** due to the reaction of **42** with H_2^{18}O water **Scheme 3-23**. Additionally, the fragment corresponding to compound **53** should also see a shift of two molecular mass units (m/z 193 to m/z 195). If **Scheme 3-22** is the predominant pathway leading to the observed product fragments, no change in the mass spectra should be observed. **Figure 3-24** shows no change in the fragmentation patterns post oxidation in the presence of H_2^{18}O . The results obtained from the H_2^{18}O water experiments are identical to those obtained in ^{16}O water, therefore it can be surmised

that the mechanism shown in **Scheme 3-21** is likely not the pathway leading to the formation of the fragments corresponding to compounds **53** and **54**.



Scheme 3-23 Predicted products from reaction of **41** with H_2^{18}O water.

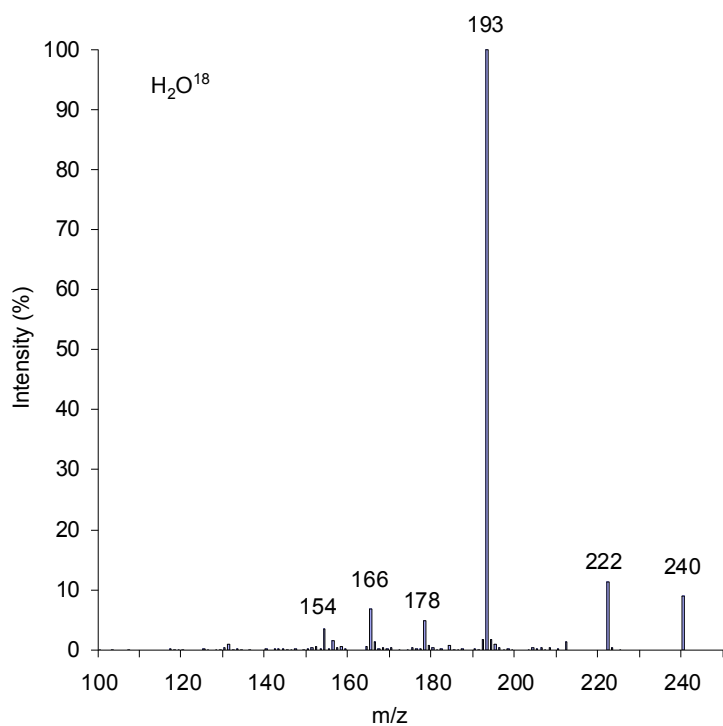
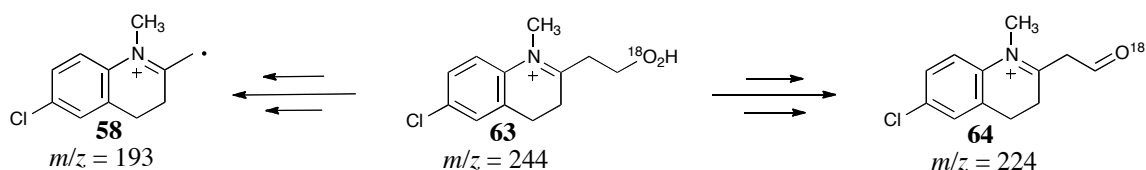


Figure 3-24 ESI MS results for experiments conducted in H_2^{18}O water.

The second set of experiments used to complement the H_2^{18}O water examinations utilized $^{18}\text{O}_2$. If the mechanism presented in **Scheme 3-22** were the predominant pathway leading to the formation of product fragments corresponding to m/z 222 and 193, one would expect the initial peak (m/z 240) to be shifted by four molecular mass units to an m/z of 244 corresponding to compound **55**. Additionally, the fragmentation patterns for this mechanistic scenario would also lead to a peak corresponding to compound **58** ($m/z = 222$) to be shifted by two molecular mass

units ($m/z = 224$) due to the reaction of **42** with ^{18}O oxygen to give product **63** (Scheme 3-24). The fragment corresponding to the β -cleavage of compound **56** would remain unchanged from the first set of experiments, and therefore the fragment corresponding to an m/z of 193 would remain unchanged. **Figure 3-25** shows the expected pattern of behavior post oxidation in the presence of ^{18}O molecular oxygen, indicating that it is likely that compound **42** does in fact react with molecular oxygen post ring opening to form products **58** and **64**.



Scheme 3-24 Predicted products from reaction of **41** with ^{18}O molecular oxygen.

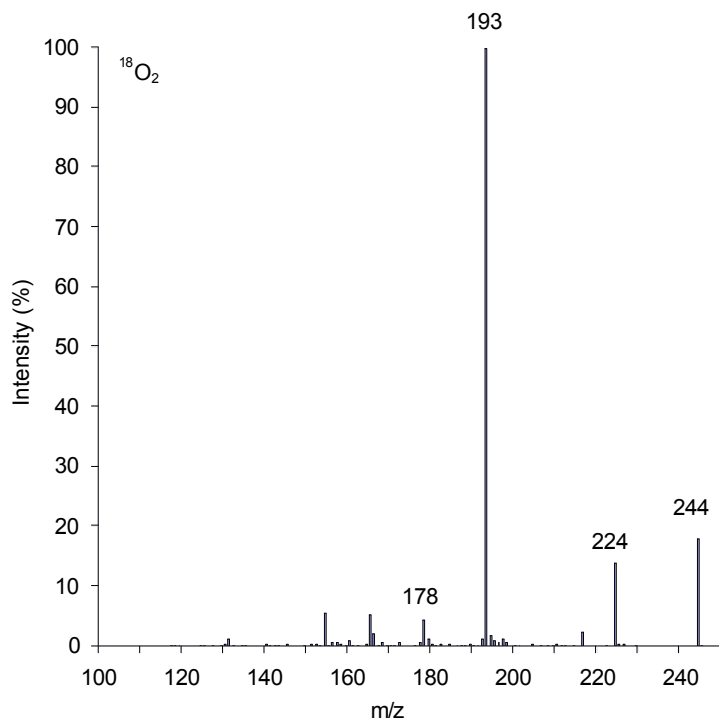


Figure 3-25 ESI MS results for experiments conducted in $^{18}\text{O}_2$.

3.3 Conclusions

Photochemical and electrochemical examinations of *N*-cyclopropyl-*N*-methylaniline revealed that the rate constant for cyclopropyl ring opening to be $4 \times 10^4 \text{ s}^{-1}$. Molecular modeling calculations revealed that the perpendicular conformation was more favorable by 2 kcal/mol, leading to the hypothesis that the cyclopropyl group did not meet the appropriate stereoelectronic requirements for ring opening. The electrochemical results reported show that the rate constant for ring opening spiro cyclopropanes: 1'-methyl-3',4'-dihydro-1'*H*-spiro[cyclopropane-1,2'-quinoline] (**25**) and 6'-chloro-1'-methyl-3',4'-dihydro-1'*H*-spiro[cyclopropane-1,2'-quinoline] (**41**) are $3.5 \times 10^2 \text{ s}^{-1}$ and $4.1 \times 10^2 \text{ s}^{-1}$ respectively. Results from preparative scale electrolysis and ESI-MS are consistent with a ring opening process being operative for the chemical step. A detailed discussion rationalizing the slowed rate constants and redox potentials of **25** and **41** is presented in Chapter 5.

3.4 Experimental Section

3.4.1 Materials and Purification

All chemicals used for this study were obtained from Aldrich and used as received unless otherwise noted. Acetonitrile was distilled over CaH_2 prior to each electrochemical run. Dry tetrahydrofuran was distilled over Na/benzophenone prior to use. All solvents used for synthesis unless otherwise specified were ACS grade solvents and were not treated in any way prior to use. Compounds **25** and **39** were purified by prep-TLC prior to kinetic evaluation.

3.4.2 Instrumentation

NMR spectra were obtained on a JOEL Eclipse Plus 500 MHz spectrometer. Chemical shifts are reported in ppm using the residual solvent peak (CDCl_3) as the linked to a HP 5973 Mass

Selective Detector interfaced to an HP series computer. Gas chromatography was performed on a Hewlett-Packard 5890A GC equipped with an FID detector and an HP 3393A integrator.

3.4.3 Synthesis

3.4.3.1 3-chloro-*N*-methyl-*N*-phenylpropanamide (32).³⁸ *N*-methylaniline (10g, 93.5 mmol) was dissolved in 50 mL distilled acetone. A solution of 3-chloropropanoyl chloride (9.9g, 77.9 mmol) in acetone (15 mL) was slowly added to the solution. The solution was refluxed for 2 hours and cooled to room temperature. The reaction mixture was added to 6M aqueous HCl (100 mL), and extracted with diethyl ether (3 x 150 mL). The organic phase was then washed with sat. NaHCO₃ and brine, then dried over Na₂SO₄. The resulting solution was then evaporated to dryness. The crude product was then purified by column chromatography (EtOAc/Hexanes 3:7) to give a pale yellow oil: ¹H NMR (CDCl₃) δ 7.46 (d, 2H), 7.30 (d, 2H), 3.88 (t, 2H), 2.82 (t, 2H).

3.4.3.2 1-methyl-3,4-dihydroquinolin-2(1*H*)-one (33).³⁸ A 100 mL round bottom flask containing compound **32** (4g, 20.2 mmol) was heated to 140 °C. AlCl₃ (13.5g, 101.4 mmol) was added over a 20 min. period and the reaction was allowed to stir for 17 hrs. The resulting mixture was cooled to 0 °C and quenched with 10% aqueous HCl (200 mL). The crude product was extracted with EtOAc (3 x 100 mL), dried over Na₂SO₄, and evaporated to dryness. The crude product was filtered over alumina (100g) and eluted with EtOAc/Hexanes (1:1) resulting in a colorless oil: ¹H NMR (CDCl₃) δ 7.55 (s, 1H), 7.14 (m, 2H), 6.65 (d, 2H), 2.94 (t, 2H), 2.63 (t, 2H).

3.4.3.3 1'-methyl-3',4'-dihydro-1'*H*-spiro[cyclopropane-1,2'-quinoline] (25). Compound **33** (1g, 6.2 mmol) was dissolved in 15 mL dry THF and degassed for 15 min with argon. The solution was cooled to -78 °C and titanium isopropoxide (2.3g, 8.1 mmol) was added to the

mixture. Ethyl magnesiumbromide (6.0 mL, 18.2 mmol) was added to the solution over a 0.5 hr. period. The reaction was allowed to proceed over a 12 hr. period. The resultant suspension was quenched with saturated NH_4Cl (50 mL), and extracted using diethyl ether (3 x 50 mL). The organic layer was washed with water, brine, and dried over Na_2SO_4 . The residual solvent was removed by rotary evaporator. The crude product was purified via column chromatography on alumina (EtOAc/hexanes 5:95) yielding a pale yellow oil: ^1H NMR (CDCl_3) δ 7.02 (m, 2H), 6.63 (d, 1H), 2.79 (t, 1H), 2.69 (s, 3H), 1.55 (t, 2H), 0.77 (t, 2H), 0.41 (t, 2H); m/z 207, 206, 192, 178, 164.

3.4.3.4 3-Chloro-N-(4-chlorophenyl)propanamide (36).³⁸ 4-Chloroaniline (10g, 78.4 mmol) was dissolved in 25 mL distilled acetone. A solution of 3-chloropropanoyl chloride (5.53g, 43.5 mmol) in acetone (5 mL) was slowly added to the solution. The solution was refluxed for 2 hrs. and cooled to room temperature. The reaction mixture was added to 6M aqueous HCl (100 mL), and extracted with diethyl ether (3 x 150 mL). The organic phase was then washed with sat. NaHCO_3 and brine, then dried over Na_2SO_4 . The resulting solution was then evaporated to dryness. The crude product was then purified by crystallization (EtOAc/Hexanes 1:1) to give white crystals: mp 123-125 °C; ^1H NMR (CDCl_3) δ 7.46 (d, 2H), 7.30 (d, 2H), 3.88 (t, 2H), 2.82 (t, 2H).

3.4.3.5 6-Chloro-3,4-dihydroquinolin-2(1H)-one (37).³⁸ A 100 mL round bottom flask containing compound **36** (4g, 18.3 mmol) was heated to 140 °C. Following the complete melting of compound **36**, AlCl_3 (12.3g, 91.9 mmol) was added over a 20 min. period and the reaction was allowed to stir for 17 hrs. The resulting mixture was cooled to 0 °C and quenched with 10% aqueous HCl (200 mL). The crude product was extracted with EtOAc (3 x 100 mL), dried over Na_2SO_4 , and evaporated to dryness. The crude product was filtered over alumina

(100g) and eluted with EtOAc/Hexanes (1:1) resulting in white crystals: mp 163-164 °C; ¹H NMR (CDCl₃) δ 7.55 (s, 1H), 7.14 (m, 2H), 6.65 (d, 2H), 2.94 (t, 2H), 2.63 (t, 2H).

3.4.3.6 6-Chloro-1-methyl-3,4-dihydroquinolin-2(1H)-one (38).²⁸ Sodium hydride (60% dispersion in mineral oil, 0.66g, 16.5 mmol) was suspended in 25 mL xylene. The mixture was placed under argon and allowed to reflux for 1hr. **37** (3g, 16.5 mmol) was added to the solution and the mixture was allowed to reflux for 1.5 hr. Dimethyl sulfate (2.08g, 16.5 mmol) was added to the suspension via syringe and the reaction was allowed to progress for an additional 2 hrs. (following the addition of amide the solids became soluble in xylene). The reaction mixture was cooled to room temperature and the solution was diluted to 100 mL with 10% aqueous NaOH, extracted with hexanes (3 x 50 mL), and dried over Na₂SO₄. Hexanes were evaporated under reduced pressure and the residual xylenes were removed from the product by column chromatography on alumina (0→30% v/v EtOAc/Hexane) resulting in a white solid: mp 74-76 °C; ¹H NMR (CDCl₃) δ 7.16 (d, 1H), 7.10 (s, 1H), 6.86 (d, 1H), 3.29 (s, 3H), 2.83 (t, 2H), 2.61 (t, 2H).

3.4.3.7 6'-Chloro-1'-methyl-3',4'-dihydro-1'H-spiro[cyclopropane-1,2'-quinoline] (39). Compound **38** (1g, 5.1mmol) was dissolved in 15 mL dry THF and degassed for 15 min with argon. The solution was cooled to -78 °C and titanium isopropoxide (1.9g, 6.6mmol) was added to the mixture. Ethyl magnesiumbromide (4.9 mL, 14.9 mmol) was added to the solution over a 0.5 hr. period. The reaction was allowed to proceed over a 12 hr. period. The resultant suspension was quenched with saturated NH₄Cl (50 mL), and extracted using diethyl ether (3 x 50 mL). The organic layer was washed with water, brine, and dried over Na₂SO₄. The residual solvent was removed by rotary evaporator. The crude product was purified via column chromatography on alumina (EtOAc/hexanes 5:95) yielding a pale yellow oil: ¹H NMR (CDCl₃)

δ 7.02 (m, 2H), 6.63 (d, 1H), 2.79 (t, 1H), 2.69 (s, 3H), 1.55 (t, 2H), 0.77 (t, 2H), 0.41 (t, 2H);
m/z 207, 206, 192, 178, 164

3.4.3.8 Sample ferrocene synthesis [1-(4-Cyanophenyl)ferrocene (36f)]. p-Cyanoaniline (5g, 42.5 mmol) was dissolved in 100 mL 20% sulfuric acid. Sodium nitrite (5.8g, 84.5 mmol) was added to the solution over a 20 minute period at 0°C. The solution was then allowed to stir for 1 hour with constant stirring. Ferrocene (15.7g, 84.5 mmol) was dissolved in a minimum volume of CH₂Cl₂ and 300 mL glacial acetic was added to the ferrocene mixture. The flask was then cooled to 0°C and the p-cyano diazonium solution was added to the ferrocene mixture. The reaction was then allowed to stir for 48 hours at room temperature. The reaction was quenched with saturated NaHCO₃, and the resulting solution was extracted with CH₂Cl₂ (3 x 200mL). The organic layer was dried with Na₂SO₄ and evaporated to dryness. The material was purified via column chromatography on silica gel (EtOAc/Hexanes 5:95) yielding a maroon solid:

3.4.3.9 Tertrabutylammonium tertafluoroborate. Tetrabutylammonium bromide (84g, 0.261 mol) was dissolved in a minimum volume of water. Fluoroboric acid (36 mL, 0.271 mol) was added to the solution. A white precipitate formed that was filtered on a buchner funnel. The resulting solid was then washed with water until the filtrate was of neutral pH. The crude salt was recrystallized three times with ethyl acetate/hexanes to yield a white powder. The resulting crystalline material was then placed under vacuum for 4 hours to remove any residual solvent.

3.4.4 Photochemical Apparatus.

Steady-state UV/Vis spectra were recorded on a Hewlett Packard diode array UV/Visible spectrophotometer (HP 8452A). Laser flash photolysis (LFP) experiments were conducted using an Applied Photophysics LKS.60 spectrometer using the third harmonic of a Continuum Surelite I-10 Nd:YAG laser (4 - 6 ns pulse, 355 nm). Absorption spectra were monitored by a Hewlett

Packard Infinium digital oscilloscope and analyzed with an Applied Photophysics SpectraKinetic Workstation software package (v. 4.59). Experiments were performed with a jacketed cell holder connected to a VWR Scientific Products (PolyScience) variable temperature circulating bath (model 1150-A) thermally equilibrated to 25C.

3.4.5 Laser Flash Photolysis (LFP).

Sample solutions were prepared in 5% methanol in acetonitrile and deoxygenated with argon prior to use. (Steady-state UV/Visible spectra were recorded to ensure that amines were the only species absorbing at the excitation wavelength). In most LFP experiments, micromolar concentrations of the amine were passed through a flow cell during the course of the experiment to maintain the integrity of the sample.

3.4.6 Direct and Indirect Electrochemistry

Electrochemical measurements were made on a Princeton Applied Research (EG & G) 273 model potentiostat. All data was processed on a 386 model PC running windows 3.1. Samples solutions were prepared in distilled acetonitrile/methanol containing 0.1M tetra-butyl ammonium tetrafluoroborate prior to use. The electroactive substrate was purified by prep-TLC prior to analysis. All solutions were degassed for 10 minutes prior to analysis. A standard three electrode cell was used for all runs. A glassy carbon electrode working electrode (area = 0.14 cm²) was prepared by polishing over 0.3 μ silica slurry until a mirror finish was obtained. The auxillary electrode was fabricated from a platinum wire coil. The (Ag/Ag⁺) reference electrode was prepared prior to each run. All runs were recorded in triplicate for direct electrochemical runs and in duplicate for reductive catalysis experiments unless otherwise noted.

3.4.7 Preparative Scale Electrolysis

Preparative scale oxidations were conducted in a standard H-cell containing a glass frit serving as a salt bridge. The electrodes for the experiments were prepared in the following way: (i) the working electrode was made from mesh platinum wire soldered on to copper wire, (ii) the auxiliary electrode was assembled from coiled copper wire, and (iii) the reference electrode was composed in the same fashion that was described for the direct and indirect electrochemical measurements. Constant current measurements were run with respect to how many molar equivalents of electrons that was passed through the reaction mixture. Constant potential experiments were run at a potential 100 mV more positive than the oxidation potential of the substrate after solution resistance was accounted for.

3.4.7.1 Sample Preparative Electrolysis

25 mL solutions containing 0.1 M LiOCl₄ in 0.5 M CH₃OH in CH₃CN were prepared for both oxidative and reductive compartments of the H-cell. Substrate in micromolar concentrations was added to the oxidative side of the H-cell. The solution was then degassed with argon or air for the duration of the experiment. Post electrolysis the solutions were treated with an excess of sodium borohydride and allowed to stir for 10 minutes. The solution was diluted with water and the organic layer was extracted with 2 x 15 mL CH₂Cl₂. Samples were then analyzed by GC and GC-MS.

3.4.8 Digital Simulations

Digital simulations were performed using Digisim 2.1 (Bioanalytical Systems Inc., Kent ave. W. Lafayette, IN 47096). Assumptions for simulation parameters were defined as follows: (i) electrode area = 1 cm², (ii) $\alpha = 0.5$, (iii) T = 298 K, (iv) D = 10⁻⁵ cm²/s, (v) scan rate (v) = 25 mV (vi) semi-infinite diffusion assumed, (vii) the reaction mechanism was modeled as shown in

Scheme 3-14, (viii) $k_{\text{ET}} = 10^5 \text{ M}^{-1}\text{s}^{-1}$ and $k_{-\text{ET}} = 1 \times 10^{10} \text{ M}^{-1}\text{s}^{-1}$, while k_0 was varied methodically from $10^2 - 10^7 \text{ s}^{-1}$, (ix) substrate concentrations were dictated by the experimental values.

References

1. Rappoport, Z., *The Chemistry of the Cyclopropyl Group, Parts 1 and 2*. Academic Press: New York, 1987.
2. Newcomb, M.; Johnson, C. C.; Manek, M. B.; Varick, T. R., Picosecond Radical Kinetics. Ring Openings of Phenyl Substituted Cyclopropylcarbinyl Radicals. *Journal of the American Chemical Society* **1992**, *114*, 10915-10921.
3. Tanko, J. M.; Li, X. Z.; Chahma, M.; Jackson, W. F.; Spencer, J. N., Cyclopropyl conjugation and ketyl anions: When do things begin to fall apart? *Journal of the American Chemical Society* **2007**, *129* (14), 4181-4192.
4. Drumright, R. E.; Mas, R. H.; Merola, J. S.; Tanko, J. M., Interplay between Conjugative and Steric Effects in Cyclopropylarenes. *Journal of Organic Chemistry* **1990**, *55* (13), 4098-4102.
5. Stevenson, J. P.; Jackson, W. F.; Tanko, J. M., Cyclopropylcarbinyl-type ring openings. Reconciling the chemistry of neutral radicals and radical anions. *Journal of the American Chemical Society* **2002**, *124* (16), 4271-4281.
6. Guengerich, F. P., Roles of Cytochrome-P-450 Enzymes in Chemical Carcinogenesis and Cancer-Chemotherapy. *Cancer Research* **1988**, *48* (11), 2946-2954.
7. Shimada, T.; Yamazaki, H.; Mimura, M.; Wakamiya, N.; Ueng, Y. F.; Guengerich, F. P.; Inui, Y., Characterization of microsomal cytochrome P450 enzymes involved in the oxidation of xenobiotic chemicals in human fetal livers and adult lungs. *Drug Metabolism and Disposition* **1996**, *24* (5), 515-522.
8. Meunier, B.; de Visser, S. P.; Shaik, S., Mechanism of oxidation reactions catalyzed by cytochrome P450 enzymes. *Chemical Reviews* **2004**, *104* (9), 3947-3980.
9. Sono, M.; Roach, M. P.; Coulter, E. D.; Dawson, J. H., Heme-containing oxygenases. *Chemical Reviews* **1996**, *96* (7), 2841-2887.
10. Guengerich, F. P.; Macdonald, T. L., Mechanisms of Cytochrome-P-450 Catalysis. *Faseb Journal* **1990**, *4* (8), 2453-2459.
11. Hanzlik, R. P.; Tullman, R. H., Suicidal Inactivation of Cytochrome-P-450 by Cyclopropylamines - Evidence for Cation-Radical Intermediates. *Journal of the American Chemical Society* **1982**, *104* (7), 2048-2050.
12. Macdonald, T. L.; Zirvi, K.; Burka, L. T.; Peyman, P.; Guengerich, F. P., Mechanism of Cytochrome-P-450 Inhibition by Cyclopropylamines. *Journal of the American Chemical Society* **1982**, *104* (7), 2050-2052.

13. Karki, S. B.; Dinnocenzo, J. P.; Jones, J. P.; Korzekwa, K. R., Mechanism of Oxidative Amine Dealkylation of Substituted N,N-Dim

ethylanilines by Cytochrome-P-450 - Application of Isotope Effect Profiles. *Journal of the American Chemical Society* **1995**, *117*(13), 3657-3657.

14. Dinnocenzo, J. P.; Karki, S. B.; Jones, J. P., On Isotope Effects for the Cytochrome-P-450 Oxidation of Substituted N,N-Dimethylanilines. *Journal of the American Chemical Society* **1993**, *115*(16), 7111-7116.

15. Manchester, J. I.; Dinnocenzo, J. P.; Higgins, L. A.; Jones, J. P., A new mechanistic probe for cytochrome P450: An application of isotope effect profiles. *Journal of the American Chemical Society* **1997**, *119*(21), 5069-5070.

16. Macdonald, T. L.; Gutheim, W. G.; Martin, R. B.; Guengerich, F. P., Oxidation of Substituted N,N-Dimethylanilines by Cytochrome-P-450 - Estimation of the Effective Oxidation Reduction Potential of Cytochrome-P-450. *Biochemistry* **1989**, *28*(5), 2071-2077.

17. Shaffer, C. L.; Morton, M. D.; Hanzlik, R. P., Enzymatic N-dealkylation of an N-cyclopropylamine: An unusual fate for the cyclopropyl group. *Journal of the American Chemical Society* **2001**, *123*(2), 349-350.

18. Loeppky, R. N.; Elomari, S., N-alkyl-N-cyclopropylanilines as mechanistic probes in the nitrosation of N,N-dialkyl aromatic amines. *Journal of Organic Chemistry* **2000**, *65*(1), 96-103.

19. Newcomb, M.; Johnson, C. C.; Manek, M. B.; Varick, T. R., *J. Am. Chem. Soc.* **1992**, *114*, 10915-10921.

20. Bouchoux, G.; Alcaraz, C.; Dutuit, O.; Nguyen, M. T., Unimolecular chemistry of the gaseous cyclopropylamine radical cation. *Journal of the American Chemical Society* **1998**, *120*(1), 152-160.

21. Qin, X. Z.; Williams, F., Electron-Spin-Resonance Studies on the Radical Cation Mechanism of the Ring-Opening of Cyclopropylamines. *Journal of the American Chemical Society* **1987**, *109*(2), 595-597.

22. Li, X. Z.; Grimm, M. L.; Igarashi, K.; Castagnoli, N.; Tanko, J. M., The first calibration of an aminiumyl radical ion clock: why N-cyclopropylanilines may be poor mechanistic probes for single electron transfer. *Chemical Communications* **2007**, (25), 2648-2650.

23. Bhakta, M. N.; Wimalasena, K., Microsomal P-450-catalyzed N-dealkylation of N,N-dialkylanilines: Evidence for a C-alpha-H abstraction mechanism. *Journal of the American Chemical Society* **2002**, *124*(9), 1844-1845.

24. Miwa, G. T.; Walsh, J. S.; Kedderis, G. L.; Hollenberg, P. F., The Use of Intramolecular Isotope Effects to Distinguish between Deprotonation and Hydrogen-Atom Abstraction

Mechanisms in Cytochrome-P-450-Catalyzed and Peroxidase-Catalyzed N-Demethylation Reactions. *Journal of Biological Chemistry* **1983**, *258* (23), 4445-4449.

25. Cerny, M. A.; Hanzlik, R. P., *J. Am. Chem. Soc.* **2006**, *128*, 3346-3354.

26. Bissel, P.; Castagnoli, N.; Penich, S., Studies on the cytochrome P450 catalyzed oxidation of C-13 labeled 1-cyclopropyl-4-phenyl-1,2,3,6-tetrahydropyridine by C-13 NMR (vol 13, pg 2975, 2005). *Bioorganic & Medicinal Chemistry* **2005**, *13* (14), 4588-4588.

27. Maslak, P.; Chapman, W. H.; Vallombroso, T. M. J.; Watson, B. A., Mesolytic Scission of C-C Bonds in Radical Cations of Amino Derivatives: Steric and Solvent Effects. *Journal of the American Chemical Society* **1995**, *117*, 12380-12389.

28. Bordwell, F. G.; Fried, H. E., Heterocyclic Aromatic Anions with $4n+2$ -Pi-Electrons. *Journal of Organic Chemistry* **1991**, *56* (13), 4218-4223.

29. de Meijere, A.; Kozhushkov, S. I.; Savchenko, A. I., Titanium-mediated syntheses of cyclopropylamines. *Journal of Organometallic Chemistry* **2004**, *689* (12), 2033-2055.

30. Nadjo, L.; Saveant, J. M., Linear Sweep Voltammetry: Kinetic Control by Charge Transfer and or Secondary Chemical Reactions. *Electroanalytical Chemistry and Interfacial Electrochemistry* **1973**, *48*.

31. Andrieux, C. P.; Blocman, C.; Dumasbouchiat, J. M.; Mhalla, F.; Saveant, J. M., Homogeneous Redox Catalysis of Electrochemical Reactions .5. Cyclic Voltammetry. *Journal of Electroanalytical Chemistry* **1980**, *113* (1), 19-40.

32. Andrieux, C. P.; Hapiot, P.; Saveant, J. M., Fast Kinetics by Means of Direct and Indirect Electrochemical Techniques. *Chemical Reviews* **1990**, *90* (5), 723-738.

33. Andrieux, C. P.; Dumas-Bouchiat, J. M.; Saveant, J. M., Homogeneous Redox Catalysis of Electrochemical Reactions. *Journal of Electroanalytical Chemistry* **1978**, *87*, 39-53.

34. Nadjo, L.; Saveant, J. M., Linear Sweep Voltammetry: Kinetic Control by Charge Transfer and or Secondary Chemical Reactions. *Electroanalytical Chemistry and Interfacial Electrochemistry* **1973**, *48*, 113-145.

35. Singleton, D. A.; Hang, C.; Szymanski, M. J.; Meyer, M. P.; Leach, A. G.; Kuwata, K. T.; Chen, J. S.; Greer, A.; Foote, C. S.; Houk, K. N., Mechanism of ene reactions of singlet oxygen. A two-step no-intermediate mechanism. *Journal of the American Chemical Society* **2003**, *125* (5), 1319-1328.

36. Volk, K. J.; Yost, R. A.; Brajtertoth, A., Electrochemistry on Line with Mass-Spectrometry - Insight into Biological Redox Reactions. *Analytical Chemistry* **1992**, *64* (1), A21-&.

37. Jurva, U.; Bissel, P.; Isin, E. M.; Igarashi, K.; Kuttub, S.; Castagnoli, N., Model electrochemical-mass spectrometric studies of the cytochrome P450-catalyzed oxidations of cyclic tertiary allylamines. *Journal of the American Chemical Society* **2005**, *127* (35), 12368-12377.
38. Occhiato, E. G.; Ferrali, A.; Menchi, G.; Guarna, A.; Danza, G.; Comerci, A.; Mancina, R.; Serio, M.; Garotta, G.; Cavalli, A.; De Vivo, M.; Recanatini, M., Synthesis, biological activity, and three-dimensional quantitative structure-activity relationship model for a series of benzo[c]quinolizin-3-ones, nonsteroidal inhibitors of human steroid 5 alpha-reductase 1. *Journal of Medicinal Chemistry* **2004**, *47* (14), 3546-3560.
39. Flaniken, J. M.; Collins, C. J.; Lanz, M.; Singaram, B., Aminoborohydrides. 11. Facile reduction of N-alkyl lactams to the corresponding amines using lithium aminoborohydrides. *Organic Letters* **1999**, *1* (5), 799-801.

Chapter 4 Development of New *N*-Cyclopropyl Based Electron Transfer Probes for Cytochrome P-450 Oxidations: Resonance Effects

Contributions

This chapter focuses on the synthesis, electrochemistry and product studies of 4-chloro-*N*-methyl-*N*-(2-phenylcyclopropyl)aniline (**7**). This manuscript (now in preparation), contributions from the authors are as follows: synthesis, electrochemistry and product studies (bulk electrolysis) of **7** were all completed by Michelle L. Grimm.¹ Selected synthetic steps were repeated by Eveline Reichert. Dr. Medhi Ashraf and Leslie Owens performed all ESI-MS examinations. Dr. Neal Castagnoli made significant intellectual contributions to the work. Dr. James M. Tanko contributed to the writing and editing of the manuscript as well as preparing the work for publication.

1. Grimm, M. L.; Hancock, A. N.; Reichert, E.; Fonovic, B.; Suleman, N. K.; Ashraf, M.; Dudding, T.; Castagnoli, N.; Tanko, J. M. Development of New *N*-cyclopropyl Based Electron Transfer Probes for Enzyme Catalyzed Reactions: Stereoelectronic Effects and Resonance Effects. (Manuscript in preparation).

Abstract

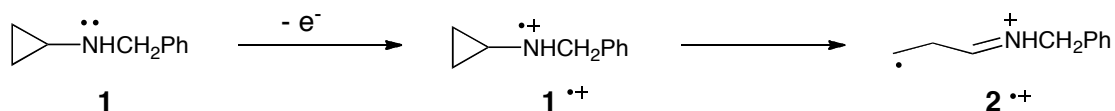
The chemistry of *N*-cyclopropyl amines has been used in enzymatic examinations of cP-450 to probe for an SET pathway. Photochemical and electrochemical examinations of *N*-methyl-*N*-cyclopropylaniline (**5**) revealed that the rate constant for cyclopropyl ring opening to be $4 \times 10^4 \text{ s}^{-1}$. This result can be explained by a resonance effect in which the spin and charge of the radical cation in the ring closed form is delocalized into the benzene ring hindering the overall rate of the ring opening reaction. Therefore a derivative of **5** was synthesized to provide a driving force for the ring opening reaction thereby accelerating the overall rate of the ring opening pathway. The electrochemical results reported herein show that the rate constant for ring opening of 4-chloro-*N*-methyl-*N*-(2-phenylcyclopropyl)aniline (**7**) to be $1.7 \times 10^8 \text{ s}^{-1}$. The formal oxidation potential (E°_{ox}) of **7** was determined to be 0.53 V. Results from preparative scale electrolysis are consistent with a ring opening process being operative for the chemical step.

4.1 Introduction

This chapter of the dissertation will focus on the cyclopropane ring opening reaction of (4-chloro-*N*-methyl-*N*-(2-phenylcyclopropyl)aniline] (**7**). A detailed discussion explaining the use of cyclopropanes to propose a single electron transfer (SET) mechanism for the oxidation of amines by cP-450 family of enzymes was presented in the previous chapter. Therefore only a brief description of the rationale for the work presented in this chapter will be discussed. This chapter will focus on the synthesis and electrochemistry of **7**, and will discuss how resonance affects the rate of ring opening of these radical cations.

4.1.1 Cyclopropyl Carbinyl Neutral Radical

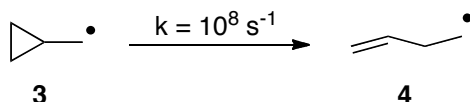
Several cyclopropyl amines have been reported to undergo oxidation by cP-450. Among these substrates, *N*-benzyl-*N*-cyclopropyl amine (**1**) has been commonly used to study the enzyme's mechanism; compound **1** renders the enzyme inert upon exposure.¹ This observation led to the hypothesis that the initial oxidation is an electron transfer step resulting in the formation of an amine radical cation (**1^{•+}**), which will rapidly ring open to generate the corresponding distonic radical cation **2^{•+}** (**Scheme 4-1**). **2^{•+}** is believed to covalently bind to the enzyme irreversibly, and render the enzyme inert.



Scheme 4-1 Ring opening of *N*-benzyl-*N*-cyclopropyl amine following an SET pathway.

The rate constants for the ring opening of *N*-cyclopropyl amines are expected to be within the same order of magnitude as the neutral cyclopropyl carbinyl free radical rearrangement (**Scheme 4-2**).^{2,3} Rate constants for the neutral carbon based radical are known to be on the order of 10^8 s^{-1} .⁴ Experimental evidence in conjunction with MO calculations imply that this assumption is

valid for aliphatic amines, but the data detailing the behavior of aromatic amines remains ambiguous.^{5,6} Due to the fact that *N*-cyclopropyl-*N*-methylaniline and several of its derivatives have been used as SET probes in cP-450 oxidations, the ring opening reaction must be competitive in relation to other competing pathways (e.g. deprotonation) for the probe to be effective.⁷

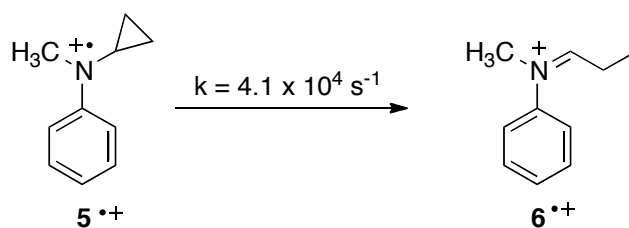


Scheme 4-2 Ring opening of the cyclopropyl carbinyl neutral radical.

4.1.2 Aromatic Amines

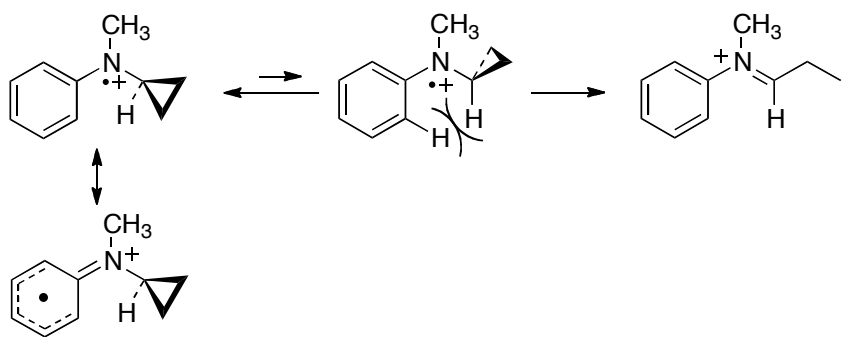
Recently in our laboratory, kinetic examinations of a series of aniline derivatives have been examined (**Figure 4-3**).⁷ Direct photoionization at 266nm (5% CH₃OH in CH₃CN) of *N,N*-dimethylaniline and *N*-methyl-*N*-cyclopropylaniline (**5**) utilizing nanosecond laser flash photolysis (LFP) showed absorption maxima in the region 460-490 nm consistent with the formation of the reactive radical cation.⁸ Although the molecules did show transient decays on the order of 10^6 s^{-1} with a λ_{max} of 460-490 nm, there exists no indication that a ring opening pathway was occurring. Photochemical experiments were augmented through linear sweep voltammetry and homogeneous redox catalysis studies. Direct electrochemical examinations of **5** showed that the compound undergoes a unimolecular rearrangement consistent with a cyclopropyl ring opening reaction (**Scheme 4-3**). Homogeneous redox catalysis experiments showed chemical step rate limiting behavior for three separate mediators. Examination of both the direct and indirect electrochemical data showed that the oxidation potential of *N,N*-dimethylaniline (+0.491 V) and *N*-methyl-*N*-cyclopropylaniline (**5**) are comparable (+0.528 V

vs. 0.1 M Ag⁺/Ag). Further examination of these results show that the rate constant for ring opening *N*-methyl-*N*-cyclopropylaniline was $4.1 \times 10^4 \text{ s}^{-1}$.



Scheme 4-3 Ring opening of *N*-methyl-*N*-cyclopropylaniline radical cation.

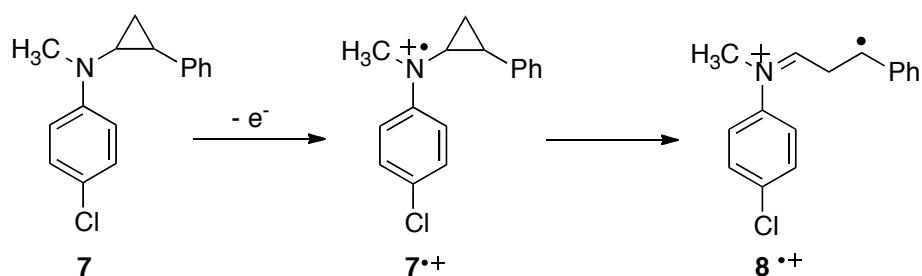
These results are best explained by two phenomena (**Scheme 4-4**): (i) a resonance effect in which the spin and charge of the radical cation in the ring closed form is delocalized into the benzene ring hindering the overall rate of the ring opening reaction, and/or (ii) the lowest energy conformation of the molecule does not meet the stereoelectronic requirements for a ring opening pathway. This chapter of the manuscript will address the resonance effects. A detailed discussion of stereoelectronic effects was presented in the previous chapter chapter.



Scheme 4-4 Depiction of (i) resonance delocalization of the radical cation, and (ii) stereoelectronic requirements for ring opening.

The hypothesis shown in **Scheme 4-4** depicts how the overall rate for the ring opening pathway of $5^{\bullet+}$ may be hindered by the ability of the spin and charge to be delocalized into the phenyl ring. This chapter aims to address the resonance effects that contribute to the hindered rate constant of the resonance stabilized radical cation ($5^{\bullet+}$) by examining the ring opening reaction

of $7^{•+}$ (Scheme 4-5). Following oxidation, compound $7^{•+}$ is expected to ring open to form the distonic radical cation $8^{•+}$. The formation of the resonance stabilized benzylic radical is expected to provide a driving force for the ring opening reaction thereby accelerating the overall rate of the ring opening pathway.



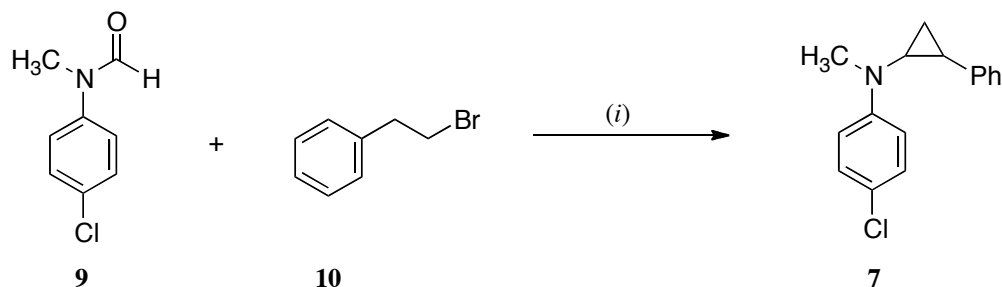
Scheme 4-5 Ring opening reaction of 4-chloro-*N*-methyl-*N*-(2-phenylcyclopropyl)aniline

4.2 Results and Discussion

4.2.1 Substrate Synthesis

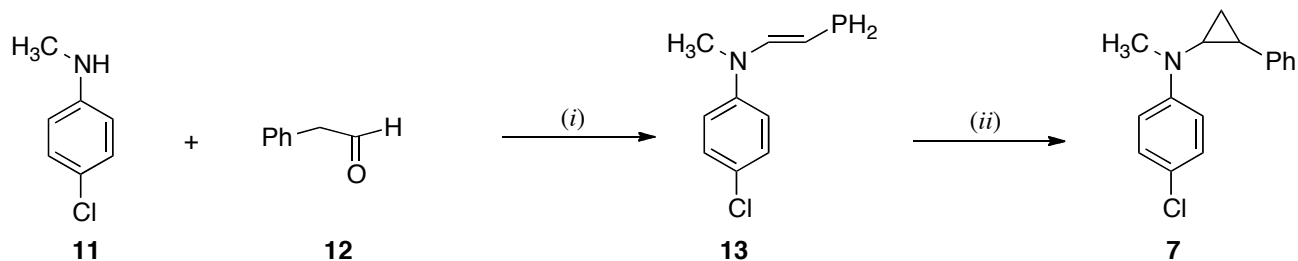
4.2.2 (4-chloro-*N*-methyl-*N*-(2-phenylcyclopropyl)aniline) (7)

Initial attempts to synthesize (4-chloro-*N*-methyl-*N*-(2-phenylcyclopropyl)aniline) (7) entailed the use of the titanium mediated cyclopropane chemistry that was very successful for the formation of the spiro cyclopropanes discussed in the previous chapter (Scheme 4-6).⁹ Compound 7 was envisioned to come from the reaction of commercially available *N*-(4-chlorophenyl)-*N*-methylformamide (9) and the Grignard reagent stemming from (2-bromoethyl)benzene (10). Multiple attempts to form the compound were attempted. No product was ever detected only recovered starting materials were ever isolated.



Scheme 4-6 Attempted synthesis of (4-chloro-*N*-methyl-*N*-(2-phenylcyclopropyl)aniline]): (i) Mg^0 , $\text{Ti}(\text{OPr})_4$, -78°C to RT, 17 hours.

Although attempts to use the titanium mediated cyclopropanation methodology were not successful, a second synthesis was devised to obtain the desired product. This chemistry involved a dehydration reaction of commercially available 4-chloro-*N*-methylaniline (**11**) and 2-phenylacetaldehyde (**12**) to give the enamine in 72% yield.³ Enamine **13** was then converted to the desired cyclopropane utilizing a modification of a Simmons-Smith reaction, in which the enamine was exposed to a diethylzinc couple in the presence of diiodomethane and trifluoroacetic acid. The final product **7** was obtained in 32% yield (**Scheme 4-7**).¹⁰

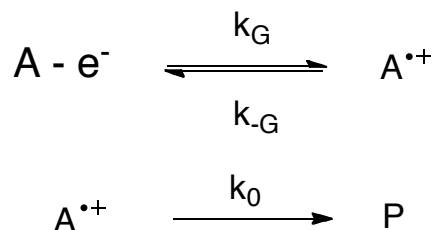


Scheme 4-7 Synthesis of (4-chloro-*N*-methyl-*N*-(2-phenylcyclopropyl)aniline): (i) reflux 17 hours, Et_2Zn , CH_2I_2 , TFA, -20°C – RT 3hrs.

4.2.3 Direct Electrochemistry

Cyclic voltammetry can be used to examine the kinetics of an electron transfer process. If a substrate can undergo a subsequent chemical transformation post electron transfer, the process is deemed to proceed via an EC mechanism (Electron transfer followed by a Chemical step) (**Scheme 4-8**).^{11, 12} During an EC process the substrate is oxidized at the electrode surface to generate $\text{A}^{\bullet+}$, and $\text{A}^{\bullet+}$ can then go on to form products. Kinetic information can be gained from voltammograms once several key components have been identified. Important components of

the voltammogram include: (i) E_p – peak potential, (ii) i_p – peak current, (iii) $E_{p/2}$ – half wave potential, and (iv) $(E_p - E_{p/2})$ – peak width.



Scheme 4-8 Representation of the EC mechanism.

An irreversible voltammogram is characterized by the lack of a wave on the reverse sweep. This phenomena can be the result of several mechanistic scenarios: (i) the electron transfer step is rate limiting, (ii) the chemical step is rate limiting, or (iii) a combination of both (mixed kinetic control). All three cases have been solved through the use of dimensionless variables (**Equations 4-1** and **4-2**) to solve the boundary value problem for each mechanistic scenario.¹² Terms are defined as follows: v is the scan rate, D is the diffusion coefficient, k_0 is the rate constant, k_G is the heterogeneous rate constant, and n is the number of electrons in the electron transfer step. These solutions will give rise to important features of the voltammogram.

$$\Lambda = k_G \left(\frac{DnFv}{RT} \right)^{-\frac{1}{2}} \quad \text{Equation 4-1}$$

$$\lambda = \frac{RTk_0}{nFv} \quad \text{Equation 4-2}$$

In the case where electron transfer is rate limiting, the EC mechanism will give rise to the following set of solutions to the boundary problem (**Equations 4-3** and **4-4**).¹² Characteristic voltammograms for an electron transfer rate limiting process are characterized by peak widths of 95 mV, and the change in peak potential with respect to scan rate will vary anodically by 59 mV per tenfold change in scan rate (v). **Equation 4-5** gives the relationship between the

heterogeneous rate constant (k_G) and the peak potential (E_p). If the formal oxidation potential is known for the substrate of interest then the heterogeneous rate constant k_G for electron transfer can be found from **4-5**.

$$\frac{dE_p}{d\log v} = \frac{29.6}{\alpha n} mV \quad \text{Equation 4-3}$$

$$E_p - E_{p/2} = \frac{1.85RT}{\alpha nF} \approx 95mV \quad \text{Equation 4-4}$$

$$E_p = E^o - \frac{0.783RT}{\alpha nF} - \frac{RT}{\alpha nF} \left(\ln \frac{D_0^{1/2}}{k_G} + \ln \left(\frac{nFv\alpha}{RT} \right)^{1/2} \right) \quad \text{Equation 4-5}$$

The circumstance where the chemical step is rate limiting will give rise to a separate set of solutions to the boundary problem (**Equations 4-6 and 4-7**).¹² Important diagnostic features for voltammograms of a system undergoing a chemical step rate limiting pathway include peak widths of 48 mV, and the change in peak potential with respect to scan rate will vary by approximately 30 mV. The substrate concentration **A** will have no bearing on the change in peak potential (**Equation 4-8**). **Equation 4-8** will hold true if the subsequent chemical transformation is a first order process. The solution to the boundary problem relating peak potential (E_p) to the rate constant for the chemical step (k_0) is shown in **Equation 4-9**. If the formal reduction potential of the compound is known, then this equation can be used to solve for the rate constant for the chemical step.

$$\frac{dE_p}{d\log v} = \frac{29.6}{n} mV \quad \text{Equation 4-6}$$

$$E_p - E_{p/2} = 1.85 \frac{RT}{nF} \approx 48mV \quad \text{Equation 4-7}$$

$$\frac{dE_p}{d\log[A]} = 0 \quad \text{Equation 4-8}$$

$$E_p = E^o - \frac{0.783RT}{nF} + \frac{RT}{2nF} \ln \frac{kRT}{vnF} \quad \text{Equation 4-9}$$

The last potential scenario is the case of mixed kinetic control. To solve for solutions of the boundary problem it is necessary to introduce two new variables, p and ξ . ξ is a dimensionless variable that defines the electrode potential and the heterogeneous rate constant for electron transfer **Equation 4-10**.^{12, 13} The parameter p measures the competition kinetics of the electron transfer step and the chemical step (for an α value of 0.5) **Equation 4-11**. The k_G term dominates as the function p approaches zero, conversely as p approaches infinity kinetic control is governed by k_0 . Experimentally one can diagnose mixed kinetic control by examining voltammograms ranging from low to high scan rate. At lower scan rates electrochemical runs will have features indicative of chemical step rate limiting, while at high scan rates voltammograms will have properties that resemble electron transfer rate limiting behavior. Characteristic features of voltammograms for a system under mixed kinetic control include, peak widths between 48-95 mV, and the change in peak potential with respect to scan rate will exhibit changes between 30 and 60 mV.

$$\xi = -\frac{\alpha F}{RT} (E - E_{A/A^{\cdot+}}) + \ln \left(k_G \sqrt{\frac{RT}{\alpha F v D}} \right) \quad \text{Equation 4-10}$$

$$p = \frac{F_v}{2RT} \frac{k_0 D^2}{k_G^4} \quad \text{Equation 4-11}$$

Experimental runs of compound **7** consisted of measuring the peak potential at multiple scan rates ($v = 100\text{-}1000$ mV/sec). Sample runs were measured at multiple concentrations. Characteristic features of the voltammograms included: (i) Peak potentials (E_p) on the order of 375 mV at 100 mV, (ii) Peak widths ($E_p - E_{p/2}$) between 78-85 mV, and (iii) a change in peak potential with respect to the scan rate ($dE_p/d\log v$) of 45.01 +/- 3 mV. A representative voltammogram is shown in **Figure 4-1**.

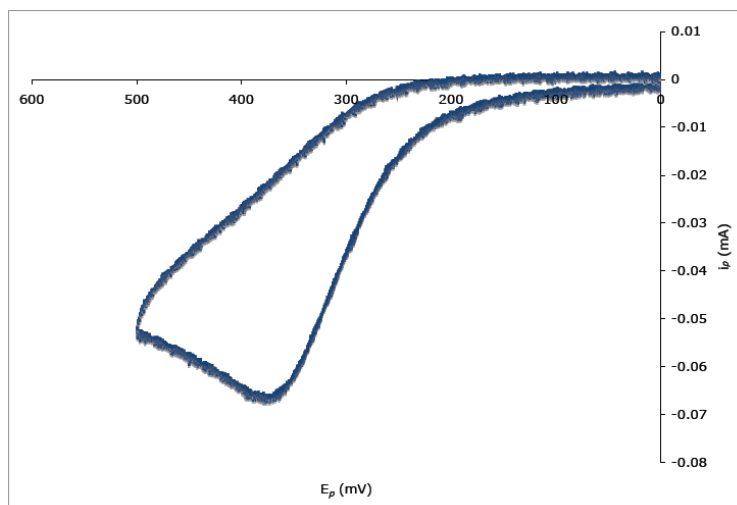


Figure 4-1 Cyclic voltammogram of **7** (0.1 M $\text{NBu}_4^+\text{BF}_4^-$, 0.5 M $\text{CH}_3\text{OH}/\text{CH}_3\text{CN}$, $\nu = 100$ mV/sec, 2.3 mM substrate)

Voltammograms for this system are indicative of mixed kinetic control. Changes in peak potential with respect to the scan rate are between 30 and 60 mV/decade. Peak widths are larger than expected for chemical step rate limiting behavior, but do not show characteristic peak broadening that is expected for an electron transfer rate limiting process. Plots showing the variation in peak potential with respect to the scan rate are shown in **Figures 4-2, 4-3, and 4-4**.

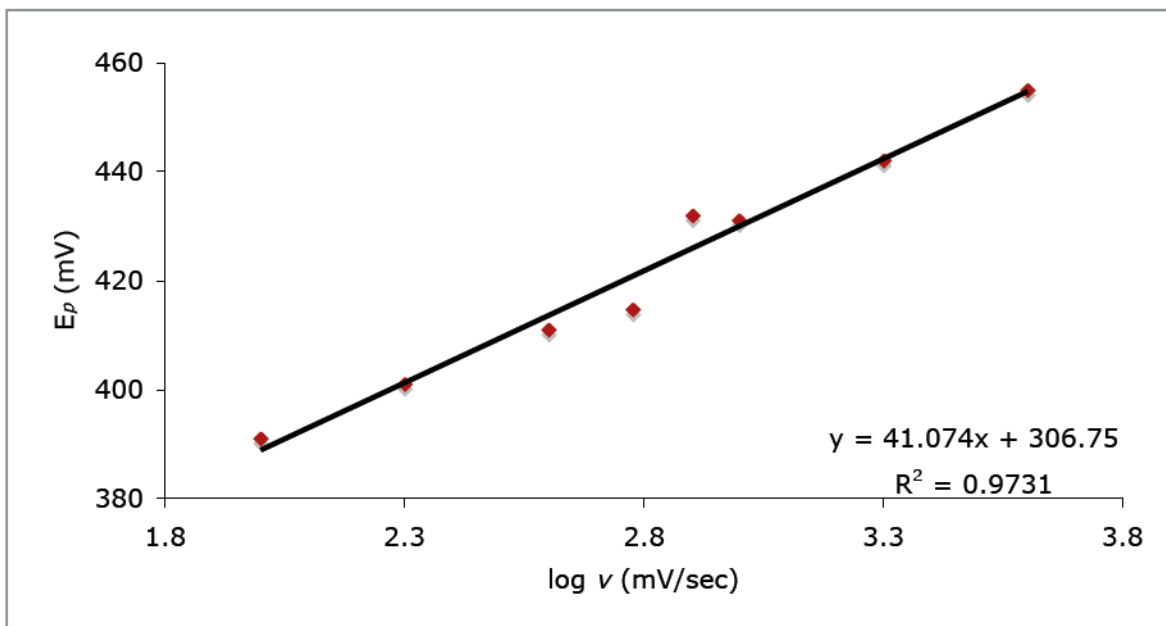


Figure 4-2 LSV analysis of 7, $\partial E_p/\partial \log v$ at 1.5 mM concentration. (0.1 M $\text{NBu}_4^+\text{BF}_4^-$, 0.5 M $\text{CH}_3\text{OH}/\text{CH}_3\text{CN}$, $v = 100\text{-}4000$ mV/sec)

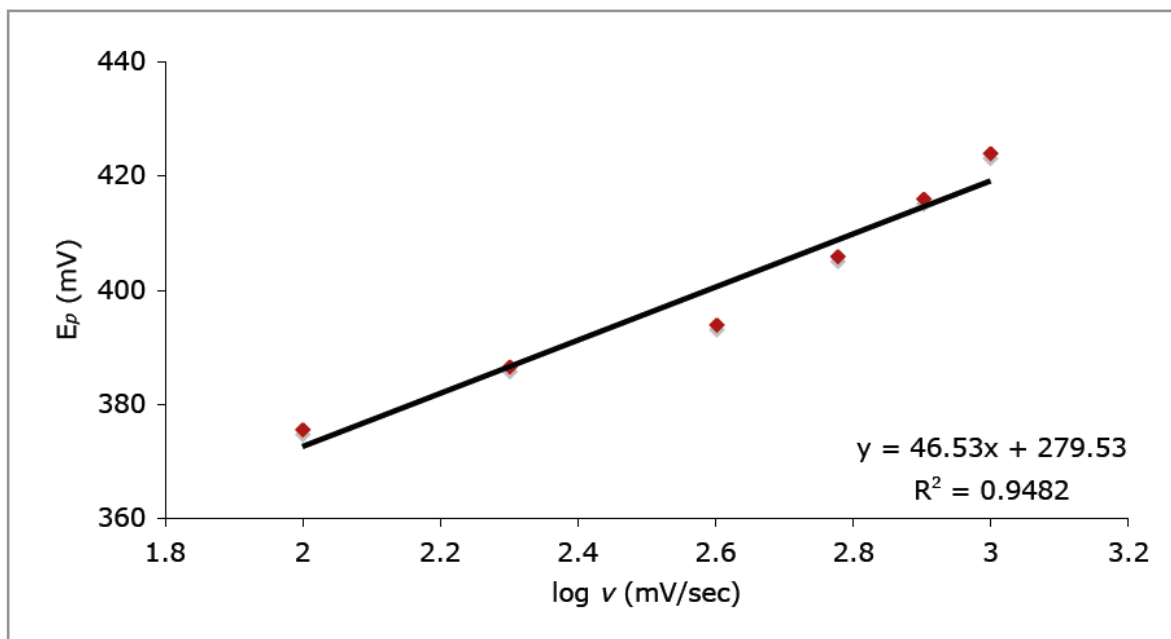


Figure 4-3 LSV analysis of 7, $\partial E_p/\partial \log v$ at 2.3 mM concentration. (0.1 M $\text{NBu}_4^+\text{BF}_4^-$, 0.5 M $\text{CH}_3\text{OH}/\text{CH}_3\text{CN}$, $v = 100\text{-}1000$ mV/sec)

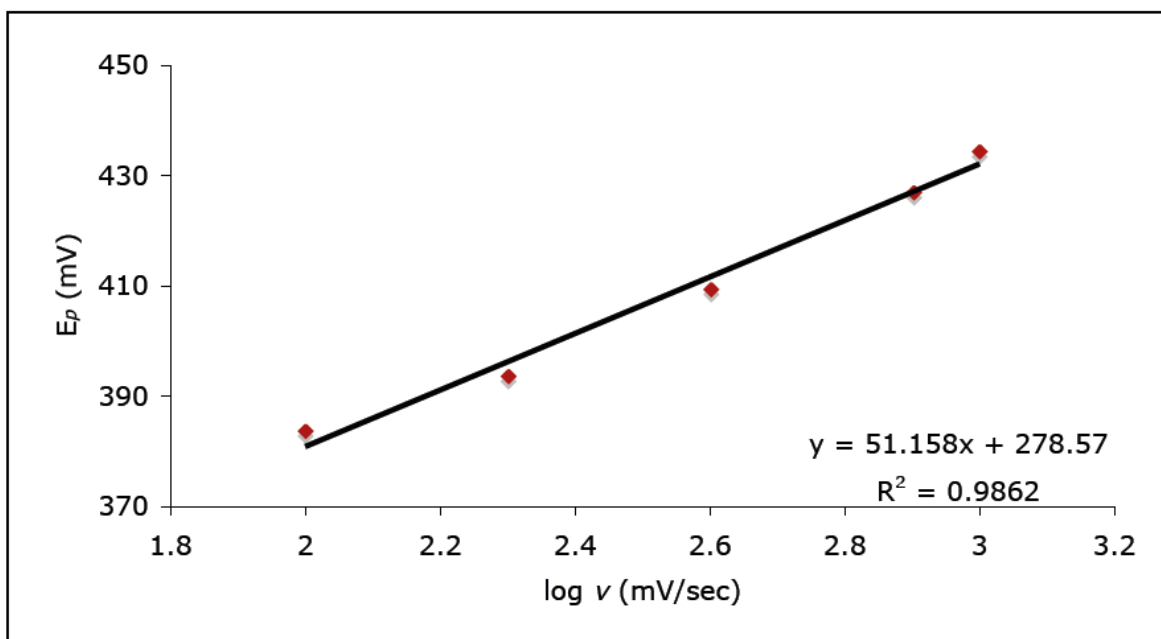


Figure 4-4 LSV analysis of **7**, $\partial E_p/\partial \log v$ at 2.5 mM concentration. (0.1 M $\text{NBu}_4^+\text{BF}_4^-$, 0.5 M $\text{CH}_3\text{OH}/\text{CH}_3\text{CN}$, $v = 100\text{-}1000$ mV/sec)

Theoretical working curves that account for the variation in peak width ($E_p - E_{p/2}$) and peak potential (E_p) with respect to the scan rate have been derived for the mixed kinetic control pathway. These working curves account for the peak potential based on **Equation 4-10** and the peak width is accounted for by **Equation 4-11**. Experimental data is then fit to these curves by plotting the data for the peak widths vs. log of v against the theoretical working curve to obtain a value for a new dimensionless variable C_1 , subsequent fitting of the experimentally obtained peak potentials against log v will yield a value for a second parameter C_2 (**Equations 4-12 and 4-13**).

$$C_1 = \log\left(\frac{F}{2RT} \frac{k_0 D^2}{k_G^4}\right) \quad \text{Equation 4-12}$$

$$C_2 = E_{A/A^{++}}^0 + \left(\frac{RT}{F} \ln 10\right) \log\left(\frac{k_0 D}{k_G^2}\right) \quad \text{Equation 4-13}$$

$$E_{A/A^{2+}}^0 + \left(\frac{RT}{2F} \ln 10\right) \log k_0 = C_2 - \left(\frac{RT}{2F} \ln 10\right) \left[C_1 - \log \left(\frac{F}{2RT} \right) \right] \quad \text{Equation 4-14}$$

Fitting the experimental data for the mixed kinetic control model results in values of 2.396 V and -0.254 V for C_1 and C_2 respectively. Values for the formal redox potential ($E_{A/A^{2+}}$) of the substrate and the rate constant for the subsequent chemical step (k_0) can be obtained by solving **Equation 4-14**. Experimental data correlated to the appropriate working curves for all runs are shown in **Figures 4-5** and **4-6**.

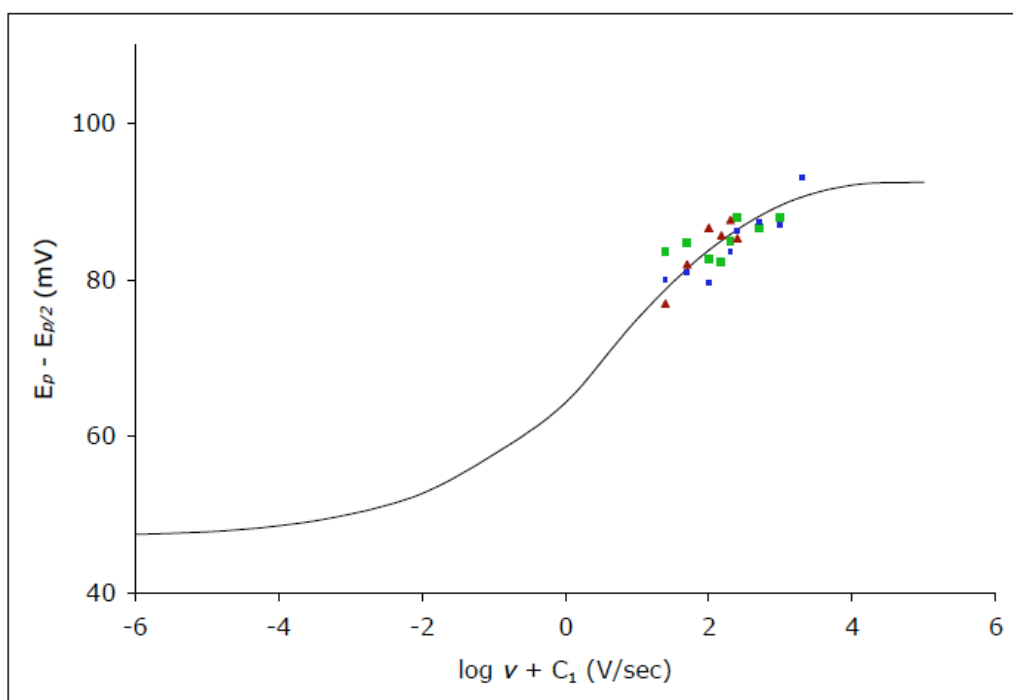


Figure 4-5 Working curve for the change in peak width ($E_p - E_{p/2}$) with respect to the log of the scan rate (v) to extract a value for C_1 .

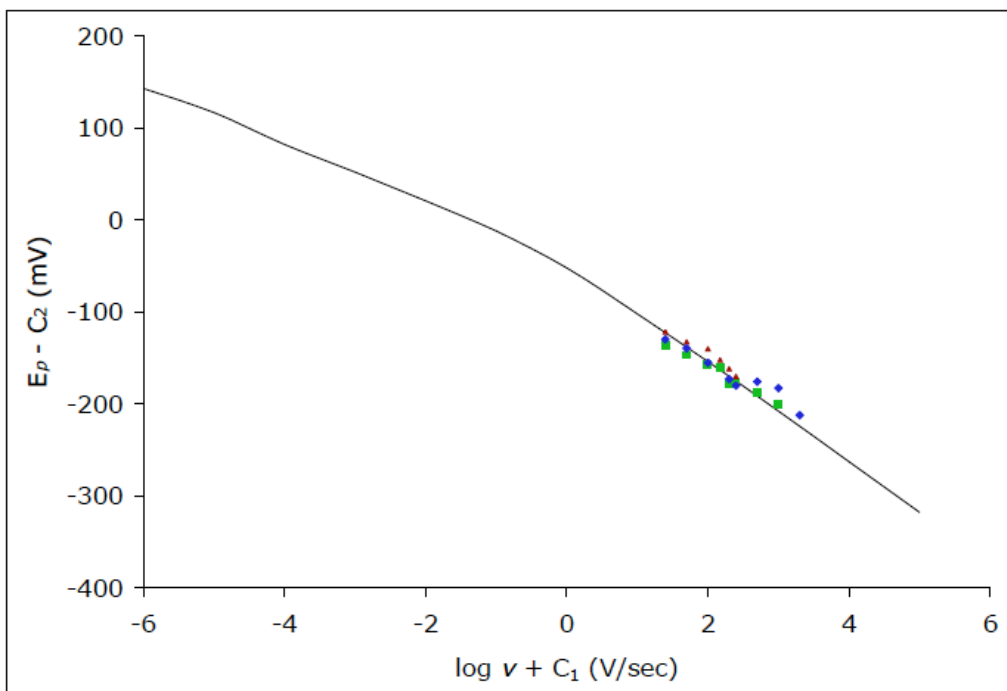
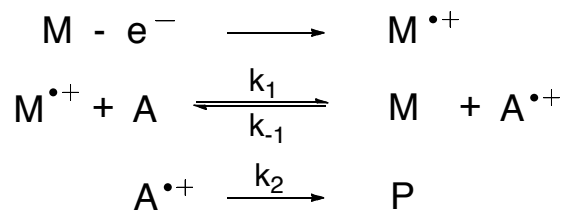


Figure 4-6 Working curve for the change in peak potential (E_p) with respect to the log of the scan rate (v) to extract a value for C_2 .

4.2.4 Indirect Electrochemistry

Mediated redox catalysis, a technique that utilizes an electro active compound to facilitate homogeneous electron transfer was used to augment the direct electrochemistry. Mediator **M** is oxidized to form $M^{\bullet+}$, $M^{\bullet+}$ will react with **A** to give $A^{\bullet+}$, and $A^{\bullet+}$ can then go onto products.



Traditional data analysis of redox catalysis data is processed from analysis of peak current ratios ((i) i_p – current drawn from mediator and substrate, (ii) i_{pd} – current drawn from mediator by itself) and plotting them against mediator concentration (C_M^0) at constant γ . When electron transfer is rate limiting the system is dependent on two dimensionless parameters λ_1 and γ

(Equations 4-15 and 4-16). As a result there will be a concentration dependence on the mediator at constant gamma.

$$\lambda_1 = \left(\frac{RT}{F} \right) \left(\frac{k_1 [M]}{v} \right) \quad \text{Equation 4-15}$$

$$\gamma = \frac{[A]}{[M]} \quad \text{Equation 4-16}$$

No kinetic information about the chemical step can be obtained if the electron transfer step is rate limiting, but two important values can be extracted from these experiments: (i) the standard redox potential compound of interest ($E^\circ_{(A/A^{•+})}$), and (ii) the rate constant for the electron transfer of the mediator and the substrate (k_1). This information can be obtained by examining a series of mediators that differ in redox potential. By plotting the rate constants of the forward electron transfer against the driving force (i.e., $E^\circ_{(M/M^{•+})} - E^\circ_{(A/A^{•+})}$), k_1 and $E^\circ_{(A/A^{•+})}$ can be obtained for the system if the data lies in the ‘activation’ and ‘counter diffusion’ regions (Figure 4-7).¹⁴ Redox catalysis measurements were necessary to obtain the rate constant between the mediator and compound **6** (k_1) as well as the standard redox potential (E°_{OX}) of **6** in order to solve Equation 14.

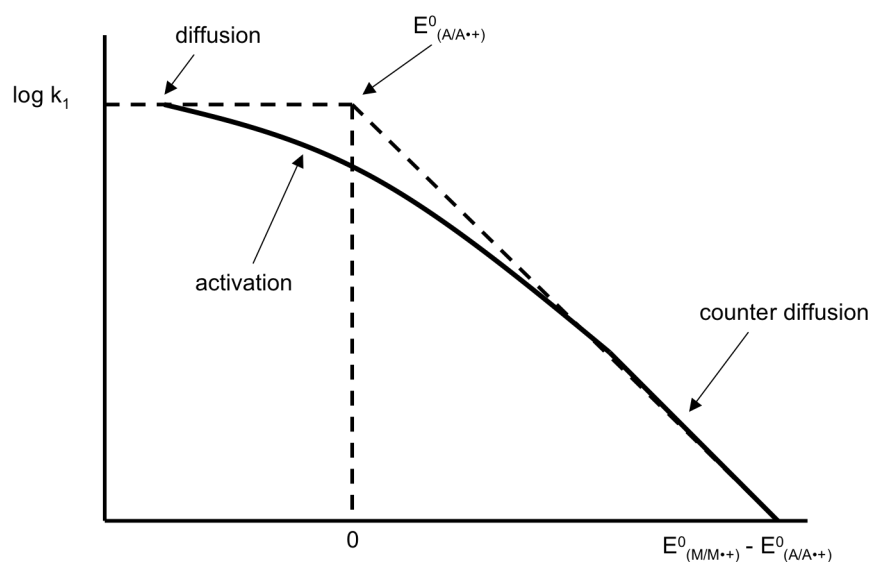


Figure 4-7 Representation of the procedure to extract k_1 and $E^\circ_{(A/A^{•+})}$ from experimental data

A series of theoretical working curves have been developed for this mechanistic regime that compare the peak current ratio (i_p/i_{pd}) to the dimensionless parameter $\lambda\lambda_1/\lambda_{-1}$. Comparison of plots [i_p/i_{pd} vs. $\log(1/\nu)$] and [i_p/i_{pd} vs. $\log C_M^\circ/\nu$] will unambiguously show any mediator dependence in the system. Peak current ratio (i_p/i_{pd}) is a function of $\log(C_M^\circ/\nu)$ when the electron transfer step is rate limiting, thus plots of [i_p/i_{pd} vs. $\log(C_M^\circ/\nu)$] will converge to one line, while plots of [i_p/i_{pd} vs. $\log 1/\nu$] will show three distinct curves. The difference between the experimental data and the theoretical values obtained from the working curves is directly related to the rate constant for the electron transfer step. **Figure 4-8** and **4-9** show some representative examples of the data obtained for reductive catalysis experiments utilizing ferrocene carboxylic acid ($E^\circ_{\text{ox}} = 0.264 \text{ V}$) as a mediator for compound **7**.

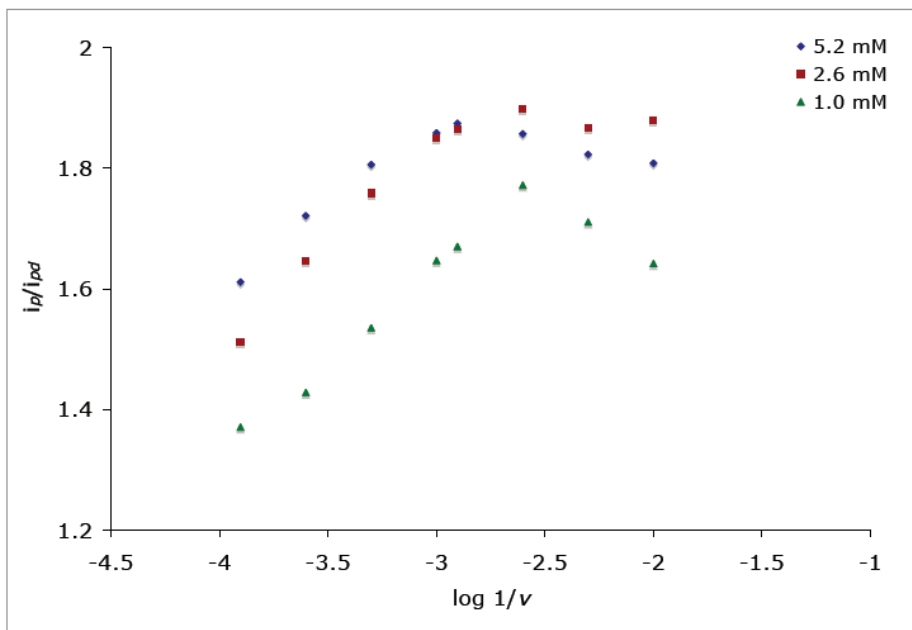


Figure 4-8 [i_p/i_{pd} vs. $\log(1/\nu)$] – Mediated redox catalysis of **7** by ferrocene carboxylic acid, (0.1M LiOCl₄, 0.5M CH₃OH/CH₃CN, $\gamma = 1$, $\nu = 100 - 8000 \text{ mV/sec}$)

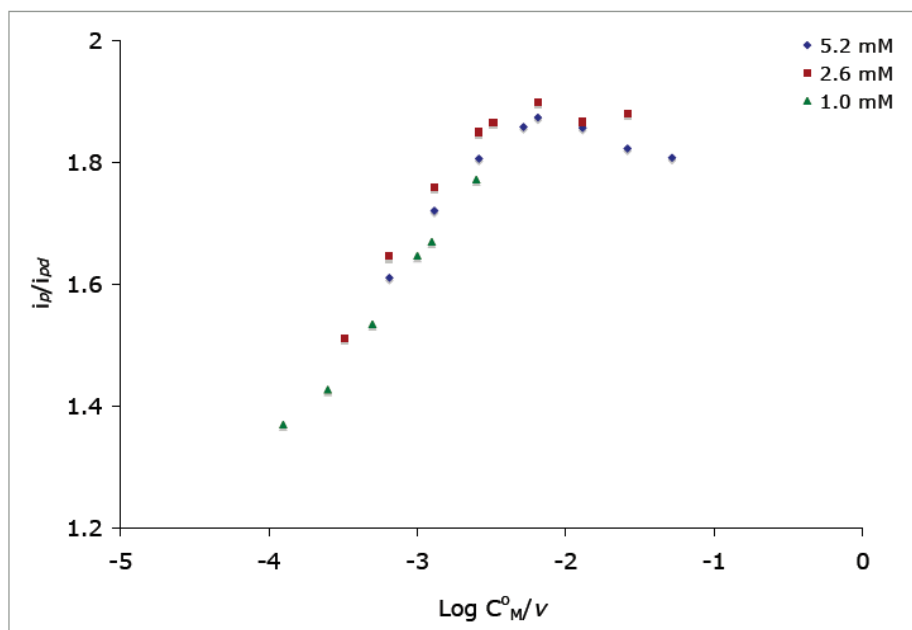


Figure 4-9 [i_p/i_{pd} vs. $\log (C_M^0/v)$] – Mediated redox catalysis of **7** by ferrocene carboxylic acid, (0.1M LiOCl₄, 0.5M CH₃OH/CH₃CN, $\gamma = 1$, $\nu = 100 - 8000$ mV/sec)

As shown by **Figures 4-8** and **4-9** i_p/i_{pd} varies with respect to mediator concentration, therefore the electron transfer step is the rate limiting. By fitting the experimental data to the appropriate published working curves the rate constant for the electron transfer between the mediator and **7** (k_1) can be obtained (**Appendix B**).^{15, 16} The driving force for electron transfer (ΔG_{ET}) can be obtained through the use of **Equation 4-15**, and the formal redox potential (E°_{OX}) for the substrate can be extracted from **Equation 4-16**.

$$\Delta G_{ET} = -RT \ln k_1 \quad \text{Equation 4-17}$$

$$K_1 = \frac{k_1}{k_{-1}} = \exp \left[\frac{F}{RT} (E_{A/A^{*+}} - E_{M/M^{*+}}) \right] \quad \text{Equation 4-18}$$

Redox catalysis data revealed the oxidation potential of **7** to be 0.527V. The formal oxidation potential (E°_{OX}) could then be used to solve **Equation 4-14** to yield a value of $1.3 \times 10^8 \text{ s}^{-1}$ for the rate constant of the chemical step (k_0).

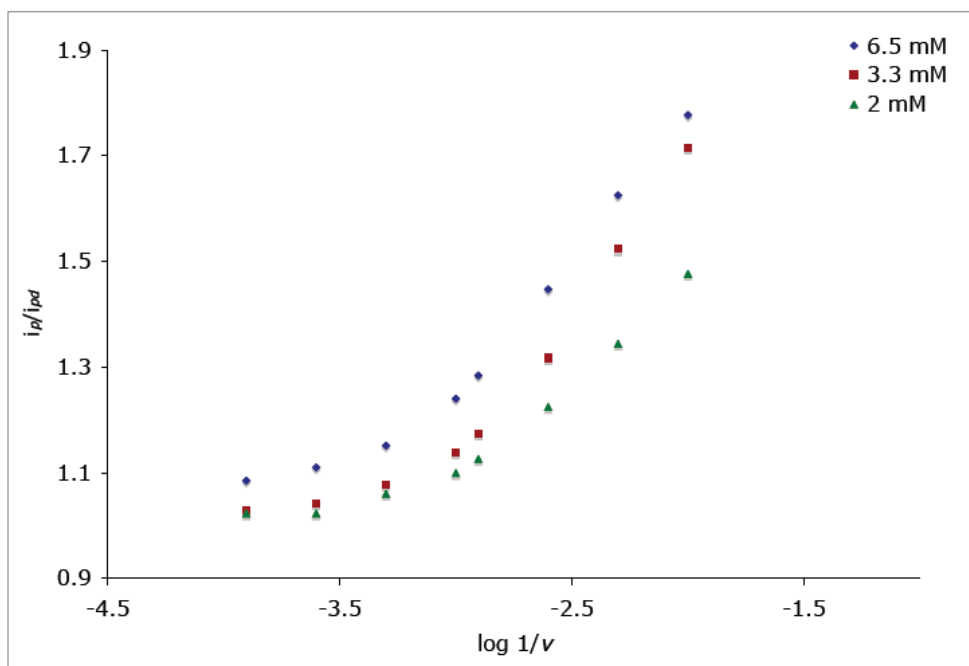


Figure 4-10 [i_p/i_{pd} vs. $\log(1/v)$] – Mediated redox catalysis of **7** by 4-cyanophenyl ferrocene, (0.1M LiOCl₄, 0.5M CH₃OH/CH₃CN, $\gamma = 1$, $v = 100 - 8000$ mV/sec)

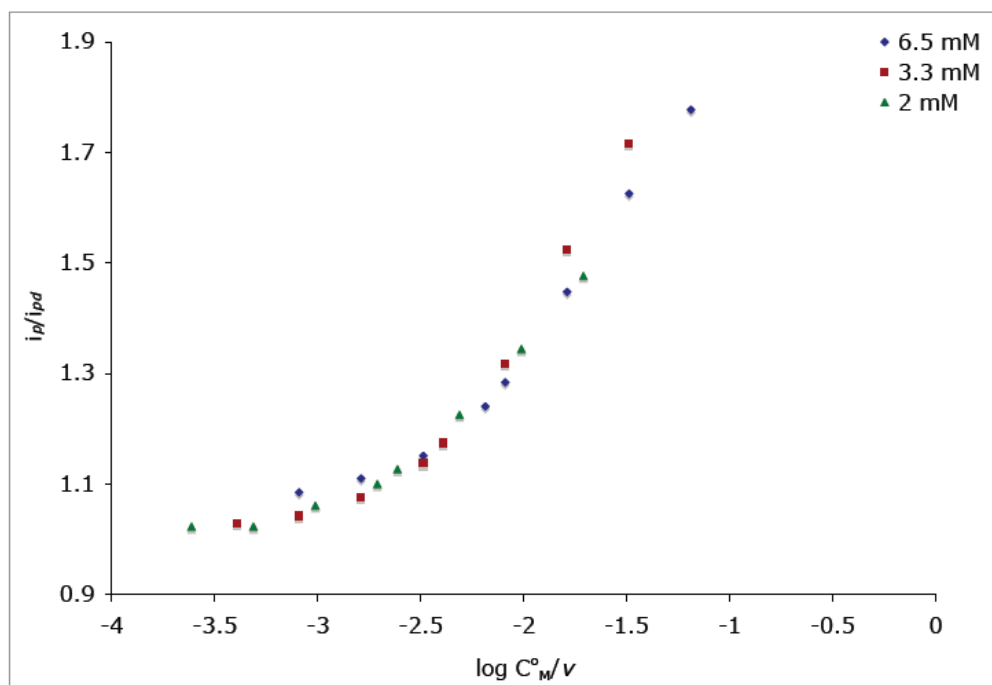


Figure 4-11 [i_p/i_{pd} vs. $\log(C_M^0/v)$] – Mediated redox catalysis of **7** by 4-cyanophenyl ferrocene, (0.1M LiOCl₄, 0.5M CH₃OH/CH₃CN, $\gamma = 1$, $v = 100 - 8000$ mV/sec)

A second set of experiments was conducted using 4-(cyanophenyl)-ferrocene as mediator ($E^{\circ}_{\text{ox}} = 0.145 \text{ V}$). **Figure 4-10** and **4-11** show some representative examples of the data obtained for this second set of runs. Analysis of the data provided a value of 0.533V was obtained for the oxidation potential, and a value of $2.1 \times 10^8 \text{ s}^{-1}$ was obtained for the rate constant for ring opening (k_0).

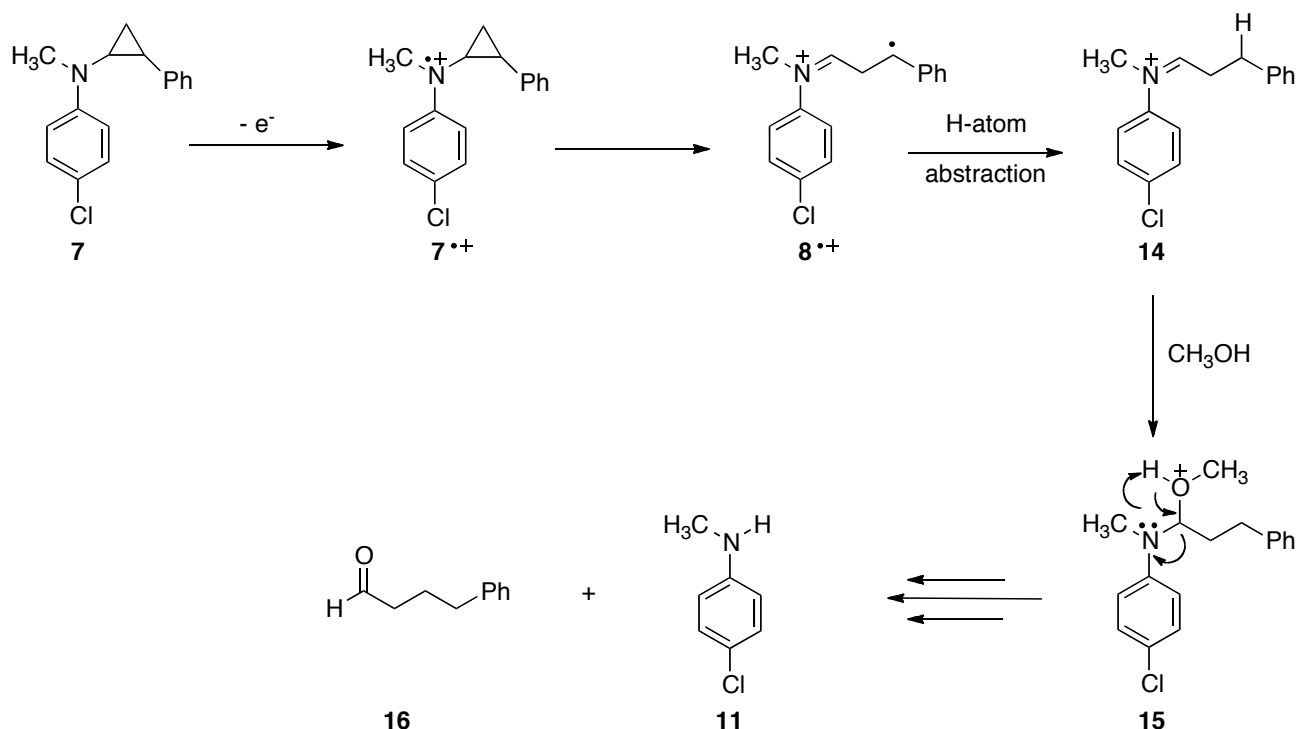
4.2.5 Preparative Scale Electrolysis (Bulk Electrolysis)

To ensure that a ring opening pathway was indeed occurring following the direct and indirect electrochemistry, preparative scale electrolysis was performed on compound **7**. Preparative scale oxidations were conducted in a standard H-cell containing a glass frit serving as a salt bridge. Compounds were oxidized for a fixed amount of time, corresponding to the number of moles of electrons passed through the solution over the course of the experiment. Sample solutions were then quenched and analyzed by GC-MS. Unfortunately, large samples (e.g. gram quantities) were unable to be examined utilizing this method due to problems with electrode fouling. For this reason micro-molar solutions had to be utilized for the work described herein; attempts to isolate and characterize products via traditional analytical techniques were not feasible.

Constant current electrolysis runs were conducted for these examinations in order to alleviate problems with electrode fouling. Two equivalents of electrons were passed through the samples in an attempt to drive the reaction to completion (initial runs utilizing one electron equivalents resulted lowered reaction yields). Analysis of samples post reaction showed the formation of 4-chloro-*N*-methyl aniline (**10**), which is consistent with a cyclopropyl ring opening pathway (**Scheme 4-9**). The proposed mechanism for the formation **10** consists of an initial oxidation of **7** at the electrode surface to yield **7^{•+}**. Compound **7^{•+}** can then subsequently ring open to yield the distonic radical cation **8^{•+}**. The benzylic radical would then undergo a hydrogen abstraction from

the solvent. The highly electrophilic imine is then susceptible to nucleophilic attack by methanol from the solvent to generate compound **15**. Under equilibrium conditions **15** will then fragment to give 4-chloro-*N*-methyl aniline (**11**) and 3-phenylpropanaldehyde (**16**).

Analysis of product mixtures following electrolysis led to the formation of one peak post reaction. Formation of compound **11** was fully characterized by comparison of mass spectral data of product solutions to authentic samples. Reduction of aldehydes by NaBH₄ are known to produce alcohols, therefore compound **16** should yield the corresponding alcohol following work up conditions. Exposure of the aldehyde **16** to bulk electrolysis conditions resulted formation of the alcohol in diminished yields. Mass balance for either product following bulk electrolysis runs were never obtained. The inability to detect the aldehyde in sample runs is presumably due to loss of products in the aqueous layer.



Scheme 4-9 Proposed mechanism for the reaction of **6** following bulk electrolysis.

4.3 Conclusions

LSV analysis of 4-chloro-*N*-methyl-*N*-(2-phenylcyclopropyl)aniline (**6**) showed mixed kinetic control behavior. Subsequent redox catalysis experiments showed rate limiting electron transfer. Fitting to the appropriate working curves revealed the formal oxidation potential (E°_{ox}) of **6** to be 0.53 V. The rate constant for the ring opening reaction of the radical cation was determined to be $1.7 \times 10^8 \text{ s}^{-1}$. A detailed discussion rationalizing the accelerated rate constant and redox potential of **7** is presented in Chapter 5.

4.4 Experimental Section

4.4.1 Materials and Purification

All chemicals used for this study were obtained from Aldrich and used as received unless otherwise noted. Acetonitrile and dichloromethane were distilled over CaH_2 prior to use. Tetrahydrofuran was distilled over Na/benzophenone prior to use. All solvents used for synthesis unless otherwise specified were ACS grade solvents and were not treated in any way prior to use.

4.4.2 Instrumentation

NMR spectra were obtained on a JOEL Eclipse Plus 500 MHz spectrometer. Chemical shifts are reported in ppm using the residual solvent peak (CDCl_3) as the internal standard. GC/MS was obtained on a Hewlett-Packard HP6890 gas chromatograph linked to a HP 5973 Mass Selective Detector interfaced to an HP series computer. Gas chromatography was performed on a Hewlett-Packard 5890A GC equipped with an FID detector and an HP 3393A integrator.

4.4.3 Synthesis

4.4.3.1 (*E*)-4-chloro-*N*-methyl-*N*-styrylaniline (13).³ Distilled 2-phenylacetaldehyde (2.2g, 18.3 mmol) and 4-chloro-*N*-methylaniline (2.8 g, 19.7 mmol) was dissolved in 100 mL dry benzene. The flask was then fitted with a Dean-Stark trap and reflux condenser. The reaction was then heated to reflux for 12 hours. Following overnight reflux the flask was allowed to cool to room temperature. Benzene was removed under reduced pressure. The resulting solid was recrystallized in hexane to give a fine yellow powder. ¹H NMR (CDCl₃) δ 7.31-7.23 (m, 7H), 7.13-7.07 (m, 1H), 6.98 (d, 2H), 5.7 (d, 1H), 3.27 (s, 3H).

4.4.3.2 4-chloro-*N*-methyl-*N*-(2-phenylcyclopropyl)aniline (7).^{3, 10} A 50 mL round bottom flask was equipped with a magnetic stir bar and placed under N₂. The flask was cooled to -78°C and 4 mL dry CH₂Cl₂ was added to the flask. Diethyl zinc (4.1 mL, 4.11 mmol) and a solution of diiodomethane in 3 mL CH₂Cl₂ (0.66 mL, 8.23 mmol) was added to the flask. The mixture was then warmed to -20°C and allowed to stir for 30 minutes. A solution of trifluoroacetic acid in 2 mL CH₂Cl₂ (0.32 mL, 4.1 mmol) was then added to the flask. The solution was allowed to stir for an additional 30 minutes, and X (0.5g, 2.05 mmol) in 2 mL CH₂Cl₂ was added to the mixture. The reaction was then allowed to stir for 3 hours. The reaction mixture was diluted with 25 mL ether and washed twice with 30 mL of 10% aqueous NH₄OH, water, and brine. The organic layer was dried over NaSO₄ and evaporated to dryness. The crude product was purified via column chromatography on alumina (EtOAc/hexanes 5:95) yielding a pale yellow oil: ¹H NMR (500 MHz, CDCl₃) δ 7.55 (s, 1H), 7.14 (m, 2H), 6.65 (d, 2H), 2.94 (t, 2H), 2.63 (t, 2H). m/z 257, 207, 117.

4.4.3.3 Sample ferrocene synthesis [1-(4-Cyanophenyl)ferrocene]. *p*-Cyanoaniline (5g, 42.5 mmol) was dissolved in 100 mL 20% sulfuric acid. Sodium nitrite (5.8g, 84.5 mmol) was added

to the solution over a 20 minute period at 0°C. The solution was then allowed to stir for 1 hour with constant stirring. Ferrocene (15.7g, 84.5 mmol) was dissolved in a minimum volume of CH₂Cl₂ and 300 mL glacial acetic was added to the ferrocene mixture. The flask was then cooled to 0°C and the p-cyano diazonium solution was added to the ferrocene mixture. The reaction was then allowed to stir for 48 hours at room temperature. The reaction was quenched with saturated NaHCO₃, and the resulting solution was extracted with CH₂Cl₂ (3 x 200mL). The organic layer was dried with Na₂SO₄ and evaporated to dryness. The material was purified via column chromatography on silica gel (EtOAc/Hexanes 5:95) yielding a maroon solid: E°_{ox} = 145 mV (Ag/AgNO₃, 0.1M in CH₃CN)

4.4.3.4 Tetrabutylammonium tertafluoroborate. Tetrabutylammonium bromide (84g, 0.261 mol) was dissolved in a minimum volume of water. Fluoroboric acid (36 mL, 0.271 mol) was added to the solution. A white precipitate formed that was filtered on a buchner funnel. The resulting solid was then washed with water until the filtrate was of neutral pH. The crude salt was recrystallized three times with ethyl acetate/hexanes to yield a white powder. The resulting crystalline material was then placed under vacuum for 4 hours to remove any residual solvent.

4.4.4 Direct and Indirect Electrochemistry

Electrochemical measurements were obtained on a Princeton Applied Research (EG & G) 273 model potentiostat/galvanostat. All data was processed on a 386 model PC running windows 3.1. Samples solutions were prepared in distilled acetonitrile/methanol containing 0.1M tetrabutyl ammonium tetrafluoroborate prior to use. The electroactive substrate was purified by prep-TLC prior to analysis. All solutions were degassed for 10 minutes prior to analysis. A standard three electrode cell was used for all runs. A glassy carbon electrode working electrode (area = 0.14 cm²) was prepared by polishing over 0.5μ silica slurry until a mirror finish was obtained.

The auxiliary electrode was fabricated from a platinum wire coil. The reference electrode was prepared prior to each run (Ag/AgNO₃, 0.1M in CH₃CN). All runs were recorded in triplicate for direct electrochemical runs and in duplicate for reductive catalysis experiments unless otherwise noted.

4.4.5 Preparative Scale Electrolysis

Preparative scale oxidations were conducted in a standard H-cell containing a glass frit serving as a salt bridge. The electrodes for the experiments were prepared in the following way: (i) the working electrode was made from mesh platinum wire soldered on to copper wire, (ii) the auxiliary electrode was assembled from coiled copper wire, and (iii) the reference electrode was composed in the same fashion that was described for the direct and indirect electrochemical measurements. Constant current measurements were run with respect to how many molar equivalents of electrons that was passed through the reaction mixture. Constant potential experiments were run at a potential 100 mV more positive than the oxidation potential of the substrate after solution resistance was accounted for.

4.4.5.1 Sample Preparative Electrolysis

25 mL solutions containing 0.1 M LiOCl₄ in 0.5 M CH₃OH in CH₃CN were prepared for both oxidative and reductive compartments of the H-cell. Substrate in micromolar concentrations was added to the oxidative side of the H-cell. The solution was then degassed with argon for the duration of the experiment. Post electrolysis the solutions were treated with an excess of sodium borohydride and allowed to stir for 10 minutes. The solution was diluted with water and the organic layer was extracted with 2 x 15 mL CH₂Cl₂. Samples were analyzed by GC and GC-MS.

4.4.6 Digital Simulations

Digital simulations were performed using Digisim 2.1 (Bioanalytical Systems Inc., Kent ave. W. Lafayette, IN 47096). Fitting the experimental data to the appropriate published working curve was aided through the use of TableCurve 2D (Jandel Scientific Software: 2591 Kerner Blvd. San Rafael, CA 94901).

Supplementary Data

Details of simulated working curves are presented in Appendix B of this dissertation.

References

1. Hanzlik, R. P.; Tullman, R. H., Suicidal Inactivation of Cytochrome-P-450 by Cyclopropylamines - Evidence for Cation-Radical Intermediates. *Journal of the American Chemical Society* **1982**, *104* (7), 2048-2050.
2. Shaffer, C. L.; Morton, M. D.; Hanzlik, R. P., Enzymatic N-dealkylation of an N-cyclopropylamine: An unusual fate for the cyclopropyl group. *Journal of the American Chemical Society* **2001**, *123* (2), 349-350.
3. Loeppky, R. N.; Elomari, S., N-alkyl-N-cyclopropylanilines as mechanistic probes in the nitrosation of N,N-dialkyl aromatic amines. *Journal of Organic Chemistry* **2000**, *65* (1), 96-103.
4. Newcomb, M.; Johnson, C. C.; Manek, M. B.; Varick, T. R., *J. Am. Chem. Soc.* **1992**, *114*, 10915-10921.
5. Bouchoux, G.; Alcaraz, C.; Dutuit, O.; Nguyen, M. T., Unimolecular chemistry of the gaseous cyclopropylamine radical cation. *Journal of the American Chemical Society* **1998**, *120* (1), 152-160.
6. Qin, X. Z.; Williams, F., Electron-Spin-Resonance Studies on the Radical Cation Mechanism of the Ring-Opening of Cyclopropylamines. *Journal of the American Chemical Society* **1987**, *109* (2), 595-597.
7. Li, X. Z.; Grimm, M. L.; Igarashi, K.; Castagnoli, N.; Tanko, J. M., The first calibration of an aminiumyl radical ion clock: why N-cyclopropylanilines may be poor mechanistic probes for single electron transfer. *Chemical Communications* **2007**, (25), 2648-2650.
8. Maslak, P.; Chapman, W. H.; Vallombroso, T. M. J.; Watson, B. A., Mesolytic Scission of C-C Bonds in Radical Cations of Amino Derivatives: Steric and Solvent Effects. *Journal of the American Chemical Society* **1995**, *117*, 12380-12389.
9. de Meijere, A.; Kozhushkov, S. I.; Savchenko, A. I., Titanium-mediated syntheses of cyclopropylamines. *Journal of Organometallic Chemistry* **2004**, *689* (12), 2033-2055.
10. Lorenz, J. C.; Long, J.; Yang, Z. Q.; Xue, S.; Xie, Y.; Shi, Y., A novel class of tunable zinc reagents (RXZnCH₂Y) for efficient cyclopropanation of olefins. *Journal of Organic Chemistry* **2004**, *69* (2), 327-334.
11. Bard, A. J.; Faulkner, L. R., *Electrochemical Methods. Fundamentals and Applications*. John Wiley & Sons, Inc.: New York, 2001.
12. Nadjo, L.; Saveant, J. M., Linear Sweep Voltammetry: Kinetic Control by Charge Transfer and or Secondary Chemical Reactions. *Electroanalytical Chemistry and Interfacial Electrochemistry* **1973**, *48*.

13. Costentin, C.; Robert, M.; Saveant, J. M., Fragmentation of aryl halide pi anion radicals. Bending of the cleaving bond and activation vs driving force relationships. *Journal of the American Chemical Society* **2004**, *126* (49), 16051-16057.
14. Andrieux, C. P.; Hapiot, P.; Saveant, J. M., Fast Kinetics by Means of Direct and Indirect Electrochemical Techniques. *Chem Rev* **1990**, *90* (5), 723-738.
15. Stevenson, J. P.; Jackson, W. F.; Tanko, J. M., Cyclopropylcarbinyl-type ring openings. Reconciling the chemistry of neutral radicals and radical anions. *Journal of the American Chemical Society* **2002**, *124* (16), 4271-4281.
16. Tanko, J. M.; Li, X. Z.; Chahma, M.; Jackson, W. F.; Spencer, J. N., Cyclopropyl conjugation and ketyl anions: When do things begin to fall apart? *Journal of the American Chemical Society* **2007**, *129* (14), 4181-4192.

Chapter 5 Rational for Experimental Findings and Concluding Remarks

Contributions

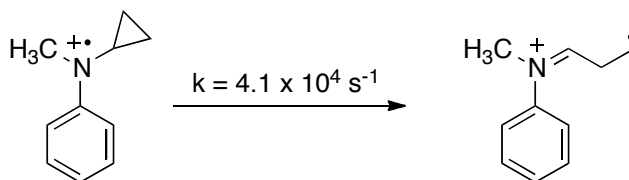
This chapter represents contributions from two sources: (i) a summary of published work describing the rate constant for the ring opening of *N*-cyclopropyl-*N*-methylaniline (**5**),¹ and (ii) the design, synthesis, and reaction kinetics of 4-chloro-*N*-methyl-*N*-(2-phenylcyclopropyl)aniline (**6**), 1'-methyl-3',4'-dihydro-1'*H*-spiro[cyclopropane-1,2'-quinoline] (**7**), and 6'-chloro-1'-methyl-3',4'-dihydro-1'*H*-spiro[cyclopropane-1,2'-quinoline] (**8**).² Contributions from the authors are as follows: Michelle L. Grimm (author of this dissertation) performed the photochemistry of all compounds.¹ Dr. Xiangzhong Li performed the electrochemistry and product studies of compounds **1** and **5**.¹ Dr. James M. Tanko and Dr. Neal Castagnoli contributed to the writing and editing of the manuscript, as well as aided in the intellectual contributions of the work. Dr. James M. Tanko prepared and submitted the manuscript.

For the second manuscript (now in preparation), contributions from the authors are as follows: synthesis, electrochemistry and product studies of compounds **6**, **7**, and **8** were all conducted by Michelle L. Grimm.² Selected synthetic steps were repeated by Eveline Reichert and Amber N. Hancock. Branden Fanovic and Justin Curtiss provided the computational data, and Dr. Travis Dudding aided significantly to the intellectual merit of the document. Dr. James M. Tanko contributed to the writing and editing of the manuscript in addition to preparing the work for publication.

1. Li, X.; Grimm, M. L.; Castagnoli, N.; Igarashi, K.; Tanko, J. M. The First Calibration of an Aminiumyl Radical Ion Clock: Why *N*-cyclopropylanilines May Be Poor Mechanistic Probes for Single Electron Transfer. *Chem. Commun.* **2007**, 2648-2650.
2. Grimm, M. L.; Hancock, A. N.; Reichert, E.; Fonovic, B.; Suleman, N. K.; Ashraf, M.; Dudding, T.; Castagnoli, N.; Tanko, J. M. Development of New *N*-cyclopropyl Based Electron Transfer Probes for Enzyme Catalyzed Reactions: Stereoelectronic and Resonance Effects. (Manuscript in preparation).

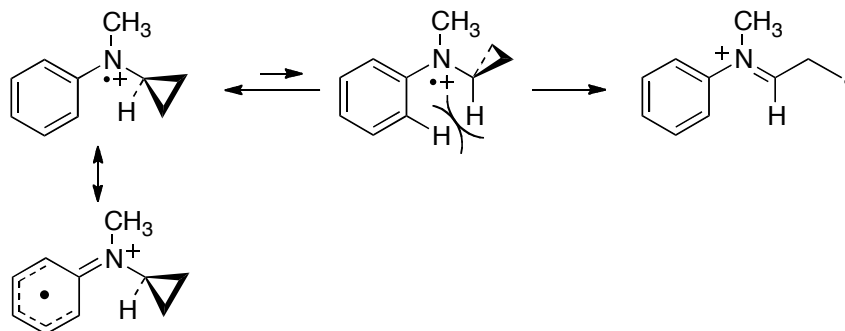
5.1 Introduction

The chemistry of *N*-cyclopropyl amines has been used to study the mechanism of amine oxidations by cP-450. Until recently, the rate constant for these ring opening reactions has not been reported.¹ Direct electrochemical examinations of **5** showed that the radical cation undergoes a unimolecular rearrangement consistent with a cyclopropyl ring opening reaction (**Scheme 5-1**). Homogeneous redox catalysis experiments showed chemical step rate limiting behavior for three separate mediators. Examination of both the direct and indirect electrochemical data showed that the oxidation potential of *N,N*-dimethylaniline (**1**) (+0.491 V) and *N*-cyclopropyl-*N*-methylaniline (**5**) are comparable (+0.528 V vs. 0.1 M Ag⁺/Ag). Further examination of these results show that the rate constant for ring opening *N*-methyl-*N*-cyclopropylaniline radical cation was $4.1 \times 10^4 \text{ s}^{-1}$.



Scheme 5-1 Ring opening of *N*-cyclopropyl-*N*-methylaniline radical cation (**5^{•+}**).

These results are best explained by two phenomena (**Scheme 5-2**): (i) a resonance effect in which the spin and charge of the radical cation in the ring closed form is delocalized into the benzene ring hindering the overall rate of the ring opening reaction, and/or (ii) the lowest energy conformation of the molecule does not meet the stereoelectronic requirements for a ring opening pathway. A detailed discussion of stereoelectronic and resonance effects were presented in chapters 3 and 4.



Scheme 5-2 Depiction of (i) resonance delocalization of the radical cation, and (ii) stereoelectronic requirements for ring opening.

5.2 Summary of Results Presented in Chapters 4 and 5

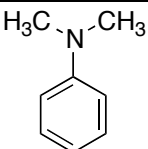
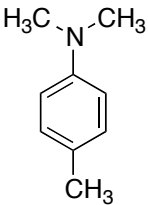
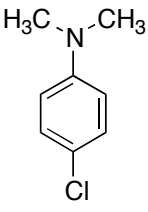
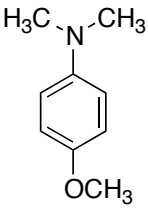
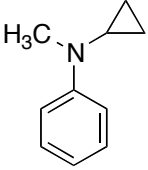
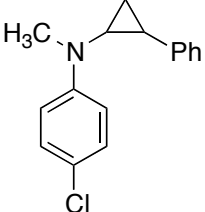
In order to probe whether a resonance or stereoelectronic effect resulted in the slowed rate constant for ring opening of *N*-methyl-*N*-cyclopropylaniline radical cation ($5^{+\bullet}$), a series of novel substrates were examined to test the assumptions presented in **Scheme 5-2**. Molecular modeling calculations revealed that the perpendicular conformation of $5^{+\bullet}$ was more favorable by 3.6 kcal/mol, leading to the hypothesis that the cyclopropyl group did not meet the appropriate stereoelectronic requirements for ring opening. Two novel cyclopropanes were synthesized that effectively lock the cyclopropyl group in the bisected conformation, thereby ensuring that the stereoelectronic requirements were met. Electrochemical examinations of, 1'-methyl-3',4'-dihydro-1'*H*-spiro[cyclopropane-1,2'-quinoline] (**7**) and 6'-chloro-1'-methyl-3',4'-dihydro-1'*H*-spiro[cyclopropane-1,2'-quinoline] (**8**), revealed the rate constants for ring opening of these radical cations to be $3.5 \times 10^2 \text{ s}^{-1}$ and $4.1 \times 10^2 \text{ s}^{-1}$ respectively. Formal redox potentials of **7** and **8** were considerably lower than the parent *N*-methyl-*N*-cyclopropylaniline (**5**); a redox potential of 0.3V was obtained for compound **7** and a value 0.366V was measured for **8**.

In order to understand how a resonance effect could potentially contribute to the overall rate constant for the ring opening of these aniline radical cations, 4-chloro-*N*-methyl-*N*-(2-

phenylcyclopropyl)aniline (**6**) was synthesized. Compound **6** was designed to provide a driving force for the ring opening reaction by providing a resonance stabilized benzylic radical following the rearrangement of the cyclopropyl amine radical cation. LSV analysis of **6** showed mixed kinetic control behavior. Subsequent redox catalysis experiments showed rate limiting electron transfer. Fitting to the appropriate working curves revealed the formal oxidation potential (E°_{ox}) of **6** to be 0.53 V. The rate constant for the ring opening reaction of the radical cation was determined to be $1.7 \times 10^8 \text{ s}^{-1}$.

5.3 Substituent Effects Correlated to Redox Potentials

In an attempt to rationalize the results presented the preceding chapters, the formal redox potentials of commercially available anilines **1-4** were examined. The redox potentials of compounds **1-4** differ by electron donating and electron withdrawing capabilities with *N,N*-dimethylaniline (**1**) being the parent structure. As the electron donating capabilities are increased the formal redox potential is lowered effectively making the compound easier to oxidize. Conversely, as electron withdrawing groups are introduced to the base structure the compound becomes more difficult to oxidize (**Table 5-1**). The redox potentials of compounds **1** and **5** are comparable, indicating that the redox potential is not greatly influenced by the addition of a cyclopropane to the base structure. In an attempt to better understand how the formal redox potential affects the rate constant for ring opening of these radical cations, the redox potentials of compounds **1-4** were compared to the experimentally determined oxidation potentials of aniline derivatives **5-8**. A detailed discussion of this analysis is presented below.

Substrate	E°_{ox} (mV)	k_0 (s^{-1})
 1	491	-----
 2	338	-----
 3	514	-----
 4	167	-----
 5	528	4.1×10^4
 6	530	1.4×10^8

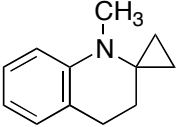
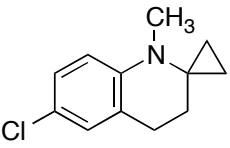
 <p style="text-align: center;">7</p>	300	3.5×10^2
 <p style="text-align: center;">8</p>	366	4.1×10^2

Table 5-1 Redox Potentials for the anilines examined and rate constants for the ring opening of the corresponding radical cations.

Computations at the B3YLP level of theory utilizing the 6-31G* basis set were conducted on compounds **1-8**. Correlation of the measured redox potentials to the ionization potentials (e.g., the difference in energy of the neutral and oxidized forms of these amines) showed a linear correlation (**Figure 5-1**). This verifies that the electrochemical methods used to extract both the redox potentials and rate constants for ring opening of radical cations **5^{+•}** - **8^{+•}** are valid. Additionally, the linear correlation between the measured redox potentials and the calculated ionization potentials provides evidence that the experimentally obtained values for k_0 of radical cations **5^{+•}** - **8^{+•}** are acceptable.

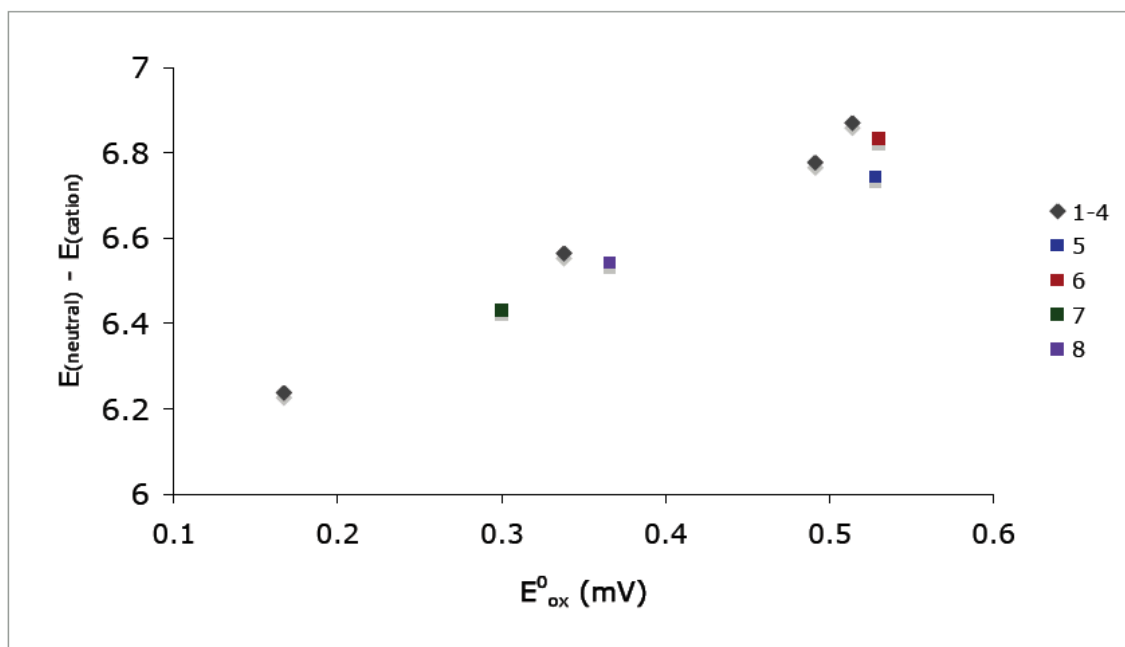


Figure 5-1 Correlation of calculated ionization potentials to experimentally determined redox potentials of compounds **1-8**.

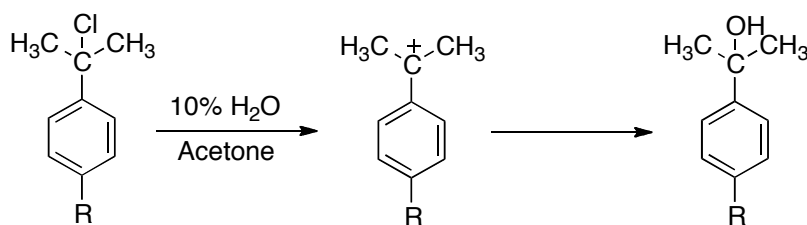
5.4 Linear Free Energy Relationships

The trends shown in **Table 5-1** can be explained through the use of a modified version of the Hammett Equation.^{2, 3} Hammett derived a mathematical expression to quantitatively assess the electronic effects of a chemical transformation based on the ionization of benzoic acid (**Equation 5-1**), where σ is an electronic constant based on the electronic nature of the substituent, ρ is the reaction constant (dependent upon the nature of the reaction, solvent, and temperature)⁴, and K_X and K_H are the ionization constants for a substituted benzoic acid and for benzoic acid, respectively. For a reaction in general, by correlating the $\log(k_X/k_H)$ or $\log(K_X/K_H)$ against the electronic substituent constants, one can deduce a value for the reaction constant ρ . A positive ρ value is indicative of a more negative transition state structure of that of the reactant, and the reaction will be accelerated by the presence of electron withdrawing groups.

Conversely a negative ρ value is indicative of a more positive transition state structure, and the reaction will be accelerated in the presence of electron donating groups.

$$\rho\sigma = \log \frac{K_X}{K_H} \quad \text{Equation 5-1}$$

The redox potentials of compounds **1-8** were correlated to σ^+ constants in order to determine if there was a relationship between the substrate's ability to lose an electron and the electron donating/electron withdrawing properties of the substituent on the aromatic ring.⁵ σ^+ values were chosen for this analysis because the chemical model for these substituent constants are based solvation reaction of cumyl chloride (**Scheme 5-3**). This chemical model takes into account how direct resonance interactions can stabilize an electron deficient intermediate.



Scheme 5-3 Solvolysis reaction of cumyl chloride that defines the σ^+ substituent constant.

The correlation between the σ^+ values show a linear relationship for all of the anilines with the exception of the two quinoline derivatives **7** and **8** (**Figure 5-2**). This trend clearly shows that electron donating substituents play a large role in stabilizing the radical cation following the oxidation of the amine. In examining the redox potentials of compounds **1-4** it is evident that the electron donating substituents will lower the redox potential of these anilines. The lowered oxidation potential of compound **4** can be directly attributed to the increased ability of the methoxyl group to stabilize the spin and charge via a resonance effect following oxidation of the neutral amine. The redox potential of **2** can be attributed to an inductive effect.

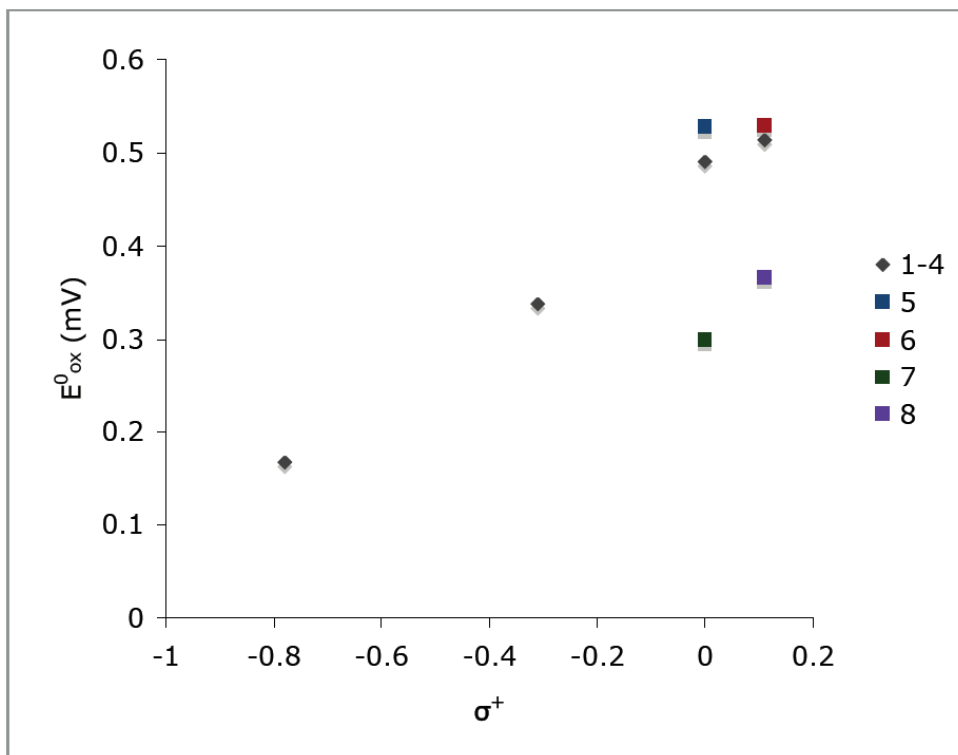


Figure 5-2 Hammett plot correlating the redox potential of **1-8** to σ^+ .

The quinoline derivatives have lower redox potentials than anilines **1-6**, indicating that another phenomena is responsible for the redox properties of compounds **7** and **8**. Two possibilities have been considered: (i) the radical cation is stabilized by the p-orbitals of the cyclopropane which are now appropriately aligned with the electron deficient center (cyclopropyl stabilization), or (ii) locking the cyclopropyl group in the bisected conformation with an alkyl chain has introduced a new substituent (i.e., the ortho alkyl group) which has significantly added to the electron donating character to the molecule. The second effect was examined by modifying the published Hammett substituent constants to account for the added contribution of the alkyl group in compounds **7** and **8**. This was accomplished through the use of **Equation 5-2**.

$$\sigma_{adjusted}^+ = \sigma_{para}^+ + \sigma_{alkyl}^+ \quad \text{Equation 5-2}$$

Correlation of the $\sigma_{adjusted}^+$ values to the experimentally obtained redox potentials show a linear relationship for all of the anilines examined in this manuscript (**Figure 5-3**). This trend clearly

shows that for novel substrates, **7** and **8**, the electron donating character of the alkyl chain plays a large role in stabilizing the radical cation following the oxidation of the amine. The effect of cyclopropyl stabilization is minimal for these compounds.

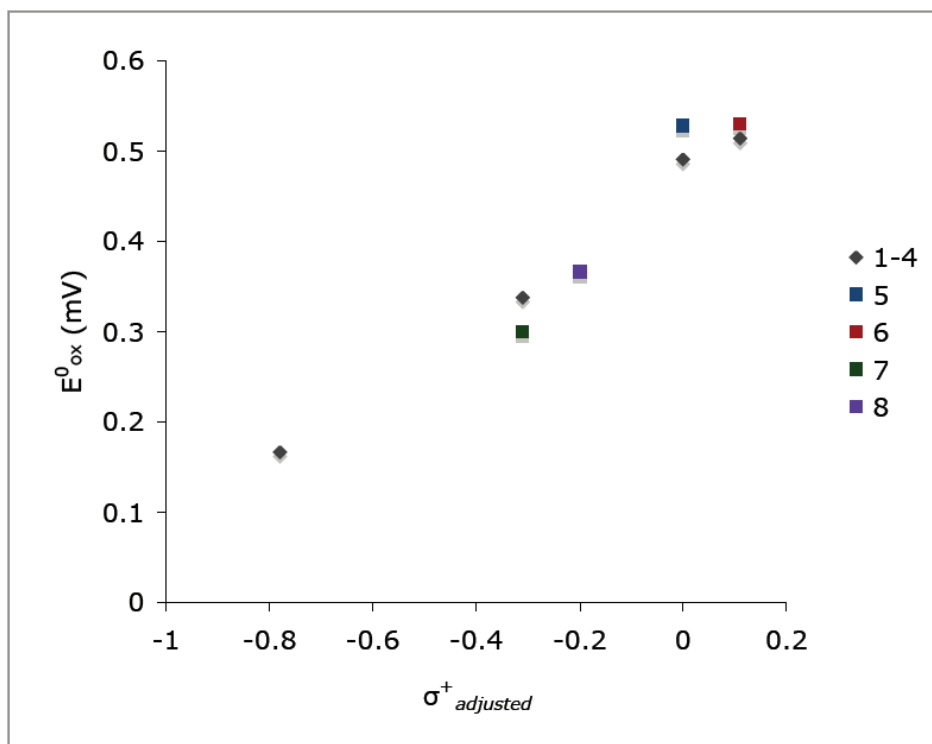


Figure 5-3 Hammett plot correlating the redox potential of **1-8** to adjusted σ^+ constants accounting for the added electron donating character of compounds **7** and **8**.

5.5 Activation Barriers and Trends in Redox Potentials

Energy profiles on $\mathbf{5}^{\bullet+}$ were constructed at the B3YLP/6-311+G(d,p) level of theory. Results reveal: a) the ring-closed and ring-opened forms of $\mathbf{5}^{\bullet+}$ reside at potential energy minima (no imaginary frequencies), and b) that there is a barrier to the ring opening reaction. A transition state for the ring opening was located, characterized by one imaginary frequency corresponding to C-C bond cleavage. The energy of activation for the ring opening pathway was found to be 7.65 kcal/mol. Ring opening was endothermic by ca. 4.3 kcal/mol.

This same computational methodology was carried out for three additional cyclopropyl anilines that differ in structure by their electron donating capabilities (**Table 5-2**). Absolute energies for each structure were normalized against the transition state energies for direct comparison of the relative energies of the ring closed radical cations.

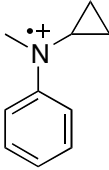
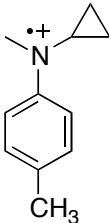
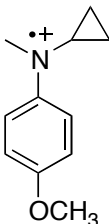
Substrate	Calculated E_a (kcal/mol)
 5^{•+}	7.65
 9^{•+}	9.96
 10^{•+}	12.91

Table 5-2 Calculated activation barriers for compounds **5^{•+}**, **9^{•+}**, and **10^{•+}** at the B3YLP/6-311+G(d,p) level of theory.

The data from modified Hammett plots predicts that cyclopropylamines containing electron donating groups will yield structures with lowered redox potentials. Comparison of the relative energies compounds **5^{•+}**, **9^{•+}** and **10^{•+}** confirms this trend **Figure 5-4**. Compound **10^{•+}** which can stabilize the electron deficient radical cation via inductive and resonance effects, yields the lowest energy ring closed radical cation: resulting in a higher activation barrier for the ring

opening reaction. The methyl group of $9^{\bullet+}$ can stabilize the radical cation through an inductive effect resulting in a lower energy ring closed structure when compared to the relative energy of compound $5^{\bullet+}$. The trends in the calculated activation barriers of compounds $5^{\bullet+}$, $9^{\bullet+}$ and $10^{\bullet+}$ all reflect the relative stability of the ring closed radical cations. For this reason compound $10^{\bullet+}$ is expected to have the smallest rate constant the ring opening reaction. Conversely, the ring opening reaction compound $5^{\bullet+}$ is expected to be the fastest of the series.

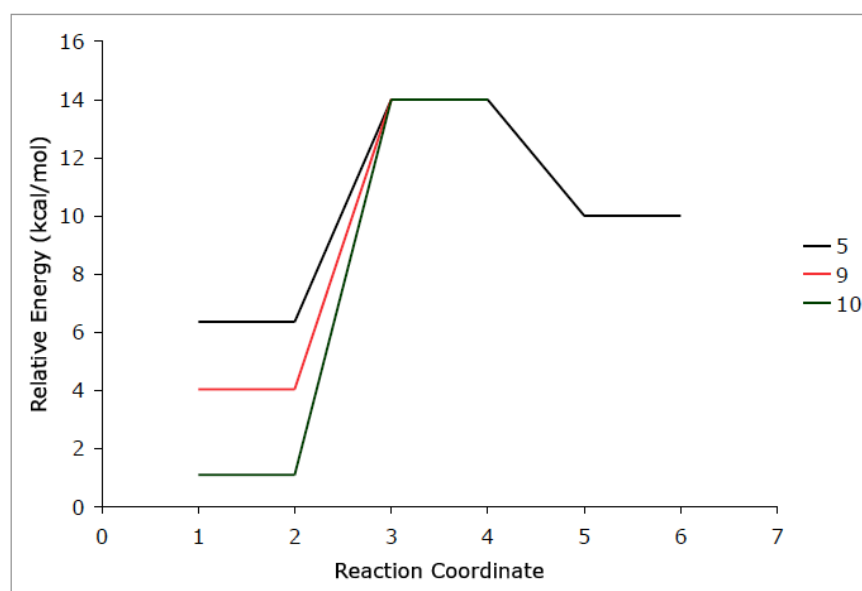
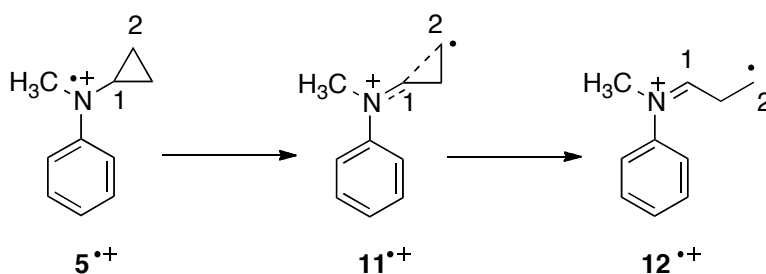


Figure 5-4 Reaction coordinate diagram depicting the relative energies of compounds $5^{\bullet+}$, $9^{\bullet+}$, and $10^{\bullet+}$.

5.6 Spin density analysis of compound $5^{\bullet+}$

The redox potentials of compounds **1** and **5** are comparable; therefore the redox potential is not significantly influenced by the addition a cyclopropyl group. The rate constant for ring opening *N*-methyl-*N*-cyclopropylaniline radical cation was experimentally determined to be $4.1 \times 10^4 \text{ s}^{-1}$. The small rate constant for the ring opening reaction of compound $5^{\bullet+}$ could potentially be explained by a resonance effect in which the spin and charge of the radical cation in the ring closed form is delocalized into the benzene ring hindering the overall rate of the ring opening

reaction. Spin density computations were conducted at the B3YLP level of theory for the three structures associated with the ring opening reaction in an attempt to understand the magnitude of the resonance contribution for this pathway. The structures examined for this analysis are: (i) the ring closed radical cation $5^{+\bullet}$, (ii) the transition state represents the C-C bond breaking step of the process ($11^{+\bullet}$) and (iii) the product corresponding to the distonic radical cation $12^{+\bullet}$ (Scheme 5-4).



Scheme 5-4 Ring opening reaction of $5^{+\bullet}$.

Figure 5-5 shows that the spin density of the ring closed radical cation is delocalized into the aromatic portion of the molecule causing a net stabilization of this structure prior to ring opening reaction. In the transition state the resonance contribution of the aromatic ring is diminished as more radical character is transferred to carbon atom **2** (Scheme 5-4) during the C-C bond breaking step. Finally in the product structure the resonance contribution of the aromatic ring is non-existent. From these computational results we can surmise that the delocalization of the radical into the aromatic ring of compound $5^{+\bullet}$ plays a significant role in the decreased rate constant for ring opening of the amine radical cation.

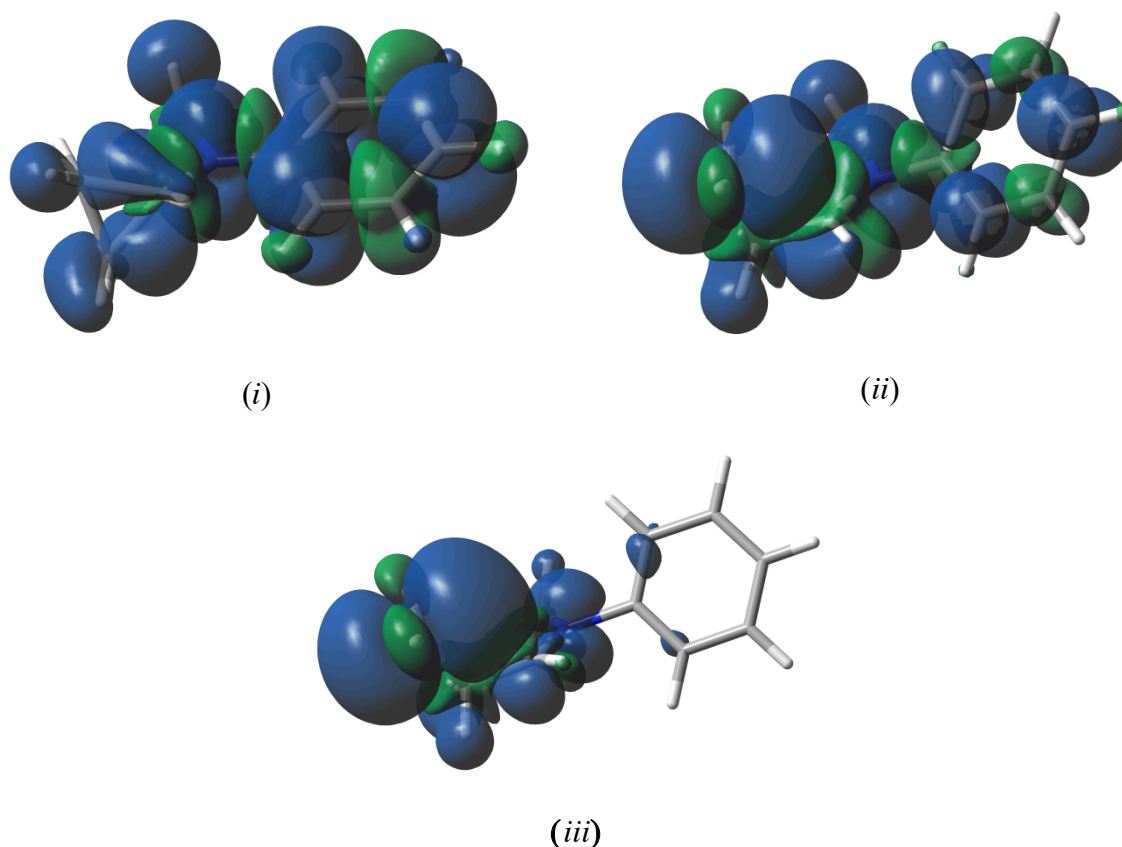


Figure 5-5 Depiction of the spin and charge delocalization of (i) the ring closed radical cation, (ii) the transition state, and (iii) the product arising from the ring opening of $5^{+\bullet}$.

5.7 Comparison of 5 to 7 and 8

In examining the major contributing structures that were used to generate the reaction coordinate diagram for compound $7^{+\bullet}$ at the B3YLP level of theory, we can see the same type of behavior that was seen for compound $5^{+\bullet}$. The structure corresponding to the ring closed radical cation shows that the spin density is delocalized into the aromatic portion of the molecule. In the transition state, as the cyclopropyl C-C bond is broken and the resonance contribution is diminished. Finally, in the product structure, the resonance contribution stemming from the aromatic ring no longer exists (**Figure 5-6**). These computational results show that the resonance contribution of the ring closed radical cation plays a major role in the slowed rate constant for

ring opening of $7^{\bullet+}$. Due to the fact that the redox potential of **7** is 190 mV lower than compound **5**, one would expect the relative energy of $7^{\bullet+}$ to be lower than $5^{\bullet+}$. For this reason a smaller rate constant for the ring opening pathway of $7^{\bullet+}$ is expected. Spin density computations of compound $8^{\bullet+}$ resulted in the same trend shown for compound $7^{\bullet+}$. Results for these computations are presented in Appendix C.

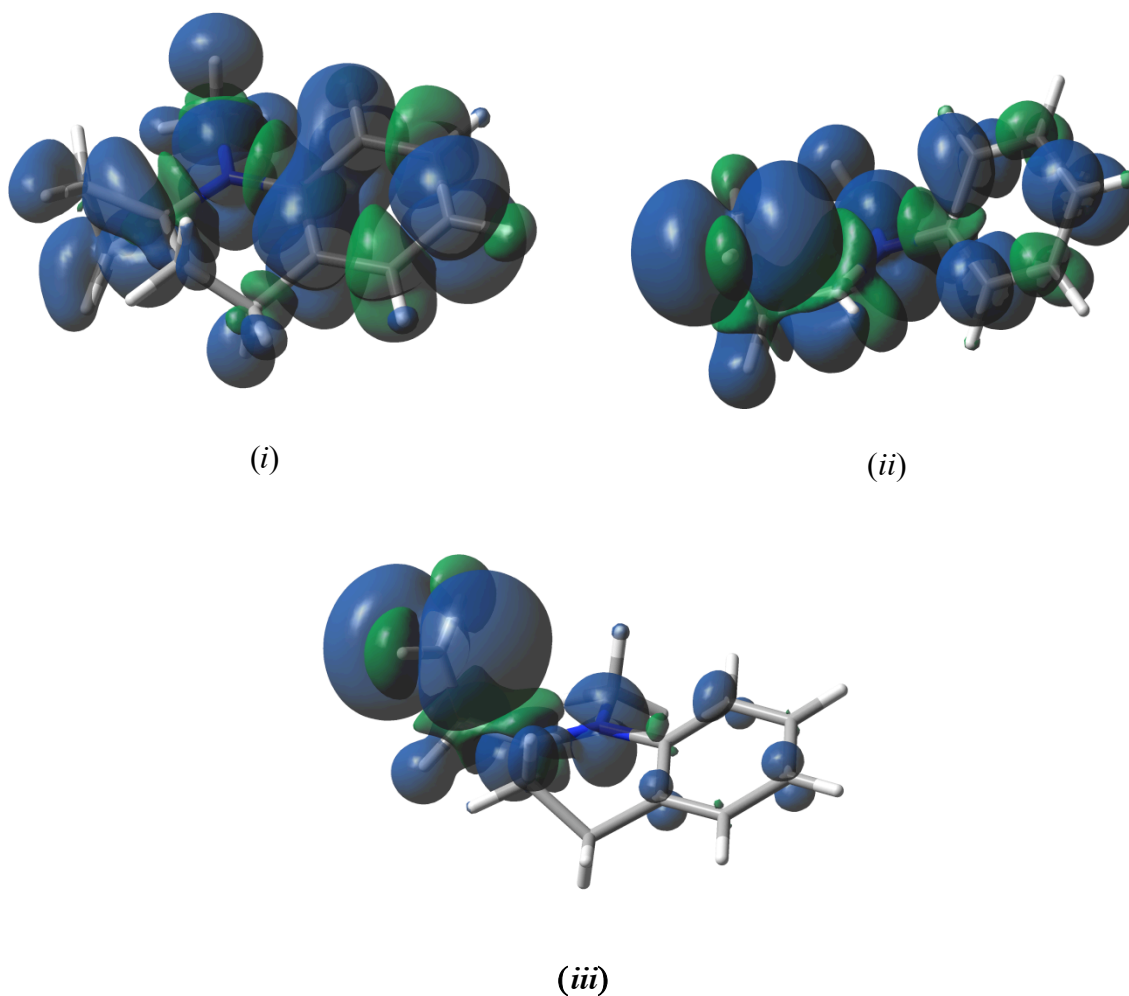
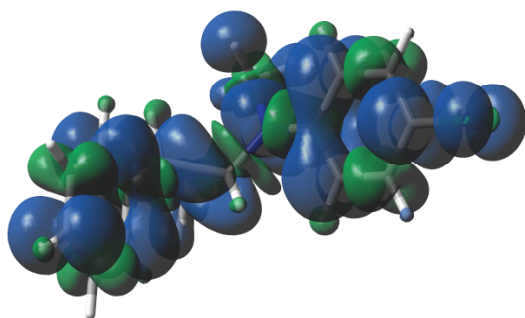


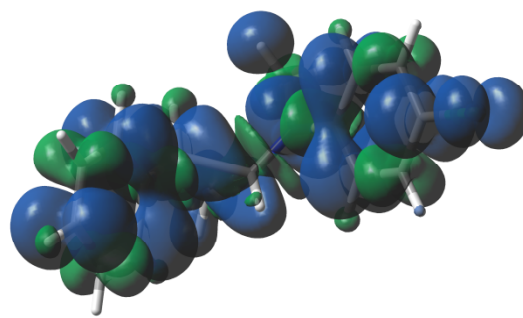
Figure 5-6 Depiction of the spin and charge delocalization of (i) the ring closed radical cation, (ii) the transition state, and (iii) the product arising from the ring opening of $7^{\bullet+}$.

5.8 Spin Density Analysis of Substrate $6^{+\bullet}$

Spin density computational examinations of compound $6^{+\bullet}$ were conducted to provide further evidence that the formation of a resonance stabilized benzylic radical in the product structure provides a driving force for the ring opening reaction. This in turn results in an increase in the overall rate constant for the ring opening pathway. The energy optimized structure for the ring closed radical cation ($6^{+\bullet}$) shows a longer than average C-C bond length for the cyclopropane bond by 0.1 Å. The spin density of the ring closed radical cation is delocalized throughout the entire molecule. The transition state structure is very similar to the reactant, indicative of a highly exothermic process. Finally, the product structure depicts how the benzylic radical is stabilized by resonance via the phenyl ring. Although the resonance contribution of the ring closed radical cation is still a major contributor to the overall energetics of the ring opening pathway, the relief of ring strain coupled with the formation of the highly resonance stabilized benzylic radical explains the rate increase for the ring opening reaction of $6^{+\bullet}$.



(i)



(ii)

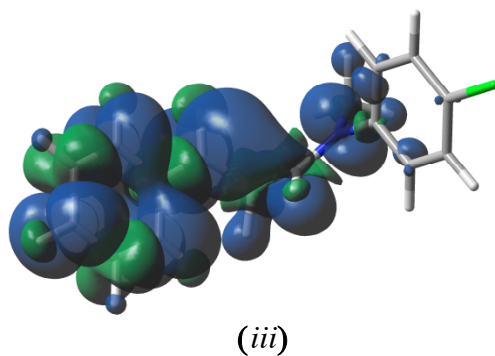


Figure 5-7 Depiction of the spin and charge delocalization of (i) the ring closed form, (ii) the transition state, and (iii) the product arising from the ring opening of $6^{+\bullet}$.

5.9 Comparison of Experimental Data with Computational Results

Examination of compounds $5^{+\bullet}$ - $8^{+\bullet}$ at the B3YLP level of theory to generate reaction coordinate diagrams for the ring opening pathway are shown in **Figure 5-8**. The calculated activation barriers for compounds $5^{+\bullet}$, $6^{+\bullet}$, and $7^{+\bullet}$ parallel the experimental trends.

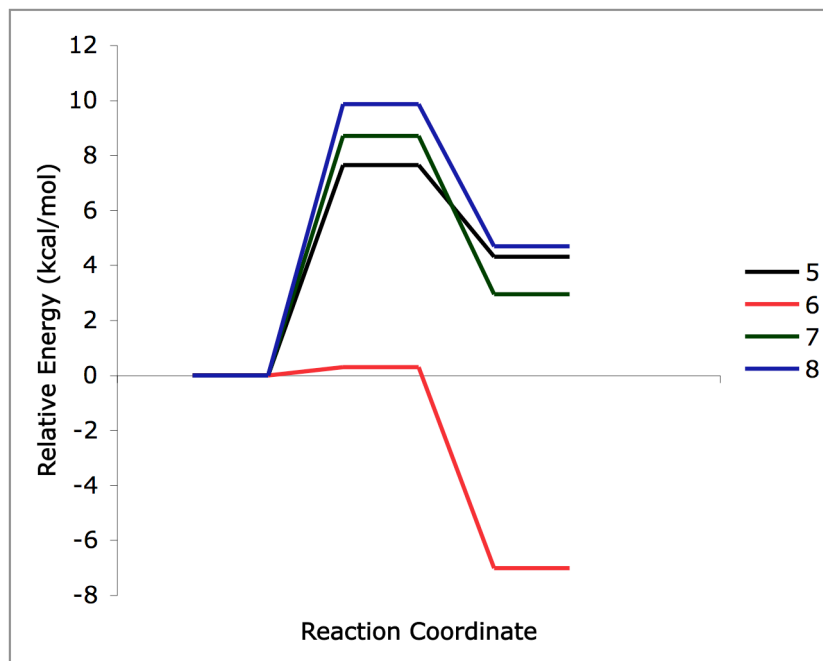


Figure 5-8 Reaction coordinate diagram for compounds **5-8**.

Table 5-3 compares the experimentally obtained rate constants for the ring opening of anilines **5⁺**, **6⁺**, **7⁺**, and **8⁺** against the calculated activation barriers. The predicted rate constants for compounds **5⁺** and **8⁺** correlate well to the experimentally obtained values.

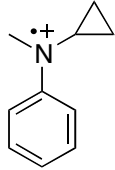
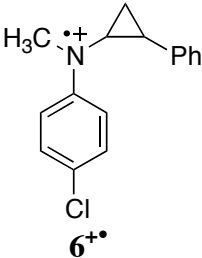
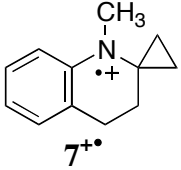
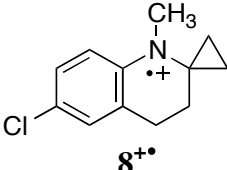
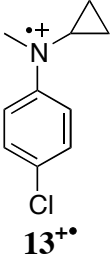
Substrate	Calculated E _a (kcal/mol)	Calculated k (s ⁻¹)	Measured k (s ⁻¹)
 5⁺	7.65	3.7 x 10 ⁴	4.1 x 10 ⁴
 6⁺	0.29	1.4 x 10 ¹⁰	1.4 x 10 ⁸
 7⁺	8.70	5.9 x 10 ³	3.5 x 10 ²
 8⁺	9.86	6.9 x 10 ²	4.1 x 10 ²
 13⁺	9.37	1.7 x 10 ³	-----

Table 5-3 Comparison of experimentally derived rate constants and computational results at the B3YLP/6-311+G(d,p) level of theory.

The computationally derived value for the ring opening of **6^{•+}** is two orders of magnitude higher than the measured value. The energy optimized structure for the ring closed radical cation (**6^{•+}**) shows a longer than average C-C bond length for the cyclopropane bond by 0.1 Å. The presence of the ‘loose’ C-C bond may potentially explain the accelerated rate constant that was obtained from the computations. Electrochemical examinations of **6** did not reveal any evidence a concerted dissociative electron transfer pathway (i.e., concerted oxidation of the amine coupled with a bond breaking step). Predicted peak widths for a concerted dissociative electron transfer pathway are predicted to be 160 mV based on **Equation 5-3**. The term α is deemed the transfer coefficient, which gives information about the symmetry of the transition state. The term α determines the fraction of change in the electrode potential that causes a change in the activation energy. For a concerted dissociative electron transfer processes this value has been measured to be 0.3 if bonds are broken concurrent with electron transfer.⁶ Linear sweep voltammetry of compound **8** showed mixed kinetic control behavior with peak widths of 85 mV. No evidence of a concerted dissociative electron transfer pathway was ever observed in the direct electrochemical runs.

$$E_p - E_{p/2} = \frac{1.85RT}{\alpha nF} \approx 160mV \quad \text{Equation 5-3}$$

Comparison of computational results for compounds **7^{•+}** and **8^{•+}** show a higher activation barrier for compound **8^{•+}**. This result does not correlate to the predicted pattern that is expected from the modified Hammett plot presented in **Figure 5-3**. Correlations of measured redox potentials

to Hammett substituent constants predicts electron donating substituents to stabilize the radical cation following oxidation of the amine. This will result in a higher activation barrier for the ring opening reaction. Conversely, electron withdrawing substituents should yield higher energy ring closed structures resulting in a faster ring opening reaction. Compound **8** may not fit the predicted trend because the chlorine atom can act as both an electron donor and an electron acceptor. If the resonance effect of the chlorine atom has more of an impact on the ring closed structure this will result in a lower energy ring closed structure. The resonance contribution was accounted for in **Equation 5-4**.

$$\sigma_{resonance} = \sigma_{para} - \sigma_{meta} \quad \text{Equation 5-4}$$

Modification of the published Hammett substituent constants to account for the added contribution of the alkyl group as well as the resonance effect for compound **8** were correlated to the formal redox potentials of all compounds examined experimentally.^{7, 8} This was accomplished through the use of **Equations 5-2** and **5-3**. **Figure 5-9** shows the results of this analysis. Although the correlation of the redox potentials to the σ^+ constants seems to show that compound **8** is an outlier for this analysis, the magnitude of the resonance contribution of this functional group may be over compensated for. This could explain the anomalous results from the computational data.

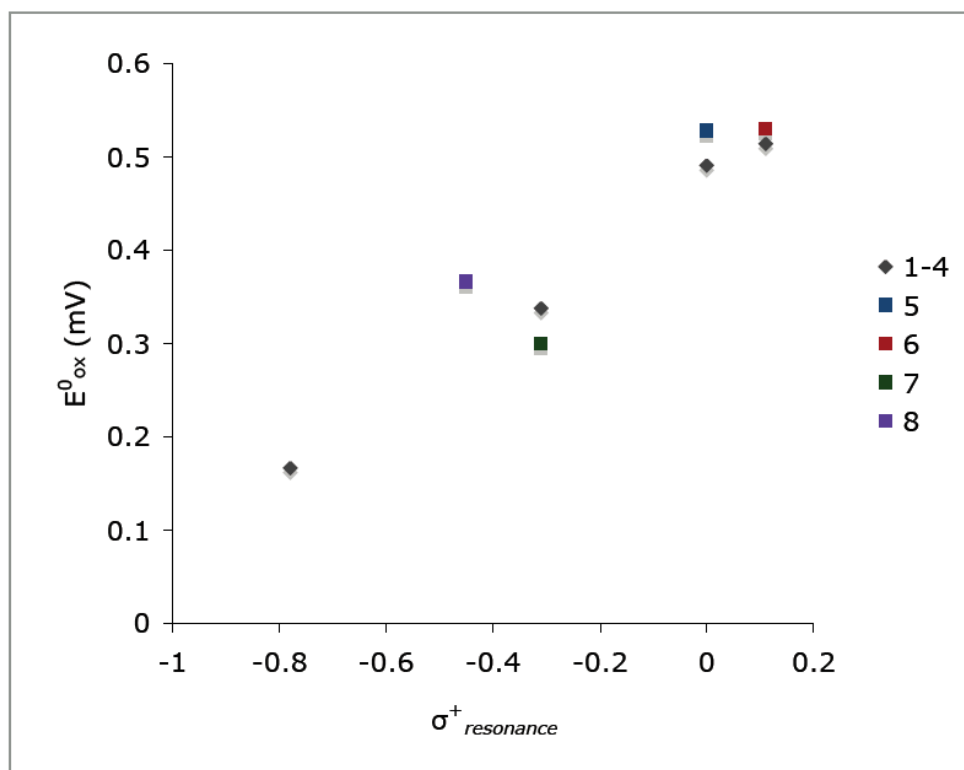


Figure 5-9 Hammett plot correlating the redox potential of **1-8** to modified σ^+ constants accounting for the added resonance effect for **8**.

Lastly, comparison of the activation barrier of **13⁺** to compounds **5⁺**, **9⁺**, and **10⁺** also showed a similar result that was seen for compound **8⁺**. The activation barrier for the ring opening reaction of compound **13⁺** is expected to be the smallest of the series. Transition state structures for all four compounds were characterized by one imaginary frequency corresponding to C-C bond cleavage. Analysis of the transition the state structures of all four compounds revealed a C-C bond cleavage, and there were no obvious anomalies for the transition state structures of all four compounds. Correlations of the redox potential to σ^+ Hammett substituent constants was not possible because the formal redox potential of compound **13** was not measured. The resonance contribution of the chlorine atom may potentially explain why the ring closed structure for compound **13⁺** is lower in relative energy when compared to compound **5⁺**.

5.10 Final Thoughts and Conclusions

Correlation of the measured redox potentials to calculated ionization potentials showed a linear correlation, verifying that the electrochemical methods used to extract both the redox potentials and rate constants for ring opening of radical cations **5**^{•+} - **8**^{•+} are valid. The correlation of experimentally measured redox potentials of compounds **1-8** to $\sigma^+_{adjusted}$ substituent constants revealed a linear trend, confirming that the electron donating character of the ortho alkyl group of compounds **7** and **8** plays a large role in stabilizing the radical cation following the oxidation of the amine. The relative energy of the ring closed radical cations (**5**^{•+}, **9**^{•+}, and **10**^{•+}) directly affects the rate of ring opening reactions as shown by computational reaction coordinate diagrams at the B3YLP/6-311+G(d,p) level of theory. Spin density computations of **6**^{•+} at the B3YLP level of theory depict the extent of the resonance contributions in the ring opening pathway. The relief of ring strain coupled with the formation of the highly resonance stabilized benzylic radical explains the rate increase for the ring opening reaction of **6**^{•+}. The effect of the chlorine atom substituent should be probed further to provide an understanding of how this functional group stabilizes the ring closed structure.

References

1. Li, X. Z.; Grimm, M. L.; Igarashi, K.; Castagnoli, N.; Tanko, J. M., The first calibration of an aminiumyl radical ion clock: why N-cyclopropylanilines may be poor mechanistic probes for single electron transfer. *Chemical Communications* **2007**, (25), 2648-2650.
2. Jaffe, H. H., A Reexamination of the Hammett Equation. *Chem Rev* **1953**, *53*, 191-261.
3. Lowry, T. H.; Richardson, K. S., *Mechanism and Theory in Organic Chemistry*. 3rd ed.; Harper Collins Publishers: New York, 1987.
4. Hammett, L. P., The Effect of Structure upon the Reactions of Organic Compounds. Benzene Derivatives. *J Am Chem Soc* **1937**, *59*, 96-103.
5. Klumpp, G. W., *Reactivity in Organic Chemistry*. John Wiley & Sons, Inc.: New York, 1982; p 103-117.
6. Andrieux, C. P.; Hapiot, P.; Saveant, J. M., Fast Kinetics by Means of Direct and Indirect Electrochemical Techniques. *Chem Rev* **1990**, *90* (5), 723-738.
7. Ehrenson, S.; Brownlee, R. T. C.; Taft, R. W., Generalized treatment of substituent effects in the benzene series. Statistical analysis by the dual substituent parameter equation. *Prog. Phys. Org. Chem* **1973**, *10*, 1-80.
8. Exner, O., *Advances in Linear Free Energy Relationships*. Plenum Press: New York, 1972.

Appendix A: Supplementary Information for Chapter 2

Reaction of Benzophenone Triplet with Aliphatic Amines. What a Potent Neurotoxin Can Tell Us About the Reaction Mechanism

Transient absorption spectra for and MPTP and N-cyclopropylphenyl MPTP as well as concentration profiles of MPTP and N-cyclopropyl MPTP in are provided as supporting information for chapter 2.

Transient Absorption Spectroscopy. Sample solutions containing approximately a 1:1 ratio of benzophenone and MPTP (4.5 mM) were prepared in distilled acetonitrile or benzene. Solutions were degassed prior to use. All experiments were conducted with the use of a flow cell to ensure that fresh solution was used for all runs. UV-Visible spectra were recorded prior to runs to ensure benzophenone was the only absorbing species.

Concentration profile for MPTP and benzophenone. Solutions containing varying concentration of amine and benzophenone (4 mM) were prepared. All solutions were degassed prior to use. Pseudo first order rate constants for the reaction of benzophenone triplet (³BP) with MPTP were obtained by plotting the experimentally observed rate (k_{obs}) constants of ³BP decay as a function of amine concentration [MPTP] (**Equation 1**).

$$k_{obs} = k_0 + k[MPTP] \quad \text{Equation 2-1}$$

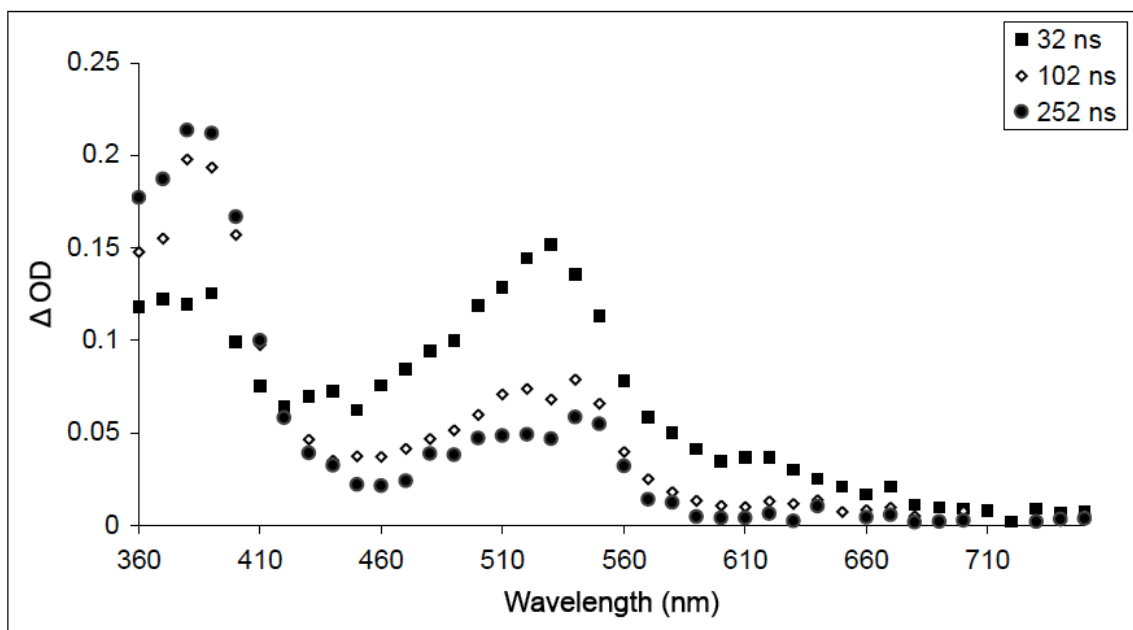


Figure 2-7 Transient absorption spectra of MPTP (1) in benzene.

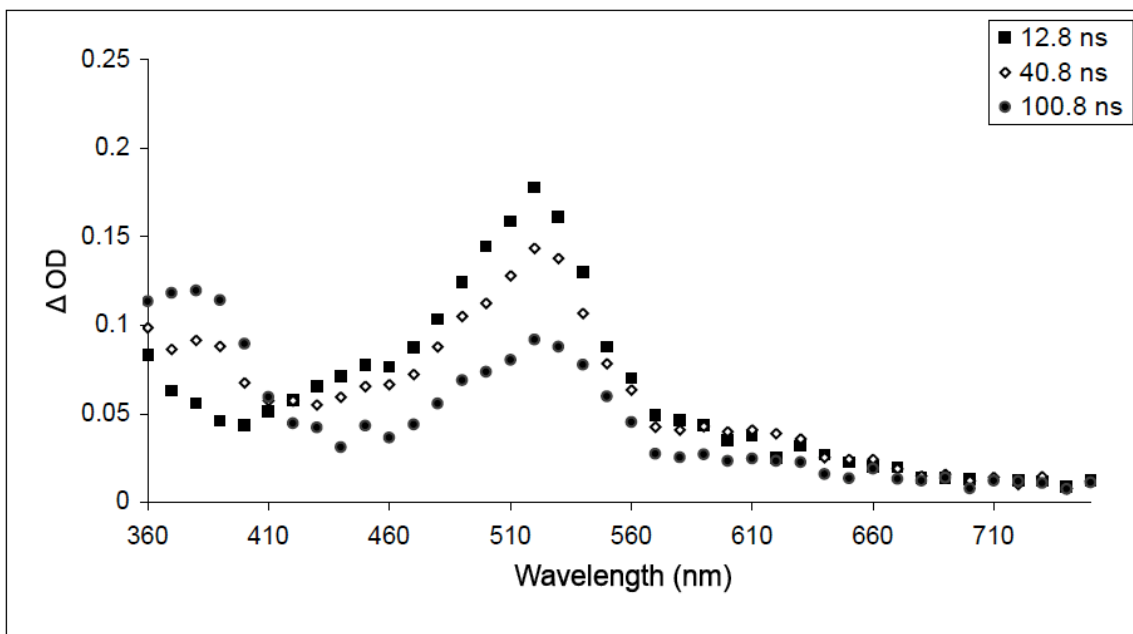


Figure 2-8 Transient absorption spectra of MPTP (1) in CH_3CN in the presence of $LiOCl_4$.

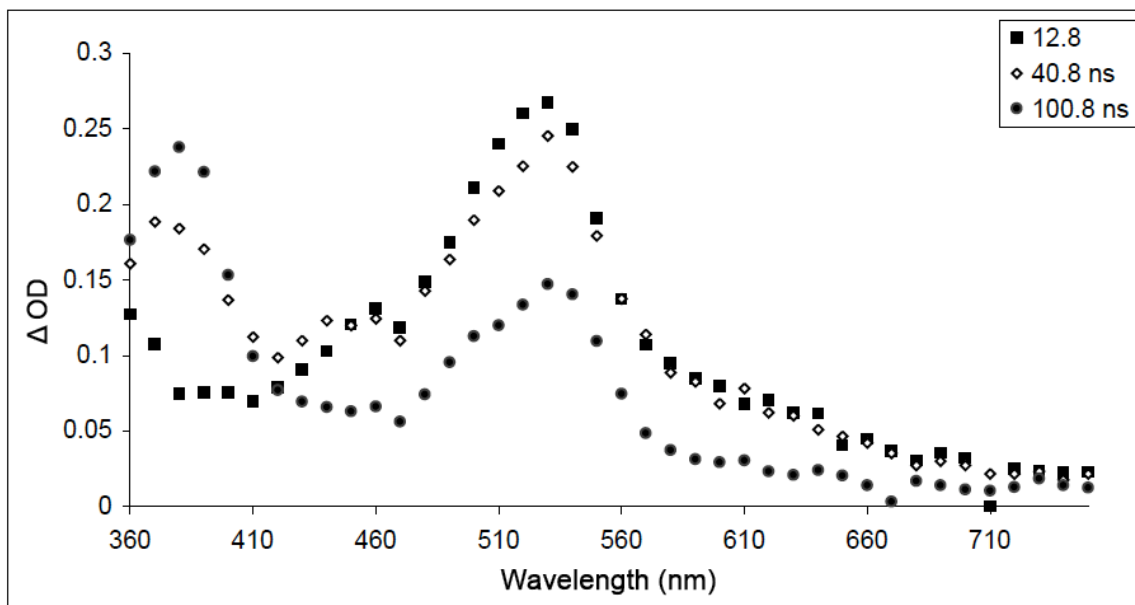


Figure 2-9 Transient absorption spectra of *N*-cyclopropylphenyl MPTP (**10**) in benzene.

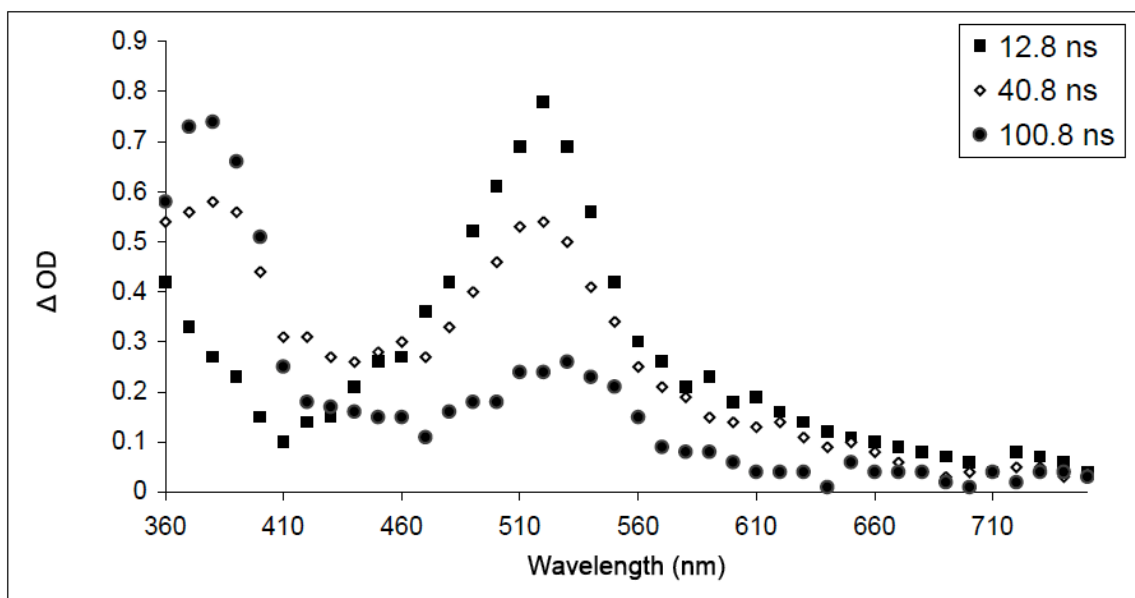


Figure 2-10 Transient absorption spectra of *N*-cyclopropylphenyl MPTP (**10**) in CH_3CN in the presence of LiOCl_4 .

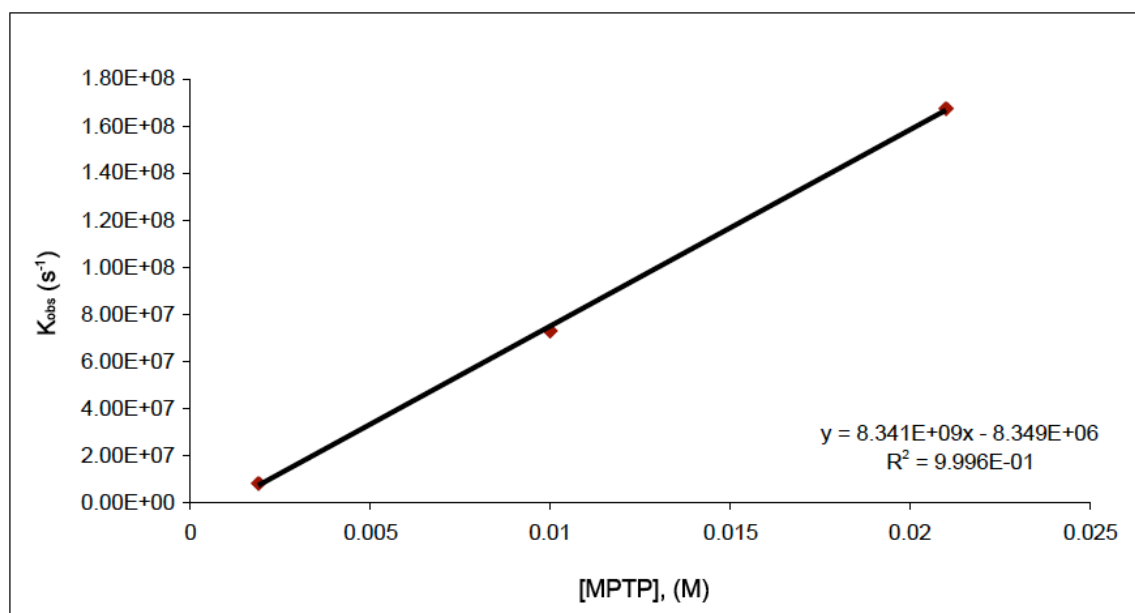


Figure 2-11 Concentration profile for the reaction of benzophenone triplet (3BP) with MPTP (**1**) in acetonitrile.

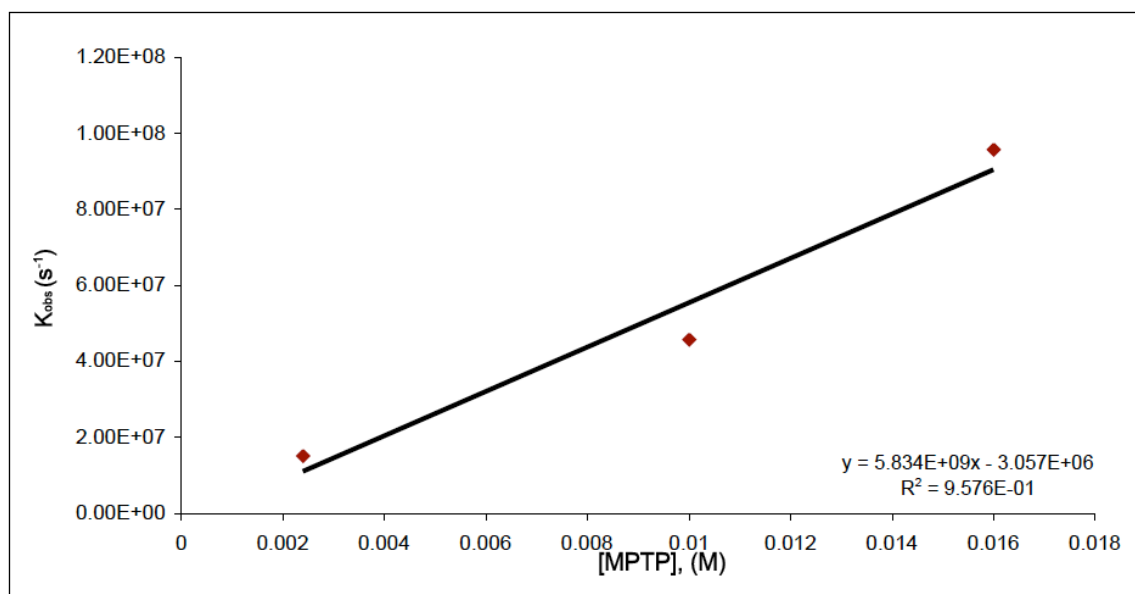


Figure 2-12 Concentration profile for the reaction of benzophenone triplet (3BP) with MPTP (**1**) in acetonitrile in the presence of 0.5M $LiOCl_4$.

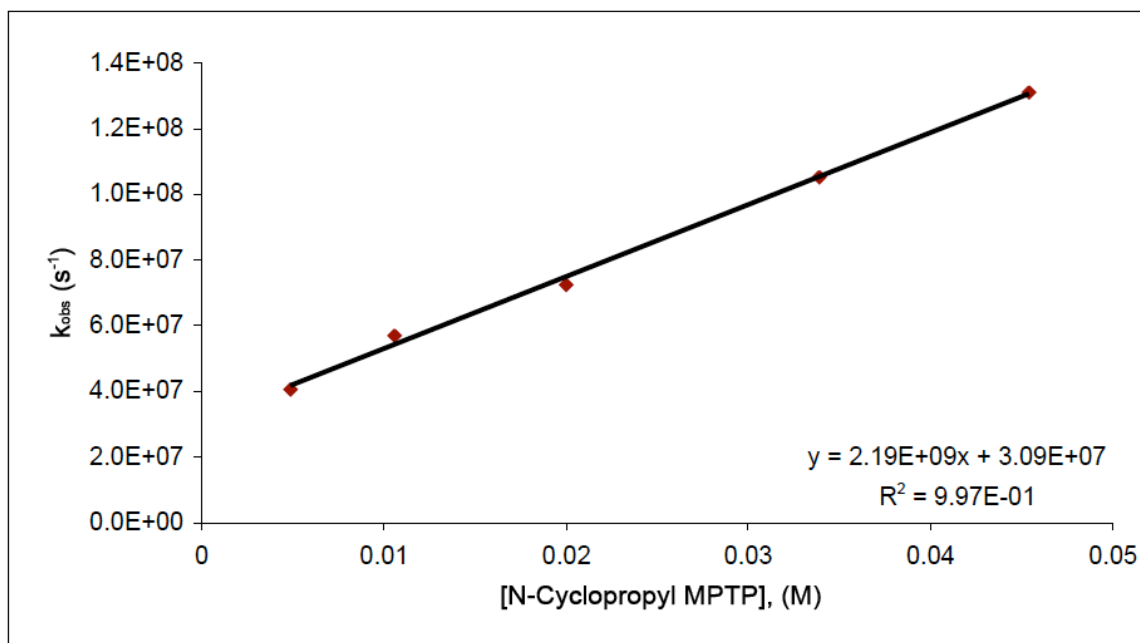


Figure 2-13 Concentration profile for the reaction of benzophenone triplet (3BP) with *N*-cyclopropyl-MPTP (**9**) in benzene.

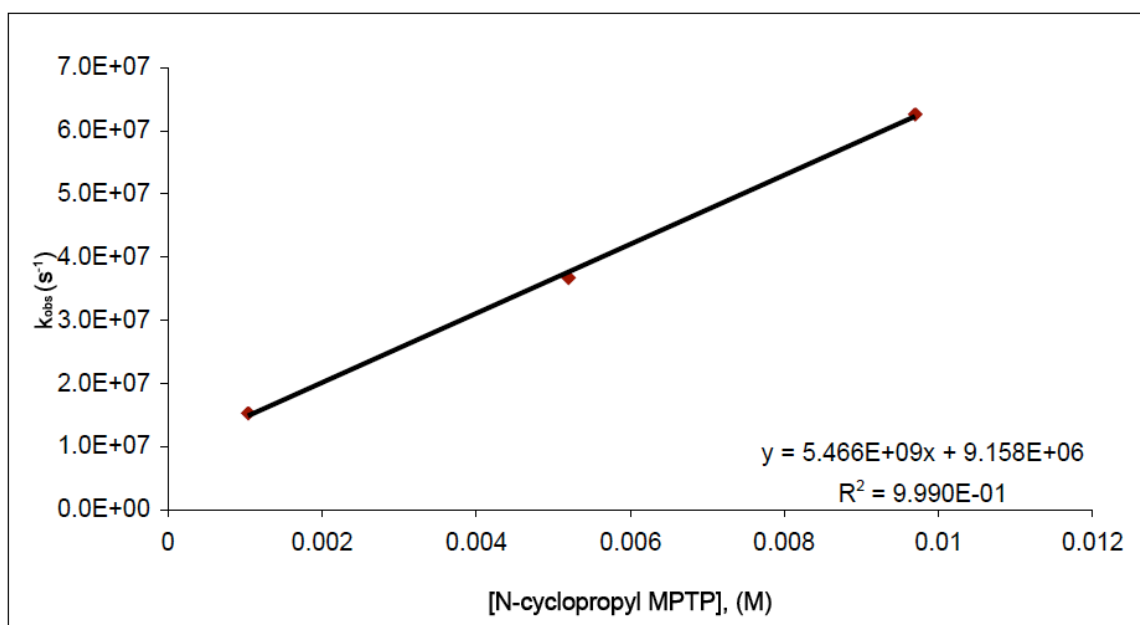


Figure 2-14 Concentration profile for the reaction of benzophenone triplet (3BP) with *N*-cyclopropyl MPTP (**9**) in acetonitrile.

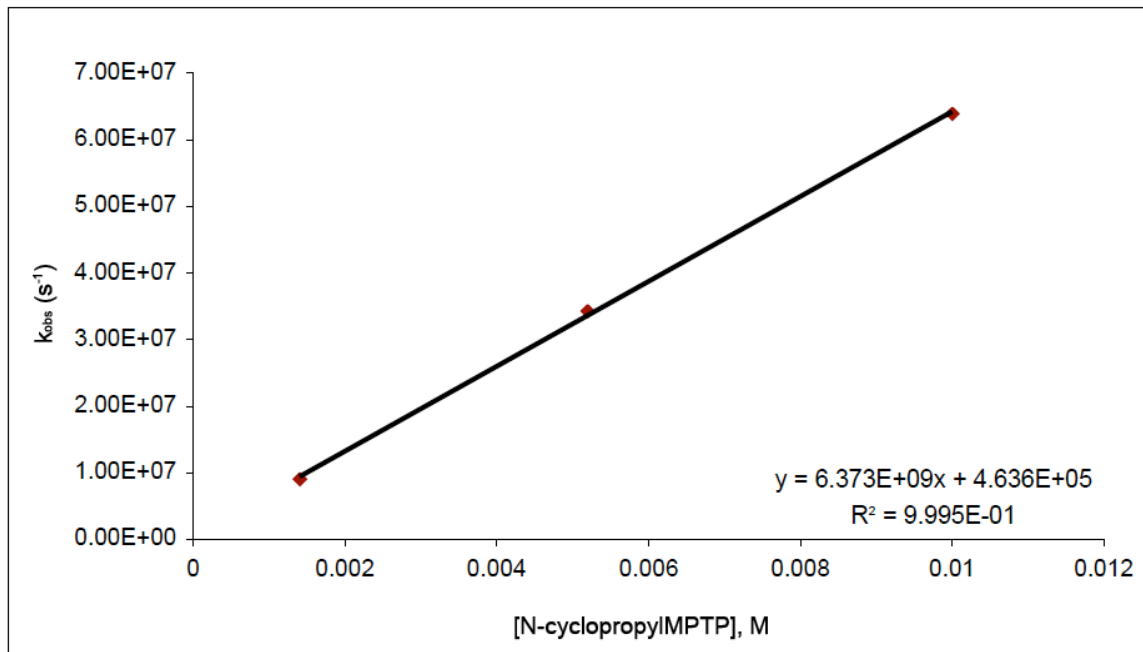


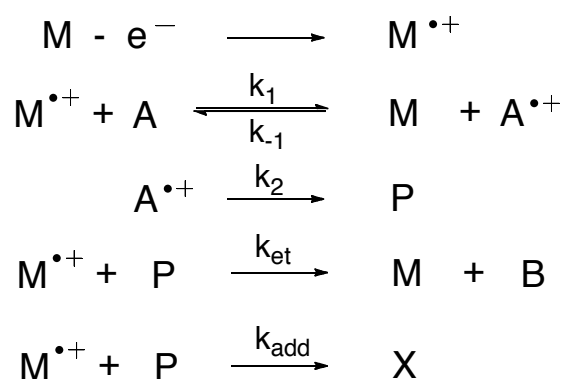
Figure 2-15 Concentration profile for the reaction of benzophenone triplet (³BP) with *N*-cyclopropyl MPTP (**9**) in acetonitrile in the presence of 0.5M LiOCl₄.

Appendix B: Supplementary Information for Chapter 4

Chapter 4 Development of New *N*-Cyclopropyl Based Electron Transfer Probes for Enzyme Catalyzed Reactions: Resonance Effects

Details of the fitting procedure for the experimental data to the appropriate published working curves for compound **6** is provided as supporting information for chapter 4.

A series of theoretical working curves have been developed for this mechanistic regime that compare the peak current ratio (i_p/i_{pd}) to the dimensionless parameter $\lambda\lambda_1/\lambda_{.1}$. By fitting the experimental data to the appropriate published working curves the rate constant for the electron transfer between the mediator and $\mathbf{6}^{\bullet+}$ (k_1) can be obtained. The kinetics of this system was complicated by a competing bimolecular reaction between the oxidized form of the mediator ($\mathbf{M}^{\bullet+}$) and ring opened product $\mathbf{6}^{\bullet+}$ (**Scheme 4-10**). A competition between a second oxidation step and the coupling of oxidized form of the mediator ($\mathbf{M}^{\bullet+}$) and $\mathbf{6}^{\bullet+}$ was considered in the fitting to the appropriate working curves. The treatment of this data introduced a new parameter ρ , that takes into account the amount of $\mathbf{6}^{\bullet+}$ that adds to the mediator ($\rho=k_{et}/k_{et} + k_{add}$).



Scheme 4-10 Mechanism used to generate the theoretical working curves.

The relevant working curves were generated using digital simulation software. Curves were derived by simulating plots of i_p/i_{pd} vs $\log \lambda_1$ for varying values of ρ . The subsequent working curves were then fit to the function $y = a + cx + ex^2 + gx^3 + ix^4 / 1 + bx + dx^2 + fx^3 + hx^4 + jx^5$. The solved solutions for the simulated working curves were then fit to the experimentally obtained curves of i_p/i_{pd} vs $\log C_M^\circ/v$. The parameter ρ was obtained from the best fit working

curve. k_1 was obtained through the use an adjustable parameter with the relationship $\log (RT/F)k_1 = \Delta$.

Appendix C: Supplementary Information for Chapter 5

Concluding Remarks

Spin density computations for compound **8^{•+}** and transition state structures for compounds **5^{•+}**, **9^{•+}**, **10^{•+}**, and **13^{•+}** are provided as supporting information for chapter 5.

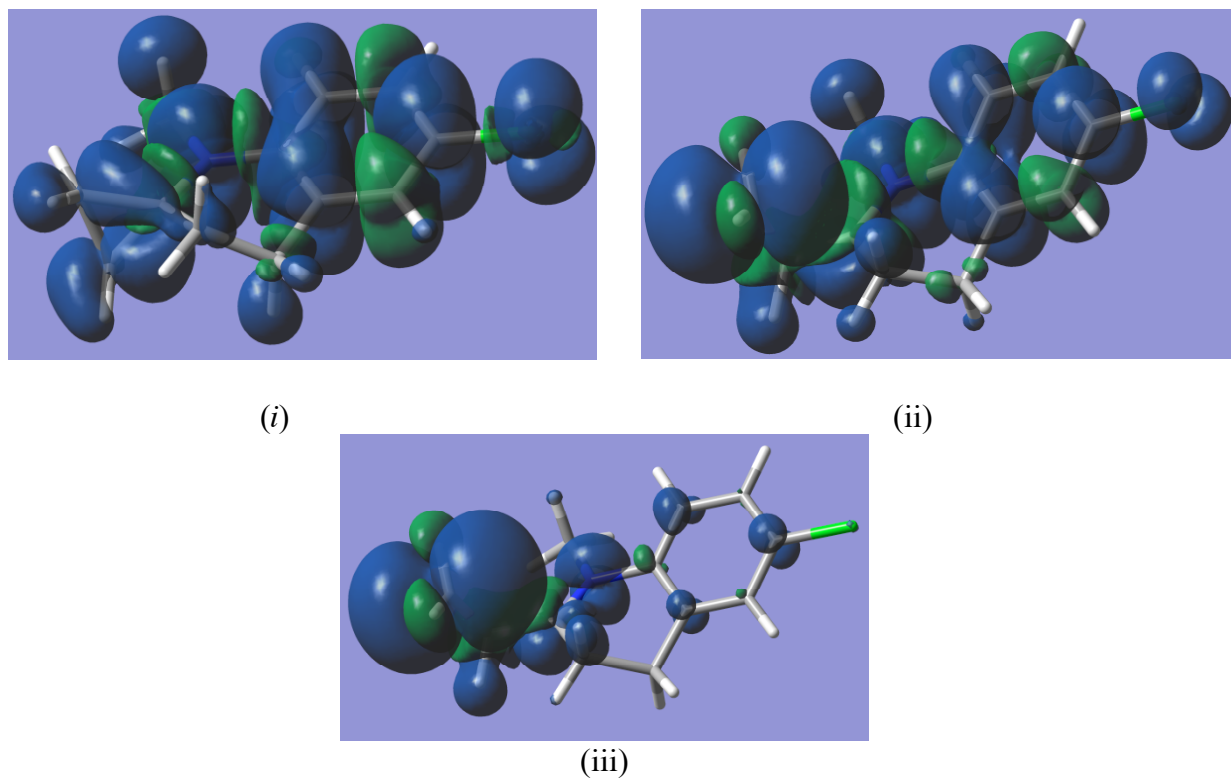


Figure 5-10 Depiction of the spin and charge delocalization of (i) the ring closed radical cation, (ii) the transition state, and (iii) the product arising from the ring opening of $8^{*\dagger}$.

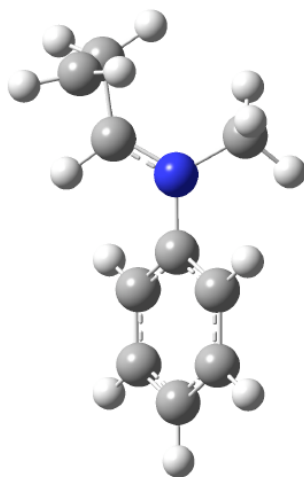


Figure 5-11 Transition state structure for compound $5^{*\dagger}$.

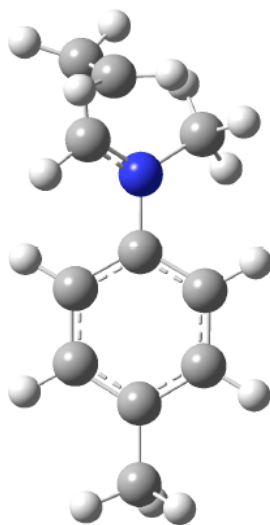


Figure 5-12 Transition state structure for compound **9^{*+}**.

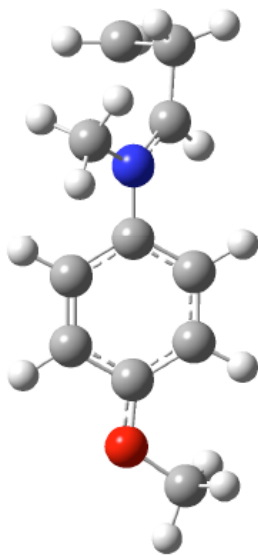


Figure 5-13 Transition state structure for compound **10^{*+}**.

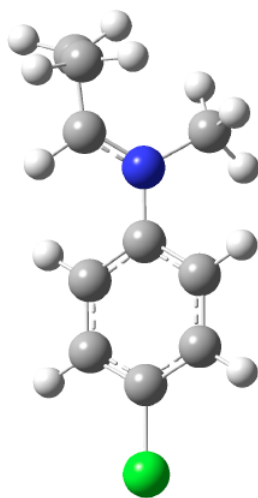


Figure 5-14 Transition state structure for compound **13^{*+}**.